Controlled delivery and release of asphaltene inhibitors

Mahmoud Kamel Getan Alhreez

Submitted in accordance with the requirements for the degree of

Doctor of Philosophy

School of Chemical and Process Engineering

The University of Leeds

April 2019

Declaration of Authorship

The candidate confirms that the work submitted is his own, except where work which has formed part of jointly authored publications has been included. The contribution of the candidate and the other authors to this work has been explicitly indicated below. The candidate confirms that appropriate credit has been given within the thesis where reference has been made to the work of others.

- Alhreez, M. and Wen, D., 2018. Controlled releases of asphaltene inhibitors by nanoemulsions. Fuel, 234, pp.538-548.

This work is attributed to Mahmoud Alhreez under supervision Dongsheng Wen. Chapter 4 is included in this work.

- Alhreez, M., Wen, D. and Ali, L., 2017, April. A novel inhibitor for controlling Iraqi asphaltene problems. In 2017 International Conference on Environmental Impacts of the Oil and Gas Industries: Kurdistan Region of Iraq as a Case Study (EIOGI) (pp. 37-41). IEEE.

This work is attributed to Mahmoud Alhreez under supervision Dongsheng Wen. Proofreading and presentation the work had been done by Lamea Ali. Chapter 4 is included part of this work.

- Alhreez, M., Xin Xiao, and Wen, D., 2019. Kinetic Study of Controlled Asphaltene Inhibitor Release from Nanoemulsions. Langmuir, **in press** at the time of thesis submission.

This work is attributed to Mahmoud Alhreez under supervision Dongsheng Wen. Proofreading and fitting curves in the manuscript have been done with assistance Xin

Xiao. The manuscript hasn't been accepted for publication yet and now under review. The results of this work have been put in Chapter 5 in the thesis.

- Alhreez, M. and Wen, D., 2019. Molecular structure characterization of asphaltene in the presence of inhibitors with nanoemulsions. *RSC Advances*, 9, 19560-19570**.**

This work is attributed to Mahmoud Alhreez under the guidance of academic supervisor Dongsheng Wen. Chapter 6 is included in this work.

- Alhreez, M., Hu Z., and Wen, D., 2019. Delivery and controlled release of inhibitor: A prospective method for enhanced oilfield asphaltene prevention, *Fuel*, **under review** at the time of thesis submission.

This work is attributed to Mahmoud Alhreez under the guidance of academic supervisor Dongsheng Wen. Proofreading has been done by Zhongliang Hu. Chapter 7 is included in this work. The manuscript hasn't been accepted for publication yet and now under review.

Acknowledgements

First and foremost, I would like to extend my deepest gratitude to my supervisor, Prof. Dongsheng Wen, for his endless guidance and support through these years. Stepping close to him can always let me feel a kind of positive energy. The regular gatherings and invitations to his place also made the entire process enjoyable.

I also would like to extend my appreciation to Dr. David Harbottle, for his support in experiment facilities, papers correction and useful suggestion at every stage of this PhD study. Thanks to Dr. Zhongliang Hu, Dr. Ehsan Nourafkan and Dr. Xin Xan for their support in materials and discussion during experiments. Thanks to the technicians: Dr. Ben Douglas and Dr. Susanne Patel and other technicians from the School of Chemical and Process Engineering, for their generous support on facilities and manufacturing.

Finally, I would like to say an eternal thank you to my family, who have been giving support and COURAGE throughout my life.

Abstract

Asphaltene is a poly-disperse distribution of the heaviest and most polarizable fraction of crude oil. The asphaltene aggregation and subsequent precipitation in nonpolar media may have a profound effect on plugging wellbores and production equipment. This thesis develops an innovative concept of using nanoemulsions (NEs) as carriers for delivering asphaltene inhibitors (AI) and control their release inside porous media to prevent asphaltene agglomeration and deposition. The new concept could provide tremendous value by i) improving the stability of asphaltene, ii) reducing the usage of AI, iii) extending the treatment time via slow release, and iv) allowing good adsorption of AIs on the formation surface to increase asphaltene treatment efficacy. Four areas were studied including i) the preparation of NEs and NEs loaded with AIs; ii) asphaltene aggregation/precipitation prevention and AI release kinetics study, iii) molecular structure alteration of asphaltene in the presence of NEs, and iv) controlled the delivery of these NEs through porous media.

Firstly, we developed a novel strategy to manipulate the occurrence of Ostwald ripening to form stable NEs by using oil-soluble inhibitors such as dodecylbenzene sulfonic acid (DBSA) and the polycyclic aromatic hydrocarbon phenanthrene (phe) to the oil phase. Two methods, one static based on Brownian motion and one dynamic based on centrifugal force, were used to evaluate and confirm the physical stability of NEs. It was found that with the help of inhibitors, the NEs were very stable even after centrifuging under 500 g for 1 hour or 4 weeks' storage under ambient conditions.

Following this, a novel approach by using NEs for controlled delivery and release of AI was proposed to minimize asphaltene precipitation with reduced AI amount. The amount of inhibitor could be significantly reduced by ~ 20 times by using the DBSA NEs, with

largely extended release time. Continuing our work on the controlled release of AIs by using NEs, a mechanistic understanding of the controlled release effect was proposed based on the effect of DBSA NEs on the asphaltene particle morphology variation, which was related to the hydrophilicity of DBSA and the strong intermolecular interactions among all DBSA NE's components. The AI release mechanism was compared with eight kinetic models, and the Korsmeyer-Peppas release model was identified. The evidence of multiple intermolecular interactions and quantitative FTIR study showed that the controlled release effect and long term asphaltene stability were due to the decrease of the aromaticity and the reduction in the aliphatic side chains of asphaltene. The refractory nature of asphaltenes was investigated by thermogravimetric analysis (TGA), which revealed that the structure of asphaltene was improved considerably and the coke yield was decreased by 62% due to the decrease of the cluster size and the increase of the stacking distance between aromatic sheets.

Finally, DBSA NEs were used as carriers for delivery and controlled release of DBSA for enhanced displacement of asphaltene on the sandstone rock surface. It showed that comparing to DBSA injection alone, the cumulative asphaltene recovery efficiency was increased by 16.4%. A combination of three possible mechanisms, including slow release kinetic, electrokinetics repulsive expansion, and interfacial and wettability properties were discussed to illustrate the mechanism of the enhanced asphaltene displacement.

Keywords: Delivery system, controlled release; asphaltene inhibitor, nanoemulsions, asphaltene precipitation and stability, enhanced oil recovery

Table of Contents

List of Figures

List of Tables

List of Abbreviations

API	American Petroleum Institute
AI	Asphaltene Inhibitor
AOT	Aerosol-OT (surfactant)
Blank NEs	Blank Nanoemulsions
BTC	Breakthrough Curve
C_{Au}	The Number of Carbons Per Aromatic Structural
CMC	Critical Micelle Concentration
COR	Cumulative Oil Recovery
DAC	dodecylammonium chloride
DBSA	dodecylbenzene sulfonic acid
DBSA NEs	Nanoemulsion Loaded with DBSA
dm	the distance between two aromatic sheets
$d\gamma$	Distance Between the Two Aliphatic Chains or Saturated Rings
DLS	Dynamic Light Scatting
E_{COR}	Cumulative Oil Recovery Efficiency
$EAAR$	Advanced Asphaltene Recovery Efficiency
EDX	Energy-dispersive X-ray spectroscopy
EOR	Enhanced Oil Recovery
FTIR	Fourier-transform infrared spectroscopy
HLB	hydrophilic-lipophilic balance
f_a	Aromaticity of Asphaltene
IFT	Interfacial Tension (N/m)
La	The Size of the Aromatic Sheets

Lc	Cluster Diameter
Me	The Average Number of Aromatic Sheets
N	the molar ratio of CH_2/CH_3
NEs	Nanoemulsions
Phe NEs	Nanoemulsion Loaded with Phenanthrene
OOIP	Original Oil in Place
R	The molar ratio of aromatic rings to aliphatic side chains
Ra	The Average Number of Aromatic Rings in Each Aromatic Sheet
R_{AI}	the reduction amount of asphaltene inhibitor
R_{TC}	the reduction of total chemicals used
PV	Pore Volume
SDS	Sodium Dodecyl Sulphate
SEM	Scanning Electron Microscopes
SS	stainless-steel
TEM	Transmission Electron Microscope
UV-Vis	Ultraviolet–visible
G’	Storage Modulus (Pa)
G’’	Loss Modulus (Pa)
tanδ	Damping factor

Publications and Conferences

- Alhreez, M. and Wen, D., 2018. Controlled releases of asphaltene inhibitors by nanoemulsions. *Fuel*, *234*, pp.538-548.
- Alhreez, M., Xin Xiao, and Wen, D., 2019. Kinetic Study of Controlled Asphaltene Inhibitor Release from Nanoemulsions. *Langmuir*, **In press**.
- Alhreez, M. and Wen, D., 2019. Molecular structure characterization of asphaltene in the presence of inhibitors with nanoemulsions. *RSC Advances, 9, pp.19560-19570.*
- Alhreez, M., Hu Z., and Wen, D., 2019. Delivery and controlled release of inhibitor: A prospective method for enhanced oilfield asphaltene prevention, *Fuel*, **In progress**.
- Alhreez, M. and Wen, D., 2018. Nanoemulsion: Stabilization, characterization, and evaluation for asphaltene removal application, **In Preparation**.
- Alhreez, M., Wen, D. and Ali, L., 2017, April. A novel inhibitor for controlling Iraqi asphaltene problems. In *2017 International Conference on Environmental Impacts of the Oil and Gas Industries: Kurdistan Region of Iraq as a Case Study (EIOGI)* (pp. 37-41). IEEE.
- **Oral presentation conference,** Effect of Polymeric Inhibitor on Asphaltene Precipitation, 3rd World Congress on Oil, Gas and Petrochemistry, 23-25 August 2017, Spain, Barcelona,
- **Oral presentation conference,** Evaluation of the Asphaltene Inhibitors Effect on Asphaltene Aggregation and Precipitation, 2nd International Conference on Petrochemistry, 25-27 April 2018, Rome, Italy

Chapter 1

Introduction

In this chapter, we introduce the background of asphaltene and describe the scope of this dissertation and the main objectives pursued and achieved in this research. In addition, we introduce the structure and the different chapters of the dissertation in the following sections.

1.1. Description of the problem

Petroleum is a fundamental source of energy for the whole world and will probably remain so for many decades in the future. Due to the global decline of conventional oil supply, oil industries and governments are investing in unconventional oil sources such as heavy oils and bitumen to supply the increasing demand for fuels. Nowadays, the hydrocarbon industry is a large part of the global economy, as well as it is the main source of energy, so there is a great interest in the optimization of processes and solution of problems of the oil industry [1]. Asphaltene fractions in oil contribute to various problems that are present in such segments of the oil industry as mining, transportation, storage and refining [2]. This is aggravated if being considered that the deposits of lighter hydrocarbons are being depleted and the vast reserves of heavy hydrocarbons become major sources of extraction of these precious materials [3,4].

Asphaltene can be defined as a poly-disperse distribution of the heaviest and most polarizable fraction of the crude oil that is insoluble in low-molecular-weight alkanes, such as n-pentane and n-heptane, but completely soluble in aromatic hydrocarbons, such

as benzene and toluene [5,6]. The asphaltene fraction is formed of associated systems of polynuclear aromatics bearing alkyl side chains, organic molecules containing oxygen, nitrogen, and sulfur as well as vanadium and nickel porphyrins which are also present in asphaltenes [7]. Asphaltene is usually responsible for many flow assurance problems like wettability changes and pore clogging in reservoir rocks and fouling in wellbore tubing and production surface facilities [8].

During brine injection into an oil reservoir, asphaltenes, present in the crude oil, may precipitate, aggregate to flocs and subsequently leading to possible deposition. Precipitated asphaltenes can deposit on the rock surfaces; thus leading to a reduction in the porosity and permeability and eventual blocking of the rock reservoir pores, which is the major focuse in this study. In addition, asphaltene precipitation and deposition may occur in production wells in the pipelines thus giving rise to flow assurance problems. Asphaltene instability in the crude oil which causes the precipitation of asphaltene is a major contributor to fouling. The delayed coking process is a favoured technology for upgrading the heavy fractions of bitumen but fouling in furnace tubes that preheat the feed results in significant cost penalties due to increased fuel consumption, and time for shut-down that is often required for cleaning. Asphaltene instability begins with the onset of insolubility, followed by the formation of colloidal scale particles, which aggregate and ultimately sediment out of solution. Asphaltene aggregation is attributed to intermolecular attractive interactions arising from charges on the rings as a result of the presence of dissociated ions, along with acid and basic functional groups, containing heteroatoms (N, S, and O). Nitrogen is mainly contained within the rings, in either pyrrolic structures (acidic) or pyridinic structures (basic). Sulfur is present in thiophenic structures, while oxygen appears in hydroxyl, carbonyl, and carboxylic groups [9]. Thereby, the dissociation of charged ions must cause opposite surface charges on

asphaltenes. Basic functional groups (e.g., pyridinic groups) should generate negative charges in nonpolar medium, whereas hydroxyl groups in carboxylic acids, alcohols, and phenols, as well as mercapto groups (associated with mercaptans) and organic sulphides, would produce positive charges [5]. The time required for asphaltenes to fully separate can be increased by varying solvent compositions, indicating that the delay of instability is possible [10].

1.2. Asphaltene dependent phenomena

In general, precipitation, flocculation, a flow of suspended particles, deposition and adsorption are instances of asphaltene-dependent phenomena which may work individually or simultaneously and result in significant changes in the fluid flow behaviour. Figure 1-1 illustrates a sequence of processes and their effects which might take place in a typical rock-fluid system due to the presence of asphaltene particles. A description for each of the mechanisms is presented afterwards.

1.2.1. Asphaltene aggregation

The mechanisms of the aggregation behaviour of asphaltenes are not completely understood yet and are generally believed to attribute to π-π interactions, acid-base interactions and hydrogen bonding between asphaltene molecules. Due to the amphiphilic nature of the asphaltenes, asphaltenes can form micelle-like aggregates similar to surfactants. The modified Yen model shows that the asphaltene nanoaggregate is around 2 nm in size and composed of about six asphaltene molecules stacked through the aromatic sheets [8,11]. The aggregation of asphaltenes can be affected by many factors such as the source of asphaltenes, concentrations, solvent conditions, temperature, pressure and in the presence of resin. Concentrations above 50-100 mg/L are believed for asphaltenes forming nanoaggregates [12-14]. The amount of the aggregation was found to increase as the solubility parameter of the solvent decreased [15]. As stated above, asphaltene nanoaggregates can further aggregate to

clusters which are believed to be the precursors of the asphaltene flocculates leading to the asphaltenes precipitation.

1.2.2. Asphaltene precipitation

Precipitation can be defined as a separation of asphaltene particles from a liquid phase that leads to the formation of a new solid phase. Precipitation occurs due to a change in thermodynamic conditions, i.e., pressure, temperature, and composition. Pressure reduction during primary recovery may cause precipitation of asphaltene. It usually starts at a pressure above the bubble point known as onset point. As pressure is reduced from the onset point toward the bubble point pressure, more asphaltene precipitates. The bubble point exhibits the highest amount of precipitation but any more pressure drop below the bubble point will reversely affect precipitation; i.e., precipitated asphaltene returns to the oil phase and the number of precipitated particle decreases [16,17]. At pressures below the bubble point, light components leave crude oil and the heavier components in the remaining mixture increase the solvency of the crude oil for asphaltene and cause it to re-dissolve into the crude oil.

However, there is still no unified observation for the effect of temperature on asphaltene precipitation and investigators have reported opposite trends for precipitation due to a temperature change [18,19].

Various injection scenarios such as CO_2 injection, recycled gas injection, solvent injection, gas-lift operations, and acidizing may destabilize the asphaltene in the oil phase and make it precipitate. This can be described as the negative effects of the incompatible injected fluid on the solubility of asphaltene [20].

1.2.3. Asphaltene flocculation

Flocculation is the intermediate stage between precipitation and deposition of asphaltene. Due to polar-polar interaction between asphaltene molecules, they may aggregate and form larger molecules. Therefore, it is very probable that deposition takes place when large flocculated particles are entrapped in porous media during flow of the oil phase [21].

1.2.4. Asphaltene deposition

Deposition of asphaltene involves the porous medium; i.e., rock properties also contribute to quality and extent of deposition. A very tortuous path due to complex rock structure, low porosity and permeability, the presence of impurities and clay in the rock structure play roles in deposition mechanisms. In general, surface precipitation, pore throat plugging, and re-entrainment are classified as different mechanisms of asphaltene deposition in porous media [22]. Surface precipitation refers to the settlement of asphaltene particles on a rock surface that might finish with gradual blocking of the pore space. Pore throat plugging occurs when flocculated asphaltene particles are larger than pore throat and plug the pathway which leads to permeability reduction. Re-entrainment may take place when shear stress is developed due to the excessive pressure drop at the location of deposited asphaltene. It might remove the deposited asphaltene and improve the permeability again.

1.2.4.1 Asphaltene adsorption

Asphaltene adsorption is the adherence of asphaltene particles on the pore surface due to interactions between the rock surface and asphaltene. It can be considered as an interfacial phenomenon in which asphaltene contributes to modification of rock-fluid properties.

Adsorption changes the nature of the surface interactions between the rock surface and the neighboring fluids and can cause considerable modifications in flow characteristics and recovery factor. It may occur before and after the asphaltene precipitation and causes modifications in surface structure and its interaction with the neighbouring fluids. Adsorption may alter rock-fluid properties, for instance, interfacial tension (IFT), contact angle (CA), wettability and relative permeability, and it affects the end-point saturations as well as recovery. Wettability controls flow properties and it is an essential concept in defining the distribution of fluids in a reservoir. It is as important as permeability and viscosity in determining the production and recovery from a petroleum-bearing formation. Therefore, asphaltene adsorption may affect multiphase flow in porous media and change the efficiency of displacement processes such as water flooding.

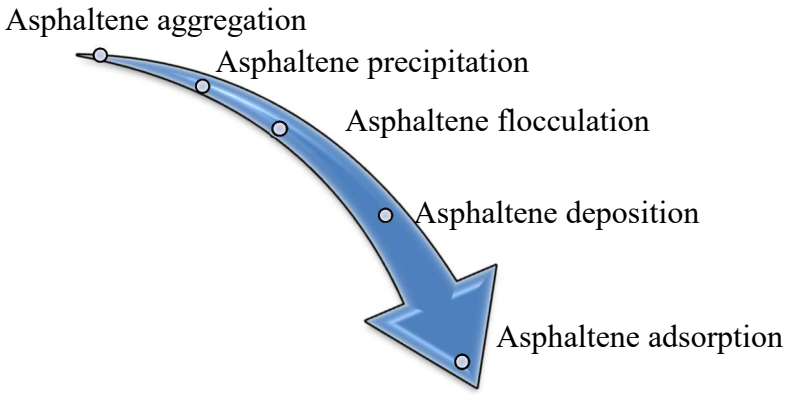

Figure 1-1. Asphaltene Dependent Processes

1.3. Delivery and controlled release systems

The delivery system is a broad field and allows for the formulation of drugs in a variety of different forms. Controlled (particularly extended) -release systems are designed to enhance drug therapy. There are several motivations for developing controlled-release systems: i) to enable superior control of drug exposure over time, ii) to assist drugs in crossing physiological barriers, and iii) to deliver drugs to the desired site of action while minimizing drug exposure elsewhere in the body. Finally, iv) use of controlled release technology may reduce the variability of performance of drug products [23].

The delivery system needs urgently carriers, vehicles, and protective systems to improve the drug performance. The search for such vehicles is the aim of many recent studies, a search that has become increasingly urgent. One important trend to mention is the nanotechnology that can help the drugs that are added to the body to become more efficient; i.e. healthier and safer. Nano-vehicles seem to be excellent candidates as solubilization carriers for insoluble active compounds. There is a growing interest in using NEs as vehicles for nutraceuticals and pharmaceutical formulations due to their physicochemical properties, such as spontaneous formation, clear appearance, low viscosity, thermodynamic stability, and high solubilisation capacity. According to the drug delivery systems, the hydrophobic drug inside NE systems remains in solution throughout its transit across the body and the dissolution step, which is the rate limiting step in the absorption of such drugs, can be bypassed. In addition, NE systems promote drug solubilization and drug release at the absorption site providing more consistent absorption of the hydrophobic drug and hence better bioavailability [24].

The mechanisms used to achieve these goals are diverse and complex and depend on the particular application. In fact, several mechanisms may operate simultaneously or at

different stages of a delivery process. An understanding of these mechanisms is important when designing and manufacturing controlled release systems, and in identifying potential failure modes [25].

In the oil and gas industries, a technology by which a substance can be delivered downhole and applied in a timely manner without causing any adverse effect has many advantages. Ideally, the system can be employed at any stage of stimulation or completion without involving additional tools or pumping time. If achieved, the scope is enormous with a multitude of applications. This will allow any chemicals, for example, viscosity modifiers, tracers, surface or pH modifiers, diverters or water shut-off gels, to be transported and placed in the well where needed and will be used as needed by delayed release or timely activation. The controlled release mechanism will also help to extend the effective treatment life of an inhibition process to prevent damage from scales, corrosions, salts or organic deposits, such as paraffin or asphaltene, for a long period of time [26].

The characteristics of this emerging nanotechnology that attract interest for oilfield applications include the resistance of NEs to sedimentation and creaming, which should translate to no separation in storage tanks or during transport through chemical feed lines, etc. Also, the droplet size is small with the comparison to the pore throats in gravel packs and in reservoir matrix rock, meaning that good injectivity and penetration without filtration should be possible [27]. As a two-phase system, they should be well-suited to carrying oil and water-soluble additives within the same fluid matrix, reducing the need for separate storage tanks and multiple delivery lines. Finally, a NE that is stable over time must, by definition, be resistant to coalescence and the exchange of the dispersed phase between droplets [28]. In this sense, they can be likened to a dispersion of nano-

meter-sized spherical containers and are potentially capable of carrying incompatible reagents without their coming into contact [29].

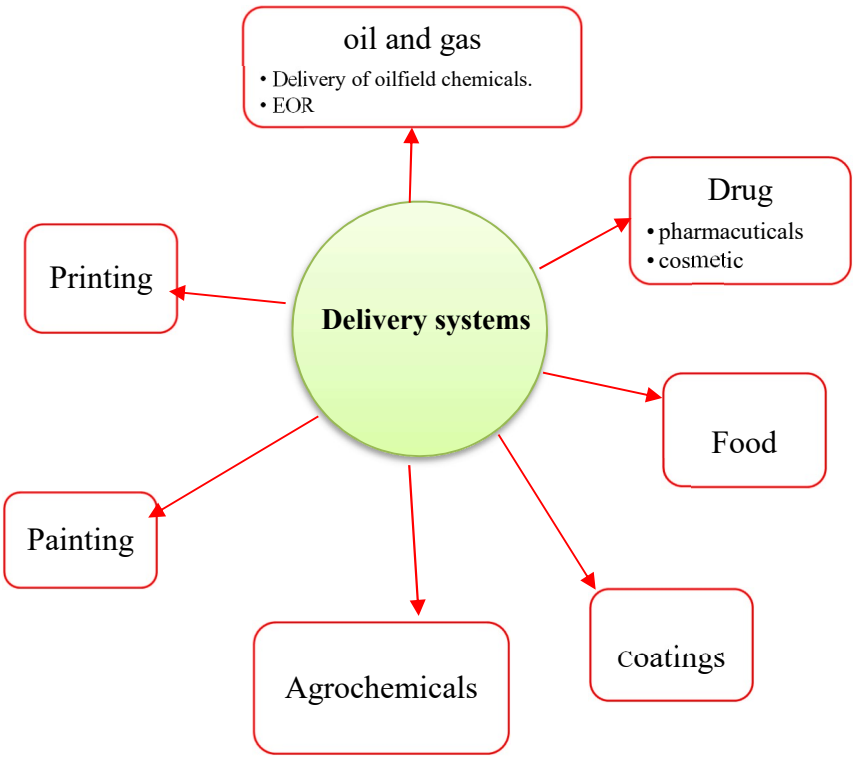

Figure 1-2. Diagram showing some of the many industrial applications of delivery systems.

1.4. Thesis outline

Borrowing the concept of controlled delivery from the nanomedicine field, this work proposes and validate a novel concept of using NE to deliver and controlled release of AI in a bulk fluid or flowing through a porous medium. The novel concept encapsulates and controls the release of AIs by using NEs, which could i) improve the stability of the asphaltene, ii) reduce the usage of inhibitors, and iii) extend the treatment time via the slow release of inhibitors.

The thesis includes 7 chapters, as shown in Figure 1-3.

Chapter One introduces the description of the asphaltene problem in the oil and gas industries. Asphaltene instability phenomena are briefly discussed. The concept of delivery and controlled release system and the objective of the work and thesis structure are presented.

Chapter Two conducts a literature review of asphaltene instability processes and the proposed mechanisms. A comprehensive review of the main current strategies for asphaltene removal is conducted. Controlled delivery in oil and gas applications are illustrated in this chapter.

Chapter Three studies the preparation and stabilisation of oil-in-water NEs for extended time. This chapter also explores a novel method by using inhibitors (as a new class of ripening inhibitor) inside NEs to reduce Ostwald ripening. Two types of analysis, including dynamic and static studies, were utilized to further evaluate and confirm the physical stability of NEs. A parametric study of the effect preparation variables on the size and size distribution and physicochemical properties of NEs is conducted to optimize the process parameters.

Chapter four proposes a novel concept to encapsulate and control the release of AIs by using NEs. A conventional inhibitor (dodecylbenzene sulfonic acid (DBSA)) is used as model inhibitor. The effects of asphaltene stability and controlled release effect via NEs are examined by the centrifugal method in three case studies, i) with DBSA, ii) with blank NEs, and iii) with NE loaded with DBSA (i.e. DBSA NE).

Chapter Five conducts a detailed release kinetic study by employing an optical technique to monitor the release profile. Three case studies are performed on the stability of

asphaltenes: i) strong organic acids (dodecylbenzene sulfonic acid (DBSA)), ii) blank NEs, and iii) DBSA NEs. Those important physical parameters, such as the AI release rate and time, are obtained. Not only providing new evidence to support our previous concept, but the data is also proceeded and compared with eight established mathematical models, to elucidate the release mechanism.

Chapter Six examines the asphaltene stability and molecular modification structure by X-ray diffraction in three case studies, i) with DBSA, ii) with blank NEs, and iii) DBSA NE. To validate the intermolecular interaction between asphaltene and DBSA NEs and allow quantitative comparison, FTIR spectroscopy is used, and the refractory nature of asphaltene after addition of DBSA NEs is investigated. The thermal stability is performed by a thermogravimetric analyser.

Chapter Seven investigates the kinetic adsorption mechanism and the level of asphaltene adsorption through a core sample of crushed sandstone grains under dynamic condition. This chapter also proposes and validates the concept of using NEs as carriers for delivery and controlled release of DBSA and a blend of surfactants mixtures at the optimum salinity to enhance the displacement of adsorbed and trapped asphaltene on the sandstone rock surface. A combination of three possible mechanisms is discussed to illustrate the mechanism of the enhanced asphaltene displacement.

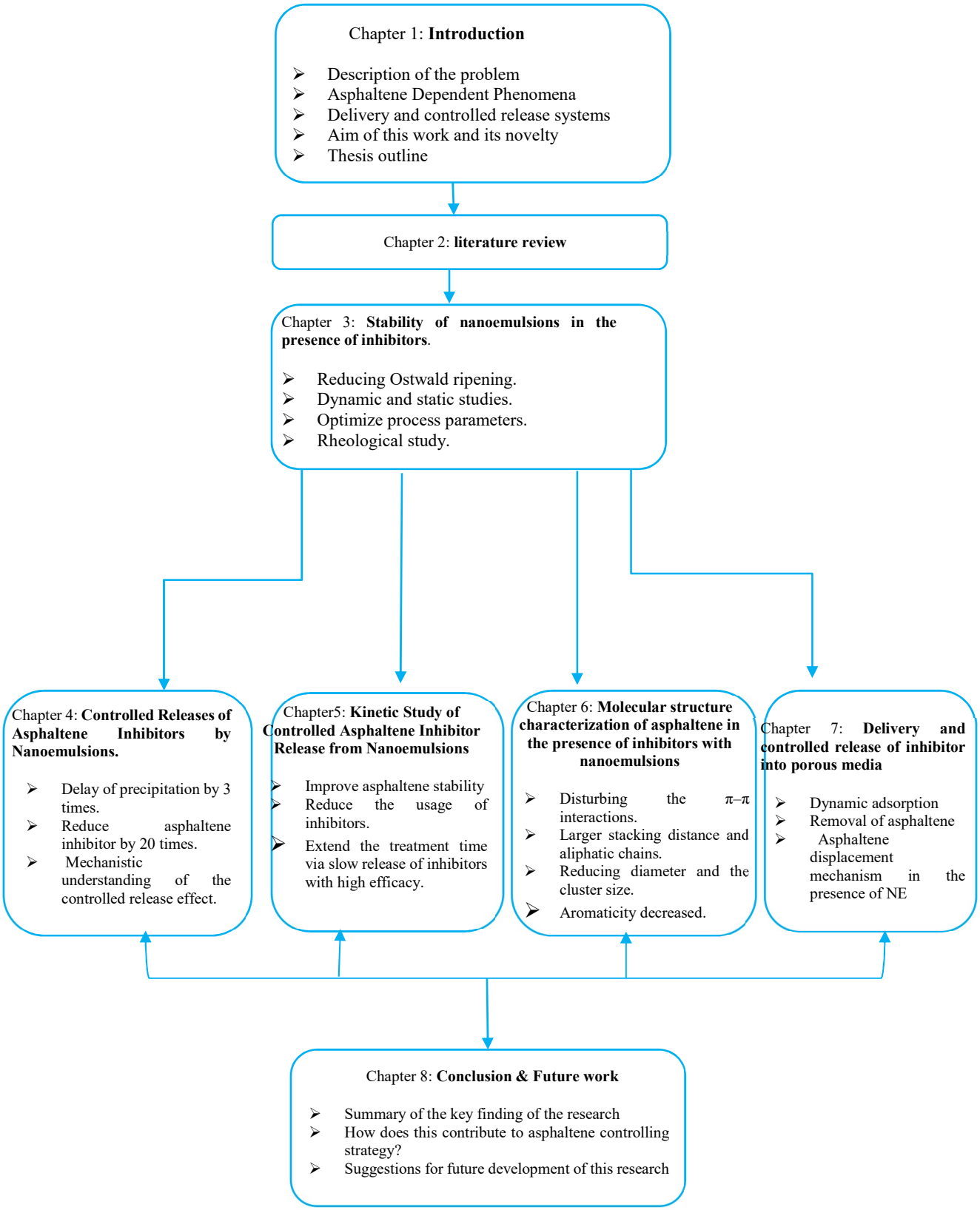

Figure 1-3. The layout of the thesis.

Chapter 2

Literature review

This chapter presents a summary of the background and detailed review of the state-of-art work on asphaltene characterisation associated with bulk/surface properties, main strategies for asphaltene removal, controlled delivery systems in oil and gas industries, NEs characterisation and stabilisation, and established the novelty of the proposed work

2.2. Asphaltene bulk properties

2.2.1. Molecular structure of asphaltene and aggregation mechanism

The mechanisms of the aggregation behaviour of asphaltenes are not completely understood yet and are generally believed to attribute to π-π interactions, acid-base interactions and hydrogen bonding between asphaltene molecules. Different models are used to describe the aggregation behaviours of asphaltenes. Colloids and micelles are two commonly used terms to describe the self-association behaviours of asphaltenes. The modified Yen model (also known as Yen-Mullins model) well described the colloidal-like properties of asphaltenes in the solvents [8,11]. Due to the amphiphilic nature of the asphaltenes, asphaltenes can form micelle-like aggregates similar to surfactants as a distribution of nanoaggregates. These nanoaggregates self-assemble in a stepwise fashion that depends on the concentration [8, 30−32], solvent [33,34], the presence of resins [35], pressure, and temperature [8, 36−38]. These nanoaggregates can further associate into clusters that are the precursors of asphaltene precipitation [15].

A variety of molecular interactions contributing to the aggregation of asphaltene molecules and to the formation of colloidal particles in crude oil include hydrogen bond

forces, aromatic π-π stacking forces [39,40], polarity induction forces [41], and electrostatic attractions between the molecules [42,43]. It is believed that the π–π interaction process between two asphaltene molecules generally involves two steps. First, the dispersion force plays a dominant role to bring the two monomers together. Then, with the two monomers approaching each other, Pauli repulsion will be produced and prevent them from getting closer [44]. Once the equilibrium distance is reached, electrostatic interaction, Pauli repulsion, dispersion, and intermolecular interaction will work together [45].

One of the best representations of the asphaltene micelle is that reported by Yen 1974. He suggests molecular weights of 1- 5×10^3, a molecular formula of approximately $(C_{79}H_{92}N_2S_2O)_3$ and molecular shape as in Figure 2-1. This structure would be formed by several flat, stacked condensed rings. Five of these rings, each containing from 8 to 16 condensed rings could be placed at distances of 0.30 - 0.37 nm, and connected by systems of sulphide, ether, aliphatic chain and/or naphthene ring linkages. The condensed sheets may contain O, S and N atoms which may act as free radicals for anchor points of bound metals like Ni, V, Mo or Fe. The whole asphaltene complex would be 0.8 – 1.6 nm in diameter and 1.6 – 2 nm in height. More complete overviews about asphaltene aggregate behaviour have been recently published by Mullins et al., which show nanoaggregates to be about 2 nm in size, while clusters of nanoaggregates are around 5 nm [46,47]. Figure 2-2 shows the stepwise aggregation of asphaltenes described by the Yen−Mullins model. Table 2-1 lists previously unresolved issues, often involving estimates spanning orders of magnitude, which had long plagued the field of asphaltene science. Fortunately, the past decade has seen huge advances in the molecular and colloidal structure of asphaltenes. However, a complete molecular analysis of asphaltene and a systematic understanding of

how asphaltene molecular structure changes with addition inhibitors have not yet been achieved.

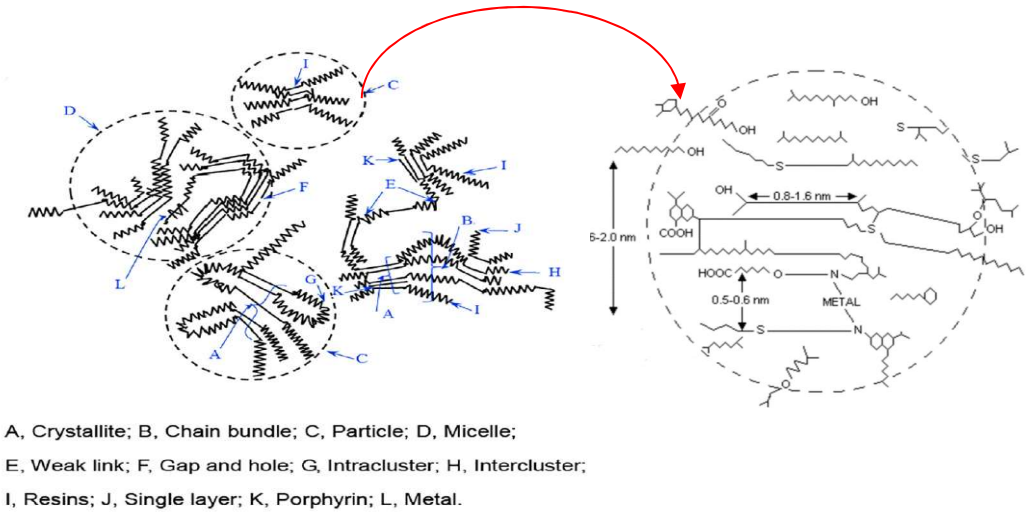

Figure 2-1: The molecular structure of asphaltene, Zig-zag lines represent saturated sheets or naphthenic rings; the straight lines represent the edge of flat sheets of condensed aromatic rings. Figure is taken from [48].

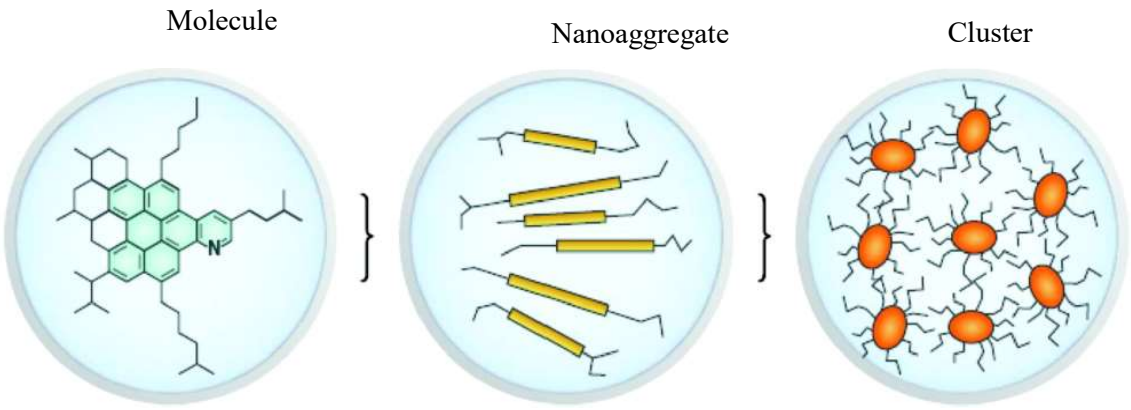

Figure 2-2. Yen−Mullins model. A typical asphaltene molecule with a polyaromatic core is shown at the left, which can then associate into nanoaggregates that contain less than 10 asphaltene molecules, shown in the middle. Groups of nanoaggregates (<10) can further associate to form clusters of nanoaggregates. The Figure is taken from [8,11,46,47].

Table 2-1: Issues in asphaltene science that have been resolved over the past 20 years.

Scientific issue	The range of reported values (as of ~1998)	Values (as of 2018)
Asphaltene molecular weight	Less than 1,000 Da to 1,000,000,000 Da [48]	750 Da [14]
Number of polycyclic aromatic hydrocarbons PAHs in an asphaltene molecule	1 to 20	1 dominates
Number of fused rings per PAH in asphaltene	2 to 20	7
Number of PAH stacks in asphaltene nanoaggregate	Unknown	1
Aggregation number of nanoaggregates	10–100 [48]	<10 [5]
Critical nanoaggregate concentration of asphaltenes	50 mg liter^{-1} to 5 g liter^{-1}[13]	100 mg litre^{-1} [14]
The concentration of cluster formation	Unknown	~3 g litre^{-1}[14]
Size of cluster	Unknown	5 nm for small clusters [45,46]
Role of resins in asphaltene Nanoaggregate.	None to necessary	~15% of crude oil nanoaggregates are resins; resins are not surfactants [7].
Relation of nanoaggregate to cluster	Unknown	Clusters consist of Nanoaggregates [8,11]
Relation of nanoaggregates in toluene to those in crude oil	Unknown	Very similar in size and composition [8,11]

2.2.2. Asphaltene precipitation and deposition mechanism

The main components of the crude oil can be divided into saturates, aromatics, resins, and asphaltenes. At normal conditions, these components are all homogenized in solution to form the crude oil. Saturates and aromatics are nonpolar compounds, while asphaltenes are considered polar compounds since they contain heteroatoms such as nitrogen, sulfur, or oxygen. For these components to be held together, a bridging agent must be present. Resins contain both polar and nonpolar sites which make them act as a good bridging agent which holds all the crude oil components together [49]. Once any change in equilibrium conditions occurs, the forces holding these components together become

severed, and thus the asphaltene, which is the solid component in the solution, begins to precipitate. Changes in equilibrium conditions may include a change in pressure, temperature, and the addition of a solvent such as CO_2, n-heptane, and n-hexane [50]. Following asphaltene precipitation, if the conditions are suitable, asphaltene will begin to form flocculations [51]. These flocculations have a high density and will thus begin to deposit in the pores of the reservoirs. The excessive deposition will result in asphaltene buildups, and eventually, pore plugging [52]. Figure 2-3 shows the main components of crude oil and the bond severance resulting in asphaltene precipitation.

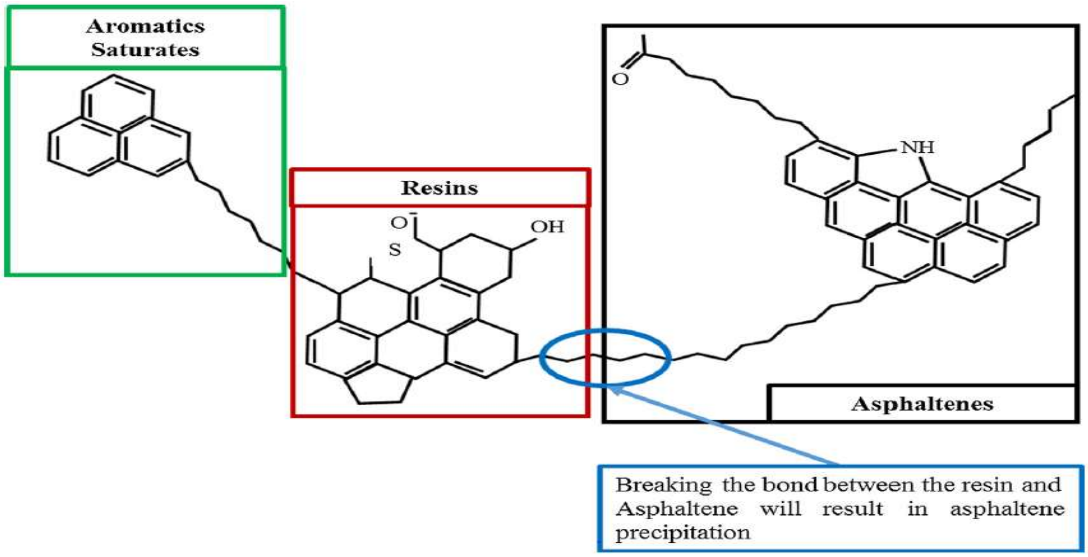

Figure 2-3. Main components of crude oil and asphaltene precipitation. Figure is taken from [53].

2.3. Asphaltene surface properties

2.3.1. Dynamic asphaltene adsorption studies

The flow and distribution of fluids in porous media are largely controlled by fluid-fluid and rock-fluid interactions [54]. Asphaltene intramolecular forces are important when considering asphaltene- asphaltene and ultimately asphaltene–surface interactions that

can facilitate asphaltene - surface adsorption [55]. Therefore, the wettability of rock may be changed to less water wet or more oil-wet. Wettability is a crucial parameter that determines the location and distribution of fluids in a reservoir. The change in wettability will affect the multi-phase flow behaviour in a porous medium when two or more immiscible fluids are flowing in the porous medium. Accordingly, rock-fluid properties such as interfacial tension, relative permeability, and capillary pressure are expected to change because of asphaltene adsorption [56].

There is a large body of literature that deals with the adsorption of asphaltenes on various rock minerals, including clays [58]. Most of these works are concerned with the measurement and modeling of adsorption isotherms on crushed minerals under static conditions [58-65]. Very little work currently exists on the adsorption kinetics of asphaltenes under flow conditions [54]. Piro et al. [66] used a sand pack of crushed dolomite and asphaltene-in-toluene solution to investigate their dynamic adsorption under different flow rates. The authors found that the amounts of adsorbed asphaltenes are rate-dependent. The continuous adsorption with time observed in their study is possibly due to uncertainties in the estimation of initial concentrations.

Toth et al., [67] filled the glass column by 15 gr of adsorbent, an asphaltene solution of 0.5 g/L concentration was continuously added to the top of glass and samples were collected from the effluent at the bottom of the column. The collected samples were analyzed by Uv-vis spectrophotometry at 600 nm to determine the concentration of effluent flow. However, most of the static adsorption tests report Langmuir type one (monolayer) adsorption, and they observed multi-layer adsorption during the dynamic flow of asphaltene solution made from dissolving extracted asphaltene in nitrobenzene. Therefore, they concluded that dynamic asphaltene adsorption is continuous that ends up

with a composite layer of asphaltene on the rock surface and wettability alternation depends on the amount of asphaltene that has settled on the solid surface.

The literature also suffers from insufficient or even non-existing investigations on dynamic adsorption of asphaltene and consequent effects on properties of a porous medium, immiscible displacement, and recovery factor. Despite numerous studies on precipitation and deposition of asphaltene in porous media, there is still no general and consistent idea about many features of the adsorption process, its involved mechanisms and effective parameters.

Summarily, above all, a better understanding of rock-asphaltenes interactions will promote commercial development of asphaltene adsorption more quickly.

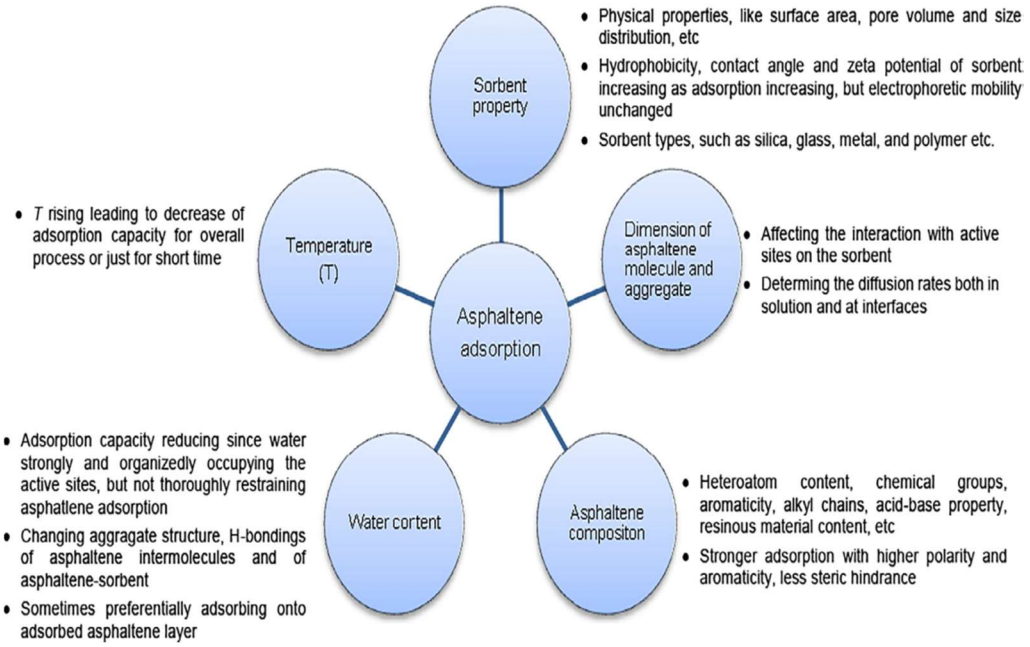

Figure 2-4. The main factors of asphaltene adsorption.

2.4. Main current strategies for asphaltene removal

As was mentioned in the previous chapter, asphaltene aggregation and subsequent precipitation/deposition cause many problems during oil production. Our focus will be on the current methods to fight these problems through the removal and the prevention of asphaltene deposition in the reservoir. There are two strategies for solving problems related to asphaltenes: their conservation and rejection.

1) The conservation of asphaltenes is based on asphaltene being kept in crude oil but decreasing the viscosity of the medium by distinct methods. Some applied techniques are as follows: the addition of organic solvents [71] and precipitation inhibitors [72]. In case of precipitation inhibitors, great knowledge of the chemical nature of the crude is required [73]; however, the addition of organic solvents is usually very expensive due to a large amount of solvent needed to achieve the required viscosity.
2) The rejection of asphaltene consists of the asphaltene removal from the medium to be used in other processes. Sometimes, solvent deasphalting [74], ultrafiltration and selective adsorption [75] are used. Application of solvent deasphalting is usually lesser practical than the other two techniques and more expensive due to use of paraffinic and naphthenic solvents, although this technique may be combined with extraction emulsion thus reducing the amount of these solvents [76]. Meanwhile, ultrafiltration has the disadvantage that the membranes easily become dirty and saturated with asphaltene agglomerates [77]. Selective adsorption is a practical strategy for removal of asphaltenes in reservoir and refineries [78]. During this process, the asphaltenes can be adsorbed and then desorbed to regenerate the adsorbent and, in some instances, they can function as catalysts [79]. Among the most investigated adsorbents for remediation of

asphaltenes, some minerals as montmorillonite, metal substrates, nanoparticles [80] and metal oxide composites, among others, are used. However, there are several factors affecting the adsorption capacity of the materials, such as the nature of asphaltenes, their concentration in the medium, temperature, pH, presence of metals, etc.

The advantages of the first method (i.e., inhibitors) are that it is usually more practical: it is not necessary to know the exact composition of the raw material and crude oil does not require further treatment. Asphaltene inhibitors (AIs) are designed to interact with asphaltene to inhibit precipitation, aggregation, and deposition, and ensure enhanced flow. Even though this approach is widely used in oilfields, it has a major problem due to the loss of a large amount of chemicals inside the reservoir, resulting in high treatment cost. [81]. For instance, the cost of chemical additive injection in Middle Eastern fields is in the range of USD $ 31,000 ~$ 46,000 per well per year [82]. In a study investigating the chemical amount required for controlling asphaltene precipitation, Subramanian et al. [83] reported that at the addition of 5 wt. % of DBSA, the asphaltene precipitation could be completely controlled. Similarly, Ortega et al. [84], suggested that the attachment of DBSA to asphaltene molecules with 3 wt. % DBSA could noticeably improve the rheological properties of bitumen. Hashmi et al. [85] studied the capability of commonly available surfactant aerosol-OT (AOT) to stabilize asphaltene suspensions in heptane. Regardless of the amount of AOT, however, the sedimentation behaviour of asphaltene was similar to that of in the absence of surfactant. Even with 20 wt. % of AOT in solution, samples collapsed within the first hour after the preparation, which indicated that it was not effective in stabilizing asphaltenes. Moreover, aromatic solvents like toluene dissolve asphaltenes, but only at very high concentrations, i.e., nearly 50% by weight [81].

2.5. Intermolecular interaction between asphaltenes and inhibitors.

The dispersing ability and changes of mean radius and polydispersity would be helpful to understand the interaction between inhibitors and asphaltene particles. The most common inhibitor/dispersant for asphaltene stabilization is DBSA, which is cheap and has been used commercially with some success in the field [86].

Wang et al, [87] investigated the effect of two typical ionic inhibitors, dodecyl benzene sulfonic acid (DBSA) and dodecyl trimethyl ammonium bromide (DTAB) on Karamay asphaltenes and Lungu asphaltenes. DBSA has good ability to stabilize Lungu asphaltenes but has no effect on Karamay asphaltenes. Differently, DTAB has good ability to disperse Karamay asphaltenes but has no obvious effect on Lungu asphaltenes. They concluded that the electric property of asphaltenes plays an important role in the interaction between asphaltenes and inhibitors. The negatively charged asphaltenes tend to be dispersed by cationic inhibitors, whereas the positively charged asphaltenes tend to be dispersed by anionic inhibitors.

Several research groups examined the properties of a number of monomeric additives. They found that increasing the polarity on the headgroup gave better asphaltene stabilization through stronger acid-base interactions. DBSA was also shown by Fourier transform infrared (FTIR) spectroscopy to interact via hydrogen bonds with asphaltenes. Besides acid-base interactions, this group also proposed that the sulfonic acid group could donate its proton to C=C bonds in asphaltenes. The strong binding of DBSA to asphaltenes makes DBSA effective enough to stabilize asphaltenes sterically [88].

Ortega et al., [84] reported that the presence of sulfonic acid groups ($-SO_3H$) in the DBSA molecules is required for the surfactant to effectively interact with asphaltenes, as shown in Figure 2-5. The interaction between DBSA and asphaltenes in crude oils has been

extensively studied in the literature [84-90], evidence that the concentration of DBSA and the chemical and structural properties of asphaltenes are major controlling variables. As shown in Figure 2-6, the modification takes place through the protonation of heteroatomic components in the asphaltenes, which are positively charged, whereas proton-donor DBSA molecules become negatively charged ions. Hence, this process leads to an ion pair with strong ionic bonding, able to promote further electrostatic interactions with other ion pairs in neighbouring molecules/aggregates.

On the other hand, DBSA amphiphiles have a strong tendency to self-associate in nonpolar medium. This association takes place between the DBSA molecules, asphaltenes then flocculate and precipitate out if the amount of DBSA is too high. Although the interaction between asphaltenes and amphiphiles has not been exactly understood at the molecular level, the electric property of asphaltenes plays an important role in the process [91]. The mechanisms by which these inhibitors interact with asphaltenes can be summarized as follows:

- π–π interactions between asphaltenes and unsaturated or aromatic groups in AI.
- Acid-base interactions.
- Hydrogen bonding.
- Dipole-dipole interactions.
- Complexing of metal ions

A key feature with nearly all inhibitors seems to be one or more polar functional groups that interact with the asphaltene monomers or aggregates, plus one or more alkyl chains that cooperatively form a less polar steric stabilization layer of alkyl tails around the asphaltenes solubilizing them in the crude oil. The alkyl tails are compatible with the crude oil, which has aliphatic hydrocarbons as its major component. The details of some

inhibitors with the mechanisms of interaction with asphaltene are summarized in Table 2-2.

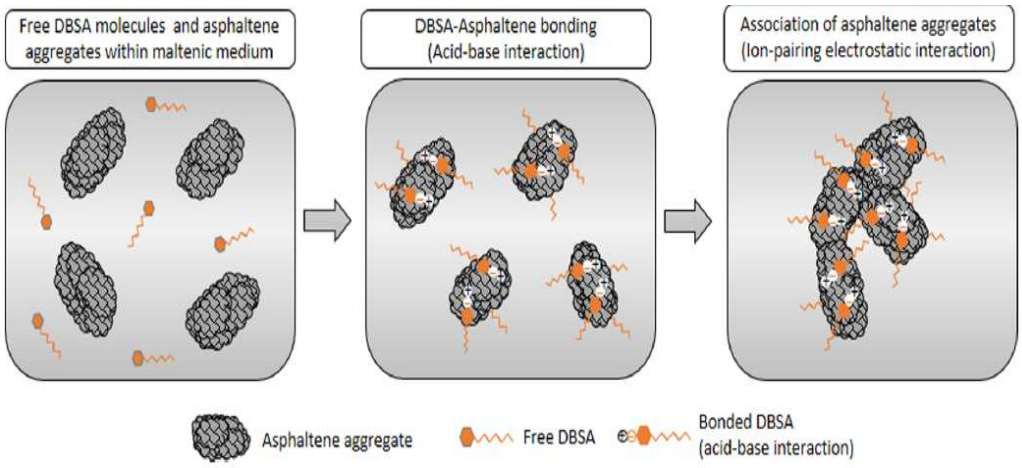

Figure 2-5. Development of the acid-base ion-pairing electrostatic interaction and association between different aggregates of DBSA−asphaltenes. Figure is taken from [84].

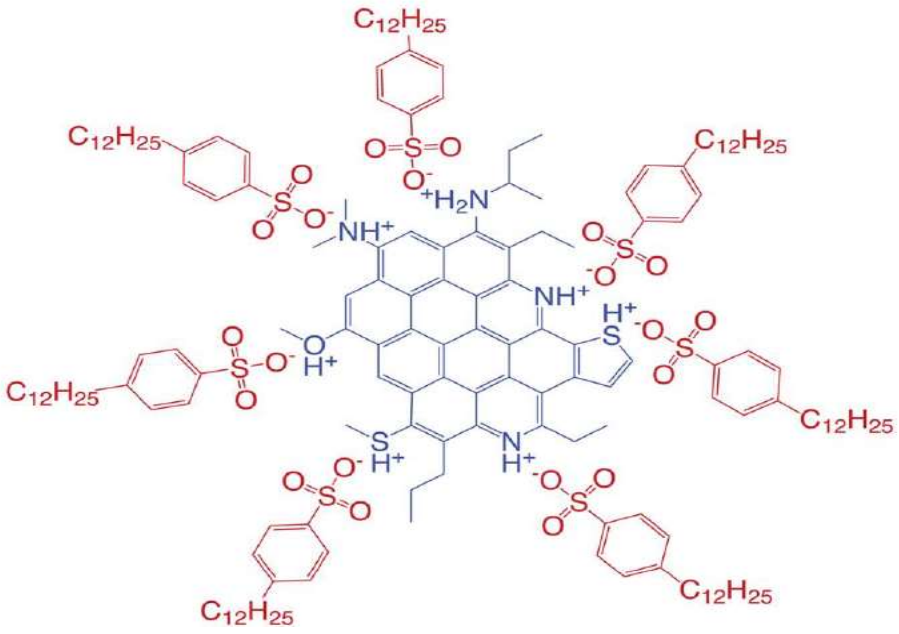

Figure 2-6. Proposed chemical mechanism for molecular assembly between asphaltene molecule with heteroatomic nitrogen protonated with DBSA, blue denotes asphaltene and red, DBSA. Figure is taken from [90].

Table 2-2. The details of some inhibitors with the mechanisms of interaction with asphaltene.

inhibitor	type	Class	Functional group	Interaction mechanism	Ref.
Hexadecylnaphthalene	Surfactant	Very low polarity alkylaromatics	hydroxyl group	π – π interaction	[91]
hexadecylnapthoxide	Surfactant	Very low polarity alkylaromatics	alkyl group	π – π interaction	[92]
N-methyl pyrrolidone (NMP)	Surfactant	Very low polarity alkylaromatics	hydroxyl group	π – π interaction	[93]
DBSA	Surfactant	Alkylaryl sulfonic acids	Sulfonic Acid, alkyl group	Acid-base interaction, π – π interaction	[94]
dodecyl resorcinol	Surfactant	Alkylaryl sulfonic acids	Sulfonic Acid	Acid-base interaction	[95–97]
dodecylphenol bis-ethoxylate hexylbenzoic acid	Surfactant	Alkylaryl sulfonic acids	benzoic acid	Acid-base interaction	[98]
hexylamine	Surfactant	alkyl amine	Amine, hydroxyl groups	Acid-base interaction	[99]
alkylphenylethoxylates blended with fatty acid diethanolamides	Surfactant	Fatty acid amides and their ethoxylates	phenyl, fatty acid, amide	Acid-base interaction, π – π interaction	[100]
Isooctyl acid phosphate blend with DBSA	Surfactant	Alkylaryl sulfonic acids	octyl acid, sulfonic Acid	Acid-base interaction, π – π interaction, ion-pair	[101]
nonylphenol–formaldehyde resins	resin	Alkylphenol-aldehyde resin	Phenol, alkyl group	π – π interaction, hydrogen bonding	[102]
blends of phosphoric esters with carboxylic acids	Surfactant	Ester carboxylic acids	Ester/carboxylic acid	π – π interaction, hydrogen bonding, acid-base interaction, ion-pair	[103]
decahydro-1-naphthalenepentanoic acid	Surfactant	carboxylic acid	carboxylic acid, hydroxyl groups	π – π interaction, hydrogen bonding, acid-base interaction	[104, 105]
sarcosinate	Surfactant	Sarcosinates	hydroxyl group, alkyl group	hydrogen bonding	[106]
Polyisobutylene succinimide	copolymer	Alkylsuccinimides	hydroxyl group, alkyl group	π – π interaction, hydrogen bonding	[107]
polyisobutylene succinic anhydride	graft copolymer	Alkylsuccinimides	hydroxyl, alkyl, imide groups	π – π interaction, hydrogen bonding	[108]
diethylenetriamine	Surfactant	Amide and Imide NonpolymericSurfactant	amide or imide groups	π – π interaction, hydrogen bonding	[109,110]
maleic anhydride and *N*-oleyl-diamino-1,3-propane 119	Surfactant	Amide and Imide Surfactant	amide or imide groups	π – π interaction, hydrogen bonding	[111]
N-stearyl methyl-1-diamino-1,3-propane	Surfactant	Amide and Imide Surfactant	amide or imide groups	π – π interaction, hydrogen bonding	[112]

NMP, *N*-ethyl pyrrolidone	Surfactant	Alkylpyrrolidones	Pyrrolidone	π – π interaction, hydrogen bonding	[131]
dodecylphenol (DDP)	Surfactant	Alkylphenols and Related	group mildly acidic phenolic	π-interacting aromatic ring and a polar hydrogen-bonding group	[114]
nonylphenolethoxylate (NPE)	Surfactant	Alkylphenols and Related	acidic phenolic	π-interacting aromatic ring and a polar hydrogen-bonding group	[115]
2-hydroxybutyric acid	Surfactant	Ion-Pair Surfactant	hydroxy group, carboxylic acid	Acid–base interactions, hydrogen bonding.	[116]
salicylic acid	Surfactant	Ion-Pair Surfactant	carboxylic acid	Acid–base interactions, Hydrogen bonding.	[117]
decaglycerol tetraoleate	Surfactant	Miscellaneous Surfactant	hydroxyl groups	π-interacting aromatic ring and a polar hydrogen-bonding group	[118]
nonylphenolic formaldehyde resin (NPR)	resin	alkylphenol–formaldehyde resin	polar anhydride groups	π – π interaction, hydrogen bonding	[119]
polycardanol	polymer	cardanol	Alkyl group, hydroxyl groups	π – π interaction, hydrogen bonding	[120]
ethoxylated triethylenetetraamine	Surfactant	oxyalkylated amines	alkyl groups, hydroxyl groups, amine	π–π interactions, hydrogen bonding	[121]
dodecylphenol–formaldehyde resin (DPR)	resin	alkylphenol–formaldehyde resin	phenolic hydroxy groups, polar anhydride groups	hydrogen bonding, π–π interactions were not considered	[122]
lauryl methacrylate/hydroxyethyl methacrylate copolymer	copolymer	lipophilic and hydrophilic monomer	alkyl groups, hydroxyl groups	hydrogen bonding	[123]
Poly(ethylene glycol) esters of maleic anhydride and α-octadecene copolymers	polymers	polyester anhydride	Polyesters, polyamides, anhydride groups	hydrogen bonding, π–π interactions	[124]
methyl methacrylate and hydroxymethylpyridines	polymer	pyridine	pyridine rings with polar ester groups	hydrogen bonding, π–π interactions	[125]
1-vinyl-4-alkyl-2-pyrrolidone polymers	polymer	polymeric amide	pyrrolidone group, carbonyl group	hydrogen- bonding	[126]
dialkanolamine	polymer	hyperbranched polyesteramide	alkyl groups, hydroxyl groups, carboxylic acid	hydrogen- bonding	[127]
lignosulfonate	polymer	arylsulfonates	phenolic and sulfonic acid groups	π–π interactions, hydrogen bonding, Acid-base interactions	[128]
4-vinylpyridine	Graft polymer	vinylic monomers	Vinyl, alkyl groups,	π–π interactions, hydrogen bonding	[129]
Xylene	dissolver	aromatic solvents	mono-ring	π–π orbital overlap	[130]
1-methylnaphthalene	dissolver	aromatic solvents	bicyclic molecules	π–π orbital overlap	[131]

2.6. Practical applications of the controlled delivery system in the oil and gas industries

The concept of delivering a chemical by utilizing a vehicle to provide a predictable and controlled release of the component holds the possibility of providing an effective and efficient means of application in a broad range of instances [132]. There are a large number of oilfield chemicals which have a potential for using in delivery system such as corrosion products removers, asphaltene inhibitors, scale inhibitors, scale dissolvers, paraffin inhibitors, gas hydrate inhibitors, biocides, pH modifiers, metal chelators, metal complexes, antioxidants, wetting agents, clay stabilizers, wax inhibitors, wax dissolvers, wax dispersants, H_2S scavengers, water flow inhibitors, sand consolidation additives, permeability modifiers, foaming agents, microorganisms, nutrients for microorganisms, salts, polymers, polymer stabilizers, crosslinkers, and breakers. These oilfield chemicals may exist in oil-soluble (nonaqueous) and/or water soluble (aqueous) forms [133]. However, research in this concept, for the controlled release of a production chemical in the well, is just at the emerging phase.

In particular, the key to effectiveness inhibitor is getting to have good adsorption on the formation surface and not be produced back too quickly. Otherwise, treatment lifetimes become uneconomically short. More recently, attention has focused on increasing the effectiveness of inhibitors by increasing the adsorption of scale inhibitors on the rock surface, hence increasing the lifetime of a squeeze treatment [134]. These studies include: (i) mixing cations or Fe (II) ions with the scale inhibitor to provide better retention than using the inhibitor alone [135], (ii) adding pH modification chemicals to the inhibitor via a temperature dependent material such as urea, (iii) using mutual solvents (such as the small alkyl glycols) to change the rock wettability (more water wet) [136], and (iv) using kaolinite or other clay to enhance the inhibitor adsorption [137].

These studies, however, only showed a limited reduction in the amount of inhibitors. To overcome these problems, a variety of inhibitor compositions have been developed. These inhibitors can be used successfully in the oil and gas industries:

• Solid Inhibitors (i.e., use of porous ceramic proppant as a carrier to deliver chemicals downhole)

• Nanoparticle

• Emulsions, microemulsions (MEs), or nanoemulsions

• Encapsulated products

The most popular approach is the incorporation of the chemicals into inert lipid vehicles such as oils, surfactant dispersions, liposomes, MEs, and NEs. Many industries use emulsion technology as a delivery vehicle for either aqueous- or oil-based chemicals (or both). The study by Al-Zahrani, [138], examined (acid-in-oil) emulsion to deliver corrosion inhibitor to the rock formation, which consists of two phases: the internal phase formed of acid with corrosion inhibitor added to it, and the external phase formed of oil with an emulsifier. Typically, the emulsified acid enters the formation and where employed successfully creates a barrier causing the acid to release slowly at a distance from the well-bore. When pumping the acid-in-oil emulsions through steel tubing and piping, a corrosion inhibitor is usually added to reduce the corrosive effects of the acid. An attempt to further reduce the amount of scale inhibitors has been done by Zhang et al., in 2016 [139] by using reverse micelles as non-aqueous scale inhibitor delivery vehicles for oilfield mineral scale control. Table 2-3 lists the previous studies of some applications of controlled delivery systems in the oil and gas industries.

Table 2-3. The details of some applications of controlled delivery systems in the oil and gas industries.

purpose	Chemical type	Carrier	Chemical additive	Author
scale inhibitor	phosphonate	Proppant	phosphonate	Brown et al. 2011[140]
scale inhibitor	Phosphonates	phosphonate–polymer nanoparticle capsules	diethylenetriamine pentakis (methylenephosphonic acid) (DTPMP)	Zhang and co-workers [141]
corrosion inhibitor	composite core-shell type nanomaterials	halloysite nanotube lumen	2-mercaptobenzothiazole	Shchukin et al. 2008 [142]
corrosion inhibitor	acid	acid-in-oil emulsion	mixture of hydro chloric acid with formic or acetic acid	Al-Zahrani, 2011 [138]
scale inhibitor	phosphonate	water-in-oil ME	diethylenetriamine pentakis(methylenephosphonic acid) (DTPMP)	Zhang et al.,2016 [139]
wax deposition	Ferrofluid (5% magnetic nanoparticles, 10% surfactants, and 85% water)	Water or organic solvent	Co-Ni nanoparticles	Haindade et al. (2012) [143]
corrosion inhibitors	nanoparticles	SiO_2 nanoparticles	benzotriazole	Shchukin, D.G. and Möhwald, H., 2007 [144]
mineral fouling	microporous	microporous polypyrrole (PPy)	1-Butyl-3-methylimidazolium bis(trifluoromethylsulfonyl) imide (BMIm)	Charpentier et al 2014 [145]
scale inhibitor	nanoparticles	carbon nanotubes (CNTs)	polyphosphinocarboxylic acid, PPCA	Ghorbani et al. 2016 [146]
scale inhibitor	nanoparticles	amorphous calcium–DTPMP solid	methylene phosphonic acid) (DTPMP)	Zhang et al., 2016 [147]
scale inhibitor	nanoemulsions	oil-in-water nanoemulsions	phosphino-polycarboxylic acids (PPCA)	Gaudio et al., 2007 [148]
Drilling bits	cement spacer	nanoemulsions	nanoemulsion	Maserati et al. (2010) [149]
corrosion inhibitor	mesoporous	Hollow mesoporous silica nanoparticles	sodium phosphomolybdate	Zea et al., 2017 [150]
corrosion inhibitor	microporous	microporous polypyrrole (PPy)	sodium phosphomolybdate	Contri et al. 2018 [151]
EOR	nanodroplets	nanodroplets	SDS and Span 80	Nourafkan et al., 2018 [152]
EOR	nanoparticles	TiO2 nanoparticles	anionic alkyl aryl sulfonic acid (AAS)	Nourafkan et al., 2018 [153]
EOR	nanoparticles	Lipid nanostructures	nonylphenol ethoxylate (NPE10)	Rosestolato et al., 2019 [154]

2.7. Nanoemulsions as a new vehicle for chemical additive delivery

There are various delivery systems that can be generally classified as liquids, semisolids, and solids. The most popular approach is the incorporation of the active substance into inert lipid vehicles such as oils, surfactant dispersions, liposomes, MEs, and NEs. The study of NEs has become a rapidly growing research field in the formulation community and the development of oil-in-water NE has attracted an immense amount of interest owing to their outstanding properties. NE is one of the most promising smart fluids that has many applications in drug delivery, cosmetics, food production, etc. [150- 157] (Figure 2-7). Recently, NE has been used successfully in the oilfield for enhancing oil recovery and for delivering chemicals in the reservoir [158,159]. NEs can be prepared either mechanically by sonication or by low energy procedures like phase inversion temperature method. Sonication technique is found to be more efficient than mechanical methods in term of production cost, handling, and maintenance [160].

The formation of stable transparent NEs poses two main challenges: the ability to initially create an emulsion where the entire droplet size is below 100 nm, and the subsequent stabilization of this emulsion against various physicochemical phenomena such as gravitational separation, coalescence, flocculation, and particularly Ostwald ripening [161]. It is well established from a variety of studies, that surfactant can be used as an emulsifier to facilitate the formation of the NE and to ensure its kinetic stability during storage [162]. The type of surfactant and its properties such as critical micelle concentration (CMC), hydrophilic-lipophilic balance (HLB), etc.) play a very important role in NE stabilization. Blend surfactants may be employed to reduce the total amount of surfactant used in particular applications, resulting in the reduction of cost and environment impact [163]. It is well known that polyoxyethylene non-ionic surfactants interact attractively with both anionic and cationic surfactants such as sodium dodecyl

sulfate (SDS) and dodecylammonium chloride (DAC) at the oil/water interface [164]. The interaction in the oil/water interface between mixed surfactants is more attractive than that between anionic surfactant molecules alone or between non-ionic molecules alone [165]. However, NEs are particularly prone to growth in particle size over time by a process known as Ostwald ripening [166]. Ostwald ripening is a process by which the fluid contained in smaller drops with high interfacial energy is transferred to larger drops, forming large droplets at the expense of smaller ones [166, 167].

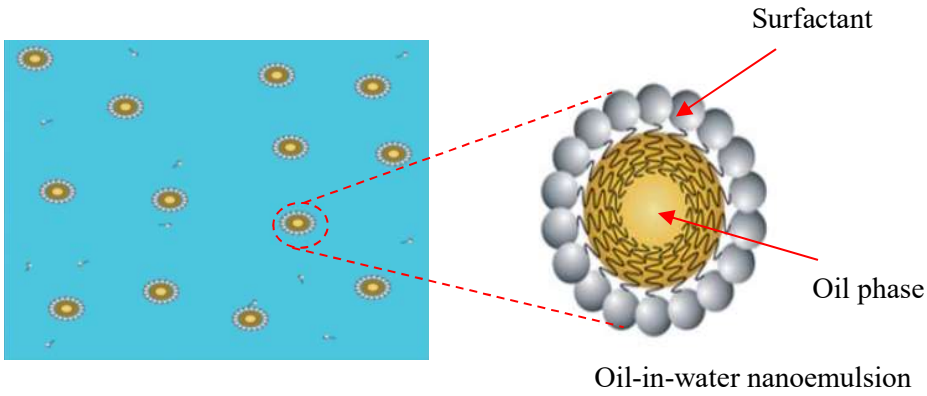

Figure 2-7. Schematic diagram of NEs fabricated from oil, water, and surfactant. Figure is taken from [168].

A considerable amount of literature has been published on two strategies for reducing the rate of Ostwald ripening in oil-in-water NEs. The first one is to use long-chain oils (as a second oil), which is insoluble in the continuous phase. This second oil is referred to as a" ripening inhibitor" and is usually a highly nonpolar substance with a relatively high molecular weight, such as corn oil [169], sunflower oil [170], and medium chain triglycerides (MCT) [171]. This would provide a kinetic stabilization of NEs and increase significantly the aging rate [172]. In 2008, Wooster et al. [161] responded to the need for reducing Ostwald ripening by adding the large molar volume of long-chain triglyceride

oil to the organic phase, which decreased the water solubility of organic phase thus providing a kinetic barrier to Ostwald ripening. Similarly, Mc- Clements et al. 2011 [173], found that by adding highly hydrophobic triglyceride molecules to the lipid phase of orange oil, a significant reduction in Ostwald ripening occurred. Recently, Chen et al., 2016 [171] used long-chain and medium-chain triglycerides with Eugenol oil at high incorporation ratio (30 wt. % to 80 wt. % in the lipid phase) when Tween 80 was used as the surfactant. Their results showed that NEs with the smallest particle size were stable within 28 days of storage. However, exactly how the second oil inhibits Ostwald ripening is still not yet fully understood.

The second way is to use polymeric stabilizers to form a strong interfacial layer around oil droplets that prevents the Ostwald ripening. In 2011, Galindo et al. examined the stability of NEs with mixtures of amphiphilic polyelectrolytes and non-ionic surfactant (tetraethylene glycol dodecylether). They showed that the shelf life of dodecane NEs was significantly extended by the presence of the non-ionic surfactant [174]. The surfactant film is responsible for the prevention of the two phases from collapsing, which must be on one hand rigid enough to give a mechanically strong interface, and on the other flexible enough so that the collision of oil droplets does not lead to the rupture of the film. Fundamentally, the stabilization of an emulsion system can be achieved by electrostatic and/or steric repulsion forces [175]. However, the formed droplets are generally large in the range of a few hundred nanometers. Although there are many reports in the literature on the reduction of Ostwald ripening [171], most are restricted to explain the mechanism of stability.

2.7.1. Characteristics of NEs

2.7.1.1. Small droplet size and narrow size distribution

The droplet size of NE is one of the most important characteristics. It influences optical, rheological, stability, and release characteristics. The small droplet size also has the potential to alter the biological fate of the delivery system [176]. The small droplet size and narrow size distribution impart several overwhelming advantages to a NE over other delivery systems. The droplet size is so small that it only scatters light weakly. This characterizes the appearance of NEs, optically clear or slightly turbid. Moreover, the small droplet size and narrow size distribution contribute to high kinetic stability of NE against aggregation and gravitational separation by Brownian motion.

In oil and gas applications, the small size of the droplets will likely increase the momentum transfer efficiency of the chemicals or other molecules inside the droplet across porous media [177].

2.7.1.2. Low concentration of surfactant

Both ME and NE systems require surface-active molecules to stabilize the interface of two immiscible phases. Surfactants serve as emulsifiers that adsorb to the surface and the interface, preventing the aggregation of droplets. ME was introduced as early as the 1940s and they are of interest as a drug delivery system due to its simplicity of manufacture, thermodynamic stability and high solubilization capacity [178]. ME is defined as a system of water, oil, and amphiphile, which is a single optically isotropic and thermodynamically stable liquid solution [179]. It shares a similar system classification as NE. The surfactant is the critical component in ME formation and a large amount of surfactant required to produce ME is a major concern of the ME due to surfactant-induced toxicity and side

effect, consumer compliance and excipients acceptability [180]. Nevertheless, it is possible to fabricate a NE with much less surfactant (~3-10 wt.%) than a ME (>20 wt.%) [181,182].

2.7.1.3. Enhanced solubility and absorption of chemicals.

NEs can encapsulate chemicals inside the dispersed phase so as to increase their release time and efficacy due to the increase of surface area resulting from the decrease in droplet size [183]. Because of enhanced release time and efficacy of chemicals, there can also be a reduction in the amount of chemicals losses. NEs also show a strong tendency to migrate and adsorb on the mineral surface due to the large surface area of the droplets and the presence of surfactants, which restored the wettability and induced ultralow interfacial tension of oil, promoting the solubilisation of the adsorbed oil layers on porous media [184].

2.7.1.4. Thermodynamically unfavorable system.

NEs are thermodynamically unstable systems because the free energy of the separated two phases (oil phase and water phase) is lower than that of the one-phase emulsion itself. Consequently, NEs always tend to breakdown over time due to various physicochemical phenomena, namely gravitational separation, coalescence, flocculation, and particularly Ostwald ripening [181,185]. Therefore, the major concern of a NE formulation is to create sufficiently small droplets in order to ensure that the system has a satisfactorily long kinetic stability for commercial applications. The long-term physical stability of a NE can be achieved by means of electrostatic or steric stabilization, static by solid particles at the interface, or increasing the viscosity of the system. Thus NE, sometimes, can be labelled as “Approaching Thermodynamic Stability” [181].

2.7.2. Advantages and formulation challenges of NEs

The attractions of NEs from personal care and health products to oil and gas applications are due to the following advantages: the transparent appearance of nanoemulsion and its fluidity at a preferable oil concentration give NE product a pleasant aesthetic character and skin feel.

With the increase in chemical solubility in the NE, the greater concentration gradient facilitates the slow release. When across the pore space in porous media, the oil droplet not only carries the chemical directly entering the porous medium but also provides an extra solvent with other components such as surfactants and induces highly permeable pathways across porous media. The small droplet size (less than 100 nm) of NE can be efficiently penetrated through the pore space in porous media [186]. The small droplet size of NE also prevents flocculation, coalescence, and gravity-induced sedimentation or creaming, phase separation and surface fluctuation during storage. Wetting, spreading and penetration can be enhanced due to the low surface tension of the whole system and low interfacial tension of the o/w phases [187].

The reduced amount of surfactant in NE formulation significantly reduces the treatment cost. NEs can be designed at much lower droplet concentration than conventional emulsions [176]. With respect to the inhibitor in a formulation, the primary goal of NE as a carrier system is to protect and deliver the chemical incorporated inside. Hence, compatibility of formulation components with the inhibitor and capacity of formulation components to solubilize and stabilize the inhibitor should be considered. Prerequisite information such as physicochemical properties of the inhibitor is needed to select a proper emulsifier system and an oil phase.

Two major concerns in formulation considerations are the efficiency of NE formation and stability of a NE [188]. The oil phase in a NE system not only influences the NE formation but also affects end-product stability. Using high viscosity oil limits droplet disruption within a high-pressure homogenizer; high level of hydrophobicity makes it difficult to prepare NEs; high interfacial tension with the aqueous phase challenges the emulsifiers to stabilize the interface. In contrast, when using oils of low viscosity, relatively high polarity, and low interfacial tension to formulate NE, it is very likely that the NE formed will easily breakdown because of Ostwald ripening or coalescence. The relatively high water-solubility of oil causes diffusion of oil molecules from small to large droplets, which leads to droplets growing. The low interfacial tension makes oil droplets more prone to coalescence [171].

2.8. Displacement/removal mechanism of asphaltenes in porous media

2.8.1. Asphaltene removal mechanism by inhibitors

Asphaltenes tend to adsorb on mineral surfaces and alter their wettability, which can reduce crude oil effective mobility by plugging pore throats, thus reducing rock permeability. Once asphaltene deposits have built up on rock surfaces, the ability to effectively mobilize and produce crude oil can be challenging [189]. Removal of asphaltenes requires the use of mechanical methods or chemical treatments (see Section 2.3).

Several investigations have been conducted to study the effect of inhibitors on the decrease and/or delay of the asphaltene precipitation and deposition. These studies suggested the injection of the surfactants into streams susceptible to asphaltene precipitation and deposition. However, there is a lack of information on the effect of the

inhibitor on the deposition of asphaltene particles on surfaces, such as rocks, stainless-steel (SS) and glass.

Al Sultan et al., 2018 [190] studied the effect of DBSA as an anionic inhibitor on asphaltene deposition on SS and glass surfaces. SS can be representative of the pipeline surface, while glass beads can be a representative of porous media. Results revealed that the inhibitor delays the asphaltene onset in the bulk system. However, asphaltene deposition on the stainless-steel surface was increased at all measured concentrations of the inhibitor, while the deposition rate on the glass surface decreased by increasing the inhibitor concentration. The results revealed that the DBSA can remove deposited asphaltene on glass surfaces at high concentrations. Similarly, Hashmi *et al.* recently showed the ability of DBSA to remove asphaltenes that have been deposited in metal capillary tubes [191].

There are two major mechanisms responsible for the removal of asphaltenes in porous media by inhibitors: mobilization and micellar solubilisation. Mobilization involves reduction of interfacial tension between the asphaltene and aqueous phase [191] and is primarily assumed to be responsible for the bulk removal of trapped oil during remediation operations [192]. Micellar solubilisation, on the other hand, is a less understood phenomenon. It is believed that inhibitor micelles dissociate near the asphaltene-water interface and then re-form around the asphaltene, essentially partitioning the hydrocarbons into the aqueous phase [193]. Micellar solubilisation of this type leads to a Winsor type I, oil-in-water emulsion [191-195]. This phenomenon has been investigated in groundwater contaminant (non-aqueous phase liquids NAPL) transport and chemical flooding in oil reservoirs for four decades [240-243]. Although most of crude oils are less dense than brine and thus considered as LNAPLs (light non-aqueous phase liquids), they often contain heavy organic macromolecules (asphaltenes)

that are denser than brine and thus classified as DNAPLs (dense non-aqueous phase liquids). However, the extent to which these two mechanisms occur is still unclear, particularly in asphaltene adsorption. Surfactant injection was very effective in mobilizing residual oil trapped in a well-controlled experimental site [196]. Although increased efficiency with surfactant mixtures has been reported in the past, some challenges may arise due to micellar agglomeration [196] or surfactant partitioning [197].

Javanbakht *et al* [198] illustrated the mobilization and micellar solubilisation mechanisms for removal of contaminants by surfactants, as shown in Figure 2-8. Fast mobilization of LNAPL (through the formation of Winsor Type III MEs) occurs first followed by the slow micellar solubilization of DNAPL (i.e., asphaltenes). The wettability reversal is due to the adsorption of surfactant molecules via their hydrophobic tails on the thin asphaltene layer causing it to detach and form Winsor Type I MEs. Mobilization here was the dominant mechanism because asphaltene nanoaggregates were colloidally stable in NAPL and their adsorption on mineral surfaces reached saturation relatively fast. However, there are situations where asphaltene aggregates may become unstable and flocculate (for instance, due to incompatible fluid mixing), leading to much larger amounts of DNAPL deposited on mineral surfaces that may hinder NAPL displacement in porous media. In this case, micellar solubilization may become the dominant mechanism. Therefore, the selection of surfactants and the effectiveness of aquifer remediation strategies depend on the colloidal stability of asphaltenes in the NAPL phase.

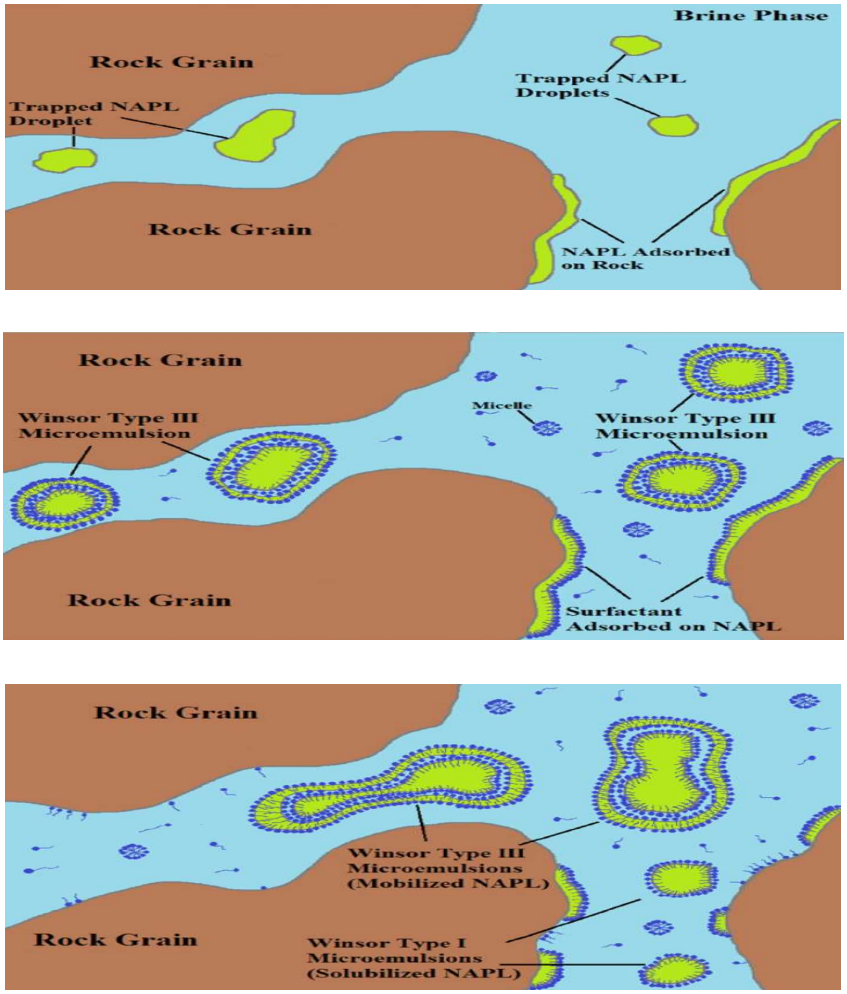

Figure 2-8. Process of NAPL removal from contaminated aquifer: (a) trapped and adsorbed NAPL, (b) mobilization of NAPL, (c) mobilization and micellar solubilisation of NAPL. Figure is taken from [198].

Besides the use of surfactant to remove asphaltenic deposits, BETX (Benzene, Ethylbenzene, Toluene, and Xylene) solvents have historically been used in the oilfield as a chemical treatment to remove deposits from pipeline tubing and near the wellbore. The use of these solvents presents serious health and safety hazards. In comparison, the use of aqueous-based treatments represents a safe alternative.

2.8.2. Molecular mechanism of contaminant removal by MEs

More recently, interest has centred on special mixtures known as MEs that may be useful for removal of contaminants. Specifically, in an O/W ME, the micellar capsules are thermodynamically stable, enabling their usage in field applications [199]. The oil phase may be an organic solvent that can be delivered to the contaminant via the ME, allowing the solvent to assist in breaking up the adsorbed contaminant. Mandal and others conducted experiments with non-ionic surfactant-stabilized MEs to prove that MEs can recover up to 30% more trapped oil phase than traditional water-flooding [200].

Qin et al. [201] observed that oil solubilization achieved by a ME was higher than that obtained using a surfactant at low concentrations in an aged Tensleep core using imbibition tests. They attributed this result to the unique ability of d-limonene swollen micelles to penetrate into microcrystalline dolomite cement and swell the crude oil leading to more effective desorption. Similarly, Oliveira et al. [202] investigated the removal of heavy crude oil from sand using MEs.

Javanbakht et al 2017 [198] studied the impact of surfactant and ME flooding on NAPL displacement in heterogeneous porous rocks. They found that ME flooding had a greater impact in displacing NAPL phase compared to surfactant flooding. They concluded the reduction of contact angle (i.e., wettability alteration) and IFT were the main mechanism for displacement of NAPL. Although the NAPL/ME IFT was slightly lower than NAPL/surfactant IFT, the increased ability of MEs to alter the wettability of contaminated rough surfaces (such as dolomite cement) was the key parameter controlling fluid displacement in this system. MEs could penetrate adsorbed DNAPL layers because of the presence of d-limonene molecules that were able to carry the surfactant even to rough surfaces and form small- emulsified NAPL droplets that were easier to displace through

narrow pores and throats. In contrast, the surfactant alone could not alter the wettability of rough surfaces and therefore left 12% more NAPL in the contaminated rock than MEs.

Lowry et al., 2016 [203] suggested that MEs may be a better option than surfactant alone for removal of oil-based contaminants from mineral surfaces. The combination of the surfactant with the limonene solvent allows the micelles to dissociate and swell the oil phase. Also, by reducing the interaction between the near irreversibly adsorbed polar molecules and the bulk oil phase, the ME can increase the mobility of otherwise adsorbed non-polar molecules. The total mechanism may be summarized as the diffusion of the micelles to the contaminant droplet, infiltration of the ME solvent, swelling of the contaminant phase and finally solubilization induced by flow (Figure 2-9).

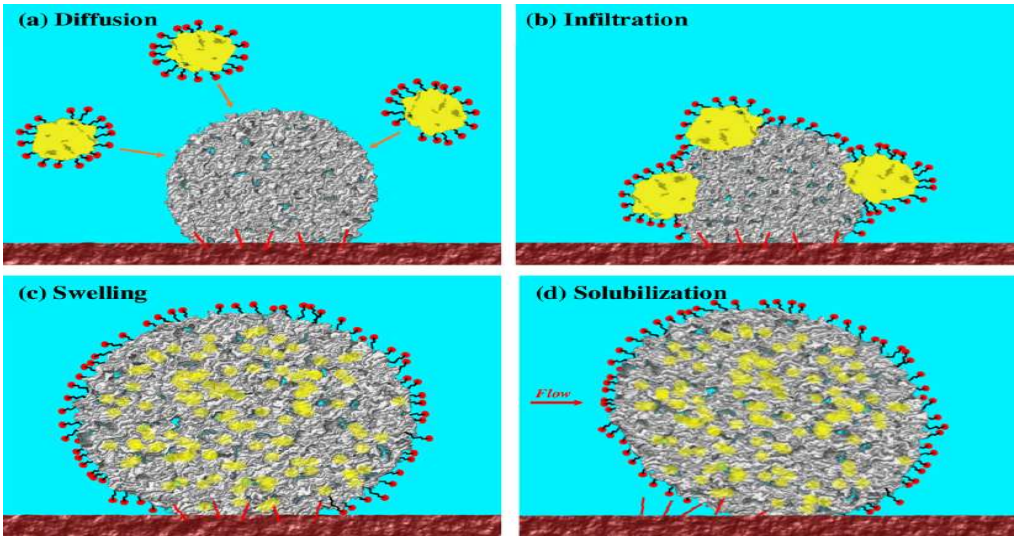

Figure 2-9. Proposed mechanism of ME interaction with NAPL on the mineral surface. Figure is taken from [203].

Hernandez et al. 2019 [204], investigated the ability of MEs to remove crude oil residue from solid surfaces using surfactant and ME in a fast and reproducible manner. ME was consisting of 23 wt.% ethoxylated nonionic surfactant (C_{12}-$15EO_7$), 23 wt.% isopropyl alcohol, 39 wt. % fresh water and 15 wt. % solvent (d-limonene). An equivalent surfactant

package (SP) was prepared by replacing the amount of solvent by water. They suggested a diagram of the removal mechanisms of solid crude oil residue from sand using MEs, as shown in Figure 2-10. They suggested that d-limonene swollen micelles will adsorb to crude oil deposits and then will diffuse and penetrate into the deposited layer, thereby softening it. The softening process is followed by removal into the aqueous phase. The ME exhibited a much higher removal than the SP for all parameters tested in this study.

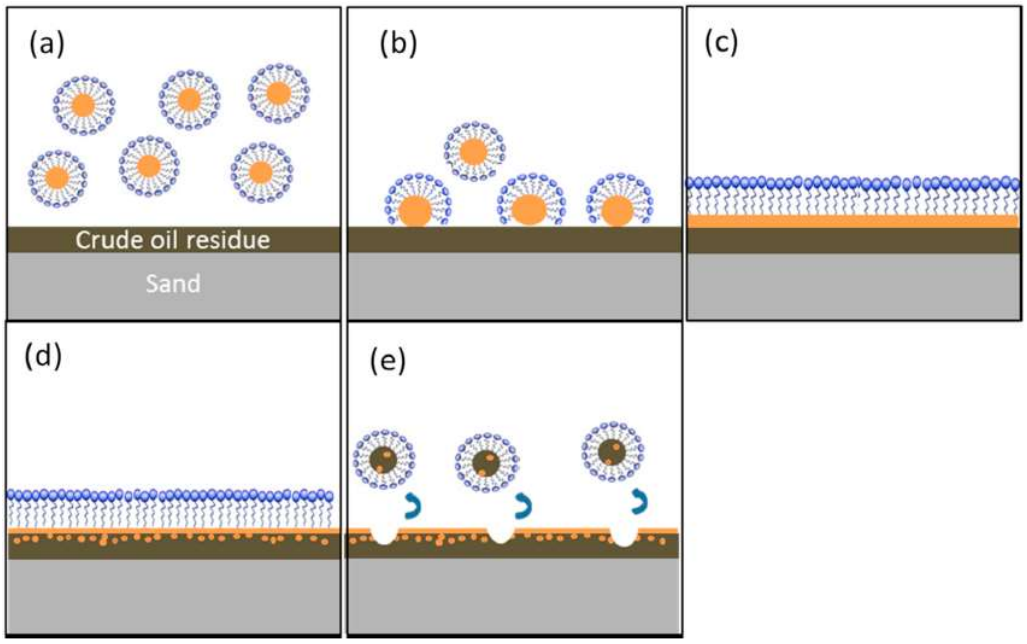

Figure 2-10. Cartoons showing the removal mechanisms of crude oil residue from sand using a ME. (a) diluted ME contacting sand, (b) and (c) adsorption of both dlimonene and surfactant contained within the ME into the sand surface, (d) d-limonene diffusing into the crude oil coated layer and softening it, (e) removal of crude oil residue. Figure is taken from [204].

2.9. Summary of the state-of-art

i) Stabilization of NEs

Over a sufficient storage time, NEs have a tendency to undergo physical changes that lead to their eventual phase separation. Previous studies reported two strategies for reducing the rate of Ostwald ripening or growth of NEs: the first one is to use long-chain oils (as a second oil) and the second way is to use polymeric stabilizers to form a strong interfacial layer around the oil droplet that prevents the coalescence and Ostwald ripening. Most of these works have failed to form droplets less than 100 nm in diameter and to be stable for a long time. In addition, previous studies are limited to explain the mechanism of NEs stability. Previous studies have also failed to understand the retention and release characteristics of chemicals from NE-based delivery systems.

ii) Stabilization of asphaltene and preventing aggregation and precipitation

Although chemical treatment is widely used in oilfields, it has a major problem due to the loss of a large amount of chemicals inside the reservoir, resulting in high treatment cost. In addition, using high concentrations of inhibitor tends to produce self-associations near the wellbore rather than adsorption on asphaltene, reducing their effectiveness. Thus, there is a strong need to develop new methods for controlled and sustained inhibitor release inside the oil reservoir.

iii) Molecular structure characterization of asphaltene

The mechanisms of the aggregation behaviour of asphaltenes are not completely understood, and a complete molecular analysis of asphaltene structure changes with the addition of inhibitors have not yet been achieved.

iv) Asphaltene adsorption/desorption into porous media (i.e. underflow conditions)

Most of the asphaltene works are concerned with the measurement and modeling of adsorption isotherms on crushed minerals under static conditions [80-87]. Very little work was conducted on the adsorption kinetics of asphaltenes under flow conditions [76] and on the effect of inhibitors on the delay of asphaltenes precipitation and deposition of asphaltene particles on porous media. Also, there are no systematic studies that establish the removal mechanisms of asphaltene from rock surface using NEs in the presence and absence of asphaltene inhibitor.

Addressing these problems, this work will develop a novel concept of using NE to deliver and controlled release of asphaltene inhibitor (AI) in a bulk fluid or flowing through a porous medium, which could i) improve the stability of the asphaltene, ii) reduce the usage of inhibitors, and iii) extend the treatment time via the slow release of inhibitors. Specifically, the thesis will:

1. Explore a novel method by using AI (i.e., as a new class of ripening inhibitor) inside NEs to reduce Ostwald ripening, which could be used as a carrier for AI in both upstream and downstream.
2. Inveterate the effect of the controlled release of AI on asphaltene stability and propose a mechanistic understanding of the controlled release effect on preventing asphaltene precipitation.
3. Conduct a detailed kinetic study of controlled AI release from NEs and elucidate the release mechanism by comparing with established mathematical models.
4. Investigate the molecular structure characterization of asphaltene in the presence of inhibitors with NEs and validate the intermolecular interaction between asphaltene and DBSA NEs.

5. Develop a novel concept of using NEs as carriers for asphaltene inhibitors and control their release inside porous media to improve the cumulative asphaltene recovery efficiency.

These are presented in the following chapters.

Chapter 3

Nanoemulsion preparation, characterisation and stability

3.1. Introduction

In many commercial applications, it is important that a NE-based product remains both physically and chemically stable when exposed to specific environmental conditions during its manufacture, storage, transportation, and utilization (such as pH, ionic strength, temperature, and mechanical forces) [200]. For emulsions to be used in the oilfield applications, emulsions need to be small size and stable for a long time [200,207]. A considerable amount of literature has been published on two strategies for stabilization of NEs: i) use long-chain oils (as a second oil) and ii) use polymeric stabilizers to form a strong interfacial layer around the oil droplet, that prevents coalescence and Ostwald ripening.

Different to the previous two methods, this Chapter explores a novel method by using AIs (as a new class of ripening inhibitor) inside NEs to reduce coalescence process or Ostwald ripening, which could not only reduce the usage of stabilizers but also produce small oil droplets stabilized for a long time. Characterization of NEs is conducted in terms of droplet size distribution, IFT measurement, surface charge determination, stability study, and rheological behaviour, which will be used in the following applications in the delivery and controlled release AI through bulk and porous media.

3.2. Experimental work and procedure

3.2.1. Materials

Analytical grade materials including: xylene (purity > 98.5%), sodium dodecyl sulfate (SDS) (Figure 3-1 A), Tween 80 (sorbitan monooleate) (Figure 3-1 B), dodecyl benzene sulfonic acid (DBSA) (Figure 3-1 C), phenanthrene (phe) (purity 98%) (Figure 3-1 D), deionized water, and sodium chloride (NaCl) were purchasing from Sigma- Aldrich Company. Figure 3-1 shows the chemical structure for the materials used.

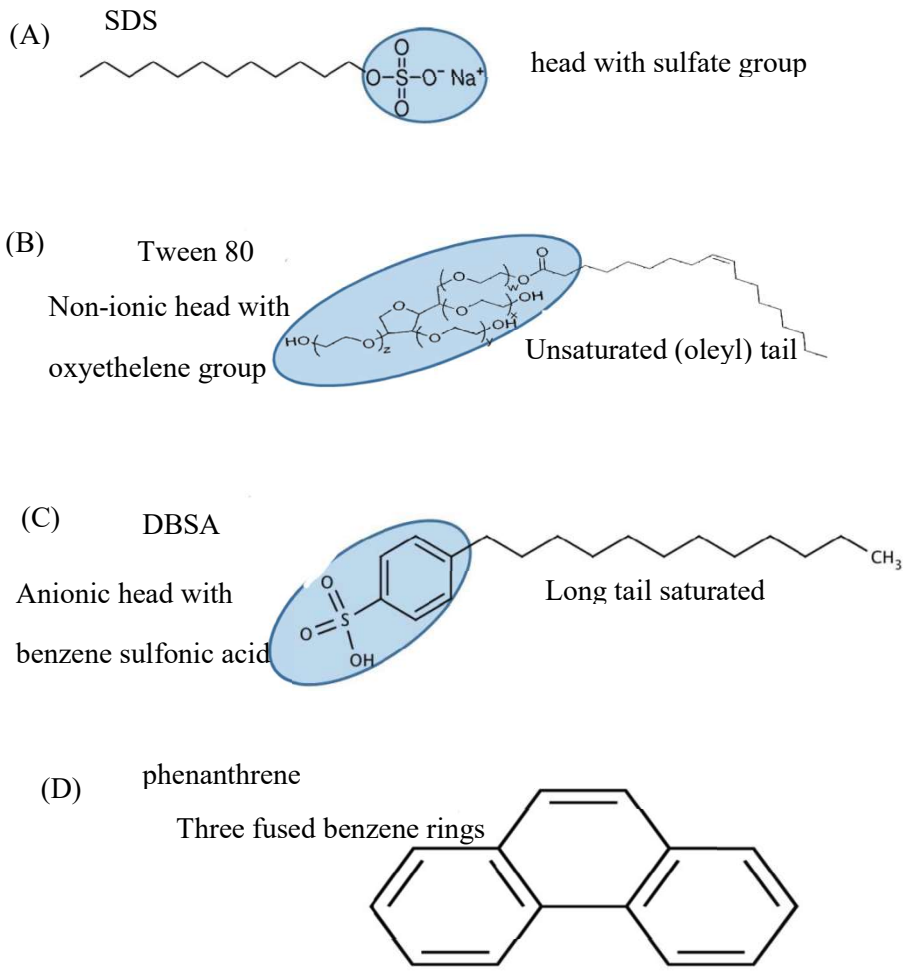

Figure 3-1: Chemical structure A) SDS, B) Tween 80, C) dodecyl benzene sulfonic acid (DBSA), D) phe.

3.2.2. Preparation of oil-in-water NEs

The properties and stability of the final NEs are largely dependent on the preparation procedures and techniques applied. NE was formulated using ultrasonication method, which is one of the most efficient high-energy homogenization techniques. Some of the potential advantages of ultrasonic homogenizers for commercial applications are their ability to produce stable NEs with very small droplet diameter and low polydispersity, low operating costs, and low energy consumption [160].

In the beginning, the formation consisting of DBSA was dissolved in xylene and mixed together by stirring using a magnetic stirrer at 1000 rpm at room temperature for 24 hours until a clear sample was obtained. At the same time, another sample consisting of a non-ionic surfactant (Tween 80), an anionic surfactant (SDS) and deionized water were mixed together by using the magnetic stirrer for 24 hours as well to ensure complete dispersion and dissolution. In the next step, the mixture of (deionized water, surfactants) was added slowly to the mixture of xylene and DBSA. Then, the samples were pre-homogenized by a high shear mixer (IKA T2S digital/Ultra- Turrax) for 4 minutes (~3000rpm) for each sample to improve the mixing and size distribution. After that, the samples were sonicated by an ultrasonic probe for 8 minutes per sample, amounting to 2 minutes of actual sonication for 4 times (i.e., 1 minute without sonication between two actual sonications). The amplitude for sonication was about 20%, the power was 26 watt, and the energy about 2000 J for each cycle. The procedure was implemented carefully to ensure the oil inside the NE is not evaporated by the elevated temperature due to the sonication. A temperature controller and a double-walled cylindrical glass container cooled by water were used to monitor and control the temperature to 25 °C during the sonication process. The low volume percent of the oil was selected to minimize the effect of droplet coalescence and the mass of the surfactants was tested to be in excess for the smallest emulsion produced.

The composition of the dispersions used to prepare blank NEs were at a concentrations of 7 vol.% xylene (oil phase), 10 vol.% mixed surfactants (9.9 vol.% Tween 80 and 0.1 vol.% SDS), and 83 vol.% deionized water, while DBSA NEs were composed of: 1 vol.% DBSA, 7 vol.% xylene, 10 vol.% mixed surfactants, and 82 vol.% deionized water. While phe NEs were composed of: 1 vol.% phe, 7 vol.% xylene, 10 vol.% mixed surfactants, and 82 vol.% deionized water.

3.2.3. Characterization of nanoemulsion

3.2.3.1. Analysis of droplet size and polydispersity index

The droplet size and size distribution for the NEs prepared with different concentrations of inhibitor were measured approximately 2–5 h after the preparation by a laser diffraction method (i.e., Zetasizer Nanoseries ZS, Malvern Instrument, Worcestershire, UK). NE droplet size was determined by 3 measurements and calculated as the mean diameter of the volume distribution (MV).

$$MV = \frac{\sum Vi\ di}{\sum Vi} \qquad \text{..... (3-1)}$$

where *V*i is the volume percentage between droplet sizes and *di* is the diameter of droplets. About 1 ml of sample was placed in a disposable cuvette (1×1×4 cm). The polydispersity index (PDI) for asphaltene particles in the suspension can be calculated from a two-parameter fit to the correlation data (the cumulants analysis) as Mw/Mn, where Mw is the weight average and Mn is the number average molecular weight [181]. Zeta potential, the electrical charge on the oil droplets in the emulsions was determined under holder temperature of 25 °C and electrical voltage 3.9 V. All NEs were stored at 25 °C and withdrawn periodically for droplet size, PDI, and zeta potential determinations.

3.2.3.2. Interfacial tension measurements

For IFT measurements of the oil/water system were carried out using a KSV CAM 200, a syringe needle with the size of the 2 inch (50.8 mm) and an outer diameter of 0.7 mm was filled with low-density fluid (i.e. xylene) and immersed in an optically clear cell filled with the aqueous phase. Then the xylene droplet was injected upwards, and a stable pendant xylene droplet was recorded by a camera. The same drop size (12 µl) was used for all experiments. A pendant drop shape was then processed by the software to fit the Young-Laplace equation, and the IFT values were determined. The measurements were repeated several times for each oil/ water system and similar trends were yielded with the standard deviation of the about ±2 unit. All the interfacial measurements were conducted at room temperature (25 °C) and atmospheric pressure.

3.2.3.3. FTIR analysis

The intermolecular forces between NE's components were investigated by FTIR-Thermo iS10 spectrometer. Infrared spectra of NEs samples were collected in the spectral range from 500 to 4000 cm^{-1}, 64 scans per spectra, and a resolution of 1 cm^{-1}. FTIR spectra were measured by the attenuated total reflectance (ATR) technique, which is a sampling technique used in conjunction with FTIR spectroscopy and enables samples to be examined directly in the solid or liquid state without further preparation. A Bruker ATR A225 sample cell equipped with a diamond crystal of quadrate area of 2 × 2 mm^2 was used. The FTIR spectrometer was controlled using the OPUS software. The background was collected every 7 min and the samples were used making sure they applied uniformly in order to get the better peaks. The equipment was cleaned in between the samples in order to avoid the chances of contamination.

3.2.4. Rheological measurements

The viscosity measurements of all NEs were performed using Bohlin Gemni rheometer at 25 °C for the shear rate range of 0−1000 s^{-1}. The sample of NE was placed into the cell (2ml Mooney). This cell is intended for use with low viscosity samples.

A fluid showing viscoelastic nature (partial viscous and partial elastic) under varying strain is known as viscoelastic fluid. Viscoelastic was measured by oscillatory mode with a frequency range between 0.1 and 20 Hz at 25 °C. For viscoelastic fluids the measurement of storage/elastic modulus (G′) and the loss/viscous (G″) modulus is possible. If, G″ > G′ = viscous or liquid-like nature, and G″< G′ = gel or solid-like nature [200].

3.2.5. Stability measurements

The static stability of NEs was evaluated by a Turbiscan instrument (Formulaction, France). The sample in the cell was at level (55 mm) and scanned every 30 minutes for 3 days and 10 hours at 25 °C, and the change in transmission, backscattering flux and delta backscattering (ΔBS) were obtained as measurements of the stability of the NEs.

Stability was evaluated as Turbiscan stability index (TSI), which is a statistical parameter used to estimate the suspension stability [207], where a low TSI value indicates high stability of the system [208,209]. The TSI value was calculated using Eq. (1) reported for [210]

$$TSI = \sqrt{\frac{\sum_{i=1}^{n}(x_i - x_{BS})}{n-1}} \quad \text{..... (3-2)}$$

Where x_i represents the average scattering intensity measured per minute, x_{BS} is the average value of x_i, and n represents the number of scans.

The dynamic stability of the NE was analyzed using LUMI-sizer (LUMiSizer, LUM Americas, Boulder, CO, USA) to determine the mechanism of instability and the

instability index as a function of time (1 hr and 4 weeks). In brief, (400 µl) of NEs was put into 8 mm x 2 mm rectangular polycarbonate cuvettes and centrifuged at 2000 rpm for 1hr. The intensity of the transmitted light through the NE is based on the movements of the droplets under the centrifugal force. The final transmission profiles of the emulsions as a function of time and height of samples in the cuvettes give an indication of kinetic stability of the NEs under accelerated gravitation.

3.3. Results and discussion

3.3.1. Influence of mixed surfactant concentration on synthesized NEs

NEs were prepared with mixed surfactants initially dissolved in the aqueous phase at mixed surfactants (SDS and Tween 80) concentration varying between 0 and 10 vol. % (with a fixed concentration of 0.1 vol. % for SDS). At low mixed surfactants concentration (i.e., 2.5 vol. %), large droplet size was observed because of high interfacial tension and coalescence of oil droplets, which is supported by a low zeta potential value. With an increase in surfactants concentration, a decrease in droplet size was observed due to a significant increase of interfacial area and reduction of interfacial energy, which in turn reduced the IFT [211], denoting less coalescence of oil droplets and an increase in the NE. The droplet size decreased from 250 nm to 200, 150, and 22 as the surfactant concentration increased from 2.5 vol. % to 5, 7.5, and 10 vol. %.

Results of zeta potential for mixed surfactants at the different concentrations studied were also shown in Table 3-1. All NEs showed negative charge with increasing Tween 80 concentration, which was not an expected result. These negative values of zeta potential may be due to the ability of oil-water interfaces to preferentially adsorb hydroxyl ions from water or due to the presence of anionic impurities in the oil or surfactant [212,213]. Samples showed an increase significantly of zeta potential absolute values from −26 to

−32 mV as Tween 80 concentration increased. NE stabilized with 10 vol.% of mixed surfactants showed zeta potential value over -30 mV, so these NEs could be considered stable; however, these results cannot guarantee NE stability, since there are other factors that affect the emulsion stability, as droplet size and distribution, interfacial tension reduction, environmental conditions, etc. [214].

In order to further investigate the co-adsorption of both surfactants at the oil/water interface, the time variation of xylene/ water interfacial tension was monitored (Figure 3-2). An IFT value of 38.31 mN/m was obtained by the pendant drop method at zero surfactant concentration, that was, between xylene and water. From Figure 3-2, the IFT values decreased with an increase in surfactant concentration. The decrease of IFT as increasing surfactant concentration can be related to faster surfactant adsorption to the oil-droplets surface. The interfacial tension for the sample with 2.5 vol. % surfactants decreased from 30.39 to 12.81 mN/m within a period of 240 s before the values became almost constant. Similarly, for the other three NE samples with 5, 7.5, and 10 vol. % concentrations, IFT decreased from 28.8 to 8.85 mN/m, from 22.8 to 5.75 mN/m, and from 20.7 to 1.9 mN/m, respectively, within a 240 s.

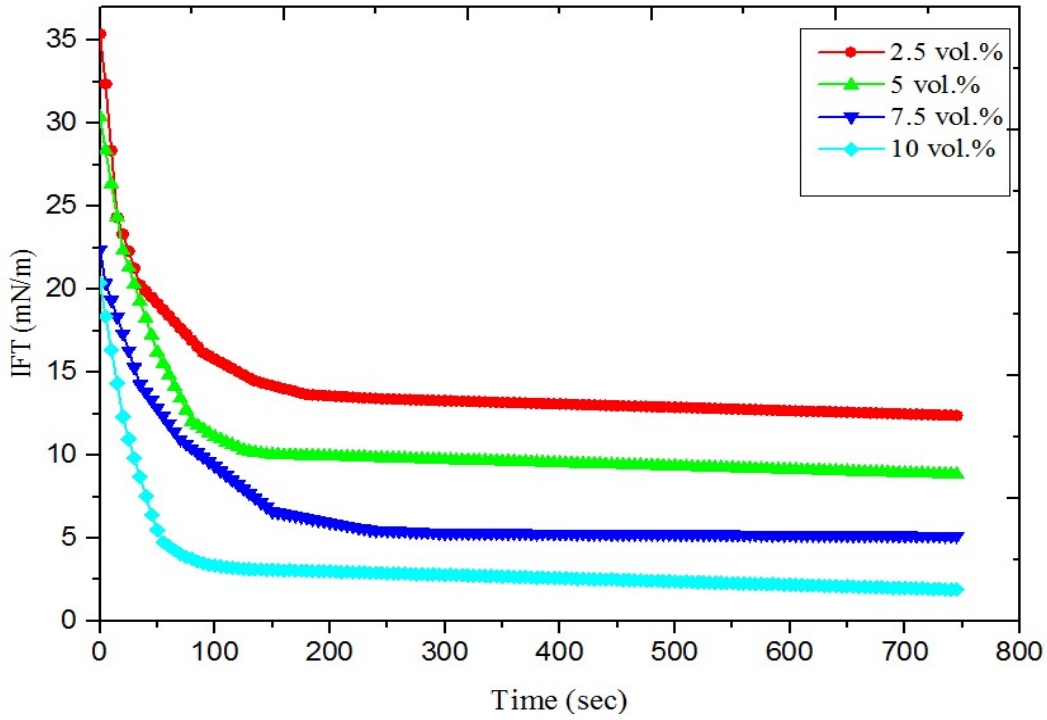

Figure 3-2. Variation of interfacial tension of the formulated NEs at different mixed surfactants concentrations.

Another significant effect was related to the storage stability of NEs. Adding Tween 80 surfactant in the aqueous phase led to a strong slowing down of emulsion aging (Figure 3-3). For a surfactant concentration of 2.5 vol. %, average droplet diameter increased during the first 100 h and level off around 700 nm over the following 250 h. Similarly, for the other three NE samples with 5, 7.5, and 10 vol. % surfactants concentrations, droplet size increased from 200 to 738 nm, from 150 to 450 nm, and from 22 to 270 nm, respectively, within 300 h time.

Although there are many reports in the literature on the outcome of using one type of surfactants, most are restricted to use mixtures of anionic and non-ionic surfactants. Mixed surfactants can provide a strong interaction at the oil/water interface. In the current study, there are two factors indicating the behavior of SDS and Tween 80 at droplet interfaces, which are discussed here. First, we expect SDS and Tween 80 can pack closely

at the oil/water interface, which may be assisted by attractive interactions between both the tails and the head groups. Note that the interactions between hydrocarbon tails are expected to be via van der Waals or dispersion forces, which become much higher if the tails can approach in close proximity [215]. The primary three hydroxyl groups on the head of Tween 80 may also undergo hydrogen bonding with the sulfate group on the head of SDS, thus serving to bind the adjacent head groups [216]. Due to these interactions, SDS and Tween 80 are anchored at the interface and thereby create a stable interfacial film. It is believed that the attractive interaction at the oil/water interface is the indirect interaction between dodecyl sulfate ions (DS^-) and the oxygen atom of polyethoxylated head group in Tween 80 through the (Na^+) countercations. Sodium ions interact with the (DS^-) ion and Tween 80 simultaneously, probably through the ion-dipole interaction and/or hydrogen bonding between them. The second aspect is the nature of Tween 80, which is largely hydrophilic and water soluble. In fact, its affinity for water is due to the three oxyethylene oligomers present on its head group. These three oxyethylene are also essential for providing steric stabilization to oil droplets and hence preventing their coalescence [217]. As a result, when droplets approach each other, a short-range repulsion (steric barrier) arises due to the presence of three oxyethylene. However, this effect is compromised if the Tween 80 molecules move from the droplet into the aqueous phase, leaving bare uncovered regions at the interface. These uncovered droplets could then undergo destabilization processes, specially Ostwald ripening or coalescence processes.

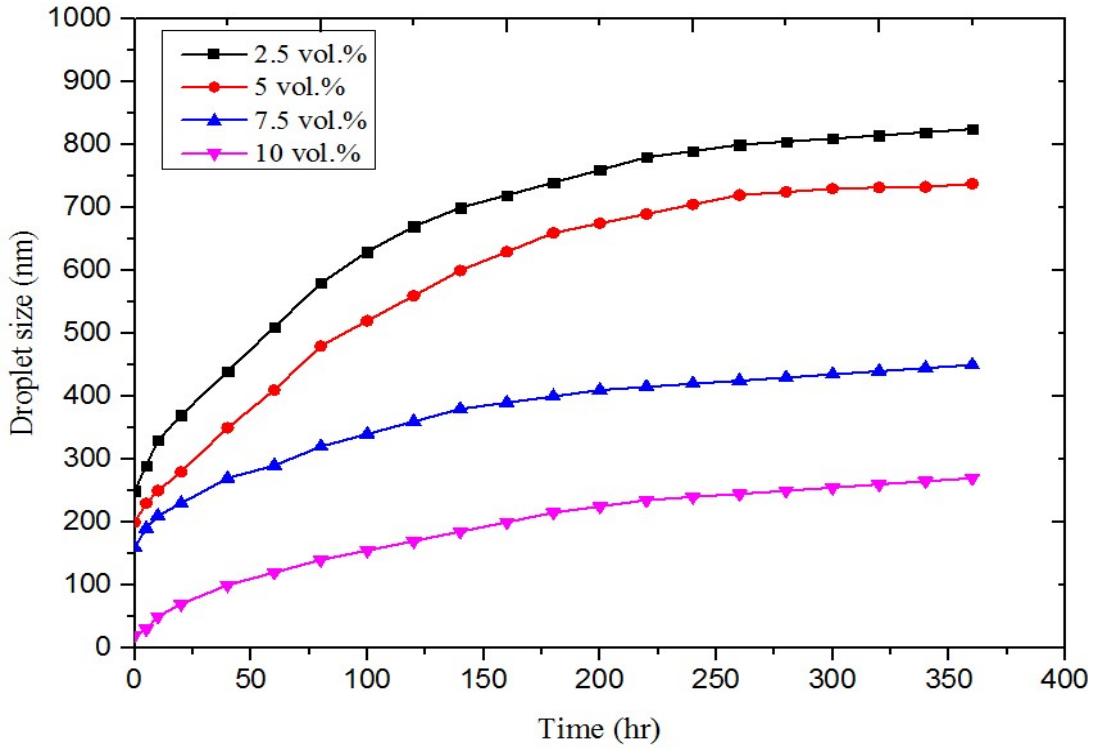

Figure 3-3. Average droplet (nm) as a function of storage time (h) for NEs at different mixed surfactants concentrations.

Table 3-1. Effect of emulsifier type and concentration on droplet size and zeta potential.

			After 1 hr			After 4 weeks		
Mixed surfactants	Tween 80	SDS	d (nm)	PDI	Zeta potential (mV)	d (nm)	PDI	Zeta potential (mV)
2.5	2.4	0.1	250	0.39	-26	825	0.59	-22
5	4.9	0.1	200	0.34	-28	738	0.48	-24
7.5	6.9	0.1	150	0.30	-30	450	0.39	-26
10	9.9	0.1	22	0.20	-32	270	0.30	-28

3.3.2. The effect of the concentration and type of carrier oil

We examined the influence of the concentration of oil phase on the physical stability and characteristic of NE. Different concentrations of oil were used to study the effect of oil concentration on particle size and the physiochemical properties of NE. Figure 3-4 revealed that with increasing oil concentration (i.e, xylene), the sample became turbid. At the concentration of less than 10 vol. %, we got a droplet size NE less than 100 nm. Therefore, all NEs were prepared and stored using oil concentration 7 vol. %. Using a low concentration of oil phase in NE makes the surfactants strongly adsorbed at the oil/water interface and tightly surrounded it. However, increasing the concentration above 10 vol. % leads to alter the physiochemical properties of NE. The viscosity of NE steadily increased and the system became more concentrated when used oil concentration more than 20 vol. %. The viscosity increased from (0.004 Pa.s) at 7 vol. % to reach about (0.0187 Pa.s) at 20 vol. % of the oil phase. The NE appearance became more unstable. However, the density of NE decreased with increasing the concentration of the oil phase.

The results of this study also indicated that the type of oil phase also affects the droplet size and size distribution of NE. Figure 3-5 showed the size droplet variation at using four different oil types. The low viscosity oils such as xylene and cyclohexane showed average droplet size 19 and 35 nm respectively. Whereas, highly viscous oils such as mineral oil and standard oil calibration (ASTM ref. S6) showed a droplet size of 411 and 601 nm respectively. It is possible that the increase in droplet size for NEs with high viscous oils may be attributed to its viscosity. Therefore, the viscosity of the oil phase plays an important role in NE size.

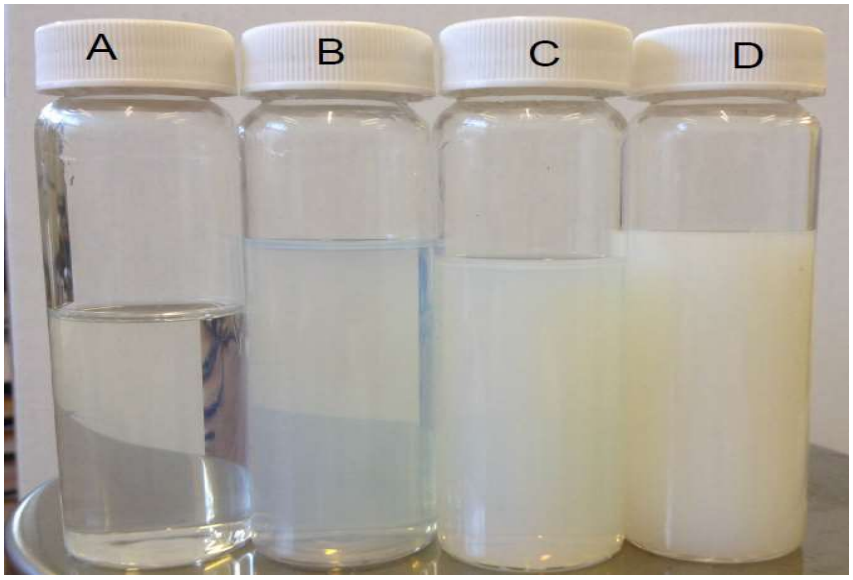

Figure 3-4. Xylene concentrations (A) 7 vol.%, (B) 10 vol.%, (C) 15 vol.%, (D) 20 vol.%

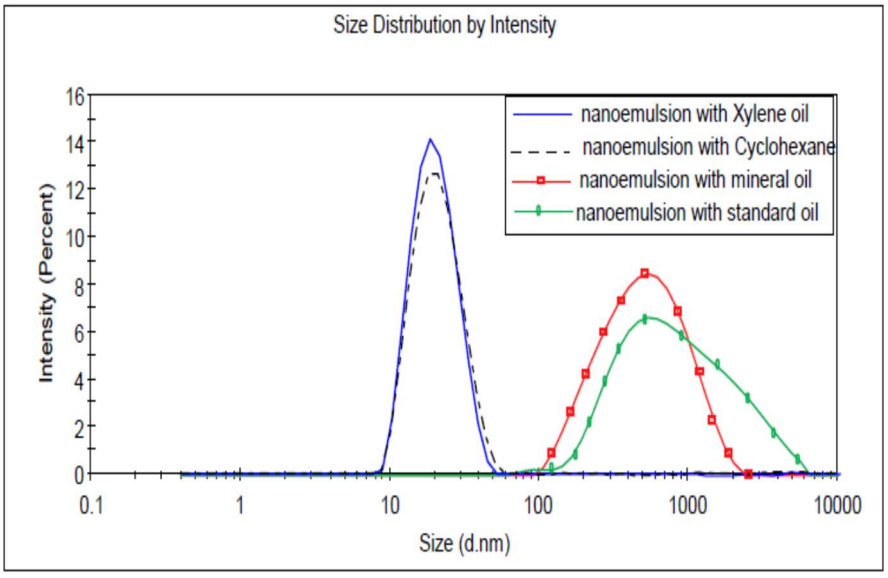

Figure 3-5. The droplet size and size distribution for NE with different oils.

3.3.3. Effect of inhibitor content on the particle size of NE

The effect of AIs loading on the properties of NEs is related to the molecular length and position of AI in the emulsion layer. Table 3-2 summarizes the features of NEs prepared with different added amounts of DBSA and phe. At low concentration of 0.5 vol. %, the AI loading reduced the droplet size of the NE, indicating that the presence of AI may play an important role in softening the phase interface and reducing its curvature then decreasing the droplet size. This effect may also be related to the localization of AI in the hydrophobic core area and provide strong interaction with the mixed surfactants molecules. At increasing of AI concentration to 1 vol. % almost did not vary droplet size values, probably because the saturation of the oil phase by AI molecules as well as the limit for droplets disruption by the sonication process used was already reached. These effects may also be related to the localization of AI in the hydrophobic core area and provide strong interaction with the mixed surfactants molecules. However, at high concentration of AIs, the system became more heterogeneous because the large droplet sizes are formed due to partition of surfactant molecules between the oil and aqueous phases and the molecules may preferentially accumulate at the oil/water interface and this may result in reduction of the Gibbs elasticity, which in turn results in an increase in the Ostwald ripening rate or coalescence [218]. However, the amount of AIs added did not significantly affect the PDI values of the NEs. All NEs exhibited a similar and narrow size distribution with the PDI ranging from 0.208 to 0.218. DBSA-based NEs did not differ significantly on PDI values ranging between 0.17 and 0.18, whilst the NEs with the highest concentrations of DBSA (2 vol. %) showed a higher polydispersity of particle size with values between 0.26 and 0.29. In general, it is considered that PDI values below 0.2 indicate uniformity among droplet sizes or monomodal distributions and therefore good physical stability during storage [219] although this effect not only depended on

particle size distribution, but also on continuous phase viscosity, electrostatic and steric repulsive interactions, density of each phase, etc. [212].

The Zeta potential value is a measure of the electrostatic repulsion of the droplet, and the higher its negative value, the better its stability. Table 3-2 shows that the Zeta potential of NEs was not significantly affected by the AI loading, and all at about -30 mV, which indicates that the NEs had good stability. NEs with an appropriate amount of AI (1 vol.%) gave consistently small droplet sizes compared to the other concentrations used in this study, thus, we have focused more on 1 vol.% DBSA in the rest of the thesis.

Table 3-2. Diameter, PDI and zeta potential of DBSA NEs with different DBSA concentrations.

	DBSA NEs			phe NEs		
Inhibitor concentration (vol. %)	d (nm)	PDI	Zeta potential (mV)	d (nm)	PDI	Zeta potential (mV)
0.0	21	0.20	-32	21	0.20	-32
0.5	18	0.19	-32	18	0.19	-30
1.0	21	0.19	-33	21	0.20	-30
1.5	35	0.26	-32	44	0.29	-29
2.0	93	0.31	-30	102	0.34	-29

3.3.4. Effects of inhibitor loading on the static stability during storage

Turbiscan is one of the most well-known tools for assessing the stability of colloidal dispersions and is used in the present study to investigate the physical stability of DBSA NEs.

Figure 3-6 (A) showed increases in the ΔT and ΔBS of blank NEs at the 3–45mm sample height within 3 days. In addition, in the bottom (0–4 mm) and the top (45–50 mm) layers, the ΔBS values changed with time, and it had a significant change after 3 days (red lines), which meant that an increase in the droplet diameter had occurred probably because of coalescence or Ostwald ripening. In addition, we can observe very easily on Figure 3-6

(A) that the ΔT increases at the bottom of the sample due to a decrease of the concentration of the particles in this part (clarification). This is caused by an increased presence of water at the bottom due to the separation of water from the NEs over time (i.e., phase separation). From the ΔBS, a high increase in signals at the top of the sample is observed. This is due to an increase in the concentration of the dispersed phase (creaming).

For DBSA NEs, Figure 3-6 (B) showed no change in ΔT and ΔBS peaks appear in the bottom of the sample, which meant that the sample was homogeneous with good physical stability. However, phe NEs showed a slight decreasing in ΔBS peaks, this is possibly caused by oil separation and absorbing the light at the top of the sample.

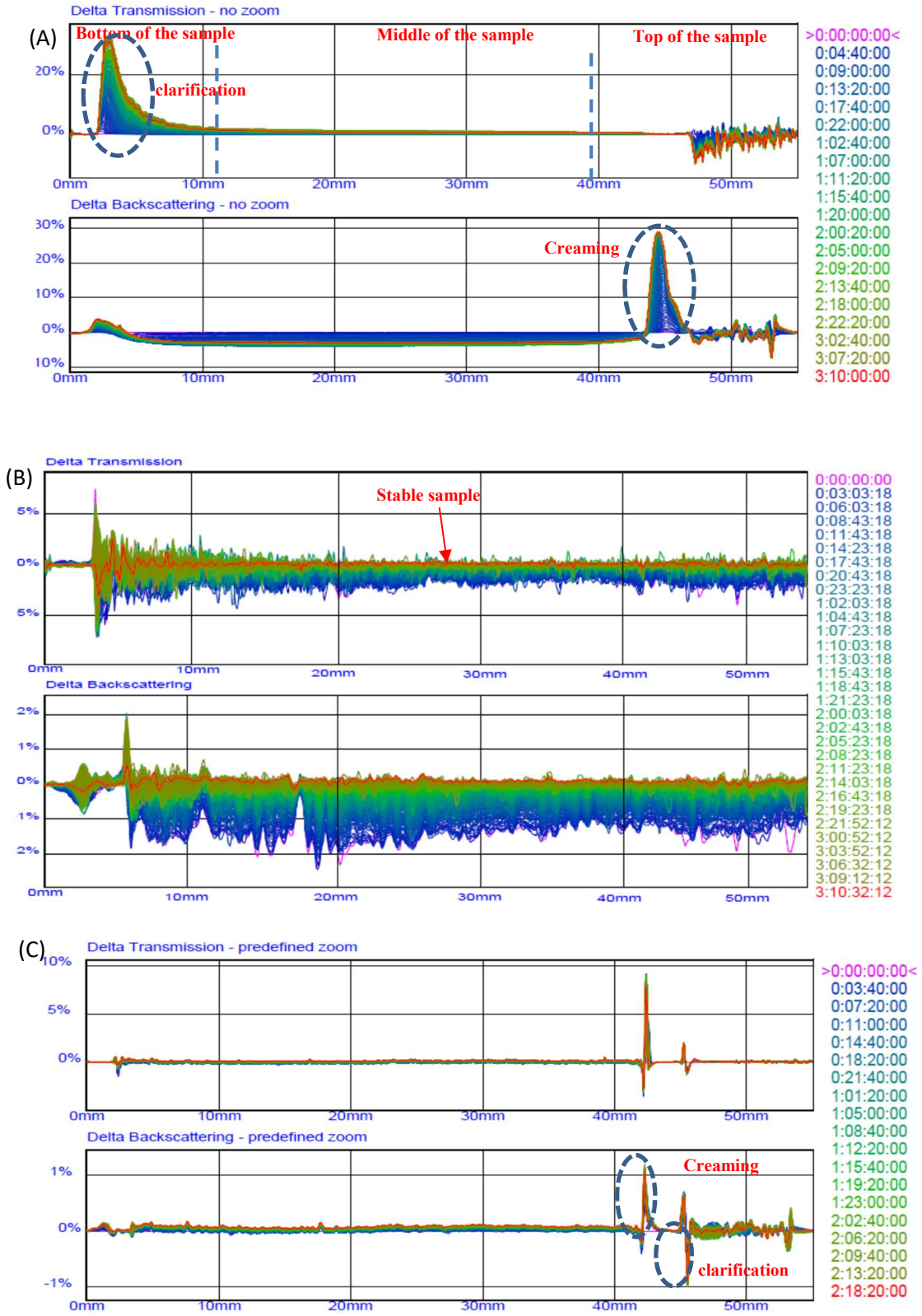

Figure 3-6. ΔT and ΔBS profiles for (A) blank NEs, (B) DBSA NEs, (C) phe NEs during 3 days of the continuous test at 25 °C.

The Turbiscan stability index (TSI) is a measure of the stability of the NEs, and the smaller its value, the better its stability. Figure 3-7 showed the changes in TSI for blank NEs and DBSA NEs, indicated that the TSI value of both samples gradually increased with time, implying that the stability of the NE decreased. However, the stability index for DBSA NEs was smaller than blank NEs. Combined with the results from DLS, it can be concluded that for samples with the presence of DBSA, the DBSA molecules were transported across the interface, and the interaction between DBSA with both oil and mixed surfactants molecules enhanced the packing of the interfacial surfactants, significantly decreasing the mean diameters of the particles and improving the stability of the NEs. Therefore, we can conclude that the stability of NEs was dramatically influenced by the location of the AI and the interaction between the AI with both oil and surfactant molecules.

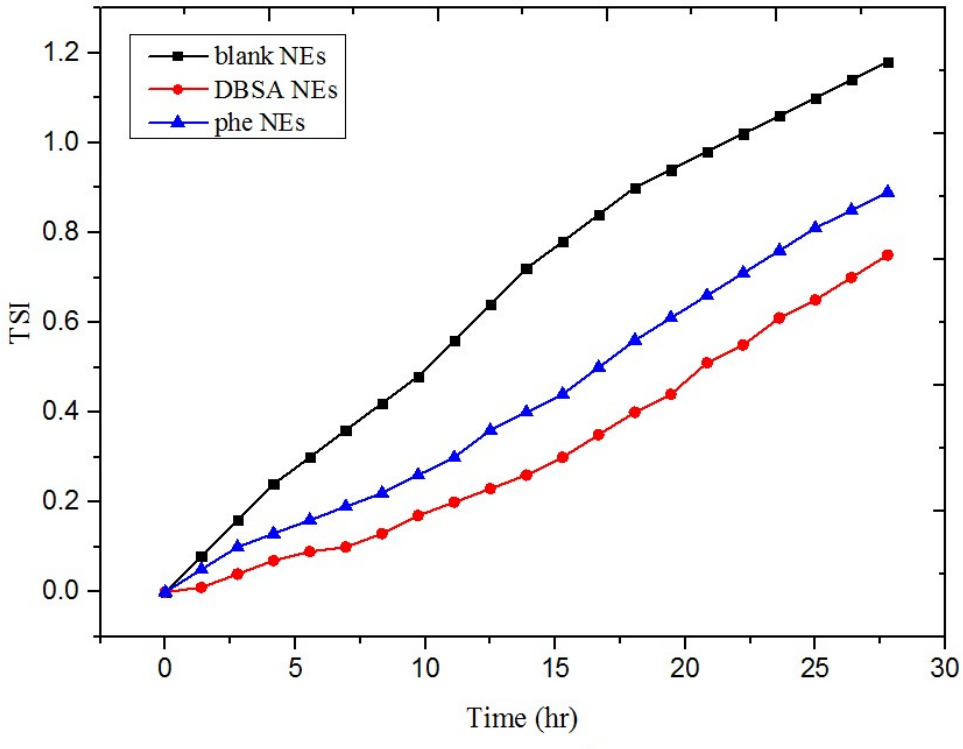

Figure 3-7. Turbiscan stability index (TSI) of blank NEs, DBSA NEs, and phe NEs.

3.3.5. Dynamic accelerated storage stability of NE in the presence of AIs.

The accelerated storage stability based on centrifugal force was carried out by using the LUMI-sizer to determine the long-time storage stability and to know which mechanism of the instability is dominating. When the transmission lines are shifted towards the bottom of the cuvette, it indicates the movement of droplets and settles down to the bottom (i.e. sedimentation mechanism). While, when the transmission profile appears on the top of the cuvette, it indicates the movement of droplets towards the surface (i.e. creaming mechanism). Looking at Figure 3-8 (A), as the time of centrifugation started, the oil droplets transferred towards the top forming a cream layer (109 mm). However, in the bottom part of the cuvette, the transmission has been decreased. The drop-in transmission near the end of the cuvette could be attributed to the sedimentation of large droplet aggregations. However, after 4 weeks (Figure 3-8 B), blank NEs showed higher phase separation. It should be noted that both creaming, and sedimentation occur. This could be due to the formation cream layer resulting from moving droplets towards the top of the sample. Creaming usually leads to coalescence of droplets that causes the destabilization of the emulsion, whereas both DBSA NEs and phe NEs showed no phase separation even after 4 weeks of storage, indicating a longer storage period (Figure 3-8 C, D, E, and F). There was no sign of creaming action in the stored sample denoting the slow recoalescence rate of oil drops because of continuous Brownian motion of the smaller droplets. This behaviour is in agreement with all dynamic stability studies in the current study.

In order to get a proper comparison of NEs long term stability it necessary to quantify the transmission profiles. Instability index, calculated from the ratio of clarification due to phase separation to the maximum possible clarification, was used to compare the accelerated stability of the NEs. Instability index is a dimensionless number between 0

and 1, where 0 represents no change in transmission usually meant higher stability; whereas, 1 indicates complete sedimentation or creaming and hence meant lower stability. In Figure 3-9, the lowest value of instability index was shown for DBSA NEs and phe NEs compared with blank NEs, which showed the highest instability index. It can be concluded that the DBSA NEs were the most stable and it showed remain stable without any measurable phase separation for a long time.

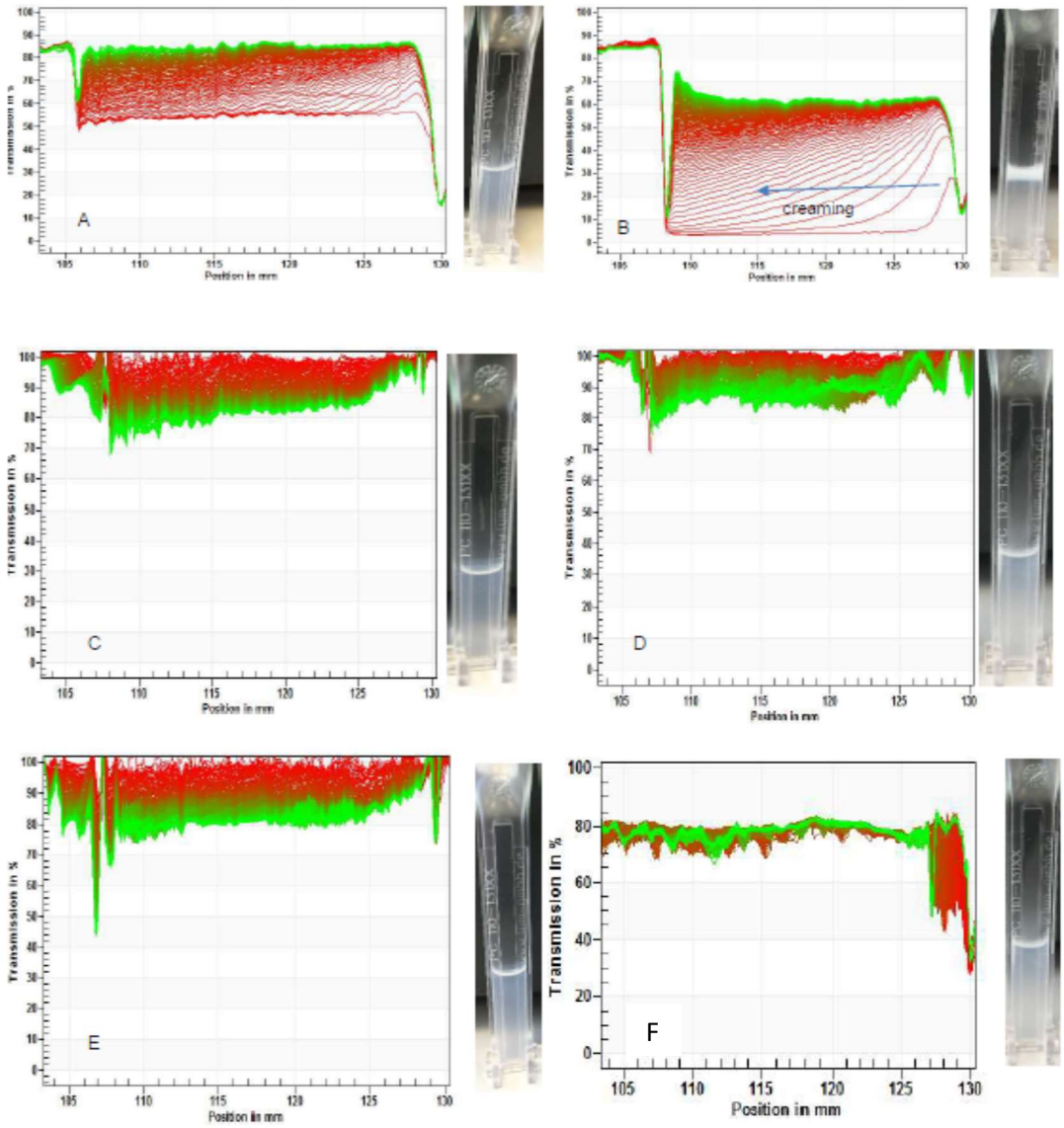

Figure 3-8. Transmission profiles as a function of length of (A) blank NEs after 1 hr, (B) blank NEs after 4 weeks, (C) DBSA NEs after 1 hr, (D) DBSA NEs after 28 day, (E) phe NEs after 1 hr, (F) phe NEs after 28 day.

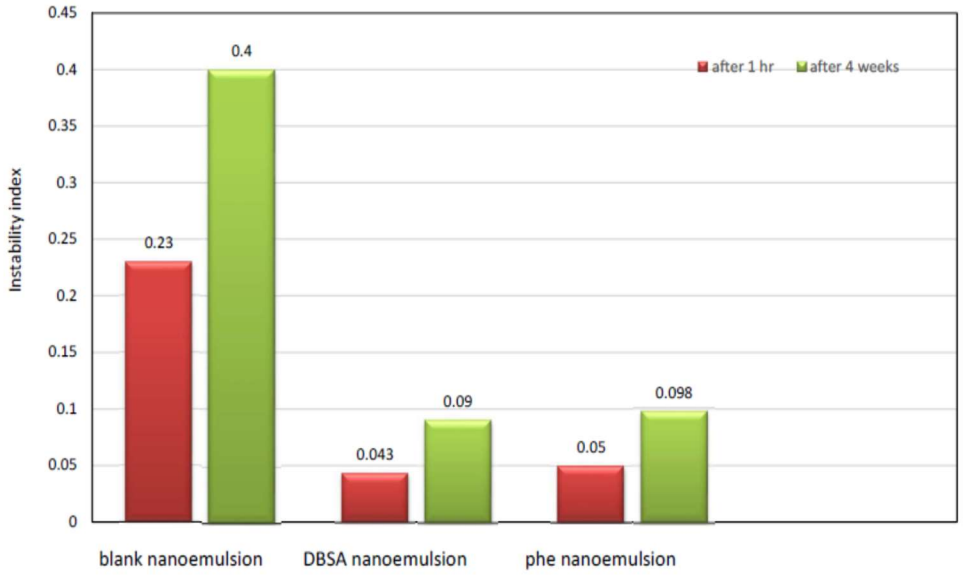

Figure 3-9. Instability index for NEs with and without AIs.

3.3.6. Rheological behaviour and characteristics of the oil-in-water NE

3.3.6.1. Viscometry (viscosity-shear rate relationship)

The purpose of the rheology study is to present the general principles of rheology, to discuss the relationship between the rheological characteristics of NEs and their colloidal properties. The rheological behaviour of NEs in the range of shear rates (0 - 1000) 1/s at 25 °C was illustrated in Figure 3-10. There is an increase in viscosity with the presence of AIs at lower shear rate due to a sharp increase of intermolecular entanglement in the solvent. The entanglement translates to increased shear stress and more pronounced pseudoplastic behaviour. It is obvious that NEs systems exhibit a non-Newtonian flow character for all samples and the viscosity strongly depends on shear rate. NE with AI has high viscosity values even at a high shear rate which indicates it has the potential to improve the mobility ratio that signifies the suitability of the NE in enhanced oil recovery (EOR) application. Shear-thinning behaviour of NEs at high shear rates is favourable during the injection process, as there is a decrease in viscosity at higher shear rates which

results in an increase in injectivity [220]. Furthermore, high consistent viscosity values are desirable when NEs moves deep into the reservoir at low shear rates, thereby improving mobility control and recovery efficiency [221].

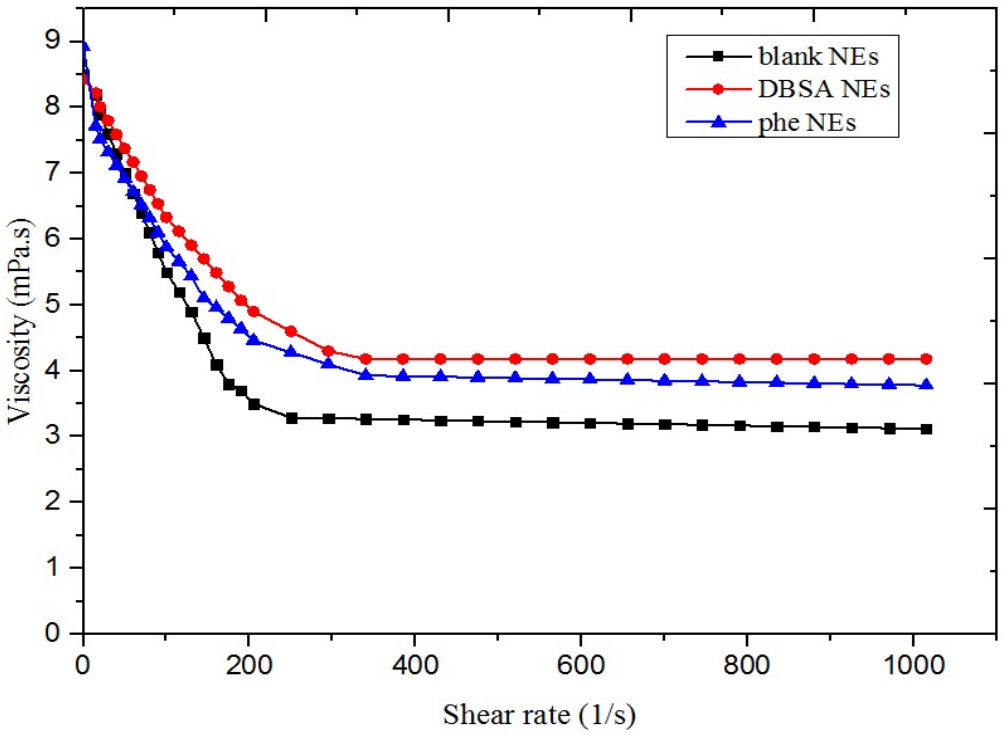

Figure 3-10. The variation of shear rate with viscosity for blank NEs, DBSA NEs, and phe NEs.

The flow curves plotted in Figure 3-10 were fitted with the power law model. The power law is usually used as a model for materials of non-Newtonian behaviour:

$$\sigma = k\,\lambda^{n} \qquad \ldots\ldots. (3\text{-}5)$$

where *k* is the consistency index and n is the flow behaviour index. Power law model can describe Newtonian, shear-thinning and shear-thickening behaviour, depending on the value of the flow behaviour index, *n*. For a Newtonian material, n is equal to 1, and the equation reduces to the Newtonian model. If n is less than 1, the fluid is shear thinning, whereas if it is greater than 1, then the fluid is shear thickening (dilatant). Therefore,

according to the power law model, all analyzed NEs are of shear-thinning nature, where the viscosity decreases with increasing the shear rate [222]. The values of n and k increase with the presence of AIs in descending order was: DBSA NEs > phe NEs > blank NEs denoting an improvement in rheological behaviour of NEs and a rise in viscosity. Thus, Power law model is essential in understanding the non-Newtonian flow behaviour of NEs solution at any desired concentration. The experimental data at 25 ˚C were fitted and analyzed with the help of the above model as shown in Table 3-3.

Table 3-3. Determination of rheological model parameters using the power law model.

Sample	20 vol. % blank NEs		20 vol. % DBSA NEs		20 vol. % phe NEs	
Modeling parameters	k	n	k	n	k	n
	0.067	0.824	0.147	0.882	0.101	0.872

3.3.6.2. Oscillatory measurements: frequency sweep profile

Oscillatory experiments were conducted to determine the dynamic moduli (G′ and G″) of the NEs with and without AIs. Storage modulus G′ is the elastic component, which indicates the amount of energy stored; while loss modulus G" is the viscous component, which indicates that the amount of energy dissipated through a generated heat. During fluid deformation, both behaviours (elastic and viscous) of the fluid are required for dynamic modulus determination. The variation of dynamic modulus with frequency is shown in Figure 3-11. Initially, for smaller values of frequency, the storage modulus (G′) values for all NEs are much smaller than the loss modulus (G″) suggesting the viscous behaviour of the emulsion. However, the storage modulus increases rapidly as compared to loss modulus with a rise in frequency, implying NES exhibit viscoelastic properties.

This suggested that not only these NEs spread easily but also their storage stability was reasonably high [223]. Looking at Figure 3-11, G′ and G″ values for NEs loaded AI are much larger than G′ and G″ for blank NEs, signifying the NEs exhibit viscoelastic properties.

The storage and loss modulus intersect each other with a further increase of frequency values. The intersection points of G′ and G″ is known as the specific frequency (SF) or cross-over frequency which indicates the transition point between the elastic and viscous phases. The value of specific frequency is helpful in signifying the point of transition between the elastic phase and viscous phase of the sample [224]. The SF values for all NEs in ascending order was: DBSA NEs > phe NEs > blank NEs. Therefore, a frequency lower than SF, the dominance of G″ can be observed indicating liquid-like behaviour. Whereas, for frequency greater than SF, elastic component G′ was the guiding factor and became more active than the viscous factor indicating solid-like behaviour. The G″ values for the NEs became almost constant after SF denoting better injectivity of the emulsions [223]. Therefore, the viscoelastic property of emulsion strongly depends on the type of AI used.

However, it was hard to judge whether the elastic behaviour NEs dominated over their viscous behaviour as a function of frequency dependence on dynamic moduli alone. A better way as to how these NEs behave under a small amplitude oscillatory shear can be found by the investigated frequency dependence of phase angle (δ) [225]. Figure 3-12 shows that the values of the phase angle of these NEs were lower than 45, it was evident that the solid-like elastic property dominated in these NEs over their liquid-like viscous property. The phase angle δ decreases from a value of 68 (viscus region) to a value of

about 6.2 and 10.5 (elastic region) for both DBSA NEs and phe NEs respectively, indicating that DBSA NEs and phe NEs are more stable than blank NEs.

Both elastic/viscous behaviour and phase angle for NEs revealed a higher prominence of elastic over viscous behavior (more stable) because of the synergy between mixed anionic/non-ionic surfactants and AI which may arise from hydrophobic interactions between the hydrophobic tails, hydrogen bonds between hydrophilic groups, and aromatic-aromatic interaction of molecules and hence produce DBSA NEs and phe NEs that are stable for long-term.

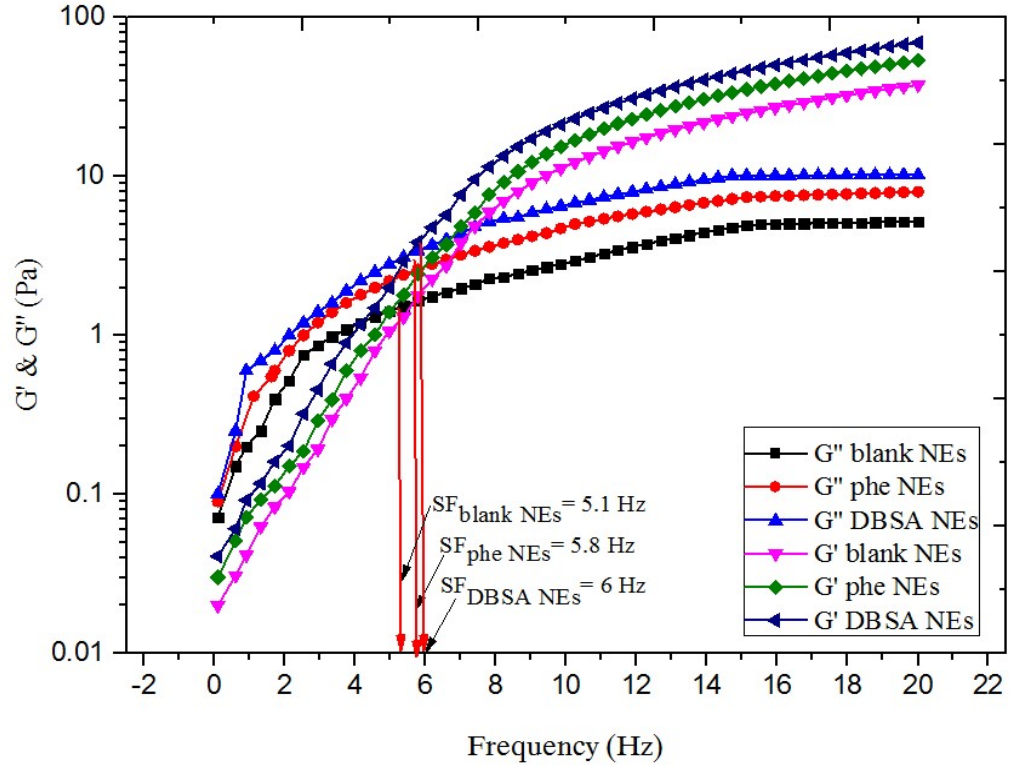

Figure 3-11. The elastic and viscous modulus for blank NEs, DBSA NEs, and phe NEs at t= 1 h storage.

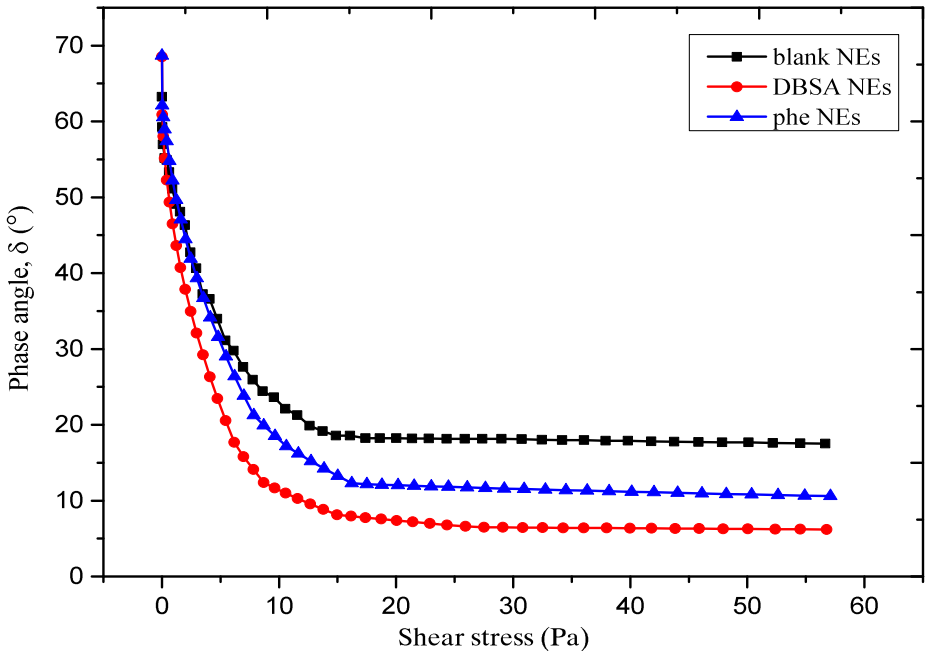

Figure 3-12. Phase angle variation with shear stress for blank NEs, DBSA NEs, and phe NEs.

3.3.7. Effect of DBSA loading on the structural properties and stability mechanism of NEs

In the present study, the intermolecular force between AI and other NE's components were investigated using FTIR spectroscopy in the wave range from 4000 to 400 cm^{-1}. In order to investigate the interaction between DBSA with mixed surfactants inside NEs, about 25 vol. % of carbon tetrachloride (CCL_4) was added to blank NEs. CCL_4 is often used as a solvent in FTIR spectroscopy to determine the free (uncomplexed) species (i.e., when it is used the spectra shows OH free) [226]. The hydrogen bonded OH band initiated at 75 vol. % of blank NE in carbon tetrachloride that is the starting point of the formation of hydrogen bonding of blank NE molecules. Looking at Figure 3-13, it is apparent that blank NEs showed broad strong absorption band centred at 3365 cm^{-1} and this can be attributed to the formation of hydrogen-bonds of interlayer water molecules with hydroxyl groups of non-ion of Tween 80 and SDS as well as the peak of free OH bond at

3606 is appeared due to the addition of carbon tetrachloride. However, for the DBSA NEs, the peak of free OH bond at 3606 disappears and the intensity of hydrogen-bonded OH at 3365 cm^{-1} is increased, which suggested that DBSA had been successfully encapsulated in the NEs [222, 225]. The C=C bands of DBSA NE molecules had also increased, and two new vibration bands, possibly related to the incorporation of DBSA, was found at 1345 cm^{-1} and 1030 cm^{-1} for sulfonic acid and sulfoxide respectively. Overall, these suggested that DBSA can only be in the hydrophobic core area and leads to hydrogen bonding of free OH groups in the DBSA NEs. In addition, the integrated areas under the IR spectrums of NEs with and without DBSA were calculated after curve deconvolution and normalizing to quantitatively evaluate any alteration. These results indicate that addition of DBSA increases the integral from 4.09 to 5.76, demonstrating that DBSA forms hydrogen bonding with a blend of surfactants (i.e., synergistic effect).

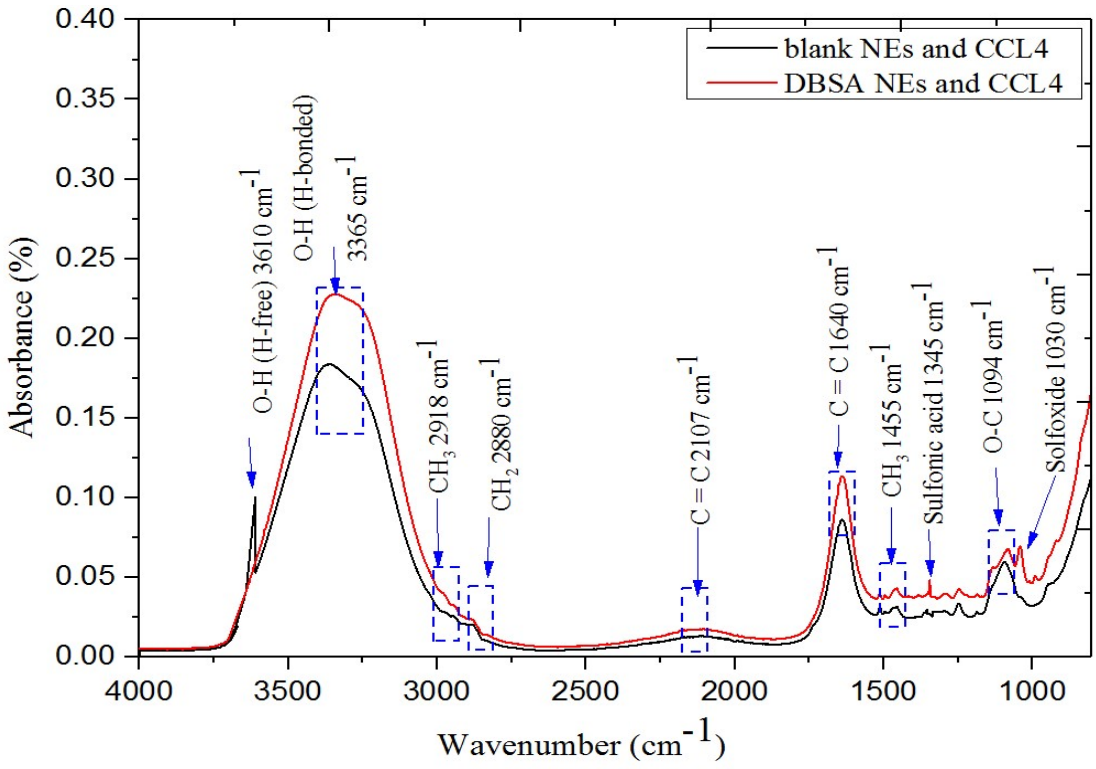

Figure 3-13. FTIR of blank NEs with 25 vol. % of carbon tetrachloride and DBSA NEs.

The overall trend of blank NEs stability is justified by the electrostatic repulsive effect due to the negative zeta potential values and the steric repulsions due to the presence of three oxyethylene side chains in Tween 80, which prefer to be surrounded by the solvent rather than interpenetration when droplets meet. As well as the synergistic effect of anionic/non-ionic surfactants is provided to pack tightly on the droplet surface. However, blank NEs undergo a growth process of droplets with time. A possible explanation for this is that Tween 80 molecules have an affinity for water due to the three oxyethylene oligomers present on its headgroup. Therefore, the Tween 80 molecules are likely to transfer from the droplet into the aqueous phase, leaving bare uncovered regions at the interface. In addition, the oil phase with relative solubility in the water phase, it has greater mobility between droplets [226]. Due to transport and diffusion of oil droplets into the water phase, the droplet size becomes larger over time. As a result, the droplet size increases with storage time.

However, addition DBSA to the organic phase makes it oil-rich or more insoluble in the continuous phase. Due to its long chain tail group and sulfonic acid group, this contains hydroxyl group that causes poorly soluble in water. During adding the continuous phase to the oil phase (xylene and DBSA), the spontaneous curvature of mixed surfactants (anionic and non-ionic) adsorb at the oil/water interface. Therefore, some of DBSA molecules adsorb at oil/water interface whereas the surplus is trapped in the oil phase due to its low affinity towards water. However, NE with DBSA may undergo electrostatic interactions, together with hydrophobic, hydrogen bonding, or acid-base interactions between DBSA and ionic/non-ionic surfactants that may enhance the binding of the DBSA to the stabilized NEs. Since Tween 80 molecules have an affinity for water and leave bare uncovered regions at the interface.

Immediately DBSA which trapped in the core of the oil droplet will adsorb on oil/water interface thereby it will cover the regions at the interface. The most interesting finding is that the DBSA NEs are more stable than blank NEs due to the synergistic effect between DBSA and blend of ionic/non-ionic surfactants as well as the long tail which makes oil phase low soluble in water.

The presence of phe in NE, the interactions between three aromatic rings of phe and aromatic ring in xylene are controlled by π-π interactions (aromatic-aromatic interaction), which play an important role in the binding interactions of both phe and xylene. Since phe is insoluble in water and the thermodynamic gradient may drive them out from the water and hence reduces the oil phase of NE to be soluble in water for the long term. In other words, phe and xylene molecules tend to clump up together rather than distributing itself in a water medium, because this allows the phe and xylene molecules to have minimal contact with water. Figure 3-14 shows the mechanism of NEs stability with and without AIs.

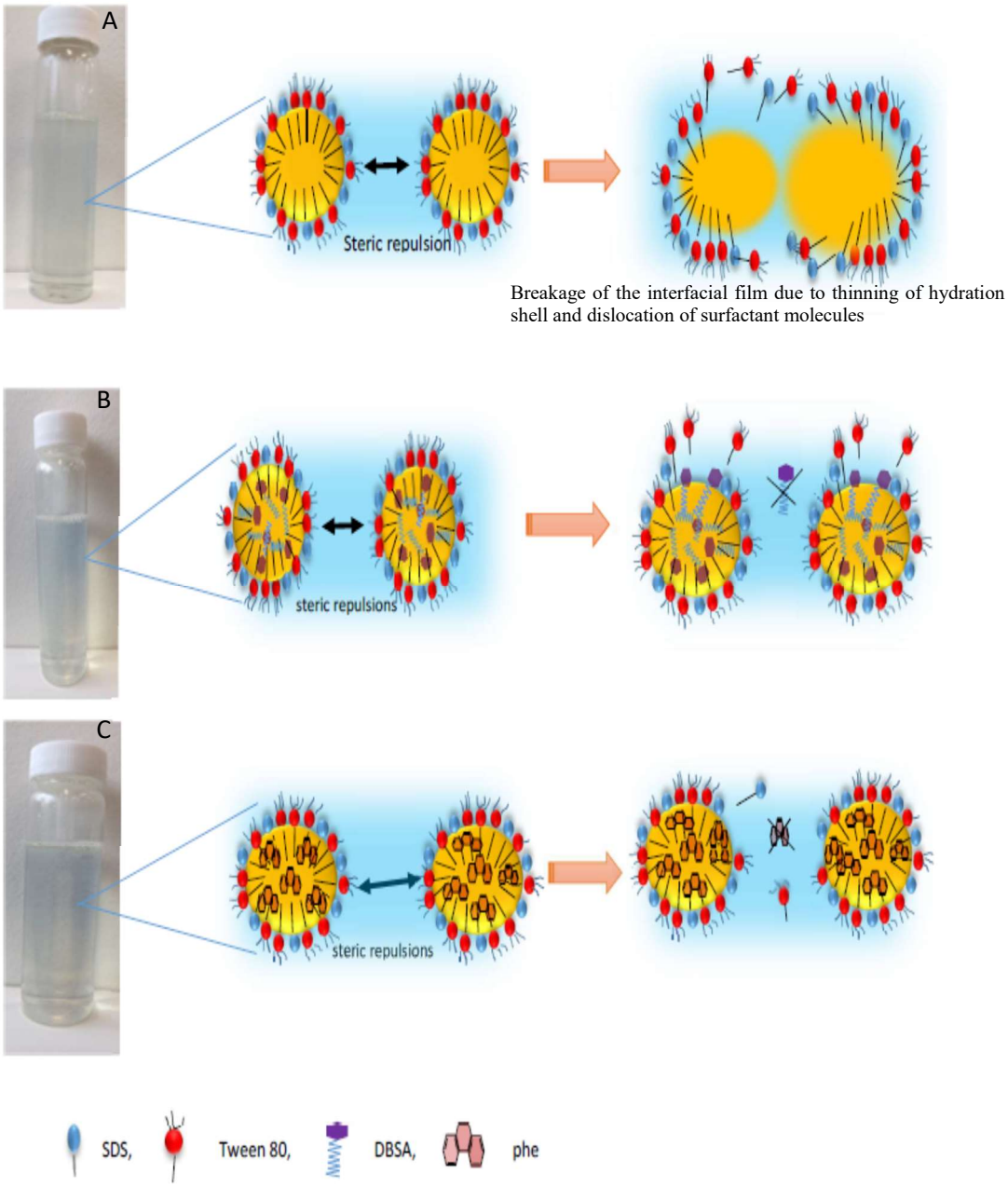

Figure 3-14. The mechanism of stability of NEs. (A) blank NEs, Tween 80 and SDS are shown to pack tightly at the surface of an oil droplet, Tween 80 stabilizes droplets by steric repulsions due to its oxyethene side chains. (B) DBSA NEs, DBSA molecules stay entrapped in the oil droplet because it has low water solubility, which makes it unfavourable for the molecules to diffuse through water from one droplet to another. (C) phe NEs, phe can provide good solubility in the oil phase and very strong intermolecular interaction with oil.

3.4. Chapter summary

This Chapter investigated the physical stability of the NEs in the presence of AIs (DBSA and phe) with high interaction between surfactants and oil phase. The results showed that:

- The type of mixed surfactants, type of oil phase, and the content of AIs are important parameters to fabricate stable NEs.
- For the blank NEs, a cream layer was formed after 4 weeks' storage or after undergoing centrifugal force. However, when AIs were introduced and put under the same condition as the blank NEs, no cream layer was produced. The NEs were remained visually homogeneous with an only slower increase in droplet size. Both static and dynamic studies revealed that inhibitor-reinforced NEs were more stable than the blank one.
- DBSA provided slightly higher stability than that of phe due to the interactions via hydrogen bonding, acid-base interactions and the presence of long chain tail group that dissolved in the oil phase. While for phe, the interactions via π - π stacking between three aromatic rings in phe and the benzene ring in xylene are dominated.
- Stable viscosity values with shear thinning nature indicated better mobility control of NEs.
- Both dynamic and static physical stability also showed that a coalescence process and Ostwald ripening were the main instability mechanism for all NEs.

Chapter 4

Controlled Releases of Asphaltene Inhibitors by Nanoemulsions

4.1. Introduction

From the literature review in Chapter 2, one of the greatest challenges related to asphaltenes is the instability, which results in precipitation in reservoirs, wells and facilities, severely impacting the oil production quality and economics. This work proposes a novel concept to encapsulate and control the release of asphaltene AIs by using NEs, which could i) improve the stability of the asphaltene, ii) reduce the usage of AIs, and iii) extend the treatment time via a slow release of AIs. As an example study, a conventional AI, dodecyl benzene sulfonic acid (DBSA), is used as model AI. The effect of asphaltene stability and controlled release effect via NEs are examined by the centrifugal method in three case studies, i) with pure inhibitors (DBSA), ii) with blank NEs, and iii) with NE loaded with DBSA (i.e. DBSA NE).

4.2. Experimental and methods

4.2.2. Preparation of oil-in-water NEs

The procedure of preparation of oil-in-water NEs with and without DBSA is illustrated in Section 3.2.2. The composition of the dispersions used to prepare blank NEs were at a concentrations of 7 vol.% xylene (oil phase), 10 vol.% mixed surfactants (9.9 vol.% Tween 80 and 0.1 vol.% SDS), and 83 vol.% deionized water, while DBSA NEs were composed of: 1 vol.% DBSA, 7 vol.% xylene, 10 vol.% mixed surfactants, and 82 vol.%

deionized water. Figure 4-1 (A and B) shows the images of DBSA, blank NE, and DBSA NE solutions.The droplet size for blank NE, and 1 vol. % DBSA NE were about 20 and 22 nm respectively.

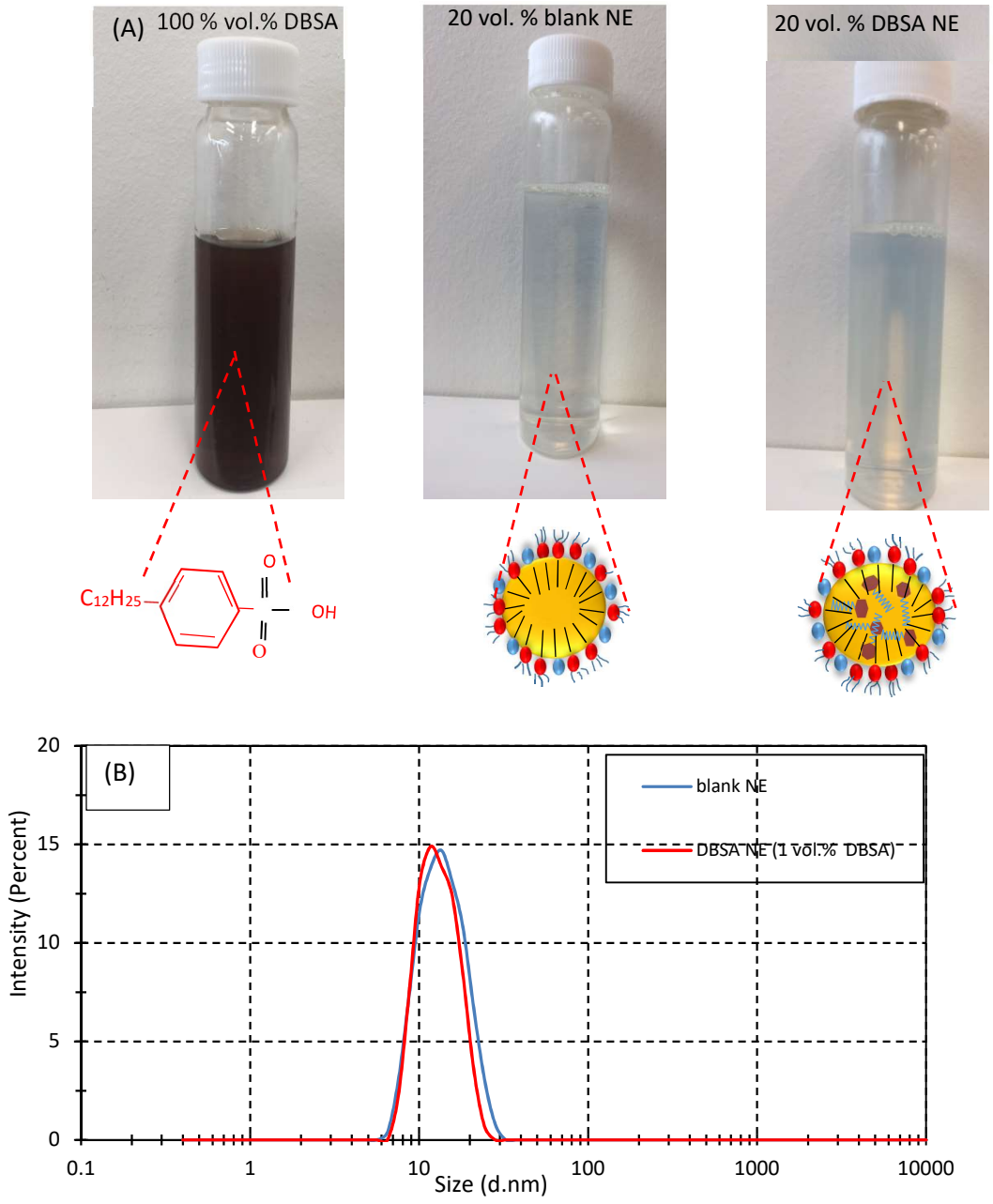

Figure 4-1. (A): The images of DBSA, blank NE, and DBSA NE solutions; (B): Droplet size for blank NE, and DBSA NE (containing 1 vol. % DBSA).

4.2.3. Asphaltene extraction and characterisation

The separation of asphaltenes was carried out according to ASTM D2007 by mixing crude oil with n-heptane at a volume ratio of 1:40, which is known to destabilize asphaltenes and to give rise in asphaltene precipitation [227]. The mixture could equilibrate after stirring and left overnight at room temperature. It was then filtered under vacuum using 0.2 µm pore size Whatman filter paper. Next, the filter cake was repeatedly washed with n-heptane to remove any resins until the effluent from the filter became colourless. Finally, the asphaltenes were recovered from the filter cake by dissolution in toluene and then dried after toluene evaporation. The asphaltene solution containing 0.5 w/v % of the asphaltene was prepared in a mixture of two solvents: toluene and n-heptane (Heptol), in different portions, which will be detailed below. FTIR allows investigating the functional groups present in a sample. The elemental composition (C, H, N, O, S) of asphaltene were determined by Elemental Analyser (CHNS-O). Figure 4-2 shows a schematic of asphaltene extraction and preparation of asphaltene solution.

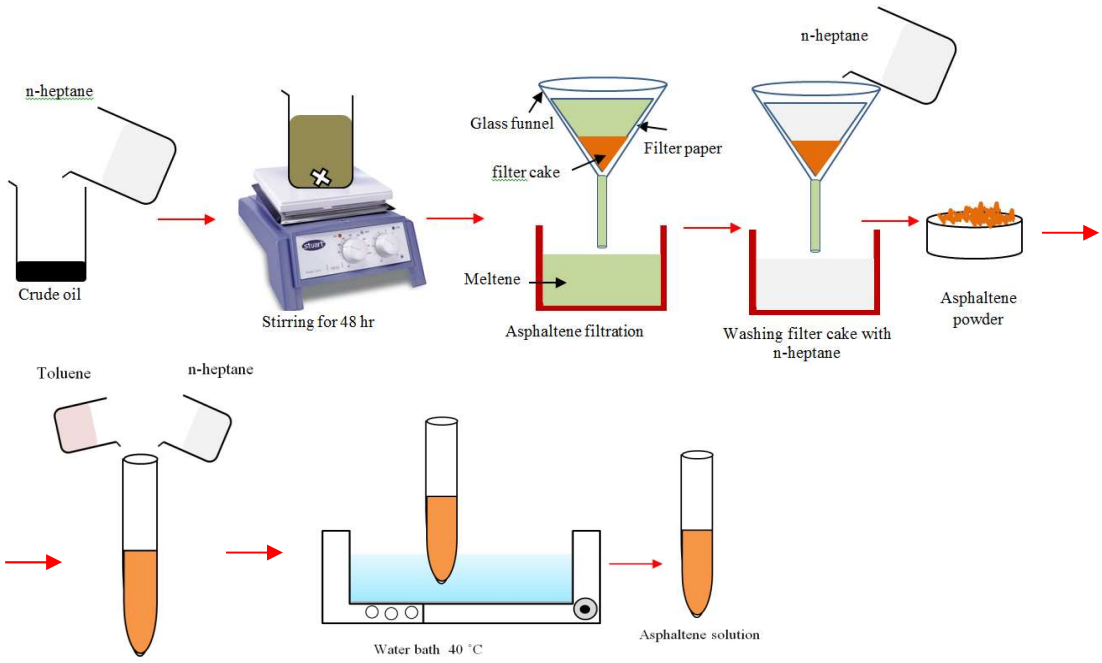

Figure 4-2. Schematic of asphaltene extraction and preparation of asphaltene solution

4.2.4. Separation analysis

Sedimentation (precipitation) analysis was performed by an analytical centrifuge (LUMiFuge, LUMiSizer; LUM, Germany). In each measurement, 400 µL of the asphaltene solution (asphaltene in 60:40 Heptol) was pipetted into a polycarbonate transparent cell with a 2 mm path length. Real-time transmission profiles across the sample were recorded at certain time intervals during the centrifugation. The sedimentation velocity was determined.

4.2.5. Optical and electron microscopy

The morphology of the asphaltene particles was examined using dynamic optical imaging (Malvern Instrument Morphology G3S Microscope (Instrument AG, Renens, Switzerland)).

A transmission electron microscope (FEI Titan Themis Cubed 300 TEM) operated at 300 kV was also used. Prior to TEM analysis, samples were dispersed on a TEM grid (holey carbon film, 400 Cu Mesh from Agar Scientific). Chemical compositions of asphaltene solutions were analysed using an Oxford Instruments INCA 350 energy dispersive x-ray spectroscopy (EDX) with 80mm X-Max SDD detector, within the FEGTEM instrument.

4.3. Results and discussion

4.3.1. Analysis of asphaltene

Asphaltenes are composed of fused benzene rings with aliphatic chains, heteroatoms (O, N, and S), and metals (Fe, V, and Ni) [228]. In asphaltenes, oxygen exists mostly in OH groups and can be found in peripheral aromatics or in aliphatic chains. Nitrogen can be found in pyrolic (5-member ring) or pyridinic (6- member ring) form. Whereas sulfur mostly exists as thiophene (5- member ring), sulfide type groups (RSR), or sulfoxide (RS

(= O) R) [229]. Infrared spectroscopy, which shows characteristic peaks that correspond to the modes of functional groups, is one of the most well-known tools for assessing the structure and functional groups for asphaltene. The current study of using FTIR spectroscopy found that asphaltene molecules consisted mainly of linear, branched, and naphthenic hydrocarbons attached to large aromatic clusters. These results are similar to those reported by Tan et al. [229]. Figure 4-3 shows that the asphaltene sample consisted of aromatic, aliphatic hydrocarbons, sulfoxide, and aliphatic primary amines functions. In the aliphatic, C-H stretch range and CH_3 stretching dominated over CH_2. Table 4-1 shows the functional groups present in asphaltenes obtained from different references using FTIR. One advantage of determining the functional groups and heteroatoms is to understand the mechanism of asphaltene stability by intermolecular interactions between these functional groups and heteroatoms with AI molecules. Table 4-2 shows the properties and SARA analysis (i.e., Saturate, Aromatic, Resin and Asphaltene) of the crude oil, whereas Table 4-3 shows the elemental analysis of the crude oil and asphaltene by the elemental analyzer.

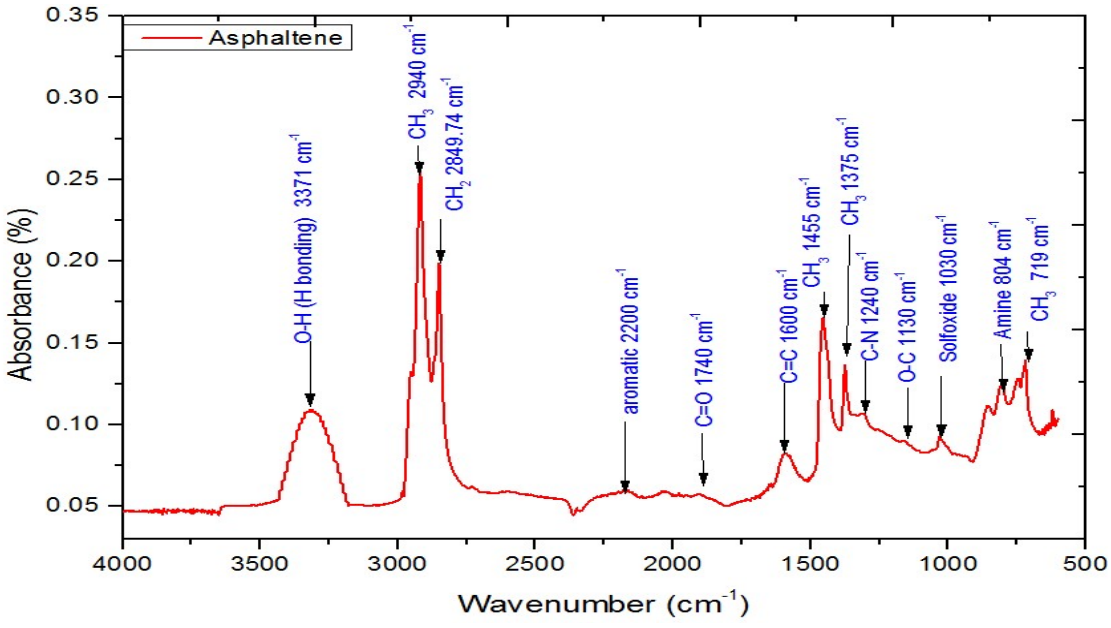

Figure 4-3: Infrared spectroscopy analyses of asphaltene.

Table 4-1: Functional groups present in asphaltenes by infrared spectroscopy.

Functional Group	Absorption Band (cm^{-1})	Ref.
- OH, - NH stretch	3600–3300	[230, 231]
OH-π hydrogen bond	3530	[230]
Self-associated *n*-mers (n >3)	3400	[231]
OH- ether O hydrogen bonds	3280	[232]
Tightly bound cyclic OH tetramers	3150	[233]
OH- N (/base structures)	2940	[234]
COOH dimmers	2640	[235]
Aromatic hydrogen	3050	[236]
Aliphatic hydrogen	2993, 2920	[231]
- CH, - CH_2, - CH_3 stretching regions	3000–2800	[237]
-SH stretching regions	~2500	[234]
C = O	1800–1600	[232]
Keton (C = O stretching)	1735–1705	[231]
Aldehide (C = O stretching)	1740–1730	[230]
Conjugated C = C	1650, 1600	[230]
Aromatic C = C	1602	[233]
-CH, -CH_2, -CH_3 bending regions	1450–1375	[233,237]
Methyl bending vibrations	1377	[232]
Ether or ester group	1306	[231]
Ester linkage	1032	[239]
Sulfoxide groups	1030	[239]
C - S, C - O, C - N stretching regions	~1000	[231,233]
Aromatic C- H bending	900–700	[230]
Alkyl chain longer than four methylene groups	725–720	[231]

Table 4-2: Properties and SARA analysis for the crude oil.

Property of the Crude oil	Value
Density, API	18.96
Density at 20 ºC, g cm^{-3}	0.936
Density at 15 ºC, g cm^{-3}	0.939
Viscosity at 25 ºC, mPa s	76
Viscosity at 50 ºC, mPa s	28
Total acid number, mg KOH g^{-1}	0.47
Asphaltenes, % m m^{-1}	3.6
Resins, % m m^{-1}	15.0
Saturates, % m m^{-1}	54.4
Aromatics, % m m^{-1}	27.0

Table 4-3: Elemental analysis of the crude oil and its asphaltene.

Samples	N (wt. %)	C (wt. %)	H (wt. %)	S (wt. %)	O (wt. %)
Asphaltene	0.80	78.64	7.56	9.04	1.21
Crude oil	0.24	81.15	10.3	2.08	2.03

4.3.2. Asphaltene precipitation test in toluene/ n-heptane mixture (Heptol)

The precipitation of asphaltene involves complex interactions among a variety of intermolecular forces, such as dispersion and van der Waals forces [240]. Gray et al. [241] proposed several mechanisms for asphaltene self-association including acid-base interactions, hydrogen bonding, metal coordination complexes, and interactions between cylcoalkyl and alkyl groups to form hydrophobic pockets driven by van der Waals interactions, in addition to aromatic π–π stacking. They suggested that all of these mechanisms interact to form a complex mixture of asphaltene nano-aggregates, leading to precipitation eventually. In order to find a practical way to prevent or treat potential problems due to asphaltene precipitation, it is necessary to determine the amount of n-heptane, which affects the stability properties of asphaltenes. It has been proposed that the refractive index, which is an indicator of the extent of the intermolecular attractions between asphaltene molecules, is a proper property to describe the asphaltene precipitation from a crude oil-hydrocarbon mixture [242,243]. The refractive index function can be calculated by:

$$RF_n = \frac{(n^2-1)}{(n^2+1)} \qquad \text{……..……. (4-2)}$$

where RF_n is the refractive index function and n is the refractive index.

In previous studies [242, 243], a linear relationship was found between the refractive index function, and the concentration of heptane for toluene/heptane mixture, as shown in Figure 4-4. However, in the present study, the asphaltene with toluene/heptane mixture, where asphaltene particles precipitate out from the solution, a gradual deviation from the linear relationship, Figure 4-5, was observed. This deviation in the refractive index function at high n-heptane concentrations is caused by the formation of asphaltene

particle flocculation and precipitation. Therefore, the point at which a departure from a linear trend on refractive index is observed is defined as the "onset precipitation point". Before the onset, asphaltenes were inherently stable and do not precipitate. This value was then used to calculate the parameters such as solubility blending and insolubility numbers [244] (Figure 4-6). The solubility parameter (δ) was derived by Hildebrand which provides a numerical estimate of the degree of interaction between materials and can be a good indication of solubility, particularly for nonpolar materials [245]. Changing the solubility parameter alters the interactive forces between asphaltenes. Several researchers have adopted the solubility parameter to describe the properties of asphaltene-Heptol systems [246, 247]. A simple method for estimating the solubility parameter of mixtures of hydrocarbons (toluene and n-heptane) makes use of the linear relationship between the solubility parameter and the refractive index function. From the data obtained from Ref. [247], we can determine the solubility parameter at different refractive index function (obtained from Figure 4-4) as shown in Figure 4-6. The solubility parameter for each volume ratio of n-heptane was found to vary from 17.0 $MPa^{0.5}$ at 40 vol. % to 15.6 $MPa^{0.5}$ at 80 vol. %.

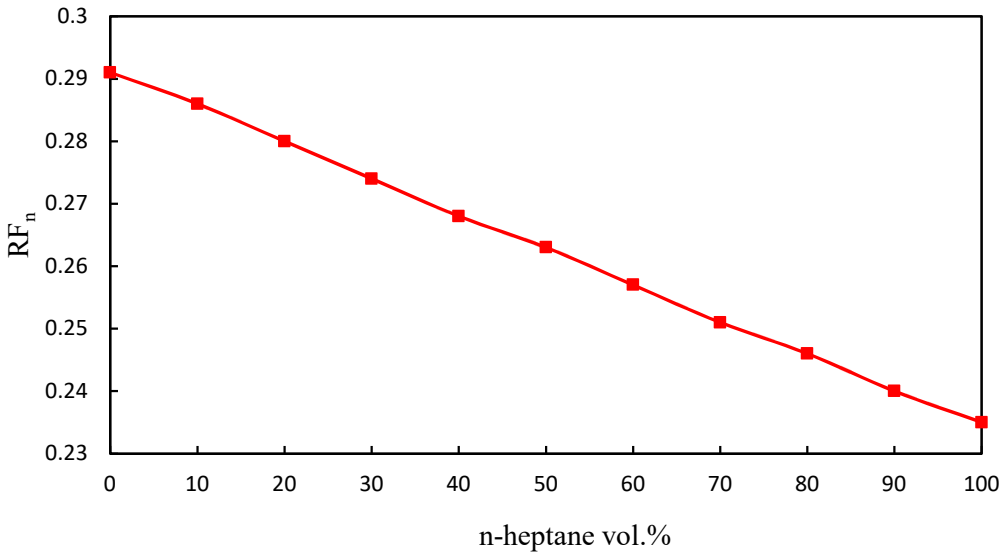

Figure 4-4. The refractive index function for toluene/heptane mixture

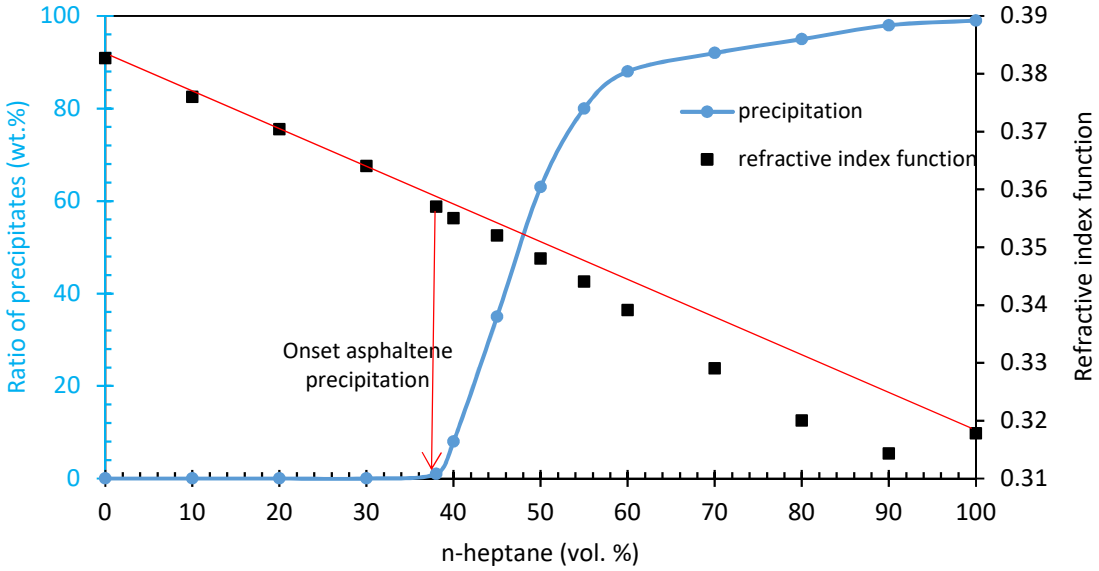

Figure 4-5. Asphaltene precipitation ratio for the asphaltene mixed with n-heptane.

Precipitation onset occurs at 38.2 vol % of n-heptane.

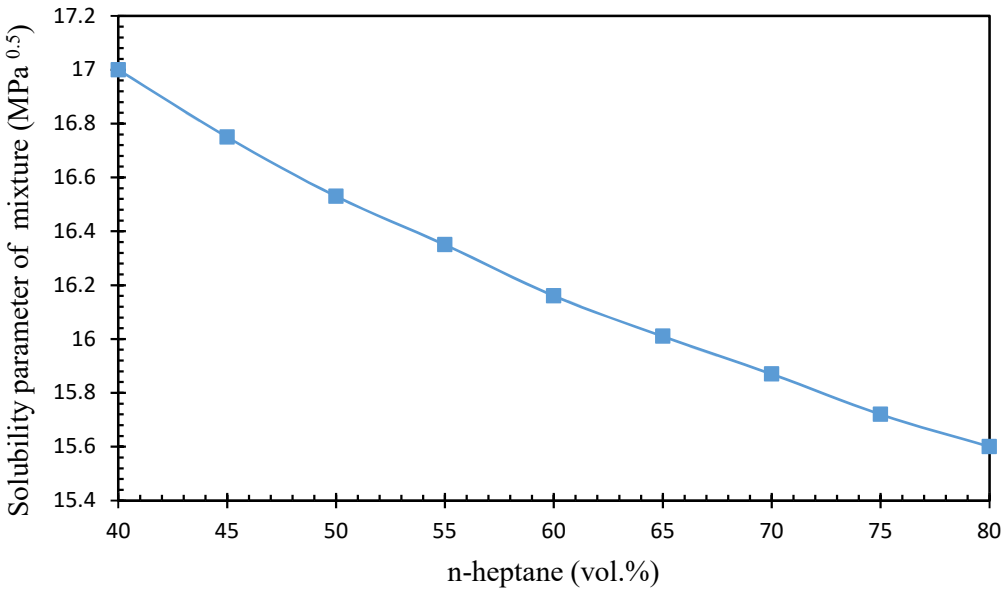

Figure 4-6. The solubility parameter of the asphaltene-heptane mixture at a different volume ratio of heptane.

4.3.3. Asphaltene stability performance by analytical centrifugation

An analytical multi-sample centrifugation technique, the LUMiSizer, has been recently used to characterize the stability of colloidal dispersions for early formulation stability within shorter timescales [248,249]. It works on centrifugal technology and detects changes in the transmitted light across the entire length of the sample. However, this technique has received little attention in the field of asphaltene sedimentation (or precipitation). By observing the asphaltene particles front moving as the sedimentation occurs, it is possible to characterize the stability of asphaltene and determine the optimum concentration of additives which affect the stability. The centrifugation method is adopted in this work to examine the effect of controlled release by investigating the stability of asphaltene particles by three case studies: i) with pure DBSA, ii) with blank NE, and iii) with DBSA NE, as below.

4.3.3.1. Asphaltene stability with pure DBSA

Asphaltene stability and sedimentation velocity with DBSA were investigated first. Sedimentation velocity is an analytical method that measures the rate at which molecules or particles move in response to centrifugal force generated in a centrifuge. From the data in (Figure 4-8 A), the DBSA can enhance the asphaltene stability. The results demonstrate that the sedimentation of asphaltene without DBSA showed high bed sediment from 24 mm (initial uniform dispersion height) to 0.8 mm (packed bed height) within 7 minutes, resulting in a quick formation of aggregation into larger structures, settling faster. It also shows that the sedimentation process decreases with the increase of DBSA concentration until approaching a plateau value. For samples with a concentration $\leqslant$ 4 vol. % DBSA, the asphaltene particles are sterically stabilized by the presence of extended DBSA

molecules on the asphaltene particle surface and the precipitate height is reduced to 0.21 mm within 24 minutes.

It can be explained by the stability behaviour of DBSA-stabilized asphaltene particles, as depicted schematically in Figure 4-7. For asphaltene solution, the asphaltene particles tend to aggregate into larger structures and settle down over a short time, resulting in instability of the asphaltene particles. Under these conditions, the aggregated asphaltene particles initially form a more open particle bed structure under the applied centrifugal field. In contrast, for asphaltene treated with DBSA, the individual particles gradually settle over time and are able to arrange into a very close-packed bed.

These larger mass aggregates, when compared to stable individual particles, settle faster, leading to shorter sediment bed formation time. The observed particle packing behaviour with respect to applied centrifugal force is consistent with other research [250,251], whereby stable particle dispersions form a pressure-insensitive packed bed while aggregated particles have a pressure-dependent network. However, with increasing the concentration of DBSA (i.e., 5 vol. %), the sedimentation only increased slightly, which is due to the self-association of DBSA.

Precipitated asphaltene particles

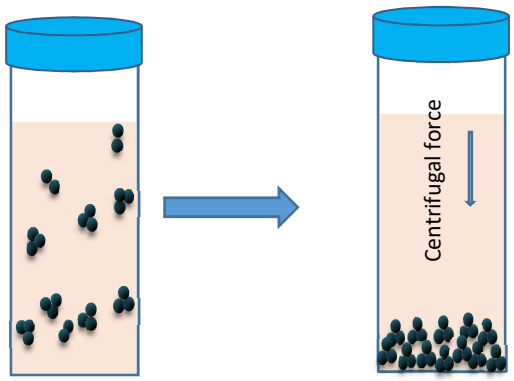

Asphaltene with DBSA (stable asphaltene)

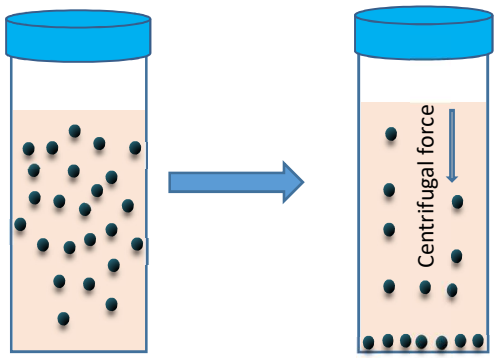

Figure 4-7. Schematic diagram for the effect of the centrifugal field on the sedimentation of (a) aggregated and precipitated asphaltene and (b) Stable asphaltene particles.

4.3.3.2. The effect of NE on asphaltene precipitation

The settling data for asphaltene particles with and without NEs has considered in Figure 4-8 B. It is obvious that the sediment time is seen to progress in a linear fashion with all volume fractions of blank NEs. For samples, with a volume fraction < 20 % (80 µl NE), a transition to a settling regime is seen after a finite time, and only a small change in the sediment height is observed over extended times. At 20 % NE, the rate of settling reduces and the time for sediment consolidation increases, i.e. within 16 minutes. Therefore, these findings suggest that the NEs have a moderate influence on asphaltene stabilization comparing with using the optimum concentration of DBSA (4 vol. %). The stability

behaviour can be attributed to the presence of blank NEs components such as water, mixed surfactants, and xylene that interact with asphaltene molecules.

4.3.3.3. The effect of DBSA NE on asphaltene precipitation

DBSA NE in this study consists of four components: xylene, DBSA soluble in xylene, mixed ionic and non-ionic surfactants (SDS and Tween-80), and water, and the detailed compositions are shown in Table 4-5. NEs with 1 vol. % DBSA remain homogeneous without any observable sediment for weeks and are used for the centrifugation tests, as shown in Figure 4-8 C. It can be observed clearly that with the addition of small volume fractions of DBSA NE (5 and 10 vol. %), the sedimentation height of asphaltene becomes considerably lower than that of pure asphaltene solution. For asphaltene sample with a volume fraction 20 vol. % DBSA NE (i.e., containing 0.8 µl DBSA), there is a significant reduction in the final settling height, which decreases from 0.8 mm to 0.2 mm, and the sedimentation time increases from 390 sec to 1470 sec comparing to pure asphaltene solution. This is indicative of reduced settling velocities of asphaltene particles. A possible explanation for these results is due to the intermolecular interactions between DBSA NE components and asphaltene molecules. It may be assumed that, in this case, the DBSA was progressively released from NE and interact with asphaltene molecules, leading to a slower settling. However, with increasing the concentration of DBSA NEs (i.e., 30 vol. %), the sedimentation only increased slightly, which may be due to the formation of large emulsion droplets.

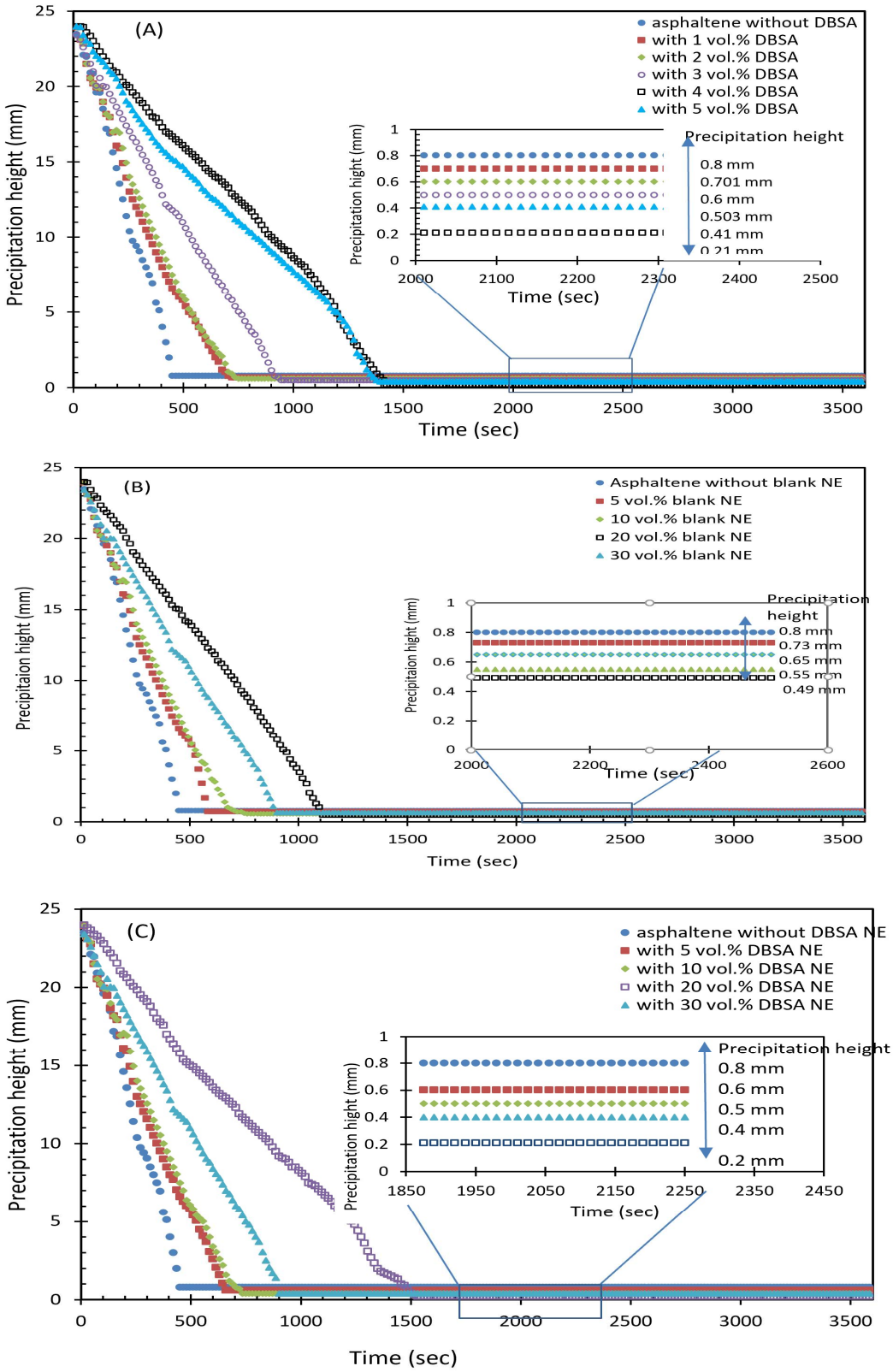

Figure 4-8. Precipitation profiles for asphaltene solution with and without different volume fractions of (A) DBSA, (B) blank NEs, and (C) DBSA NEs. The data indicate the sedimentation rate and the final height of the precipitation.

Figures 4-9 and 4-10 further compare the four cases under the optimum conditions, which shows that asphaltenes treated by 20 vol. % DBSA NE has a similar effect as that of 4 vol. % DBSA. The treatment by 20 vol. % blank NE still has some effect but less strong the other two. The analytical centrifuge technique also allows the determination of an instability index and sedimentation velocity based on the sedimentation behaviour during centrifugation. Instability index is a dimensionless number between 0 and 1, where 0 indicates to the higher stability of the dispersion, and 1 represents complete precipitation of particles and hence lowest stability under the centrifugal field [252-254]. This sedimentation rate provides information about the sedimentation time of particles and hence its stability [255]. To illustrate the effect of DBSA reduction, the instability index and sedimentation velocity are plotted as a function of DBSA volume. Using 20 vol.% DBSA NEs (i.e., containing 0.8 µl DBSA) give nearly the same values of instability index and the sedimentation rate as that of 4 vol.% DBSA (i.e., about 16 µl). Therefore, the amount of asphaltene inhibitor (% R_{AI}) is decreased by 95%. Although DBSA NEs contain different chemicals such as xylene, surfactants, and DBSA, the total chemicals (% R_{TC}) are again lower than 4 vol. % DBSA by a factor of 10%, as shown clearly in the detailed materials balance in Tables 4-4, 4-5, and 4-6. Using NEs for DBSA delivery can significantly reduce the inhibitor and chemical amounts.

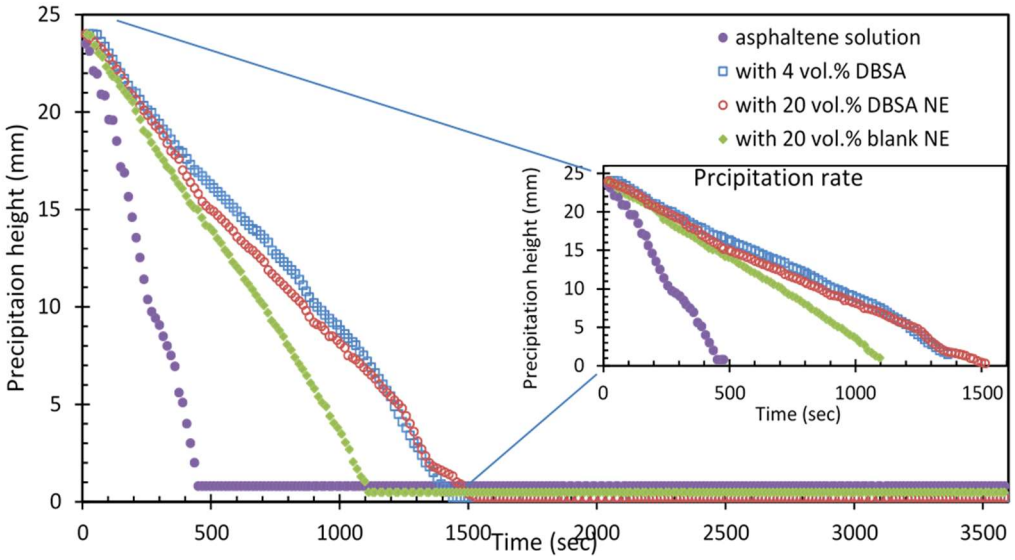

Figure 4-9. The precipitation rate and the effect of optimum concentrations of DBSA, blank NE, and DBSA NE on asphaltene precipitation.

Table 4-4. Volume and volume fraction of DBSA.

DBSA	Vol. DBSA (µL)
1 vol.%	4.0
2 vol.%	8.0
3 vol.%	12.0
4 vol.%	16.0
5 vol.%	20.0

Table 4-5. Blank NE components and material balance.

Vol%. of blank NE	Vol. of blank NE (µL)	xylene vol.%	Vol. xylene (µL)	Tween 80 vol.%	Vol. Tween 80 (µL)	SDS vol. %	Vol. SDS (µL)	Water vol.%	Vol. Water (µL)
5	20	7	1.4	9.9	2.475	0.1	0.02	83	16.6
10	40	7	2.8	9.9	3.96	0.1	0.04	83	33.2
20	80	7	5.6	9.9	7.92	0.1	0.08	83	66.4
30	120	7	8.4	9.9	11.88	0.1	0.12	83	99.6

Table 4-6. DBSA NE components and material balance.

Vol.% of DBSA NE	Vol. of DBSA NE (µL)	xylene vol.%	Vol. xylene (µL)	Tween 80 vol.%	Vol. Tween 80 (µL)	SDS vol.%	Vol. SDS (µL)	DBSA Vol. %	Vol. DBSA (µL)	Water vol.%	Vol. Water (µL)	% R_{AI}*	% R_{TC}**
5	20	7	1.4	9.9	1.98	0.1	0.02	1.0	0.2	82	16.4	98.7	74.4
10	40	7	2.8	9.9	3.96	0.1	0.04	1.0	0.4	82	32.8	97.5	55.0
20	80	7	5.6	9.9	7.92	0.1	0.08	1.0	0.8	82	65.6	95	10.0
30	120	7	8.4	9.9	11.88	0.1	0.12	1.0	1.2	82	98.4	92	< 1

*: $vol.of\ component = \frac{Total\ volume\ of\ sample\ x\ vol.\%}{100}$ ..... (4-3)

**: $\%\ R_{TC} = \left(\frac{Total\ chemicals\ vol.\ withou\ \ NE - Total\ chemicals\ vol.with\ NE}{Total\ chemicals\ vol.\ without\ NE}\right) x\ 100\%$ ..... (4-4)

$\%\ R_{AI} = \left(\frac{vol.without\ NE - vol.with\ NE}{vol.without\ NE}\right) x\ 100\%$ ..... (4-5)

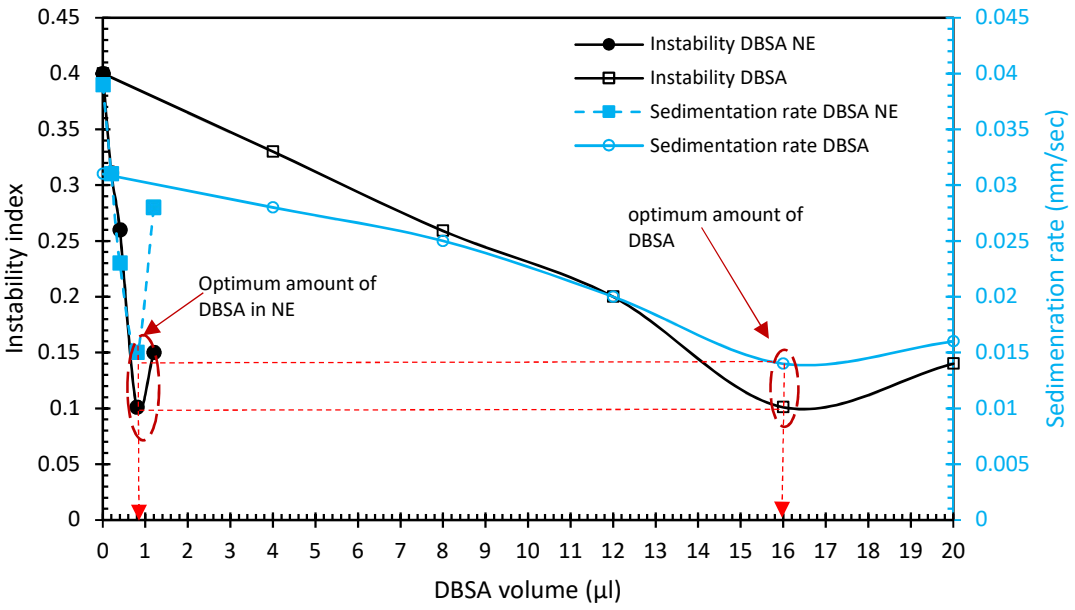

Figure 4-10. Instability index and sedimentation rate for asphalting solution with different amounts of DBSA and DBSA NEs.

4.3.4. Potential asphaltene stability mechanisms

4.3.4.1. Intermolecular interaction between asphaltene and the presence of DBSA NEs.

The DBSA NEs can modify the colloidal structure of asphaltene by promoting the interactions between the asphaltene molecules and the components of DBSA NEs (i.e., DBSA, xylene, surfactants (Tween 80 and SDS) and water). The DBSA is the most important component of DBSA NE and its head group plays a major role in the asphaltene stabilization. Consequently, the presence of sulfonic acid groups ($-SO_3H$) is required for DBSA to effectively interact with asphaltenes. The interaction between DBSA and asphaltenes takes place through the protonation of heteroatoms functional groups in the asphaltenes, which are positively charged, while proton-donor DBSA molecules become negatively charged ions. Hence, this process leads to an ion pair with a strong ionic bonding, able to promote further electrostatic interactions with other ion pairs in neighbouring molecules/aggregates [256-261]. In addition to the DBSA's head group, DBSA's tail length plays a key part in the asphaltene stabilization. DBSA's tail length (12 carbon atoms) can provide a steric-stabilization effect to prevent asphaltenes from aggregating [259]. When the alkyl tail has six carbon atoms or more, this polar moiety becomes sufficiently large to form a stable aliphatic layer to prevent asphaltene particles from aggregation. As the length of the AI tails increases, the steric exclusion effect becomes successively important [257].

The second component in DBSA NE may affect asphaltene precipitation is xylene, which is one of the most effective solvents for asphaltenes [262]. The third component is surfactant; Souza et al [263] suggested that the diffusion of the surfactant molecules to the water/oil interface can reduce the aggregation size of the asphaltene. Therefore, in this study, it was found that the use of mixed surfactants (Tween 80 and SDS) in DBSA NE

can provide good interactions with asphaltene molecules. In addition, water can appear in three different forms in oil systems: solubilized, emulsified, or free water. Non-polar oils dissolve very small amounts of water depending on the saturation limit of the type of oil. Beyond the saturation limit, water becomes either emulsified when surfactants are added or separated as free water [261, 262]. According to Sjöblom et al. [261] and Aslan et al. [262], water delays the precipitation of asphaltene, which could be due to i) water forms a layer around asphaltene and prevents asphaltene from precipitation or ii) water molecules act as a bridge between asphaltene molecules via hydrogen bonds between water molecules and heteroatoms in asphaltenes.

This system can provide very strong and different bonding interactions between asphaltene and DBSA NE components such as acid-base interaction, hydrogen bond, polar-π interaction, cation-π interaction, and aromatic-aromatic interaction. These interactions can promote further electrostatic interactions with other ion pairs. For example, the hydroxyl group in the chain length can form H- bonding with water or surfactants, whereas the nitrogen in the aromatic core can provide acid-base as well as H-bonding interactions with DBSA. Therefore, using a small amount of DBSA (1 vol. %) with other components in the DBSA NEs is sufficient to produce complete coverage of the individual aggregates. Figure 4-11 shows a proposed chemical mechanism for molecular assembly of DBSA NE components: DBSA, xylene, Tween 80, SDS, and water to an active site at the asphaltene molecular structure, through very strong interactions.

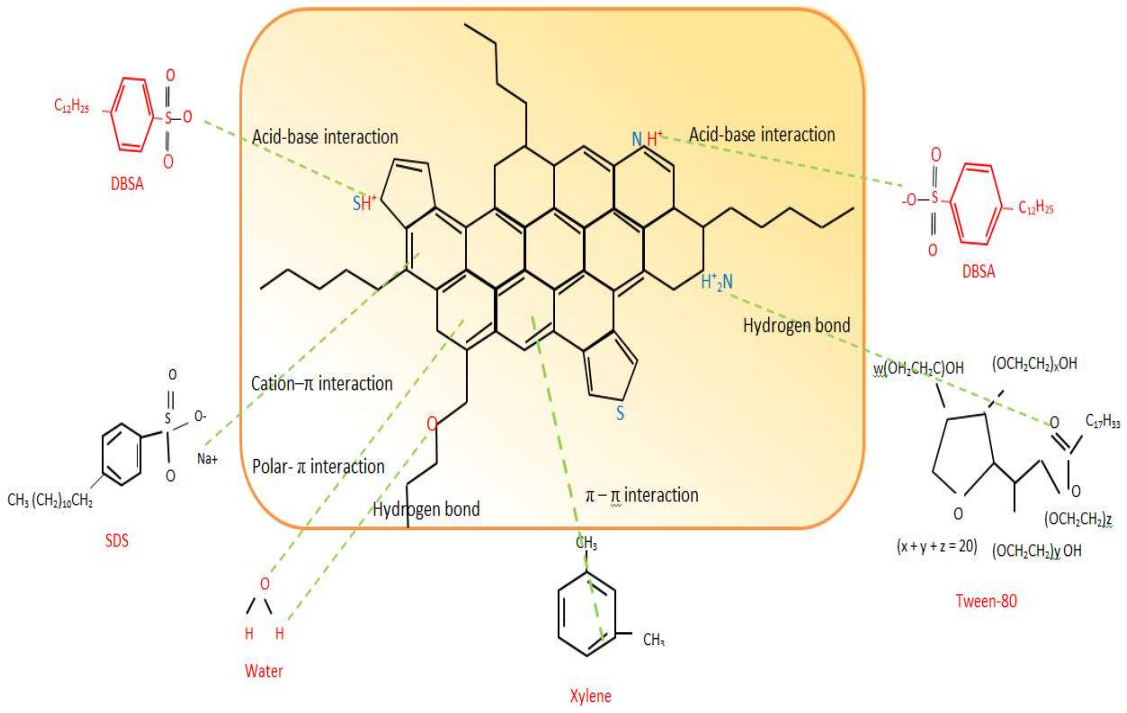

Figure 4-11. Proposed chemical mechanism for molecular assembly shows a schematic attachment of DBSA NE components: DBSA, xylene, Tween 80, SDS, and water to an active site at the asphaltene molecular structure, through very strong interactions, the heteroatomic such as nitrogen, oxygen, and sulfur groups are all protonated.

4.3.4.2. Water/asphaltene dispersion interface in the presence of the NEs.

To evaluate the influence of the blank NEs and DBSA NE and their composition on the asphaltene aggregates/ clusters present at the water/oil interface, the interfacial tension (IFT) was studied. Figure 4-12 shows the IFT for four cases: i) water/Heptol mixture (60:40 vol.%), ii) water with and without surfactants/asphaltene solution (asphaltene in 60:40 Heptol), iii) blank NE/asphaltene solution, and iv) DBSA NE/asphaltene solution. Interestingly, the IFT of water/Heptol was decreased from 28.0 to 22.0 mN m^{-1} when the asphaltenes were added to Heptol.

In the case of using blank NE or 1vol. % DBSA inside NE in asphaltene solution, 1vol. % DBSA did not cause a significant change in the IFT. Thus, DBSA is likely located inside nanodroplets (in xylene) and stabilised by mixed surfactants, which acts as a very good carrier for DBSA. DBSA NEs shows a strong tendency to migrate and adsorb at the water/oil interface due to the large surface area of the droplets and the presence of ionic/non-ionic surfactants, which reduces the IFT to 3.7 mN m^{-1}. This interfacial activity explains the effectiveness of DBSA NE in controlling asphaltene precipitation, as it allows the displacement of asphaltenes from the water/oil interface, thereby stabilizing the asphaltene in solution. Subsequently, DBSA is slowly released and interact with asphaltene molecules.

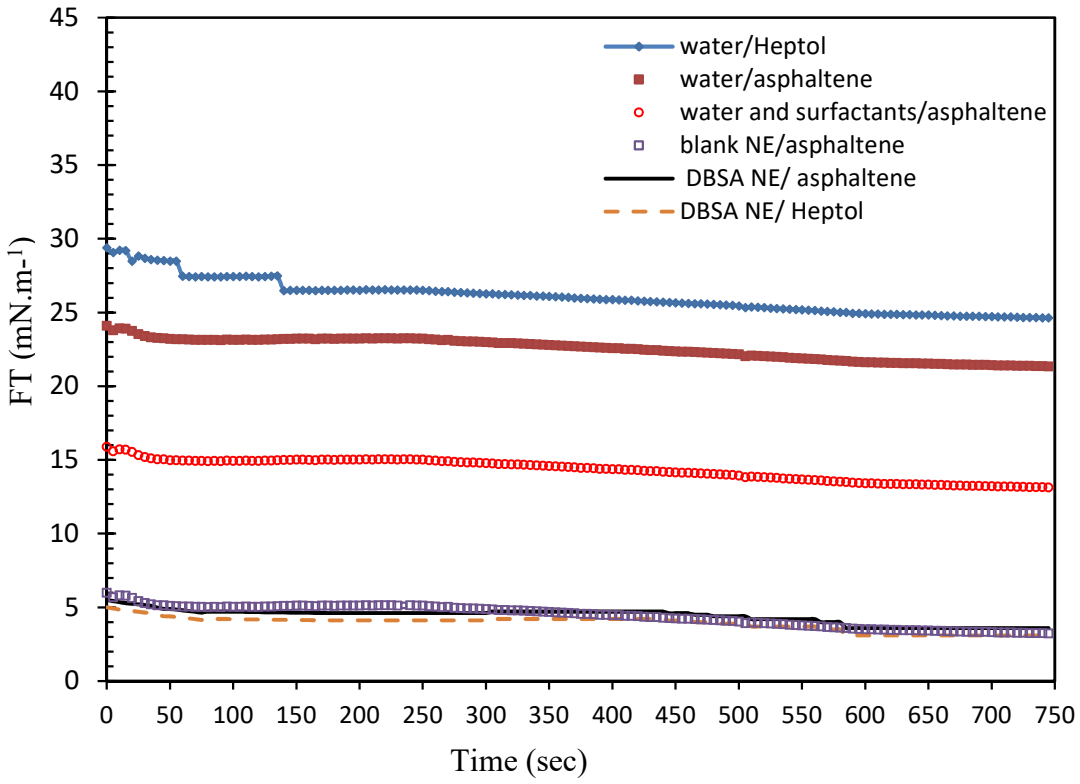

Figure 4-12. Water/oil interfacial tensions in the presence or absence of NEs containing 10 vol. % surfactants with 7 vol. % xylene.

4.3.4.3. Controlled release of DBSA and its effect on asphaltene stability.

Two possible mechanisms can be used to explain the role of DBSA NEs to control asphaltene precipitation in both the oil phase and water/oil interface. The first mechanism may occur in the oil phase (asphaltene in 60:40 Heptol), i.e., the bulk effect. The water phase (oil-in-water NEs) forms a layer around the asphaltene particles. Nanodroplets adsorb on asphaltene particles due to its high lipophilicity and higher affinity to the asphaltene as well as its small size (about 20 nm). Figure (4-13 B) shows the micrograph obtained from morphology G3S microscope for the asphaltene with DBSA NEs before the centrifugation. It is obvious that asphaltene particles are surrounded by the water phase (i.e., containing DBSA NEs). However, very long chains of asphaltene flocculate linked together (like filaments) were clearly observed before centrifugation experiment. When asphaltene with DBSA NEs are centrifuged, the stresses exerted on the asphaltene particles with NEs can be amplified and may make Tween 80 molecules move towards the water phase (i.e., around asphaltene particles) due to its affinity toward the water, leaving the oil droplet uncovered. As a result, the DBSA inside oil droplets can be released to interact with asphaltene particles, hence preventing asphaltene precipitation. Figure (4-13 C) shows the TEM micrographs obtained for the asphaltene with DBSA NEs after the centrifugation, which shows that asphaltenes are formed by nanometric particles having a diameter of around 5 to 30 nm with a large distance in between. The evidence here confirms that the DBSA NEs are able to reduce asphaltene particles from the precipitate and form good dispersion in the medium, due to the effectiveness of DBSA NEs for asphaltene stabilization.

The possible second mechanism occurs at the water/oil interface, i.e. the surface effect, as described in Section 4.4.4.2. Therefore, DBSA NEs (containing DBSA dissolved in xylene) and surfactants can displace all the asphaltenes from the interface via the release

of DBSA and other components from DBSA NEs. Therefore, DBSA NEs interact with asphaltene aggregates/ clusters at the oil/water interface due to the high lipophilicity and higher affinity to the oil than water, which consequently keep asphaltene particles in the solution with smaller average size.

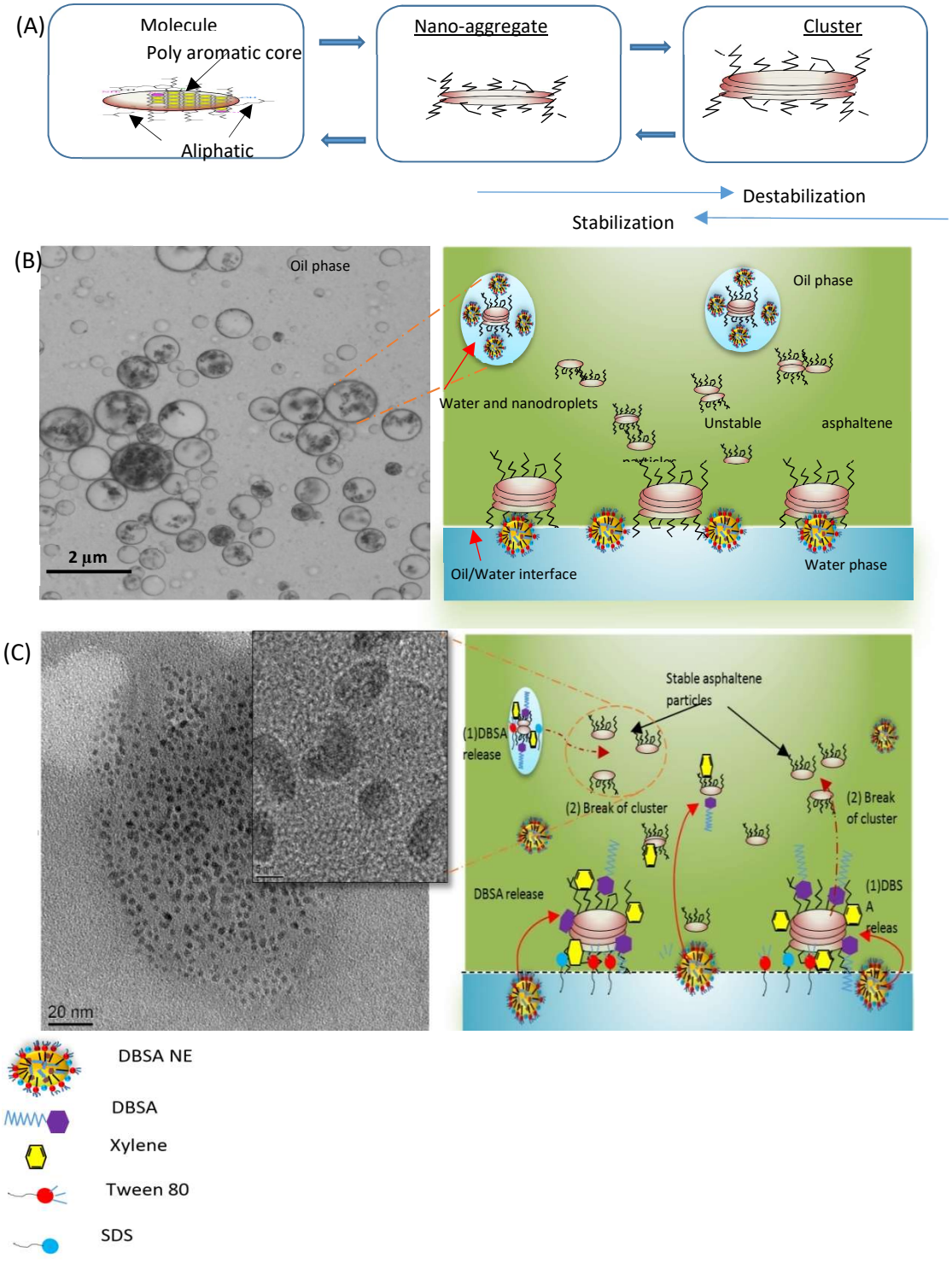

Figure 4-13. The mechanism scheme of (A) asphaltene molecule and formation of aggregates and clusters; (B) G3S morphology micrographs obtained for the asphaltene with DBSA NEs before centrifugation; (C) TEM micrographs obtained for the asphaltene with DBSA NEs after centrifugation and releasing DBSA from DBSA NEs.

4.4. Chapter summary

This Chapter explored the concept of controlled delivery of AIs by using NEs, and validated the concept by centrifugal experiments:

- NEs allowed a significant reduction of inhibitor and chemical amounts in stabilizing the asphaltene. The inhibitor amount and total chemical usage could be reduced by 95 and 10 % respectively compared with the case of using pure DBSA.
- DBSA NEs allowed a significant delay of asphaltene precipitation, i.e., a delay from pure asphaltene solution of 450 sec to 1400 sec in the presence of NEs.
- The presence of DBSA NE also reduced the precipitation thickness of asphaltene up to 75 %.
- The release of DBSA from NE depended on the interactions of surfactants used for the fabrication of NEs, and the subsequent change of the overall polarity and hydrophobic characteristics.
- Both the surface effect and bulk effect were contributing to effectiveness the NE in releasing inhibitors, including the migration of NEs to the water/oil interface and slowly release of chemicals at the interface, and the formation of hydration layers around asphaltene particles in the bulk.

Chapter 5

Kinetic Study of Controlled Asphaltene Inhibitor Release from Nanoemulsions

5.1. Introduction

Continuing our work on the controlled release of asphaltene inhibitor by using NEs, this Chapter provides new evidence from optical measurements and reveals the release mechanisms kinetically. Three case studies are performed on the stability of asphaltene: i) DBSA), ii) blank NEs, and iii) DBSA NEs. The kinetic processes of DBSA transport and release through the dialysis membrane are examined for two cases: NEs loaded DBSA and DBSA directly dissolved in xylene. Those important physical parameters, such as the AI release rate and time, are obtained. Not only providing new evidence to support our previous concept in Chapter 4, but the data are also proceeded and compared with eight established mathematical models, to elucidate the release mechanism.

5.2. Experimental and methods

5.2.1. Asphaltene preparation of solution and characterization.

The separation of asphaltenes was carried out according to ASTM D2007 by mixing crude oil with n-heptane at a volume ratio of 1:40, which is known to destabilize asphaltenes and to give rise in asphaltene precipitation. The procedure of asphaltene extraction was reported previously in Chapter 4 (see Section 4.3). For the preparation of asphaltene solution, a (0.025 w/v %) of the asphaltene was prepared in a mixture of two solvents:

toluene/heptane (Heptol) volume ratio of 60:40. To examine the effect of DBSA, blank NEs, and DBSA NEs on asphaltene precipitation, samples were slowly added to asphaltene solutions under shear action in an (IKA T2S digital/Ultra-Turrax) homogenizer at a rotation speed of 8000 rpm until complete incorporation of the NEs into the asphaltene solution. TEM (FEI Titan Themis Cubed 300 TEM) was employed to the influence of DBSA NEs on the asphaltene particles sizes and the morphology of these particles after the adsorption and slowly release. Prior to TEM analysis, samples were dispersed on a TEM grid (holey carbon film, 400 Cu Mesh from Agar Scientific).

5.2.2. The stability of asphaltene using multiple light scattering

The static stability of asphaltene was evaluated *In-situ* by a Turbiscan instrument (Formulaction, France). The sample in the cell was at level (40 mm), and two types of measurements were carried out: i) whole sample scanning continuously for 15 hours where the change in transmissions with position of sample was recorded, and ii) fixed position scanning where the transmissions as a function of time were measured at 25 mm from the top of the sample. Unstable asphaltene forms particles that precipitate quickly, while stable asphaltene tends to form small aggregates that show small changes in the transmittance profile. Moreover, stability is also assessed by means of the separability number (SN), which is defined as the standard deviation of the average transmittance. A value lower than 5 indicates high asphaltene stability, and greater than 10 suggests that the asphaltene is unstable, whereas a value between 5 and 10 means medium stability [264, 265]. The transmission of asphaltene sample and treated samples are recorded as ($\%T_{asph.}$) and ($\%T_{treated}$) respectively. The asphaltene sample is shaken again on the vortexer such that all the asphaltenes are dispersed in the solution and the transmission is

recorded as 100% dispersion (100% Asph. $_{dispersion}$). The percent inhibition (A.I %) is calculated from transmission measurements as per the equation [266]:

$$\text{A.I}\,(\%) = 100 - \left[\frac{\%T_{treated} - \%\,Asph._{dispersion}}{\%T_{As} - \%\,Asph._{dispersion}}\right] x\ 100 \qquad \ldots\ldots\ldots\ldots\ (5\text{-}1)$$

5.2.3. Asphaltene inhibitor release study

Membrane diffusion (i.e. dialysis) method is considered as one of the most convenient techniques for determining the drug release profiles of nano-sized drug delivery systems like nanoparticles, liposomes, nanosuspensions, emulsions [267-269]. With the same mechanism and methodology, the dialysis bag (12 kDa) was filled with a known amount of DBSA NEs, which was immersed into 300 ml of Heptol/ethanol mixture (7:3 in volume) (i.e., acceptor) [269]. Similarly, DBSA dissolved directly in xylene was also filled into the dialysis bag by adding of 1 vol. % of DBSA in xylene. The release and transport of DBSA from the dialysis bag into the acceptor medium can be accelerated using a magnetic stirrer and was set to 400 rpm to assure constant agitation of the acceptor compartment. A total of 1 ml of sample was collected at a predetermined time interval and an equal volume of acceptor medium was replaced. DBSA was quantified using UV-visible spectrophotometry, at the wavelength of 320 nm, on the basis of a previously prepared calibration curve using the following equation:

$$\text{DBSA released}\,(\%) = \frac{\text{DBSA in acceptor media}}{\text{Total DBSA added}} \times 100 \qquad (5\text{-}2)$$

The existing experimental method for measuring inhibitor release kinetics is shown in Figure 5-1.

Once the profile of released and transport DBSA through the membrane from NEs loaded with DBSA and DBSA dissolved directly in xylene is obtained, different models can be used to fit the results in order to study the kinetics of DBSA released through the membrane between 0 and 24 h. The release kinetics was determined by linear regression

analysis of the release curves in eight models: zero order (cumulative amount (%) of inhibitor released with time), first order (log cumulative amount (%) of inhibitor released with time), Higuchi (cumulative amount (%) of inhibitor released with the square root of time), Korsemeyer-Peppas (log cumulative amount (%) of inhibitor released with log time), Hixon–Crowell, square root of mass, three seconds root of mass and Baker–Lonsdale models [270,271]. The best-fit kinetics model was selected based on the highest coefficient of determination (R^2).

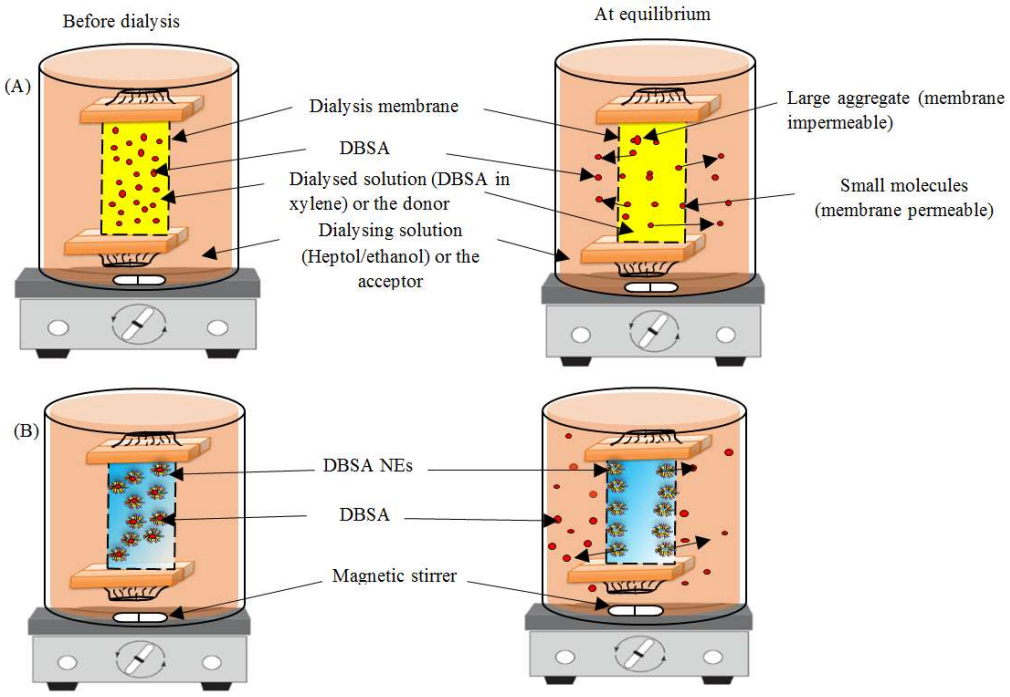

Figure 5-1. Schematic of the inhibitor release through a dialysis membrane. A) Direct loading method (DBSA in xylene) and B) NEs loaded DBSA. Inhibitor releases through the dialysis membrane into the outer compartment holding release medium.

5.2.4. Methodology applied in the construction of transmission % – cumulative inhibitor released %

In order to validate the best-fit kinetics release model to stabilise asphaltene, the membrane dialysis method data (% cumulative of DBSA released versus time) was

retrieved from studies described in Section 5.2.3, and the Turbiscan technique data (% transmission versus time) was obtained from a study described in Section 5.2.2. This relationship was generated by plotting the % cumulative of DBSA released on the X-axis and the corresponding % transmission on the Y-axis at same time points. The model (linear or polynomial) with the best regression coefficient was selected and used for validation.

5.3. Results and discussion

5.3.1. The stability of asphaltene using optical techniques

Analytical stability of asphaltene technique, the Turbiscan, has been recently used as "*in situ*" tool to characterize the stability of colloidal dispersions for early formulation stability within shorter and longer timescales [272-274]. However, this technique has received little attention in the field of asphaltene sedimentation or precipitation. The multiple scan method is adopted in this work to examine the effect of controlled release by investigating the stability of asphaltene particles by three case studies with: i) DBSA, ii) blank NE, and iii) DBSA NE, as below:

The results demonstrate that when the asphaltene is destabilized by the addition of n-heptane (0.025 w/v % asphaltene in 60:40 volume ratio Heptol), the transmission of asphaltene showed an increase with time, resulting in a quick formation of aggregation into larger structures, settling down faster. However, after the addition of 4 vol. % DBSA to the asphaltene solution, the asphaltene particles are sterically stabilized by the presence of DBSA molecules on the asphaltene particle. Under this condition, the individual particles are kept into the asphaltene sample without any aggregation or sedimentation. In addition, no significant change in transmission for asphaltene solution was observed after 24 h under gravity force, as shown in Figures (5-2 B) and 5-3. This

can be attributed to the effectiveness of DBSA to interact with asphaltene molecules, which is kept the asphaltenes well-solubilized in the solution; as a result, the transmission remains unchanged within 24 h.

The transmission data for asphaltene particles with blank NEs is considered in Figure (5-2 C) and 5-3. It is obvious that the transmission is seen to progress in a linear fashion with time. For asphaltene with 20 vol. % blank NE sample, the transmission decreases compared with the transmission for asphaltene solution over extended times; therefore, these findings suggest that the NEs have a moderate influence on asphaltene stabilization comparing with using 4 vol. % DBSA. The stability behaviour can be attributed to the presence of components of blank NEs such as water, surfactants, and xylene that interact with asphaltene molecules.

In the case of the addition of DBSA NEs, as shown in Figure (5-3 D), the transmission slightly increases after 2 h due to settling down of large asphaltene particles and then gradually decreases within the extended time, which indicates that the release effect plays a significant role in the process. It may be assumed that, in this case, the DBSA and other NE's components were progressively released from NE and interact with asphaltene molecules, which is saturated the H-bonding sites of asphaltenes and the fact that it interacted with both the periphery and aromatic cores of asphaltenes, suggesting that the asphaltene is prevented from interacting laterally between themselves and kept well-solubilized in the solution i.e., increasing the stability of asphaltene. These interactions are almost certainly due to acid-base interaction, hydrogen bond, polar-π interaction, cation-π interaction, and aromatic-aromatic interaction. These interactions can also promote further electrostatic interactions with other ion pairs. For example, the hydroxyl group in the chain length can form H- bonding with water or surfactants, whereas the nitrogen in the aromatic core can provide acid-base as well as H-bonding interactions

with DBSA. Therefore, using a small amount of DBSA (1 vol. %) with other components in the DBSA NEs is sufficient to produce complete coverage of the individual aggregates.

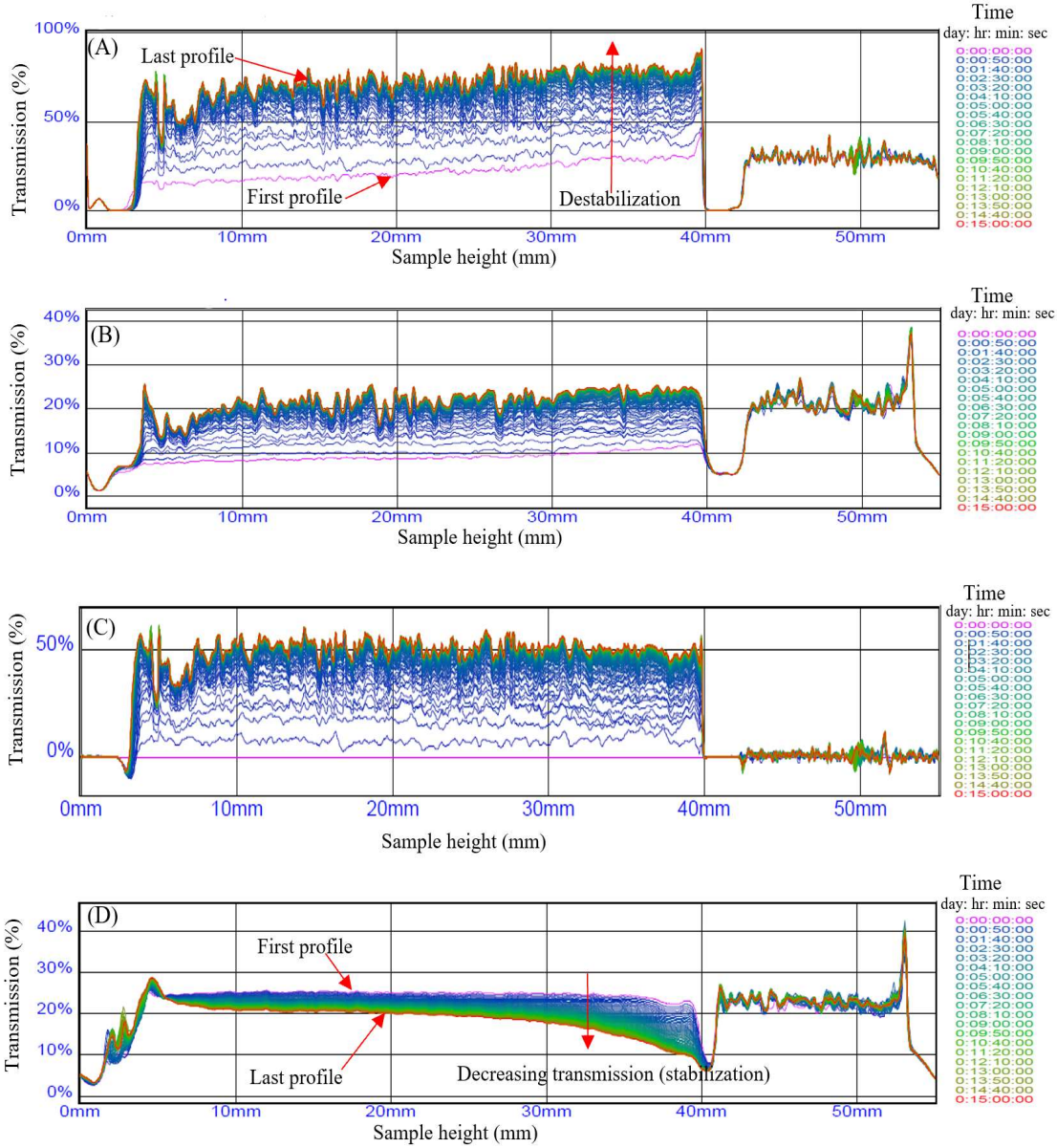

Figure 5-2. Transmission profiles for (A) asphaltene, (B) 4 vol. % DBSA, (C) 20 vol. % blank NE, and (D) 20 vol.% DBSA NE during 15 h of continuous test at 25 °C.

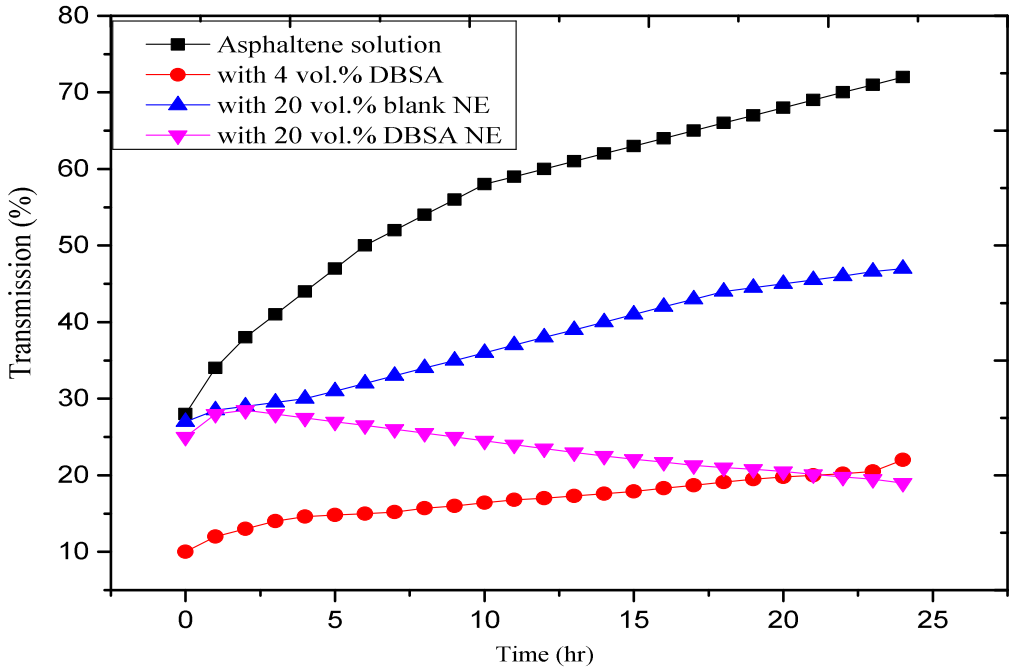

Figure 5-3. Transmission profiles at a fixed position (25 mm) for asphaltene, 4 vol.% DBSA, 20 vol.% blank NE, and 20 vol.% DBSA NE during 15 h of the continuous test.

The effect of these three cases on the stability of asphaltene is further examined by determining the separability number (SN) (%). Interestingly, the asphaltene with 4 vol. % DBSA reduces SN from 12.18 (for asphaltene solution) to 2.76, indicating that asphaltene stability is increased. However, asphaltene with blank NEs reduces SN to 7.22. It can thus be suggested that the addition of blank NEs to asphaltene solution categorizes them as "moderately stable" when the separability number is between 5 and 10.

Coming back to the topic of the role of DBSA NEs in asphaltene stability, these experiments have shown that there is a significant effect of the DBSA NEs on asphaltene stability by reducing SN from 12.18 to 2.9. Therefore, the results of stability as found by separability number are more superior, accurate and highly sensitive.

The percent of asphaltene inhibition (A.I %) was also calculated from each transmission by using Eq. (5-1) to evaluate the performance of three cases on asphaltene stability. These findings for average transmission, A.I % and SN data provide a further comparison

between the three cases, which show that asphaltenes treated by 20 vol. % DBSA NE has a similar effect as that of 4 vol. % DBSA. However, the treatment by 20 vol. % blank NE still has some effect but less strong the other two. To illustrate the effect of inhibitor (i.e. DBSA) reduction, the transmission, A.I %, and SN are plotted in Figure 5-4. Using 20 vol.% DBSA NEs (i.e., containing 0.04ml DBSA) give nearly the same values of average transmission, SN, and A.I % as that of 4 vol.% DBSA (i.e., about 0.8 ml). Therefore, the amount of asphaltene inhibitor (% R_{AI}) is decreased by 95%. Although DBSA NEs contain different chemicals such as xylene, surfactants, and DBSA, the total chemicals (% R_{TC}) are again lower than 4 vol.% DBSA by a factor of 10%, as shown in clearly in the detailed materials balance are shown in Tables S1 in the Supplementary Information. These results in good agreement with the previous chapter for reducing AI amount and the total chemicals used, which found that 4 vol. % DBSA and 20 vol. % of DBSA NEs gave the same values of instability index and sedimentation rate.

Furthermore, the results of the efficiency of asphaltene inhibition provide compelling evidence for long-term stability with high efficacy and suggest that this approach appears to be effective with increasing release time. From the data in Figure 5-5, it is apparent that, for asphaltene with DBSA NEs after 24 h of aging, the A.I % increases with time (i.e. increasing from 15 to 84.12 % gradually) due to the release effect, while for asphaltene with 4 vol. % DBSA the A.I % decreases with time (i.e. decreasing from 89 % to 79.3 %). Consequently, it can be suggested that the DBSA NEs provide cost-effective and long-lasting stability, and this is an invaluable method to control asphaltene precipitation.

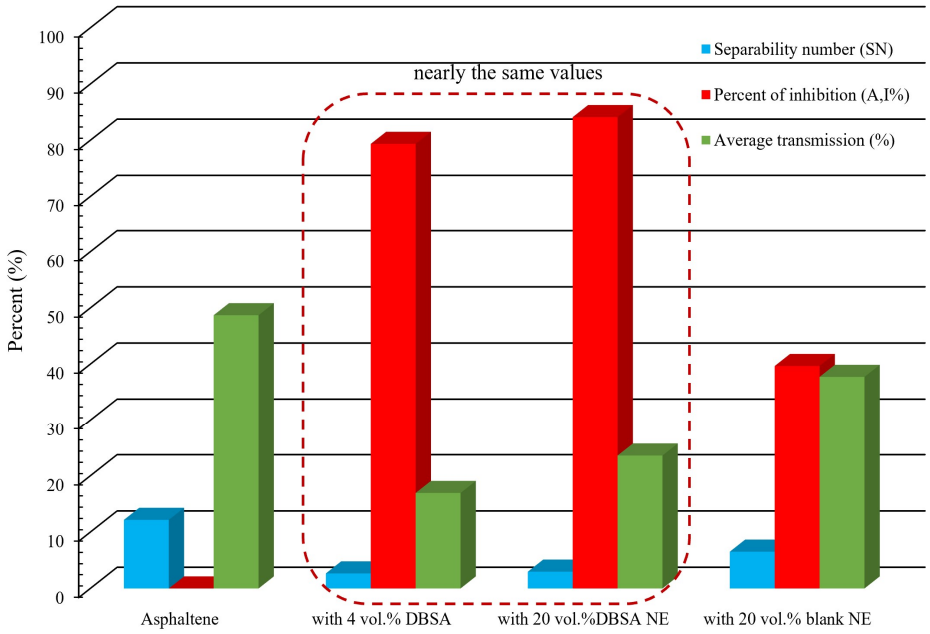

Figure 5-4. Separability number and average transmission for asphaltene,4 vol.% DBSA, 20 vol.% blank NE, and 20 vol.% DBSA NE.

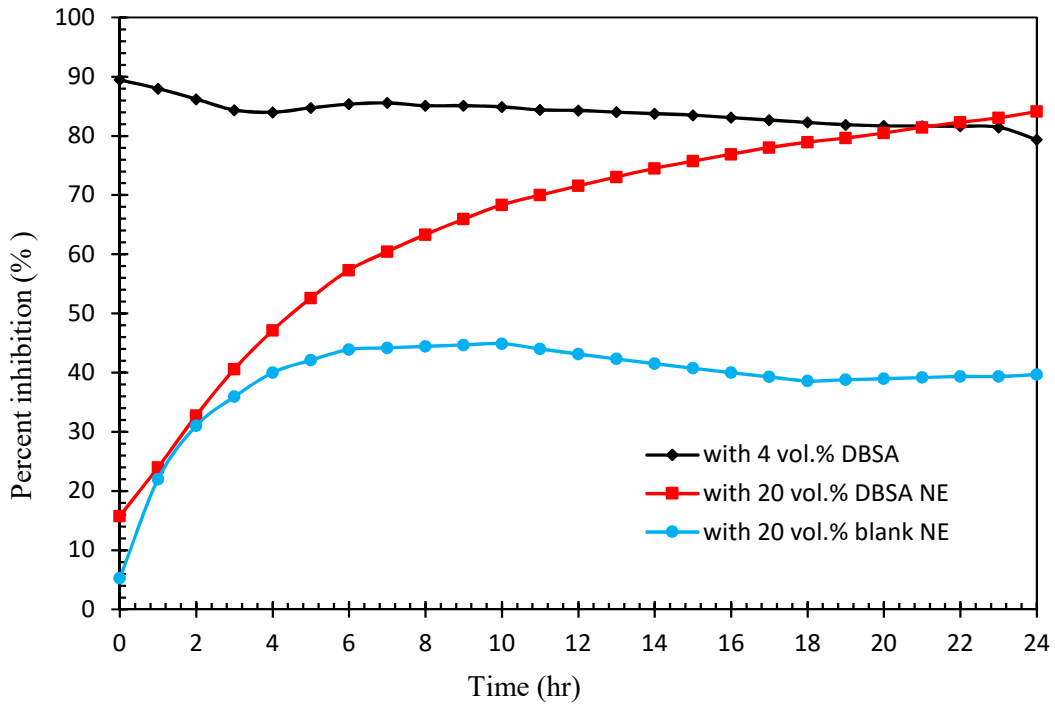

Figure 5-5. The percent of inhibition (A.I %) for asphaltene with 4 vol. % DBSA, blank NEs, and DBSA NEs with time.

5.3.2. The effect of DBSA NEs on the size and morphology of asphaltene

To validate the effect of DBSA NEs on the sizes of asphaltene precipitates, samples were collected from both the bulk and the bottom of the sample (i.e. sediment bed) for asphaltene in the presence and absence of DBSA NEs after 24 h of aging time to measure particle sizes using dynamic light scattering (DLS). We found that the asphaltene bulk contains fine particles of 5 – 20 nm, suggests that all larger particles in the bulk are precipitated down towards the bottom of the sample. Whilst the sediment bed showed formation asphaltene precipitates into larger structures within the ranges of 1000 – 3073 nm. On the other hand, asphaltene solution with DBSA NEs was shown to contain some small particles of 10 - 60 nm in the bulk, suggests that DBSA NEs make the bulk more size polydisperse than asphaltene without DBSA NEs. Moreover, the sample taken from the sediment bed shows no significant change in asphaltene particle sizes due to the stability of the sample without sedimentation or precipitation. It can be seen in Figure 5-6 (A and B) that the size distribution of the asphaltenes particles in both bulk and sediment bed was narrower compared with asphaltene without DBSA NEs, that also is evidence to indicate that the DBSA NEs are able to reduce asphaltene particles from precipitation and form a good dispersion in the medium. The data presented in Figure (8 B) also confirmed that using 4 vol. % DBSA and 20 vol. % of DBSA NEs gave nearly the same values of particle sizes and size distribution of the asphaltenes in both bulk and sediment bed. These findings are broadly consistent with the data collected using the Turbiscan and with those obtained by Mansur et al. [275]. Table 5-1 shows the particle sizes and polydispersity index data of both supernatant and sedimentation bed for asphaltene with and without 4 vol. % DBSA and 20 vol. % DBSA NEs after 24 h.

The release mechanism is supported by the evidence of the transmission electron microscopy that the DBSA NEs were firstly added to the dispersion of asphaltenes under

shear action in a homogenizer until complete incorporation of the DBSA NEs into the oil phase. The water phase which contains nanodroplets forms a layer around the asphaltene particles [276,277]. Nanodroplets adsorb on asphaltene particles due to its high lipophilicity and higher affinity to the asphaltene. Eventually, the DBSA inside NEs can be slowly released to interact with asphaltene clusters, and hence the larger asphaltene particles are reduced and kept well-stabilized in the bulk. Figure 5-7 shows the optical and transmission electron microscopy at different steps of asphaltene stability via the slow release of DBSA from NEs.

Although the proposed mechanism is well presented and evaluated by the effect of DBSA NEs on the asphaltene particle size, more validation about its effect on the morphology is still demanded. Figure 5-7c presents the micrographs of asphaltenes in 60:40 Heptol solution with and without DBSA NE after 24 h of releasing test. Without DBSA NE, large asphaltene clusters interacted with each other and grew into asphaltene precipitates to form rodlike shape structures. However, DBSA NEs can reduce asphaltenes from precipitate to spherical nanometric particles having a diameter of around 5 to 30 nm. It is evident that these results are in good agreement with those obtained by DLS. A possible explanation for this might due to very strong intermolecular interactions, which provide complete coverage of the individual aggregates to interact with both all periphery and aromatic cores of asphaltenes. This explained why DBSA NEs favoured the formation of nanoaggregates with spherical rather than rodlike shape structures. However, the formation of rodlike shape structures is might be contributed to the onset of asphaltene precipitation is near 60:40 Heptol, in excellent agreement with recent studies [275, 278]. These rodlike shape structures have an average size of 500 nm, while the spherical particles equivalent size of these structures is approximately 10 nm in the same volume

ratio of Heptol. This indicates that DBSA NEs can delay the precipitation onset in 60:40 toluene/heptane solutions.

Table 5-1. Particle sizes and polydispersity index data of both supernatant and sedimentation bed for pure asphaltene and asphaltene with 4 vol. % DBSA and DBSA NEs DBSA NEs after 24 h.

Sample	Size (nm)	PDI
Asphaltene (bulk)	5.577	0.570
Asphaltene (sediment bed)	3019	0.350
Asphaltene with 4 vol. % DBSA (bulk)	28	0.200
Asphaltene with 4 vol. % DBSA (sediment bed)	95	0.293
Asphaltene with DBSA NE (bulk)	19	0.120
Asphaltene with DBSA NE (sediment bed)	58.44	0.223

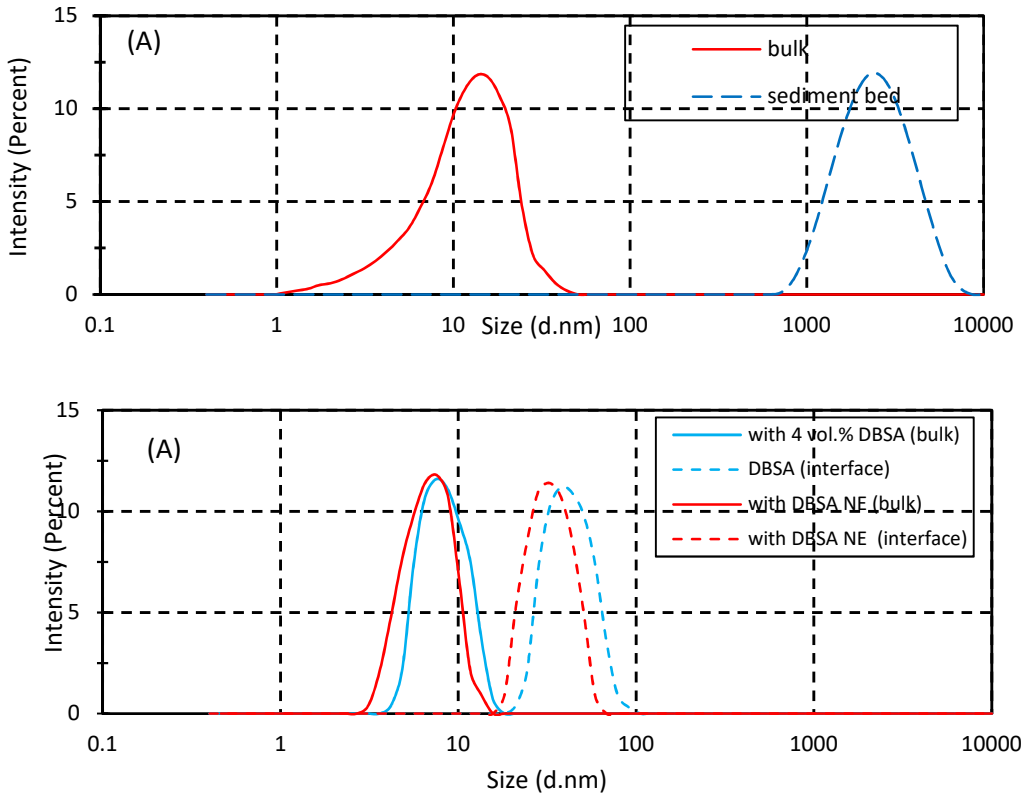

Figure 5-6. Size distribution data of both bulk and sedimentation bed or interface for (A) asphaltene, and (B) asphaltene with DBSA NEs.

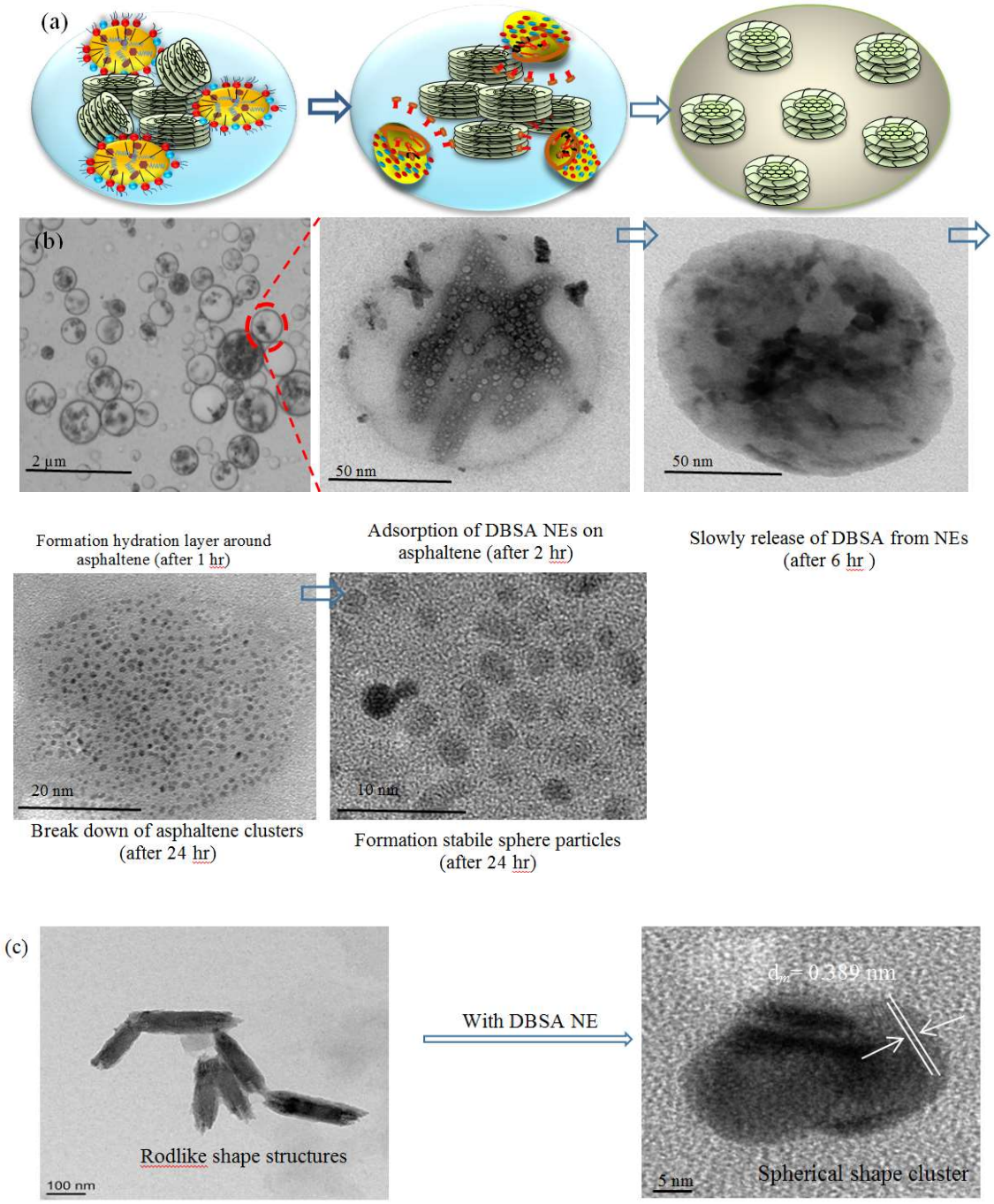

Figure 5-7. Schematic diagrams of different steps of asphaltene stability via slowly release DBSA from NEs; (b) optical and electron microscopy images of the asphaltene with DBSA NEs. The micrographs correspond to different times and are chosen to illustrate the release effect; (c) the effect DBSA NEs on the shape and size particles.

5.3.3. Kinetic study of inhibitor release

The kinetic processes of AI transport and release through the dialysis membrane are examined for two cases: NEs loaded DBSA and DBSA directly dissolved in xylene. This procedure is similar to drug release in the area of nanomedicine by using the dialysis bag method [279-281] (see Section 5.2.3). The release rate is calculated from the slope of the released amount-time profiles of DBSA. The rate of DBSA released through the dialysis membrane was measured for both cases at different DBSA concentrations: 1 vol. %, 2 vol. %, 3 vol. %, and 4 vol. %, as shown in Figure 5-8. At low concentration (1vol. %), it is noticed that the transport of DBSA from xylene shows initial burst behaviour during the first three hours followed by a steady transport through the membrane for the following 22 hours, which means that the inhibitor transport is not completely controlled. Initial burst behaviour kinetics and uncontrolled transport through the membrane are very common in the use of drug directly with oil [267-269]. This behaviour could cause aggregation near the wellbore, leading to the loss of a large amount of chemicals inside the reservoir, resulting in high treatment cost. Thus, there is a need to develop methods for controlled and sustained inhibitor release inside the oil reservoir. The data presented in Figure 5-8b confirmed that the beneficial effect of NEs for controlled DBSA release as compared to burst and uncontrolled DBSA transport from xylene. It is clear that DBSA NEs demonstrated lower DBSA release at initial time points in comparison with DBSA in xylene, ascribable to the use of mixed surfactants, which offers a physical barrier to inhibitor release from NEs and efficiently control its release. Moreover, the slower release rate from DBSA NEs with mixed surfactants could be attributed to the small size of DBSA NEs (i.e., 21 nm), which can provide a high surface area of the system. In fact, higher surface area means a higher surface from which the inhibitor can be released. Therefore, the relatively small burst release and higher sustained release rate of DBSA

from NEs can be achieved. However, our results also suggest that the cumulative release or transport of DBSA clearly depended on the amount of inhibitor. The release profiles of DBSA from NEs tended to decrease as the DBSA concentration increased. This may have been due to droplet growth with increasing the concentration of DBSA inside NEs, which means an appreciable amount of DBSA is not released from the droplets into the acceptor media. Similarly, the transport profiles of DBSA molecules from xylene decrease as the DBSA concentration increased in xylene. The drop in the transport profiles of DBSA with increasing the inhibitor concentration may have been due to the formation of large molecules in the donor compartment. Table 5-2 shows the influence of DBSA concentration and droplet size on the total amount of DBSA released or transported for both cases.

Table 5.2. Influence of DBSA concentration and droplet sizes on the cumulative of DBSA released % through the dialysis membrane after 24 hr.

	DBSA NEs				DBSA in xylene
DBSA concentration (vol. %)	d (nm)	PDI	Zeta potential (mV)	DBSA released (%)	DBSA transported (%)
1.0	21	0.19	-33	99.0	13.7
2.0	93	0.21	-34	87.6	12.25
3.0	135	0.36	-33	72.2	11.65
4.0	274	0.44	-30	67.2	11.15

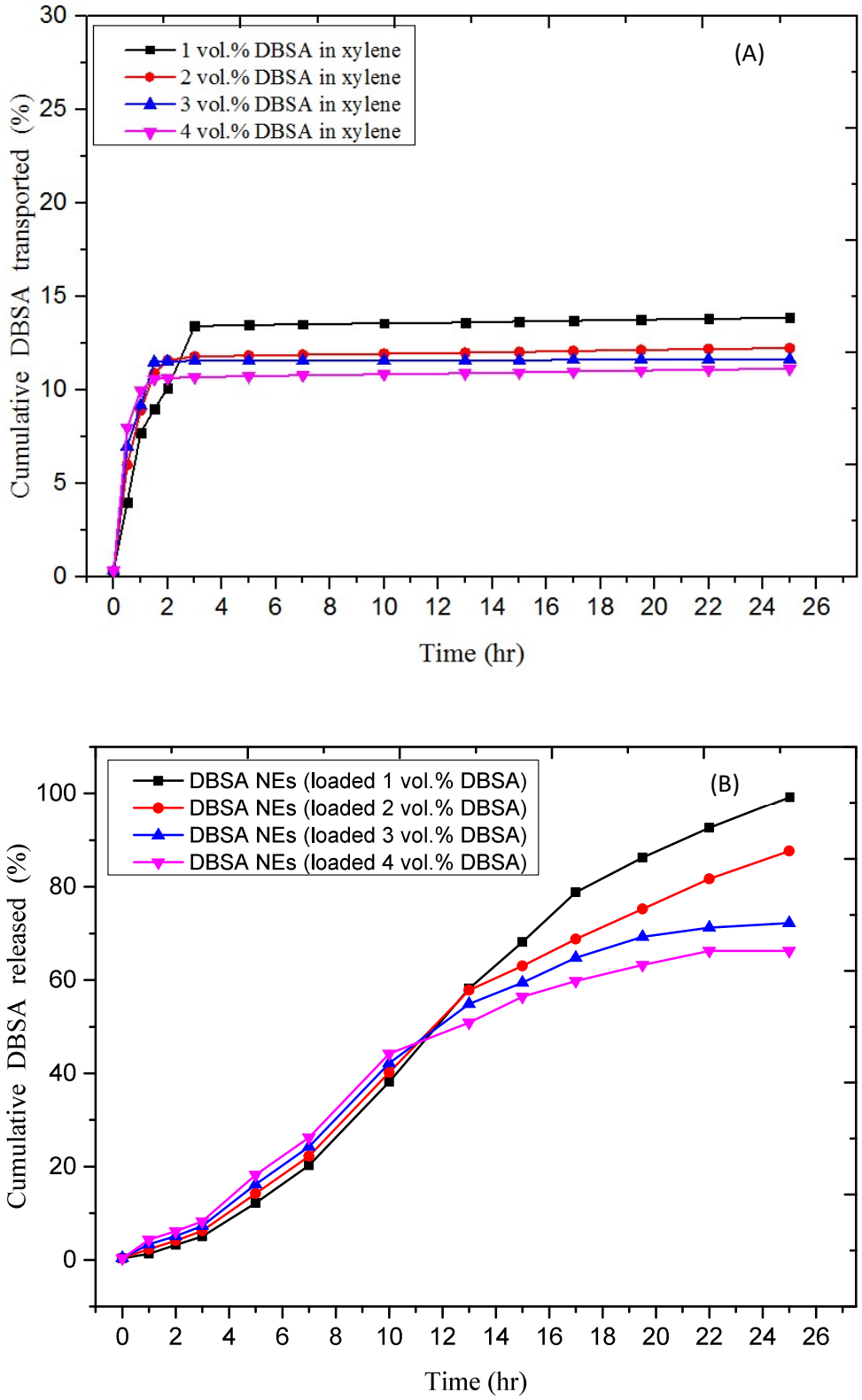

Figure 5-8. Release or transport profiles of DBSA through the dialysis membrane from (A) xylene and (B)DBSA NEs.

In the dialysis membrane testing, there are two kinetics steps involved in the total inhibitor release: 1) the inhibitor is released from the NEs to the medium inside the donor (k_1, see Figure 5-9 A & B), and 2) the released inhibitor inside the donor diffuses across the membrane to the acceptor due to concentration gradient and its high affinity for oil phase in the acceptor (k_2, see Figure 5-9 A & B). On the other hand, a poor membrane permeation of DBSA from xylene in comparison to DBSA NEs clearly indicated a higher intermolecular interaction between DBSA and xylene in the donor media; this may result in aggregation and formation of self-assembly in the donor compartment (k_3 and $-k_3$, see Figure 5-9 B). This could explain why the accumulative DBSA transported through the membrane is small in the case of using DBSA in xylene.

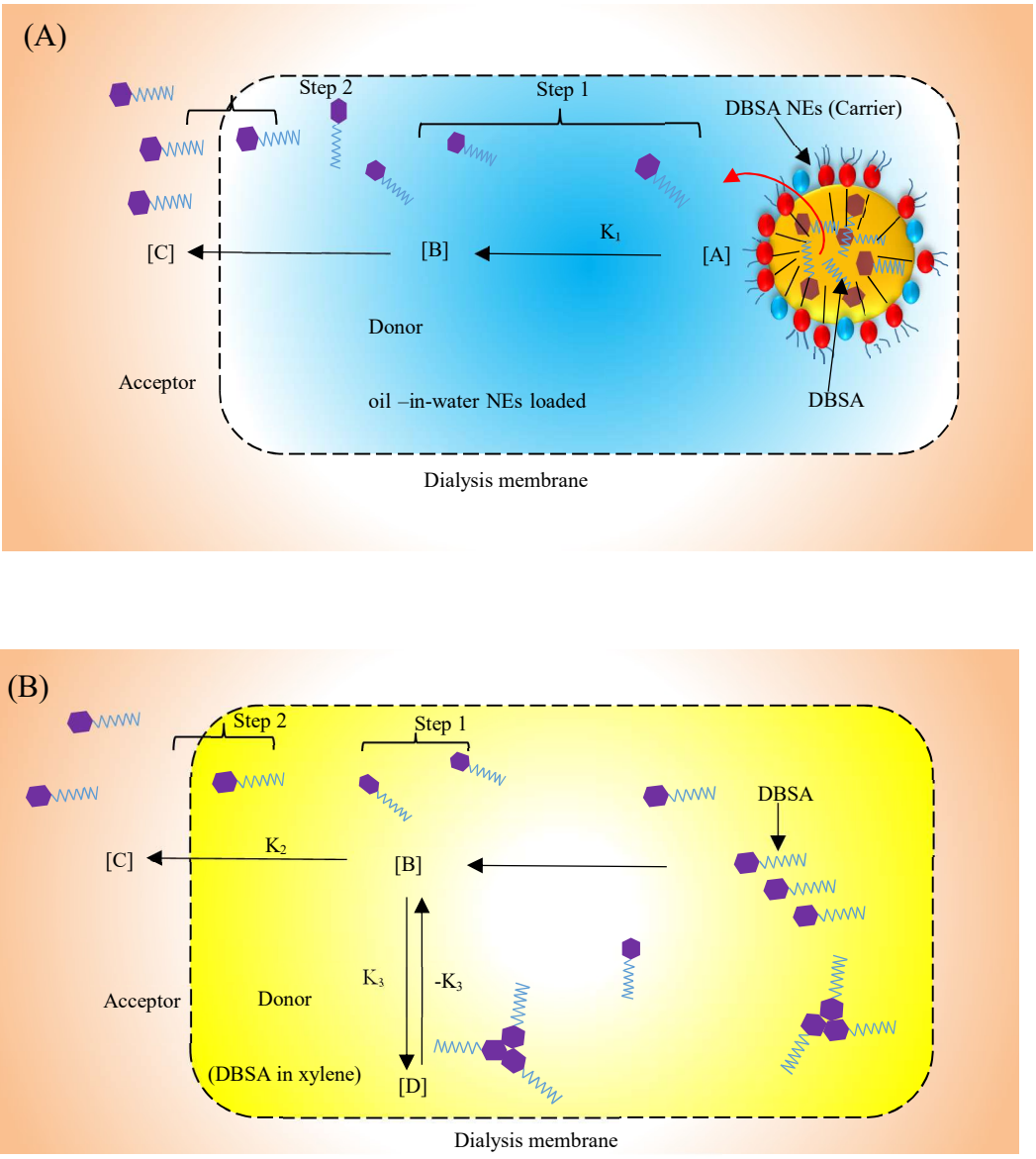

Figure 5-9. Schematic of the kinetic processes of AI transport and release through the dialysis membrane for (A) DBSA NEs and (B) DBSA in xylene.

[A] – DBSA concentration in the NEs, [B] – DBSA concentration in the donor, [C] – AI concentration in the receptor, and [D] – DBSA concentration in the donor. K_1 is the diffusion rate constants of AI inside the dialysis bag, K_2 is the diffusion rate constant of AI through a dialysis membrane to the receptor, and, K_3 and $-K_3$ are the diffusion rate constant of AI at formation aggregates in the donor.

It is essential to study the release kinetics for a better understanding of the efficacy of NE to deliver and release DBSA. The selection of a suitable kinetic model for fitting the AI release data helps determine the release characteristics. There are number of kinetic models, which describe the overall release of drug from the carrier. The most common mathematical models used in this study to investigate the release of DBSA from NEs and DBSA transport from xylene through the dialysis membrane are presented in Table 5-3.

Table 5-3. The kinetic model parameters fitting to the DBSA release results.

Models	Mathematical models	Parameters	DBSA in NEs	DBSA in xylene
Zero-order	$F = F_0 + K_0.t$	R^2	0.98151	0.96981
		K_0	0.000627722	0.0000949912
First order	$\ln(1-F) = -K_1 \cdot t$	R^2	0.61938	0.97217
		K_1	0.00251	0.000102931
Higuchi	$F = F_0 + K_H.t^{1/2}$	R2	0.98204	0.97142
		K_H	0.02585	0.00389
Korsmeyer-Peppas	$F_t = F_0 + K_{HP}.t^n$	R^2	0.99805	0.96414
		K_{HP}	0.00628	0.000768552
		n	0.68991	0.51113
Baker-Lonsdale	$3/2[1-(1-Ft)^{\frac{2}{3}}] - F_t = K_{BL}t$	R^2	0.72421	0.96702
		K_{BL}	0.000328911	0.000110438
Hixon-Crowell	$1-(1-F_t)^{\frac{1}{3}} - F_t = K_{HC}t$	R^2	0.88113	0.97146
		K_{HC}	0.00045031	0.0000333992
Square root of mass	$1-(1-F_t)^{\frac{1}{2}} - F_t = K_{SR}t$	R^2	0.95244	0.97107
		K_{SR}	0.000534237	0.000049432
Three seconds root of mass	$1-(1-F_t)^{\frac{2}{3}} = K_{TS}t$	R^2	0.98463	0.97067
		K_{TS}	0.000582836	0.0000650347

where: F_t: the amount of drug released in time t,

F_0 : the initial amount of drug,

K_0: zero order kinetic constant,

K_1 : first order kinetic constant,

K_H :Higuchi kinetic constant,

K_{HP}: Korsmeyer-Peppas release constant,

K_{BL}: Baker-Lonsdale release constant,

K_{HC}: Hixon- Crowell release constant,

K_{SR} : Square root of mass release constant,

K_{TS} : Three second root of mass release constant,

n − diffusional release exponent,

t − time.

It can be seen from the data in Table 3 that the best kinetic fit of AI release from NE was described by Korsmeyer-Peppas model, also confirmed by the coefficient of determination, $R^2 = 0.99805$ (highest value). The parameter "n" in the Korsmeyer-Peppas equation is related to the mechanism of release of the inhibitor, i.e. if the exponent $n < 0.43$, then the release mechanism is Fickian diffusion, if $0.43 < n < 0.85$, then it is non-Fickian or anomalous diffusion and an exponent value is 0.85 or greater is indicative of Case-II Transport or typical zero-order release [280, 281]. In this case, DBSA NEs give a value of n of 0.68, so their release mechanism followed a non-Fickian or anomalous diffusion. This suggested, there is a strong interaction among DBSA molecules and the NE components, which confirms that the DBSA is released slowly, dependent on the inhibitor concentration in the NE. A slow release DBSA from NEs overtime can provide long-lasting stability and minimize the amount of inhibitor. Therefore, this result clearly highlights that DBSA NE systems can act as a better inhibitor carrier for controlled

release of DBSA with a prolonged release profile. This data is in accordance with many recent drug release studies Rodríguez-Burneo et al. [282], Alvarado et al. [283], which showed that the Korsmeyer-Peppas model best describes a release process of drugs from NEs.

On the other hand, in the case of using DBSA in xylene, the DBSA transported profiles through the dialysis membrane could be best explained by first order or Higuchi models. Both regression lines are characterized by higher R^2 values than the initial (R^2> 0.97). This indicates an initial burst transport of DBSA from xylene; however, only a small amount of DBSA is released, and no significant cumulative transport efficacy is achieved. The results also suggested that it takes times for the DBSA incorporated in xylene to be released. This result is in agreement with those obtained by Miastkowska et al. [284], and Nanjwade et al. [285], who suggested that the release oil-soluble drug from the oil phase could be best explained by Higuchi or first order. Figure 5-10 (a and b) shows the release profiles of 1 vol.% DBSA from NEs and fitted to the Korsmeyer-Peppas mode, and the transport profiles of 1 vol. % DBSA from xylene and fitted to the first order mode. All the kinetic models fitting to the DBSA release from NEs and transport from xylene are illustrated in Figure A-1 (See Appendix A).

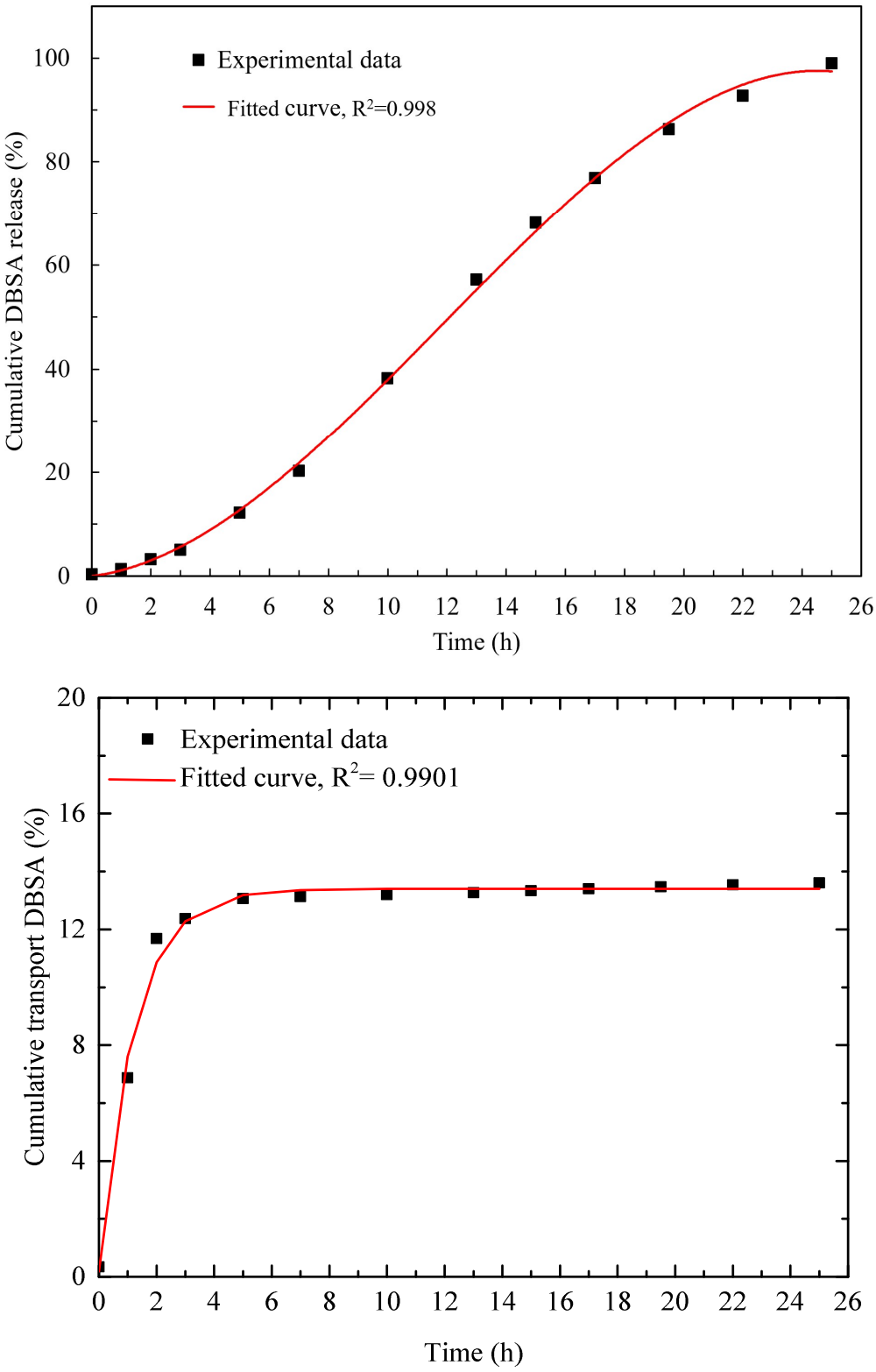

Figure 5-10: (A) The release profiles of 1 vol.% DBSA from NEs and fitted to the Korsmeyer-Peppas mode (n = 0.68), and (B) The transport profiles of 1 vol.% DBSA from xylene and fitted to the first order mode.

5.4. Relationship between DBSA released from NEs in asphaltene solution and its release through the membrane

In order to provide robust evidence for supporting the mechanism of asphaltene stability and the kinetic release mechanism of DBSA from NE, a relationship between the Turbiscan technique data (% transmission, see Figure 5-3) and membrane dialysis method data (% cumulative of DBSA released, see Figure 5-8 B) was correlated at the same time points (point-to-point) without any change in the time scale.

It is interesting to note that a second order polynomial correlation is found between % cumulative release obtained from the membrane dialysis method (X-axis) and % transmission obtained from Turbiscan technique data (Y-axis) with a correlation coefficient (R^2) of 0.9315, as shown in Figure 5-11. This may indicate a strong correlation between the mechanism of release DBSA with the mechanism of stabilization of asphaltene particles. Furthermore, the good correlation among the measurements obtained by the different techniques indicates that this methodology is useful to quantify the time needed for the release to occur and to determine the minimum DBSA concentration that starts to interact with asphaltene.

It can also be observed that, up to 3h, light transmission can increase along with the measuring cell because the settle down of some asphaltene clusters and the corresponding cumulative release of DBSA was about 5 %, which can not affect asphaltene clusters. There is, however, after 4 h, the transmission dropped progressively when the release rate increases, confirming that small particles are formed, and therefore this is an indicator of keeping the asphaltenes well-stable in the solution, which is in perfect agreement with data obtained by particle size measurements.

Figure 5-11 also presents the overall possible mechanism of asphaltene stability, based upon the kinetic processes of DBSA released from NEs and their influence on

transmission within 24 h. This proposed mechanism suggests that the release kinetics and asphaltene stability can occur within three stages: 1) the first plateau corresponds to the adsorption of self-assembled asphaltene at the w/o interface; 2) DBSA NEs are adsorbed at w/o interface and induced release of entrapped DBSA from NEs, and 3) with time, the asphaltene undergoes disassembly (break down clusters) into the bulk due to the release of DBSA NEs components, and the final transmission decreased corresponds to the increase in the release rate.

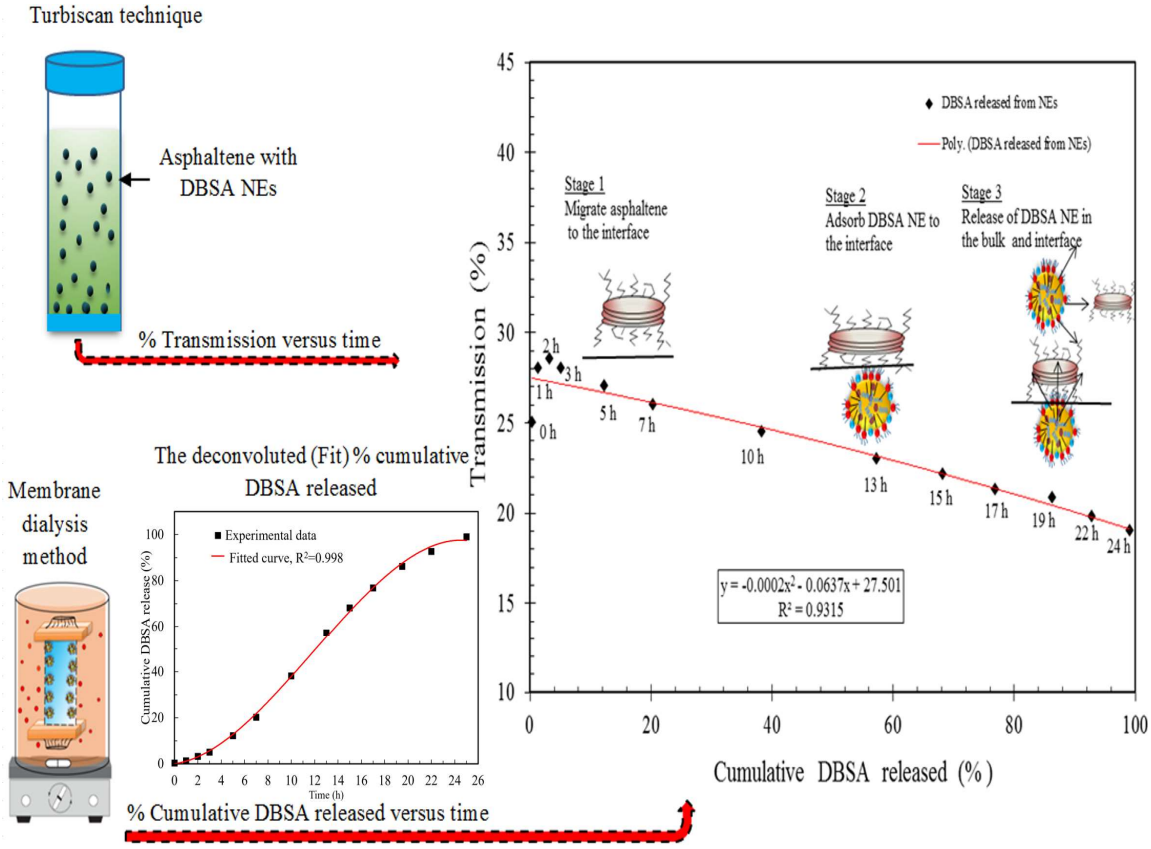

Figure 5-11. The relationship between the transmission and cumulative DBSA released and the overall possible mechanism of stabilization of asphaltene particles.

5.4. Chapter summary

This Chapter further studied the stability of NEs by using *in situ* Turbiscan and examined the detailed kinetic release mechanism, which can be summarised as:

- The DBSA and other components were progressively released from NE and interact with asphaltene molecules, increasing the stability of asphaltene.
- DBSA NEs could significantly increase the efficiency of AI by 84.12 % after 24 h, showing its effectiveness with increasing release time.
- DBSA NEs were able to reduce asphaltenes from precipitate to spherical nanometric particles (5 to 30 nm), delaying the onset of asphaltene precipitation.
- The rate of DBSA released through the dialysis membrane increases as the droplet size decreases, which is attributed to the increase in the surface area of the NEs.
- The released amount of DBSA from NEs (99 %) was much higher than form the xylene (13 %). The release profile of DASA NEs follows that Korsmeyer-Peppas mode kinetic model.
- The strong correlation between % DBSA released and % transmission clearly indicated the possibility of predicting the release time and the minimum DBSA released amount to interact with asphaltene based on the kinetic processes of inhibitor release through the dialysis membrane studies.
- It suggests that there is a significant advantage in using NEs loaded DBSA to achieve prolonged asphaltene treatment with a reduced amount of inhibitor, rather than DBSA in xylene, to encapsulate and deliver lipophilic functional components. These results also suggest that utilisation of the direct treatment of asphaltene with DBSA in both upstream and downstream should be avoided because any extended and efficient treatment may not be available.

Chapter 6

Molecular structure characterization of asphaltene in the presence of inhibitors with nanoemulsions

6.1. Introduction

From the literature review in Chapter 2, a complete molecular analysis of asphaltene and a systematic understanding of how asphaltene molecular structure changes with the addition of inhibitors have not yet been achieved. To address this limitation, we attempt to provide novel insights into the stability and molecular modification structure of asphaltene in the presence of three cases: i) pure DBSA, ii) blank NEs, and iii) DBSA NE. Based on the structural parameters obtained from combined X-ray diffraction, transmission electron microscopy TEM, and FTIR spectroscopy, a stability mechanism is proposed to describe changes in asphaltenes and the effects of DBSA NEs thereon. The thermal stability and the refractory nature of asphaltene are also performed by a thermogravimetric analyser (TGA).

6.2. Experimental and methods

6.2.1. Synthesis of NEs with the presence and absence of AI

The successful long-term stability of AI inside NEs requires different materials than currently used (surfactants) to create impermeable barriers that can arrest the diffusion of AI from the nanodroplet core. As an example, DBSA can provide steric and electrostatic repulsion together with hydrophobic and acid-base interactions between its molecules and ionic/non-ionic surfactants. Such a synergistic effect may overcome the hydrogen bonds

of water molecules and enhance the bounded molecules at the interface, resulting in more hydrophobicity of the oil phase. The procedure of synthesis of NEs with the presence and absence of AI was elaborated in the previous chapter (see Section 3.2.2). Table 6-1 shows the composition and concentrations of all three cases used in this work.

Table 6-1. The composition and concentrations of all three cases.

Sample	DBSA (vol.%)	xylene (vol.%)	Tween 80 (vol.%)	SDS (vol.%)	Water (vol.%)
DBSA	4.0	------	------	------	------
Blank NE	------	7	9.9	0.1	83
DBSA NE	1.0	7	9.9	0.1	82

6.2.2. Asphaltene extraction and preparation of samples.

The procedure of asphaltene extraction was reported previously in Chapter 4 (see Section 4.3). For preparation asphaltene solution in this Chapter, a 0.5 w/v % of the asphaltene was prepared in a mixture of two solvents: toluene/heptane (Heptol) volume ratio of 60:40. To observe the effect of DBSA, blank NEs, and DBSA NEs on asphaltene precipitation structure, samples were slowly added to the asphaltene solution under shear action in an (IKA T2S digital/Ultra-Turrax) homogenizer at a rotation speed of 8000 rpm until complete incorporation of the NEs into the asphaltene solution. Then the asphaltene solution with and without DBSA, blank NEs, and DBSA NEs were kept for 3 days for totally evaporation at room temperature. The dried solid asphaltene was used for XRD characterization and TGA.

6.2.3. Molecular structure characterization of asphaltene

Analysis of the asphaltene structure was characterised using the x-ray diffraction (XRD) technique (Bruker D8, UK). The diffraction patterns ($6° \leq 2\theta \leq 90°$) were recorded at room temperature using Cu Kα radiation (λ = 1.54055 Å) at a scanning rate of 1 deg·min^{-1} and a step size of 0.02 (2θ). The dried solid asphaltene without and with 4 vol. % DBSA, 20 vol. % blank NEs, and 20 vol. % DBSA NEs samples should be finely ground, and are prepared directly onto the sample holder. This sample arrangement provides a good signal to noise ratio, and therefore avoid fluctuations in the intensities. The main parameters required for the technique is the radiation source, in this case, it is a copper source (Cu Kα) with an electron beam of 40 keV hitting the sample. The wavelength is known to be 1.54 Å and 1.6 kW of energy in the radiation source.

To obtain any quantitative information from X-ray diffraction patterns of asphaltenes it is necessary to fit a theoretical distribution to the pattern. In the present study, Gaussian fitting procedure was employed and applied by using Origin software. The fitting procedure starts with estimating initial values for the peaks of patterns that are γ band, graphene band, 10 band, and 11 band for asphaltene. Then the regression initiates with an estimation of the peak width and intensity.

The final procedure includes the following steps:

- Go to the menu **Analysis: Peaks and Baseline :Multiple Peak Fit** to open a dialog.
- Select a function from **Peak Function** drop-down list for fitting and click **OK** to proceed to locate peaks.
- Point your mouse and double-click on the desired peak positions to add peaks.

- Click the **Fit** button in the **Get Points** dialog to fit all specified peaks and the detailed results about each peak will be summarized in a table (regression analysis of each peak).

Then peak position, peak intensity, peak area, interplanar distance, and full width at half maximum (*FWHM*) were calculated. Asphaltenes aromaticity and crystalline parameters obtained by the above procedure in the presence and absence of three cases: DBSA, blank NEs, and DBSA NEs are given in Table 6-2.

Infrared spectra of 20 vol. % DBSA NEs and asphaltene samples without and with 20 vol. % DBSA NEs were collected on a FTIR-Thermo iS10 spectrometer in the spectral range from 500 to 4000 cm^{-1}, 64 scans per spectra, and a resolution of 1 cm^{-1}. FTIR is carried out to obtain an infrared spectrum which could identify different chemical bonds of samples.

Studying the thermal behaviour of asphaltene in the presence of oxygen is necessary to have a better understanding of the thermal stability of asphaltenes. In a general thermogravimetric analysis (TGA) (a Perkin- Elmer analyzer model TGA-7HT), a known amount (9‑15 mg) of a solid sample was placed in an alumina or a platinum pan and placed in a small furnace. The weight of the sample was constantly measured at a heating rate of 10 ˚C/min. In the case of the presence of oxygen, oxidation cracking was the dominant phenomenon. For all cases, the temperature interval ranged from room temperature up to 800 ˚C.

6.3. Results and discussion

6.3.1. XRD Studies of Asphaltenes

Generally, four peaks can be detected in the X-ray diffraction pattern of petroleum asphaltene. Their origin is due to the scattering of X-ray from the periodic molecular structure of asphaltenes [276- 278]:

- γ peak: originates from aliphatic chains and condensed saturated rings and can be used to determine the packing distance of saturated structures, which appears around 2θ = 20˚.
- Graphene (*002*) peak: initiated by the stacks of aromatic molecules, which appears around $2\theta = 20^{\circ}$.
- 10 peak: originates from the in-plane structure of the aromatics (the first nearest neighbor in the ring compound).
- 11 peak: originates from the in-plane structure of the aromatics (the second nearest neighbor in the ring compound).

The (10) and (11) bands reflections come from the inplan structure of aromatics, which reveal the average diameter of the aromatic sheets. The (11) band is generally very weak and often not seen for its very low intensity compared to the (10) band and, therefore, the (10) band at around 2θ = 40˚ is normally adopted in the calculation [286]. These findings reflect those of Afra et al. [287] and AlHumaidan et al. [288].

6.3.1.1. The effect of DBSA on asphaltene structure.

The structural parameters for the asphaltene samples were determined from the deconvoluted XRD patterns (using Origin software), which use in equations in Table 6-2. The procedure of deconvoluted XRD patterns of asphaltene used in this investigation is similar to that used by other researchers [286-288]. Figure 6-1 shows that when the asphaltene is stabilized by the addition of 4 vol. % DBSA, the crystalline parameters are changed. The distance between two aromatic sheets d_m of asphaltene is 3.26 Å, which increases to 3.70 Å for the asphaltene with DBSA. These results are compatible with those reported in the literature [289-291]. Correspondingly, the distance between the two aliphatic chains or saturated rings d_γ also increased from 4.70 to 5.25 Å. However, the height stack of the aromatic sheets vertical to the plane (L_c) is decreased from 13.3 to

10.31 Å. The average number of aromatic sheets (M_e) in asphaltene cluster is 4.65 Å and it decreases to 3.9 Å after the addition of DBSA molecules. The average diameter of the aromatic sheet L_a and the number of aromatic rings in the aromatic sheet (R_a) are significantly changed with the addition of DBSA from an average of 7.1 Å and 2.66 for asphaltene to 6.2 Å and 3 for asphaltene with DBSA respectively. This can be attributed to the effectiveness of DBSA to interact with asphaltene molecules via acid-base interaction, which suggests that the asphaltene becomes looser.

6.3.1.2. The effect of blank NE on asphaltene structure

3.1.2. Effect of blank NEs on asphaltene structure

The average interlayer distance d_m for asphaltene stacks with blank NEs are not significantly changed, gradually, from 3.26 Å for the asphaltene sample to 3.42 Å. Therefore, despite the fact that observed changes are considerably small, they give a good indication that the distance between two aromatic sheets of asphaltene cluster is slightly affected and loosened by the addition of blank NEs. The distance between the two aliphatic chains or saturated rings was around 5.01 Å for the asphaltene with blank NEs. The average diameter of the aromatic sheet L_a and the cluster diameter L_c for asphaltene have also decreased with the addition of blank NEs and ranges from an average of 7.1 and 13.3 Å to 6.7 and 11.3 Å respectively. However, the insignificant change in the average number of aromatic sheets M_e, the average number of aromatic rings in each aromatic sheet R_a, and the number of carbons per aromatic structural C_{Au} compared with asphaltene sample were observed. Thus, these results suggest that blank NEs have a moderate effect on asphaltene structure comparing with using 4 vol. % DBSA. This performance may be owing to the presence of different components in blank NEs such as

surfactants, water, and xylene that provide intermolecular interactions with asphaltene molecules.

6.3.1.3. The effect of DBSA NE on asphaltene structure

One interesting finding is the distance between the aromatic sheets (stacking space), which is significantly increased from 3.26 Å to 3.96 Å with the addition of DBSA NE to the asphaltene sample. The distance between the aliphatic chains and naphthenic sheets (d_γ) was also affected by the addition of DBSA NE and increased to 5.35 Å. In addition, the average diameter of the aromatic sheet (L_a) has significantly changed with the addition of DBSA NEs from 7.1 Å to 6.1 Å. This finding is associated with a reduction of the number of aromatic rings in the aromatic sheet (R_a) from 3 to 2. The significant change in the average diameter of the aromatic sheet is mainly due to the fact that at the addition of DBSA NEs, the aromatic C = C-bond is changed. The M_e, Ra, and C_{Au} decreased to 3.9, 2.2, and 11.27 respectively. The cluster diameter (L_c), on the other hand, decreased in size to 10.2 Å as the DBSA NEs is added. The decrease in cluster diameter is due to the loss of aliphatic carbon in the side chains and naphthenes that is clearly reflected by the parameter (f_a), which represents the ratio of aromatic to total carbon per stack cluster. Since aromaticity plays a key role in the asphaltenes stacking mechanism, its alteration due to the addition of DBSA NEs should be investigated to provide more information about the parameters that would change aromaticity. The main advantage of determining aromaticity is to give the aromaticity of aromatic carbon that has the ability to stack. The results of Table 6-2 show that the primary aromaticity of the asphaltenes sample was 0.35, however, after the addition of DBSA NEs this value decreased to 0.22. It is possible that these results are due to altering the structure of asphaltenes cluster and made it less aromatic. Less aromaticity can be the result of the shortening of alkyl side chains or removal of aromatic rings. These results also suggest that the increasing trend for (d_m)

values after addition of DBSA NEs is in agreement with the aromaticity decreasing trend. Aromaticity reduction is indicative of the decrease in the molecular moieties that initiate the stacking and leads to a less ordered structure. It may be assumed that, in this case, the DBSA and other NE's components were progressively released from NE to provide various interactions with asphaltene and involve mainly the breaking of alkyl groups that weakly bond the poly-aromatic basic units, which are saturated the H-bonding sites of asphaltenes and the fact that it interacted with both the periphery and aromatic cores of asphaltenes. This suggests that the asphaltene is prevented from interacting laterally between themselves and kept well-solubilized in the solution (i.e., increasing the stability of asphaltene). The considerable cleavage in alkyl side chains also caused a decrease in asphaltene cluster diameter (L_c) as well as the average diameter of the aromatic sheet (L_a) and the number of aromatic rings per sheet (R_a) were affected.

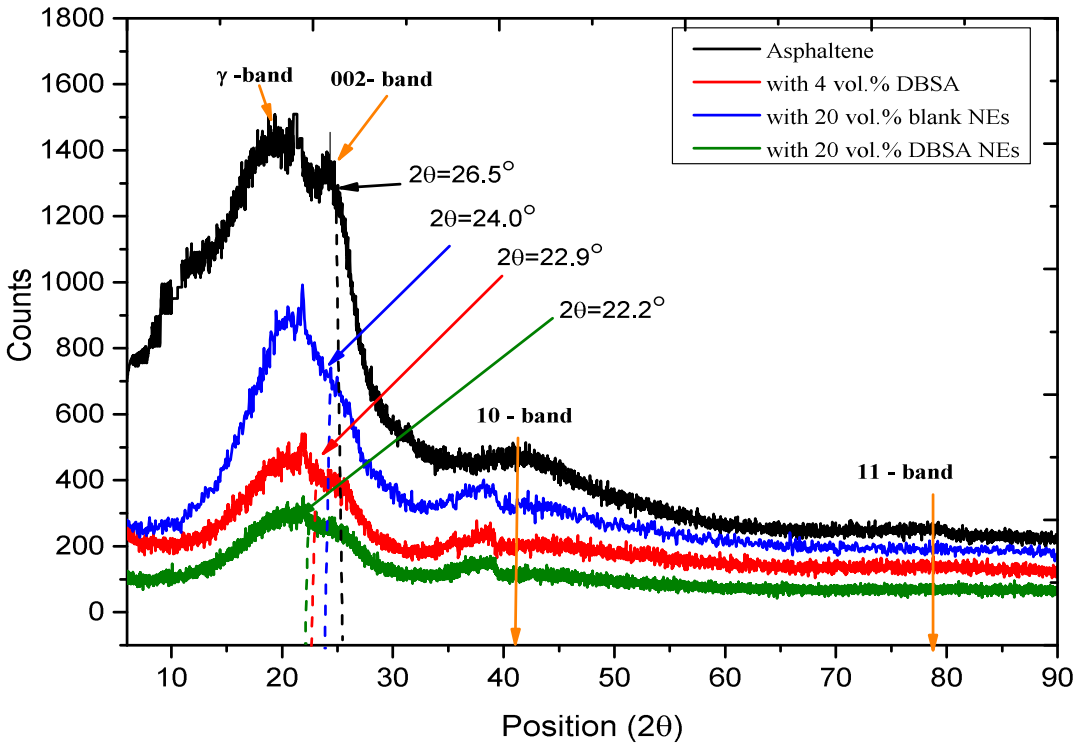

Figure 6-1. XRD pattern of asphaltenes with 4 vol. % DBSA, 20 vol. % blank NEs, and 20 vol. % DBSA NEs.

These findings for crystallite parameters of the asphaltene clusters and its aromaticity provide a further comparison between the three cases, which show that asphaltenes treated by 20 vol. % DBSA NE has a similar effect as that of 4 vol. % DBSA. However, the treatment by 20 vol. % blank NE still has some effect but less strong the other two. Using 20 vol.% DBSA NEs (i.e., containing 0.04ml DBSA) give nearly the same values of crystallite parameters and aromaticity as that of 4 vol.% DBSA (i.e., about 0.8 ml). Therefore, the amount of AI is decreased by 95%. Although DBSA NEs contain different chemicals such as xylene, surfactants, and DBSA, the total chemicals are again lower than 4 vol. % DBSA by a factor of 10%. These results in good agreement with the previous chapter for reducing AI amount and the total chemicals used, which found that 4 vol. % DBSA and 20 vol. % of DBSA NEs gave the same values of instability index and sedimentation rate.

Table 6-2. Crystalline parameters derived from XRD data for asphaltene without and with DBSA, blank NE, and DBSA NE.

	asphaltene	With DBSA	With blank NE	With DBSA NE	Equation*	Ref.
$d\gamma$, Å	4.70	5.25	5.01	5.35	$d_\gamma = \frac{5\,\lambda}{8\,sin\,\theta_{(\gamma)}}$	[279]
d_m, Å	3.26	3.65	3.42	3.96	$d_m = \frac{\lambda}{\sin\theta_{(002)}}$	[279]
L_c, Å	13.3	10.3	11.3	10.2	$L_C = \frac{0.45}{FWHM_{002-band}}$	[279]
M_e	5	4	4	4	$M = \frac{L_C}{d_m} + 1$	[279]
L_a, Å	7.1	6.2	6.7	6.1	$L_a = \frac{0.92}{FWHM_{10-band}}$	[279]
R_a	3	2	3	2	$R_a = \frac{L_a}{2.667}$	[279]

C_{Au}	13	11	12	11	$C_{Au} = \frac{L_a + 1.23}{0.65}$	[282]
f_a	0.35	0.27	0.31	0.22	$f_a = \frac{A_{(002)}}{A_{(002)} + A_{(\gamma)}}$	[282]

∗Where λ = 1.54055 Å ; $\theta\gamma$, θ002, and θ10 are the diffraction angles of γ, 002, and 10 bands, respectively; FMHM is the full width at half maximum of diffraction peak, all these values are reported in the Table 6-3.

d_γ: the distance between the two aliphatic chains or saturated rings,

d_m: the distance between two aromatic sheets,

L_a: the size of the aromatic sheets,

L_c: cluster diameter,

M_e: the average number of aromatic sheets,

R_a: the average number of aromatic rings in each aromatic sheet,

C_{Au}: the number of carbons per aromatic structural.

f_a: the aromaticity

Table 6-3. XRD values obtained from Origin 2017 software (as explained in Section 6.2.3).

	asphaltene	With DBSA	With blank NE	With DBSA NE
2θγ	19.68	20.1	20.92	20.85
$2\theta_{002}$	26.5	22.9	24.0	22.2
$FWHM_{002-band}$	0.012	0.043	0.039	0.044
$FWHM_{10-band}$	0.129	0.148	0.137	0.15

To see if the evidence from experiments supports the theoretical predictions, we investigated the effects of DBSA NEs on asphaltene stacking with transmission electron microscopy. TEM is especially effective at providing direct images of asphaltene nanoaggregate stacks in asphaltene samples. As shown in Figure (6-2 A), with the addition of DBSA NEs, the cluster size of asphaltene is significantly decreased to about (5 nm), while the average interlayer spacing between aromatic rings is increased, indicating a gradual stabilization process. Figure (6-2 B) shows the selected area electron diffraction (SAED) images of asphaltene with and without DBSA NEs, which further indicated the transformation of asphaltene sample from unstable to stable by reduction of the π-π stacking distance of the asphaltene molecules. The interlayer distance between the periodic lattice fringes from the (002) plane of asphaltene with DBSA NEs was approximately 0.310 nm. This suggests that DBSA NEs allow significant change about 22.2 % increase in the stacking distance between aromatic rings of asphaltene. This is in agreement with the findings from our XRD that show the π-π stacking distance of asphaltene molecules is reduced in the presence of DBSA NEs (d_m) value of 0.396 nm.

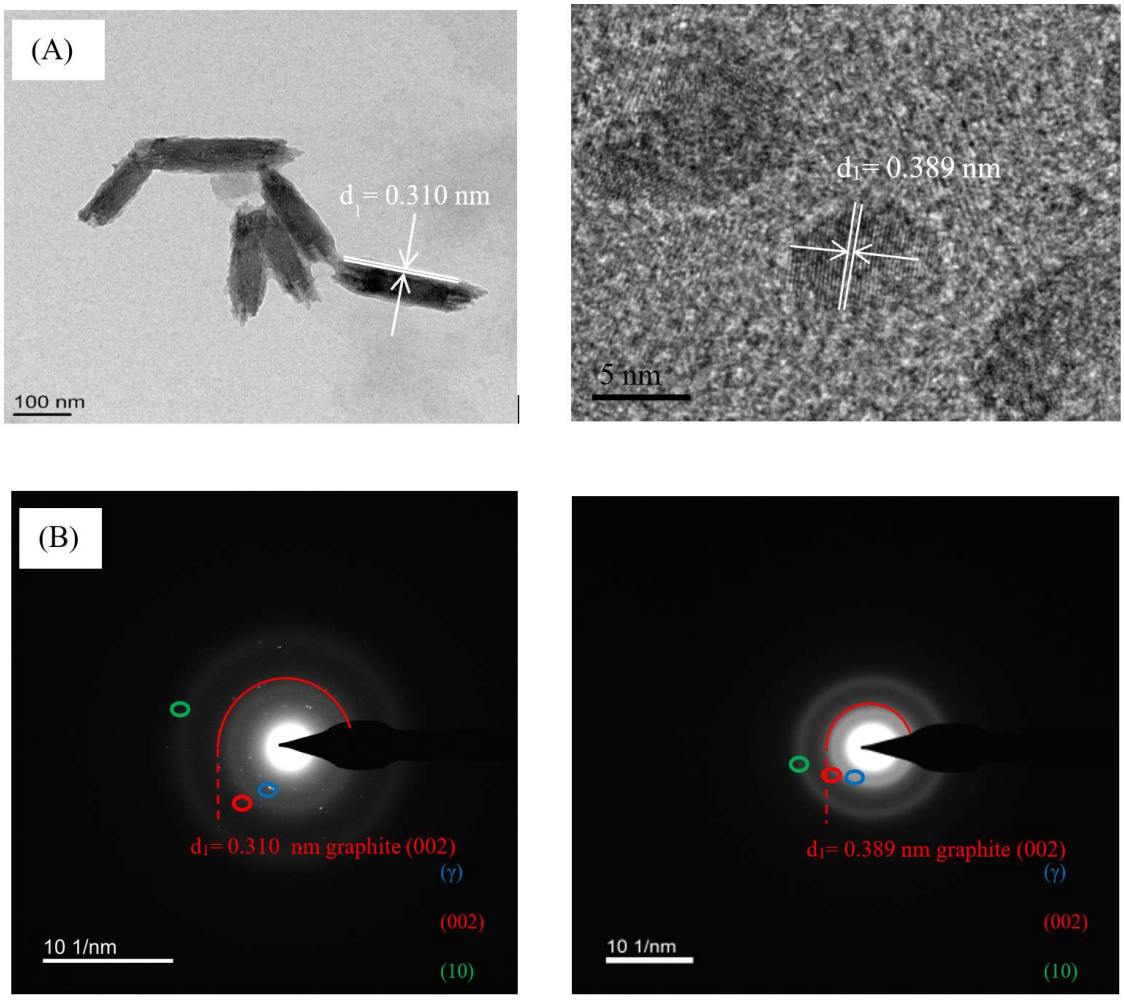

Figure 6-2. A) TEM image of asphaltene, and B) HRTEM image of asphaltene in the presence of DBSA NEs. The insets are the selected area electron diffraction pattern (SAED), which show the stacking distance measured d_{002} = 0.310 and d_{002} = 0.389 nm for asphaltene without and with the presence of DBSA NEs respectively.

6.3.2. Intermolecular interaction between asphaltene and the presence of DBSA NEs

One of the analytical techniques used for the determination of functional properties of asphaltenes is FTIR. Despite its versatility, this technique has received little attention to the study of asphaltenes [292, 293]. In addition, FTIR has been seldom mentioned in the

literature regarding quantitative [292, 294-296] and qualitative [266,297] studies for the functional resolution of asphaltenes. The FTIR analysis not only identifies the presence and quantity of functional groups in crude oil but also provides the information on the ratio of CH_2 to CH_3 and the relative amounts of aliphatic and aromatic groups, which are important criteria for crude oil [298].

The obtained FTIR absorption spectrum of extracted asphaltene is shown in Figure 6-4, which exhibited similar characteristic peaks as seen in previous studies [299-301]. Based on its complicated molecular structure, the featured peaks could be categorized into three sections: aromaticity, aliphaticity, and polar functionality [300]. Especially, for the aromatic moiety, the detected adsorption bands at 750, 808, and 866 cm^{-1} corresponded to the out-of-plane C–H bending in 1,2-disubstituted aromatic, 1,4-substituted aromatic, and 1,3-disubstituted aromatic, respectively; C=C stretching vibration in the aromatic structure was assigned at 1602 cm^{-1}. For the aliphatic characteristic, C–H stretching vibrations of CH_2 and CH_3 were assigned at 2922 and 2852 cm^{-1}, while the peaks at 1458 and 1375 cm^{-1} represented the C–H bending vibration of CH_2 and CH_3. For polar functionalities, stretching vibrations of –OH and/or –NH appeared at around 3458 cm^{-1}; and stretching vibrations of S = O in sulfoxides was observed at 1031 cm^{-1}.

Looking at Figure 6-3, it is apparent that DBSA NEs showed broad strong absorption band centred at 3365 cm^{-1} and this can be attributed to the formation of hydrogen bonds of interlayer water molecules with an anion (DBSA) as well as with hydroxyl groups of non-ion of Tween 80 and SDBS. The DBSA NEs can modify the colloidal structure of asphaltene by promoting the interactions between the asphaltene molecules and the components of DBSA NEs (i.e., DBSA, xylene, surfactants (Tween 80 and SDS) and water). The ability of DBSA NEs in reducing π-π stacking and hence increase the stability of asphaltene can be attributed to two main mechanisms: hydrogen bonding and acid-base

interaction. The hydrogen bonding interaction of asphaltenes and OH functional group of DBSA NE molecules was further investigated by observing the OH peak at the wave range of 3150 cm^{-1} to 3650 cm^{-1}. At the first step, the intensity of free and hydrogen-bonded OH of different concentrations of DBSA NE in carbon tetrachloride was characterized. The hydrogen bonded OH band initiated at 75 vol. % of DBSA NE in carbon tetrachloride that is the starting point of the formation of hydrogen bonding of DBSA NE molecules. Then this solution (DBSA NE and carbon tetrachloride) was added to asphaltene solution (0.5 w/v % of asphaltene dissolved with 60/40 vol. % Heptol) and IR spectrum was collected (Figure 6-4).

This figure shows that after addition of asphaltene, the peak of free OH bond at 3606 cm^{-1} disappears and the intensity of hydrogen-bonded OH at 3365 cm^{-1} is increased. These observations demonstrate that addition of DBSA NEs to asphaltenes leads to hydrogen bonding of free OH groups in the DBSA NEs. In addition, the integrated areas under the IR spectrums of asphaltene with and without DBSA NEs were calculated after curve deconvolution and normalizing to quantitatively evaluate any alteration. These results indicate that addition of DBSA NEs increases the integral from 2.59 to 5.36, demonstrating that asphaltenes form hydrogen bonding with DBSA NEs.

Furthermore, the addition of DBSA NEs to asphaltene largely exhibited several additional peaks. For instance, a peak from the O=S= O stretching vibration around 1300− 1000 cm^{-1} in the fingerprint region of FTIR spectrum of asphaltene shifts of the sulfonic group stretching vibration of asphaltene with DBSA NEs should be the result of bonding between functional groups of DBSA and the surface heteroatoms of asphaltenes. Therefore, it can be speculated that the release of DBSA molecules could contact asphaltenes and absorb onto the surfaces, via hydrogen bonding of O=S=O with O−H or C− H. Besides, the peaks between 660 – 900 cm^{-1} were higher than for asphaltene without

DBSA NEs, which were caused by the intensity vibration of NH_3 and N-H wagging (shifts on H- bonding). The peak intensity at 1740 cm^{-1} can be assigned to C=O (saturated aldehyde) or cis – RCH=CHR. The changes in out-of-plane O–H bending in aromatic rings of the asphaltene appeared at 675 cm^{-1}, while the peak intensity at 1510 cm^{-1} caused by NH_2 scissoring.

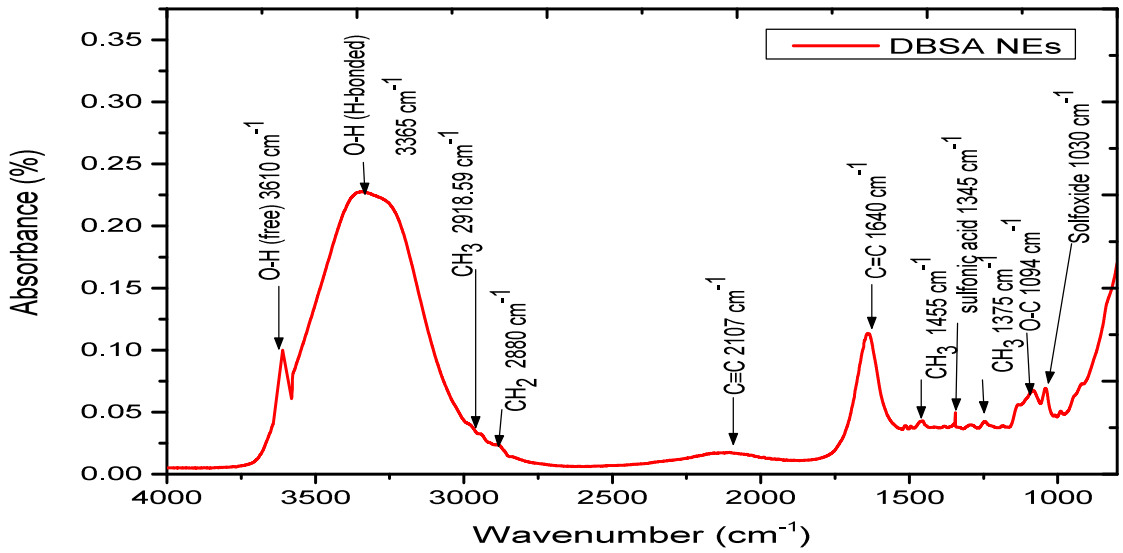

Figure 6-3. FTIR of DBSA NEs with 25 vol. % of carbon tetrachloride.

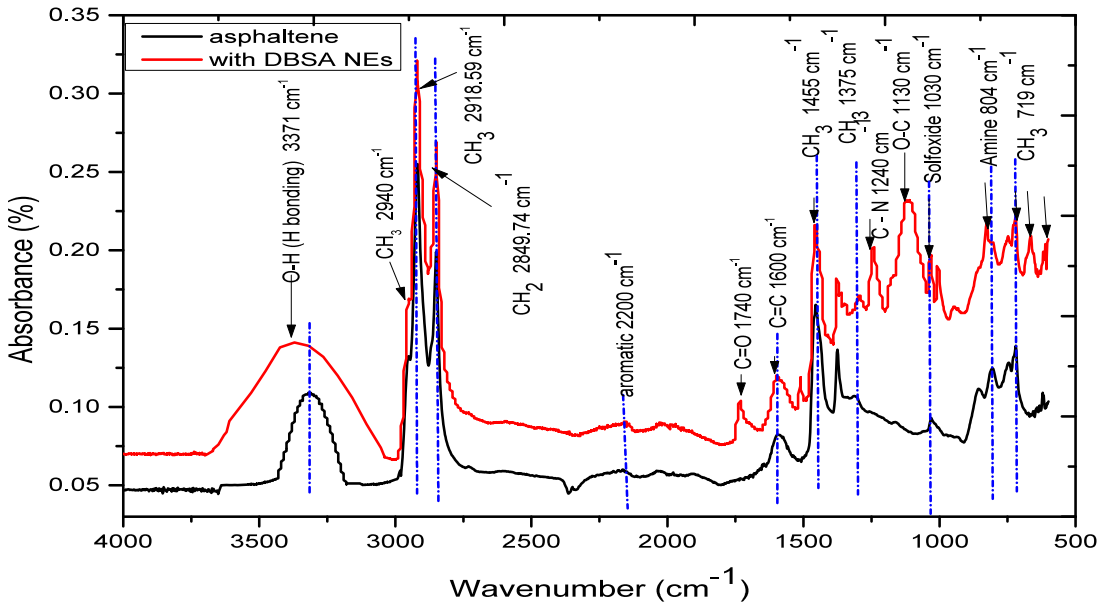

Figure 6-4. FTIR of asphaltene with and without DBSA NEs, showing the characteristic bands.

As discussed in the previous chapter, this system can overcome asphaltene intramolecular forces, creating new spaces, and involves multiple interactions between asphaltene and DBSA NE components such as acid-base interaction, hydrogen bond, polar-π interaction, cation-π interaction and aromatic-aromatic interaction. These interactions can promote further electrostatic interactions with other ion pairs. For example, the hydroxyl group in the chain length can form H- bonding with water or surfactants, whereas the nitrogen in the aromatic core can provide acid-base as well as H-bonding interactions with DBSA. Therefore, using a small amount of DBSA (1 vol. %) with other components in the DBSA NEs is sufficient to produce complete coverage of the individual aggregates.

For quantitative comparison of major functional groups in asphaltene, the integrated area of peaks (obtained from Origin 2017 software and explained in Section 6.2.3) and the intensities of specific wavelength were investigated. To calculate the number of carbon atoms per alkyl side chain, the molar ratio of CH_2/CH_3 is required which can be attributed to the ratio of absorbance intensities at wavelengths of 2,927 and 2,957 cm^{-1}. Also, this ratio is the measure of the length and the degree of the aliphatic chain by the Eq. 6-1 [301-304]:

$$N = \frac{n(CH_2)}{n(CH_3)} = \frac{A_{2927}}{A_{2957}}\ x\ K \qquad \text{…….. (6-1)}$$

Where K is a constant and determined to be 1.243 from correlating of 20 chemicals [305]. The molar ratio of aromatic rings to aliphatic side chains can be correlated with the absorbance intensities of 1450 and 1600 cm^{-1} by Eq. 2:

$$R = \frac{n(aromatic\ C{=}C)}{n(aliphatic\ C{-}H)} = \frac{A_{1600}}{A_{1450}} \qquad \text{…….. (6-2)}$$

Also, the ratios of the integrated area I_1 (2500–3000 cm^{-1}/1600 cm^{-1}) and I_2 (2500–3000 cm^{-1}/ 630–930 cm^{-1}) are relative indicators of how many aliphatic and aromatic groups are [306].

Table 6-4 shows the values of N and R for asphaltene with and without DBSA NEs samples. It can be seen from the results that asphaltene with DBSA NEs has lower the higher number of carbon atoms per alkyl side chain and it also has lower aromaticity compared with pure asphaltene. It means that the pure asphaltene is the most aromatic asphaltene and the asphaltene with DBSA NEs is the least aromatic sample. On the other hand, asphaltene with DBSA NEs shows a higher ratio of I_1 and I_2 than asphaltene without DBSA NEs, which means the shorter side chain of aliphatic substituents and more amount of aliphatic and aromatic groups.

Table 6-4. Asphaltene structure parameters with and without DBSA NEs from FTIR.

Sample	N	R	I_1	I_2	I_{3435}/I_{3100}
asphaltene	2.2	0.5	1.29	0.85	0.23
With DBSA NE	1.8	0.42	1.52	1.05	0.188

The tendency of asphaltene toward the formation of hydrogen bonding can be evaluated by calculating the ratio of the N–H and O–H intensities (3435 cm^{-1}) over the intensity of aromatic fraction (3100 cm^{-1}). These values in Table 6-4 imply that the pure asphaltene has the highest propensity toward aggregation by forming hydrogen bonding. The length of alkyl side chain can be attributed to the ratio of the intensities at a wavelength of 1455 and 1376 cm^{-1}. On the other world, the higher the ratio, the longer the side chain. These results are in the good agreement with the aromaticity results from XRD.

6.3.3. Mechanism on the effect of DBSA NEs on asphaltene structure

According to the experimental results, a possible mechanism was proposed and discussed as followed. The DBSA NEs can modify the colloidal structure of asphaltene by promoting the interactions between the asphaltene molecules and the components of DBSA NEs (i.e., DBSA, xylene, surfactants (Tween 80 and SDS) and water). Therefore, the ability of DBSA NEs to stabilize asphaltene can be attributed to several mechanisms such as i) the slow release of DBSA from NEs can provide the electrophilic addition reaction between DBSA and the π-electron of asphaltenes by initial breaking of its SO_3-H bond and subsequently bonding its dodecylbenzenesulfonate group with asphaltene molecules. It is worth noting that the DBSA NEs exhibit effective release kinetics due to the use mixture of anionic and non-ionic surfactants, which can pack closely at the oil/water interface and thereby make DBSA diffusion from NE slower. Moreover, the slower release rate could be attributed to the small size of DBSA NE (i.e., 21 nm), which can provide a high surface area of the system. In fact, higher surface area means higher surface from which the inhibitor can be released; ii) the presence of the relatively large lipophilic group (i.e., long-chain alkyl) of DBSA molecules shaped adsorbed DBSA similar to a wedge with a thick tail in the periphery of the new structure [307]. Likewise, the molecular structures of Tween 80 and SDS would shape themselves similar to a wedge with a thin tail aliphatic side chains that can hinder the π-π interactions of the asphaltenes neighbouring polyaromatic cores by introducing steric interferences in those interactions which consequently prevent the growth of asphaltenes aggregates. The length and shape of aliphatic side chains were proved to be vital factors that control the effectiveness of asphaltenes inhibitors. With an increase of the aliphatic chain length, the ability of inhibitors to surround molecules of asphaltene increases resulting in higher efficiency of the inhibitors [308, 309]; iii) aromatic compounds of Tween 80, SDS, and

xylene with a certain rigidity in the DBSA head capable of interacting with asphaltene aggregates by π–π stacking and hydrogen-bond formation; iv) H_2O may also undergo an electrophilic addition to the asphaltene's π-electron by the catalysis of acids (e.g., DBSA) and cause the absorption band in the range of 2000-3000 cm^{-1} as well as water molecules act as a bridge between asphaltene molecules via hydrogen bonds between water molecules and heteroatoms in asphaltenes. Figure 6-5 shows asphaltene molecules with two distinct nanocolloidal species are obtained after asphaltene molecules stacking. The smaller species is a nanoaggregate of small aggregation number with an aromatic core and an alkane shell. A cluster with a small aggregation number of nanoaggregates is obtained. While the overall length scales for the nanospecies are obtained from TEM and XRD results share many similarities with the Yen−Mullins model [310]. However, our proposed model involves the molecular structure of asphaltene after the addition of AI or NE loaded with AI and this must be explicitly accounted for the energetics of ring systems, as discussed.

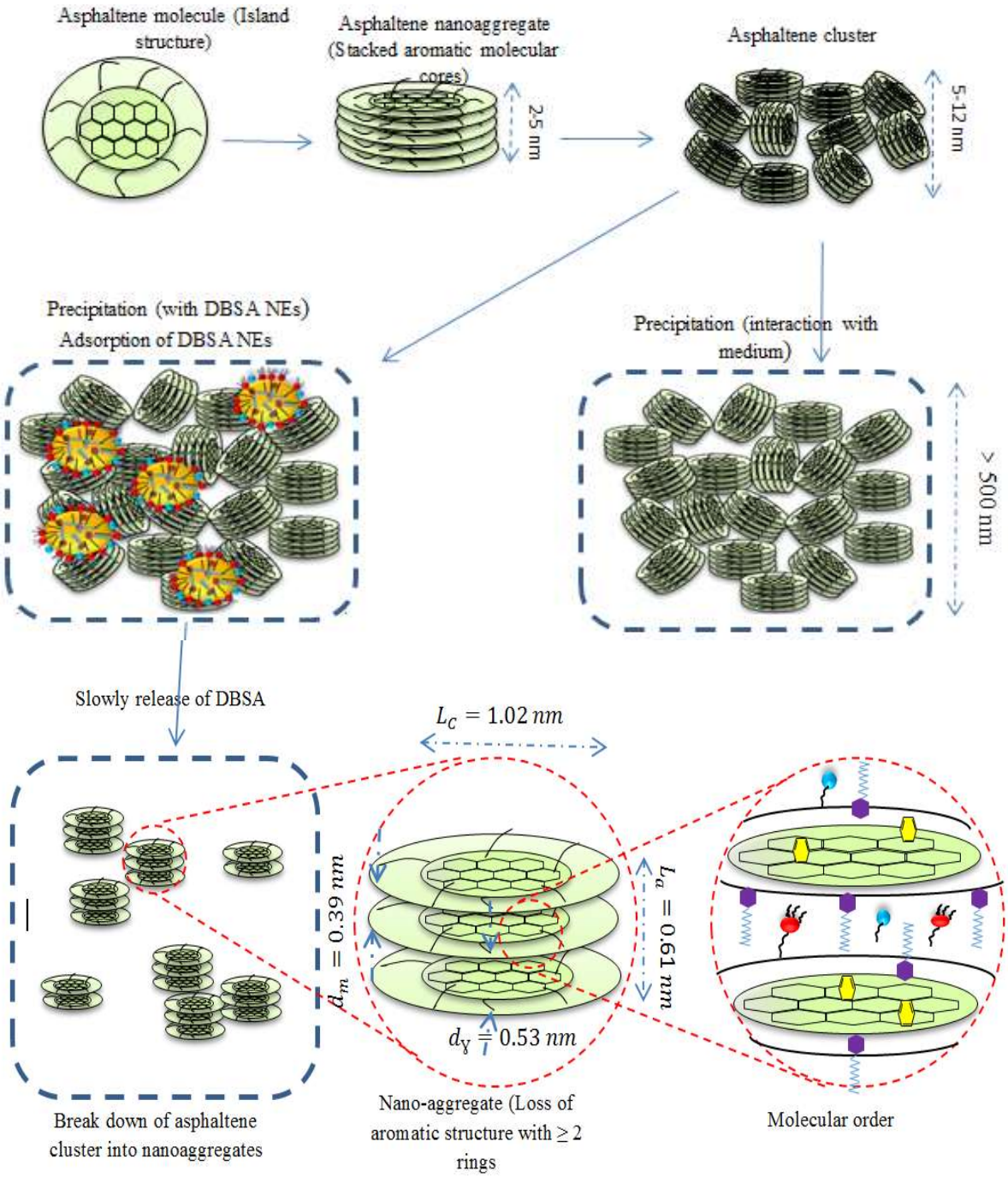

Figure 6-5. Schematic representation of the progression of asphaltene molecule and formation of nanoaggregates, with most aging being seen in larger asphaltene clusters (or primary particles). The mechanism of the adsorption of DBSA NEs on asphaltene and the slow release of DBSA from NE affect the stacking distance and the cluster size.

6.3.4. Thermogravimetric analysis (TGA)

The wide difference in the weight loss confirms the refractory nature of asphaltenes, which is relatively insensitive to the temperature. Weight loss due to the combustion of asphaltenes and asphaltene with DBSA NEs has been measured by thermogravimetric analysis purposes in the presence of air and it is presented in Figure (6-6 A). The role of air is to start the oxidation reaction; therefore, the decomposition rate is very fast at a higher temperature. This figure shows that the behaviour of asphaltenes toward coke formation is completely burned off having a maximum weight loss at 600 ˚C. Similar results were reported by Savel'ev et al., [311] and Maity et al., [312] using air in the degradation of asphaltene and functionalized asphaltene. However, around 97 wt. % another sample (asphaltene with DBSA NEs) is burned in the presence of air at around 600 ˚C.

The derivative curve clearly shows two principal weight losses at around 460 ˚C and at 585 ˚C, indicating that two types of asphaltenes are present in Figure (6-6 B). One is burned at a lower temperature, named as soft asphaltene and other at a higher temperature, named as hard asphaltene. Both peaks are sharp in nature. The presence of two types of coke (obtained mainly polymerization of asphaltene) is also reported in the literature [313-315]. Two peaks were situated at 390 and 460 °C which could mean decomposition of heavier asphaltenes with higher molecular weight or very highly associated asphaltenes. Total volatilization is achieved at 550 ˚C; asphaltenes at this temperature were fully burned off by the presence of oxygen in the air and the maximum weight loss is seen. In this stage, intermolecular associations and weaker chemical bonds are destroyed such as sulfur bridges. However, asphaltenes are not only converted into coke but also expected to be transformed into lighter compounds such as gases, oils, and resins. Above 450 ˚C temperature, asphaltenes are subjected to very severe conditions making condensation

reactions to form coke as final residue [315]. The final residue from asphaltene decomposition was 12.57 % (2.33 mg) of the initial mass, which may consist of typical of polycyclic condensed aromatic hydrocarbon compounds with large aggregates as well as elements like Ni, Fe, and VI that are stable at higher temperatures.

Comparing the thermal profile of asphaltene with the asphaltene with DBSA NEs, the derivative curve clearly develops three consecutive weight loss processes at around 300 °C, 460 °C and at 585 °C, indicating that three types of asphaltenes are present. TGA curves show that asphaltene with DBSA presented an oscillation peak from 50 to 200 °C that can be attributed to the loss of light organic compounds and the residual water (dehydration) obtained from the addition DBSA NEs to the asphaltene. The water molecules are directly bonded to the asphaltene molecules via hydrogen bonding. Hence, it is very remarkable that the water loss in asphaltene is accompanied by minor structural changes, but the framework is maintained as the overall shape of the pattern changes little between room temperature and 220 °C. This monohydrate phase is stable up to approximately 200 °C. After 200 °C asphaltenes with DBSA NEs suffer continuous decomposition up to around 600 °C. This can be attributed to releasing CO, CO_2 and some hydrocarbons from asphaltene as well as to the loss of long alkyl chains of DBSA NEs components which linked with asphaltene molecules. However, the 2nd peak of the asphaltene sample appears at 550 °C and it is shifted to a higher temperature around 585 °C for the sample asphaltene with DBSA NEs. The residue at the highest temperature for asphaltene with DBSA is very low about 4.71 %, suggesting that formation of multiple intermolecular interactions such as hydrogen bonding, acid-base interaction, and π-π stacking between the adjacent molecules of DBSA NEs with asphaltene molecules, which give rise to the high temperature [316].

The conversion of asphaltene to coke decreased when DBSA NEs were added to asphaltene, meaning that the effect of DBSA NEs tends to stabilize a proportion of the asphaltene. The DBSA NEs can promote the loss of labile points of long alkyl chains in DBSA NEs components which linked with asphaltene molecules giving more volatile compounds such as gases. Nevertheless, low coke formation was observed in asphaltene with DBSA NEs, it is possible that due to many of lighter compounds present in asphaltene with DBSA NEs have been volatilized in the initial stages only a few amounts of formed asphaltenes remains during the reaction to finally decompose toward coke which appears in less amount compared with original asphaltenes. This could explain why asphaltene with DBSA NEs continuously change in a wide range of temperature (200 – 585 °C) and why a broad range of reaction temperatures as such is not observed even for original asphaltenes. This behaviour could indicate that the coke yield is sensitive to the presence of DBSA NEs components, decreasing it around 62 %. Besides, similarities in the shape of the weight loss curves indicate that DBSA NEs did not change the main degradation pathways of asphaltene and no new material is formed due to the reaction of DBSA NEs with asphaltene. However, the nature and the structure of hard asphaltene become softer when this is treated with the DBSA NEs as well as the coke yield is decreased. These findings of TGA are in the good agreement with the other results of XRD, TEM, and IFIR for both asphaltenes with and without DBSA NEs presented in this work.

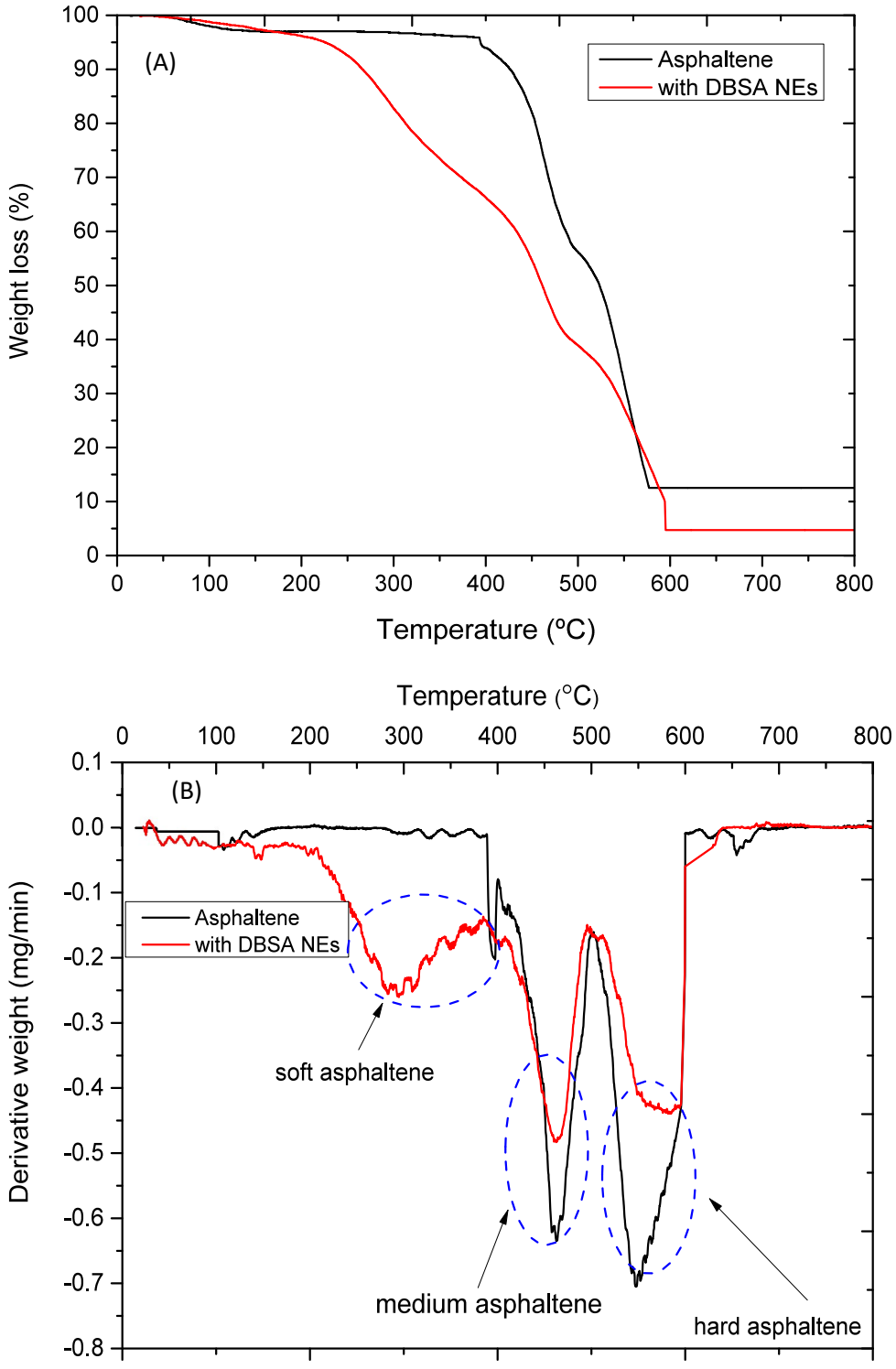

Figure 6-6. (A) TG, and (B) the derivative weight of asphaltene and asphaltene with DBSA NEs in the air.

6.4. Chapter summary

This Chapter examined the detailed molecular structure of asphaltene in the presence of NEs, and proposed a mechanism of modification structure and stabilizing asphaltene as summarized in the following points:

- Controlled release of AI by NEs could affect both morphological and structural of asphaltene.
- The results from XRD and TEM confirmed the validity of asphaltene stability mechanism by the release of DBSA and other NE's components, which were able to increase both the stacking distance between aromatic rings (about 22.2 %) and aliphatic chains and reduce the diameter of the aromatic sheet and the cluster size.
- These alterations in the molecular structure of asphaltene led to decrease in the aromaticity of asphaltene, which in turn increased the solubility of aromatic compounds in oil and improved the liberation of asphaltene aggregates. As a result, the disruption of the aromaticity implied a change of the π system over the aromatic zone that in turn disturbed eventual π–π interactions between asphaltene stacks, which was the main mechanism responsible for the formation of clusters at the nanoscale.
- The FTIR spectroscopic study verified that DBSA NE involved multiple interactions with asphaltene, building up a multicentric electron density in this region, which led to deeper isosurfaces of van der Waals forces in the interacting zone.
- In addition, the quantitative study indicated that asphaltenes with DBSA NEs had a lower number of carbon atoms per alkyl side chain, lower

aromaticity, shorter side chain of aliphatic substituents, and more amount of aliphatic and aromatic groups compared with pure asphaltene.

- The TGA results further demonstrated the alteration of asphaltene structure. It was found that during the chemical reaction between asphaltene and DBSA NEs, the structure of asphaltene was improved considerably and the coke yield was decreased around 62% due to the decrease of the cluster sizes and the increase of the stacking distance between aromatic sheets.

Chapter 7

Delivery and controlled release of inhibitor: A prospective method for enhanced oilfield asphaltene prevention

7.1. Introduction

As reviewed in Section 1.5, there is a large body of literature that deals with the adsorption of asphaltenes on various rock minerals, including clays. Most of these works are concerned with the measurement and modeling of adsorption isotherms on crushed minerals under static conditions [318-326]. Very little work currently exists on the adsorption kinetics of asphaltenes under flow conditions [327, 328].

In this chapter, we develop a novel concept of using NEs as carriers for AIs and control their release inside porous media to improve the cumulative asphaltene removal efficiency. A series of dynamic experiments are conducted to study asphaltene adsorption from monolayer to multilayer in order to understand rock-asphaltene interactions under flow conditions. The level of asphaltene transport and adsorption in sandstone packed column is evaluated and based on the evaluation a kinetic adsorption mechanism is proposed. Asphaltene removal experiments are also examined by using a core-flooding facility in three case studies, i) with pure DBSA, ii) with blank NEs, and iii) with NE loaded with DBSA (i.e. DBSA NE). Several possible mechanisms for asphaltene removal are also proposed.

7.2. Materials and experimental procedure

7.2.1. Porous medium preparation and characterization

Water-wet Berea sandstones with permeability ranging from 98.73 to 195.46 mD were selected as the porous medium in this study. The sandstone rock was crushed into single grains, sieved into narrow grain size fractions (ASTM Standard Testing Sieves, Retsch Ltd) and washed with water for several times, which was followed by settling and decanting to remove all dust particles. The residual wet sand particles were dried at 70 °C for 7 days. The porosity, absolute permeability, and dry sandstone rock weight were measured. The porosity was determined by both helium pycnometry and Archimedes (buoyancy) methods.

An investigation of the morphology of grains and pores in the sandstone rock, as well as an elemental analysis, was carried out using a scanning electron microscope (SEM, FEI Quanta 650 FEG-ESEM) and integrated energy-dispersive X-ray spectroscopy (EDX, Oxford Xmax 80 SDD) with INCA 350 software. Verification for the structure of sandstone rock is done using an X-ray diffractometer (Bruker, D8 Advanced, Germany). The sample was irradiated using a Cu target tube and exposed to all lines. The scanning angle ranged from 10° to 80° of the diffraction angle (2θ) for 45 min. The chemical composition of the sandstone rock sample is determined by X-ray fluorescence (XRF by Bruker AXS S4 Pioneer) and presented in Table 7- 1. It can be seen from Figure 7-1 and 7-2 and Table 7-1 that most of the pore sizes were above several micrometers, while confirming that the grains were composed of silica (SiO_2) with a minor fraction of alumina silicate mineral.

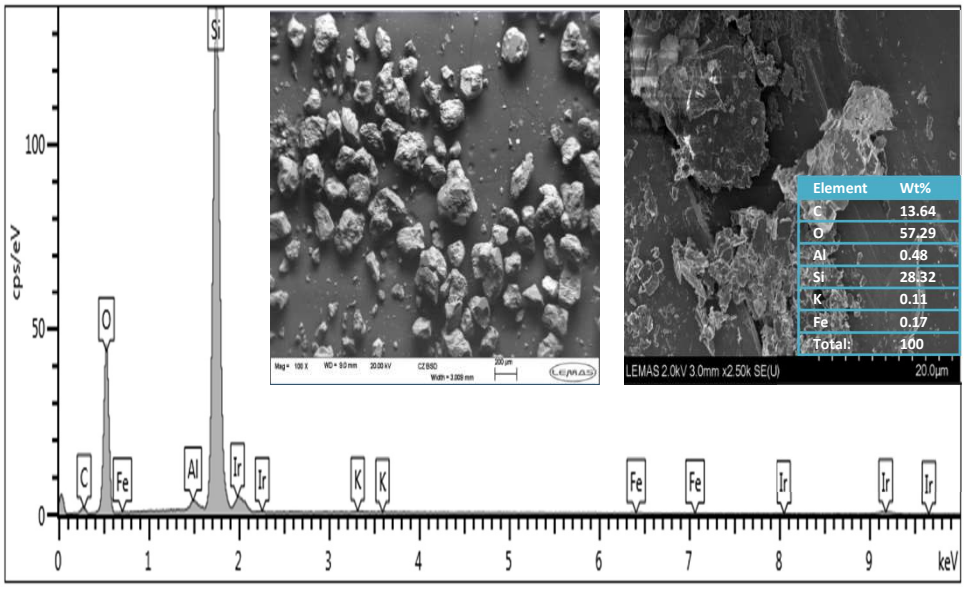

Figure 7-1. (a) High magnification SEM image of feldspar and porosity between silica grains and elemental mapping of rock using an energy dispersive X-ray spectroscopic.

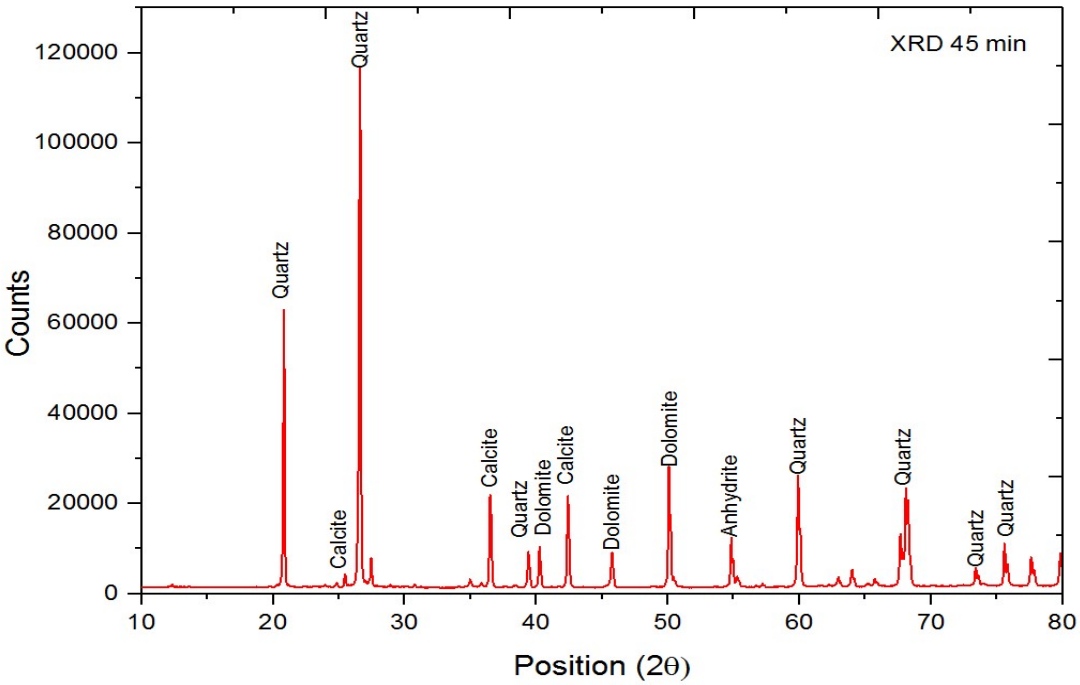

Figure 7-2. Results of XRD of the reservoir rock used in this study.

Table 7-1. The chemical composition of Berea sandstone by X-ray fluorescence

Component	Result in mass%
SiO_2	92.2518
Al_2O_3	3.3719
Na_2O	0.2473
MgO	0.1963
P_2O_5	0.0188
SO_3	0.0454
K_2O	1.2543
CaO	0.2245
TiO_2	0.1285
Cr_2O_3	0.0394
Fe_2O_3	0.7332
NiO	0.0109
Br	0.4685
ZrO_2	0.0091

7.2.2. Zeta potential measurements

For these analyses, Berea sandstone rock was crushed and classified by sieving, the particles size less than 45 µm were selected. Brine solution prepared in 1 wt. % kaolinite and crushed Berea sandstone and centrifuged for 6000 rpm for 20 min. The sample of supernatant was transferred to polystyrene cuvette to measure the zeta potential of rock by Zetasizer Nanoseries ZS, Malvern Instrument, Worcestershire, UK.

Zeta potential of NEs at different salinity was also evaluated. Furthermore, asphaltene-in-water emulsions were prepared by emulsifying 100 mg L^{-1} of the asphaltene in the aqueous phases using the ultrasonic probe (Unique) at 25 Hz for 10 min to measure the zeta potential of asphaltene droplets. All zeta potential values are the average of three independent runs carried out at room temperature.

7.2.3. Interfacial tension and contact angle measurements

The IFT and contact angle were measured by the pendant drop method using a goniometer (CAM 200, KSV instruments Ltd. Finland). The interfacial tension (IFT) between

asphaltene and different samples: deionized water, brine, DBSA, blank NEs, and DBSA NEs were measured based on the Young-Laplace equation by the pendant drop.

Measurements of the static contact angle (CA) of asphaltene/brine/rock systems were performed using the IFT/CA apparatus. The rocks were cut into small substrates that were polished two sides, and then vacuumed at 10−7 psi for 2 h, and then immersed in asphaltene solution. After aging in asphaltene for 0, 7, 14, and 21 days, they were gently placed in the IFT/CA cell. Brine (with and without NEs) was then transferred to the cell until the substrates were fully immersed. Figure 7-3 shows the schematic diagram of the experimental setup for Interfacial tension and contact angle measurements.

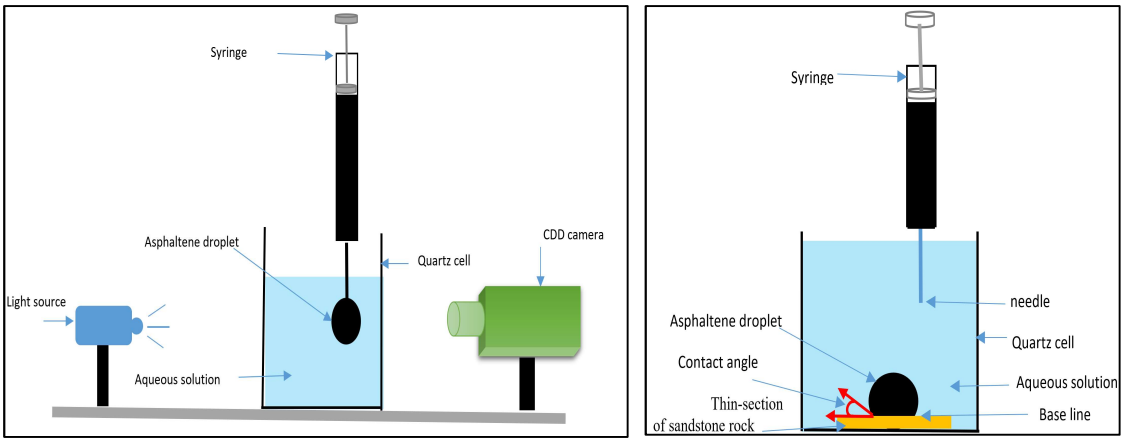

Figure 7-3. Schematic diagram of experimental setup for Interfacial tension and contact angle measurements.

7.2.4. Core-flooding experiments

Figure 7-4 shows the experimental core flooding set-up. First, the sieved, washed, and dried porous media were packed inside the holder. A piston pump (Cole-Parmer Instrument Co. Ltd.) was used for injecting brine during the core flooding experiments. Two syringe pumps (KDS 410, KD Scientific Inc. USA) were used; one for injecting asphaltene solution and another one for injection four different displacing fluids: brine,

pure DBSA, blank NEs, and DBSA NEs to avoid cross-contamination by different samples. The concentration of asphaltene was on-line measured by an UV spectrophotometer (Shimadzu, UV 1800), when it flowing through a built-in flow cell. A pressure transducer (PX409-150DWUV, Omega Engineering Ltd.), which was connected to Lab View software, was used to measure the pressure drop during experiments. The parameters of packed sandstone grains column are listed in Table 7-2, where the permeability was calculated based on Darcy's law by using the equilibrium pressure drop at a specific flow rate during brine saturation.

Table 7-2. Parameters in average value for packed glass beads column from over 20 times of practice for packing.

Porous media properties	Value
Bulk volume (mL)	33.7 ± 1.4
Pore volume (mL)	12.9 ± 0.5
Porosity (%)	38.01 ± 1.57
Absolute permeability (mD)	90-112
Mass of wet sandstone beads (g)	72.60 ± 3.10
Mass of dry sandstone beads (g)	59.80 ± 2.60
Liquid in the pore space (g)	12.8 ± 0.5
Length (mm)	72 ± 2
Diameter (mm)	24
Specific surface area (m^2/g)	0.877 ± 0.001
Electrophoretic mobility (μm cmV^{-1} s^{-1})	-1.58 ± 0.09
Zeta potential (mV)	- 20.6

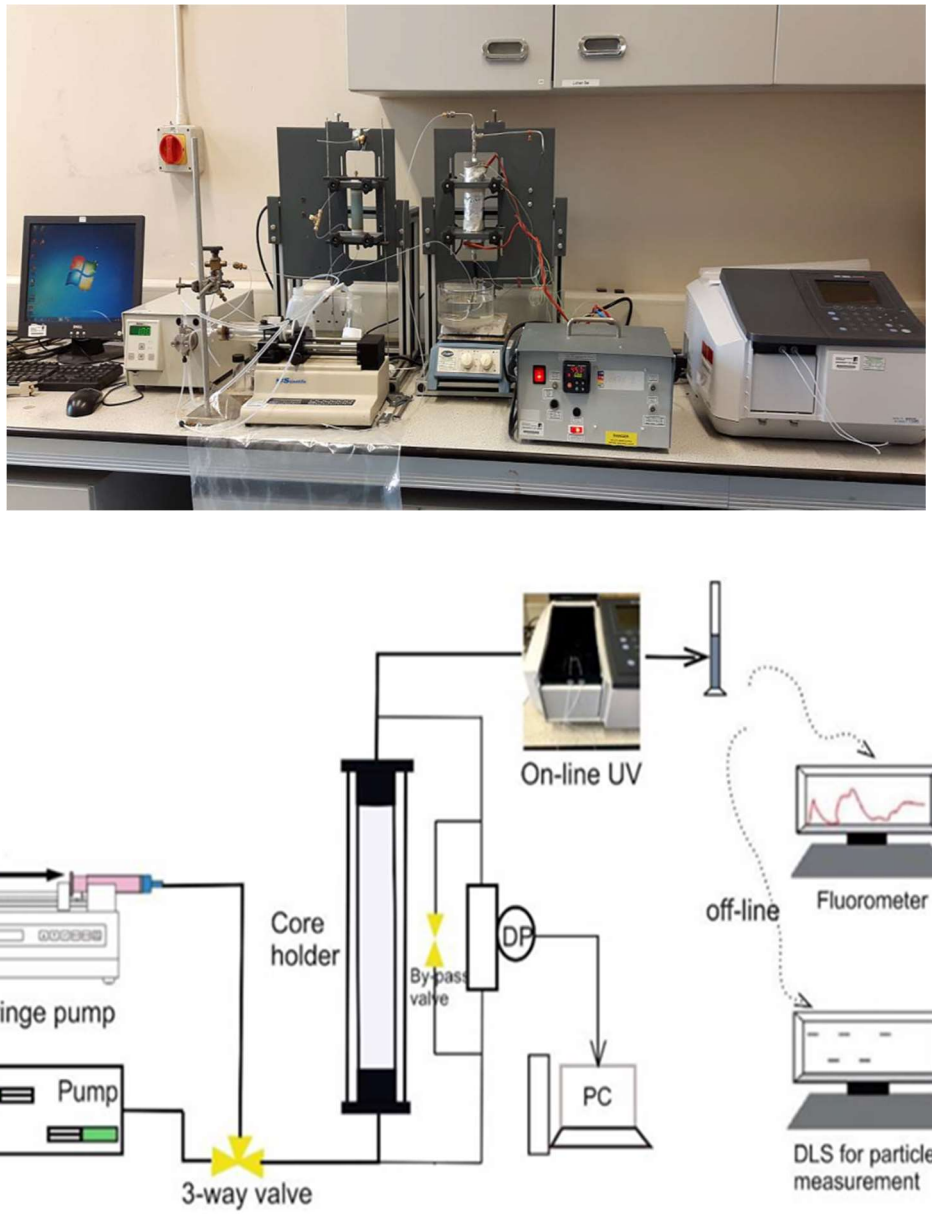

Figure 7-4. Experimental core flooding set-up.

The core flooding experiments were divided into two parts. The first part was for dynamic asphaltene adsorption measurement and the second one for asphaltene recovery evolution.

7.2.4.1. Dynamic adsorption experiments

In the first part of the experiments, below procedures were used:

- Injection of 100 ml brine (4% NaCl) flooding at a flow rate of 2 ml/min (0.156 PV/min) to fully saturate the column by brine.

- Asphaltene solution injection until desired irreducible water saturation (S_{wi}= 25%) was achieved, and the original oil in place (OOIP) is determined by the volume of water collected.
- Injection of 20 ml brine post flooding (4% NaCl) at a flow rate of 0.5 ml/min (0.078 PV/min).

At the same time, the effluent solution was flowed through a UV–visible spectroscopy meter and was collected. The asphaltene effluent concentrations were measured based on the absorption of asphaltene for UV light at a wavelength of 423 nm. The breakthrough curves (BTCs) of asphaltene in the column outlet were generated by using the relative concentration (i.e., the effluent concentration C_e divided by the original sample concentration C_0), against the injection time expressed in pore volumes (PVs).

The amount of asphaltene adsorbed (Γ) on the solid surface (mg/g rock) for the core flooding was estimated following the mass balance according to equation [319,320]:

$$\Gamma = \frac{C_o - C_e}{W} V \qquad \text{..... (7-1)}$$

where C_o (mg/L) and C_e (mg/L) are the initial and equilibrium concentrations, respectively, V (L) is the solution volume and W (g) is the mass of solid dry sandstone.

7.2.4.2. Asphaltene displacement Tests

The second part of the experiments concerns the removal of asphaltene inside a sand packing in core flooding experiments, as below:

- Brine saturation by injecting 10 PV of brine at the optimum salinity (4 wt. % NaCl) at 2 ml/min (0.156 PV/min).

- Place the sandstone in asphaltene solution (asphaltene in 60:40 Heptol) and centrifuge them at 2000 rpm for 30 minutes. The preceding step was to displace the water droplet on the rock surface to keep only the irreducible water (S_{wi}). The sand-pack system was then allowed to oil-wet for 21 days with asphaltene solution.
- Brine injecting 3 PV of brine at the optimum salinity (4 wt. % NaCl) into the packed bed column at 0.5 ml/min (0.038 PV/min).
- Three different displacing fluids were injected including (4 vol. % of pure inhibitor, 20 ml of blank NEs, and 20 ml DBSA NEs) at a flow rate of 0.5 ml/min for 1.5 PV. Following the pure AI injection, the brine solution will be injected to push the previously injected AI deeper into the sand column. This step is called injection of "overflush fluid''. The traditional inhibitor squeeze treatment uses AI usually as a 5%–20% in the reservoir [331], thus the total pure AI amount equal to 4 ml (20% from 1.5 PV).
- Then the column was shut-in for 24 h to allow the displacing fluids to be able to affix to the surfaces of formation (i.e. the slow release).
- 40 ml brine post flooding was conducted at a flow rate of 1 ml/min.
- The effluent liquid was collected in a 50 ml graduated cylinder marked in 0.1 ml divisions in order to determine the amount of oil recovered. Table 7-3 shows the number of experiments pertaining to each pair of concentration, flow rate, heptane and clay content tests.

To calculate the cumulative asphaltene recovery efficiency, three tertiary flooding experiments were conducted with pure AI, blank NEs, and DBSA NEs. As described in the core flooding experiment (asphaltene displacement procedure), all the effluent materials, including asphaltene, brine and NE suspensions, were collected by using a

long slim graduated tube marked in 0.1 mL divisions. Due to the density difference, the asphaltene solution/water phase can be separated instantly and automatically. The cumulative asphaltene recovery efficiency (ECAR) is calculated by using the amount of cumulative asphaltene production divided by the OOIP (Original Oil in Place) at the residual water saturation (Swi) of 25%. The advanced asphaltene displacement efficiency (EAAD) is calculated by using the amount of asphaltene solution produced in the process of displacing fluids/ brine post flooding divided by the asphaltene left at end of brine/ displacing fluids.

The reduction of asphaltene inhibitor amount (% R_{AI}) and the total chemicals usage (% R_{TC}) in the NE were calculated following the material balance according to equations 4-3, 4-4, and 4-5 in Section 4.3.3.

Table 7-3: Experimental analysis for the effect of asphaltene concentration, flow rate, heptane, and clay content.

Experiment	Concentration (mg/L)	Flow rate (ml/min)	Heptane (vol. %)	Kaolinite (wt.%)
1	10000	0.5	-	-
2	10000	1	-	-
3	10000	3	-	-
4	5000	0.5	-	-
5	10000	0.5	-	-
6	10000	0.5	-	5 %
7	10000	0.5	40%	-
8	10000	0.5	40%	5%

7.3. Results and discussion

7.3.1. Formation of NE at the optimum salinity

As reported in Section 3.2.2, the formation of stable NEs against coalescence or Ostwald ripening processes, a mixture of surfactants can form a strong interfacial layer around oil droplet. However, in this Chapter, another way to reduce the number of surfactants

needed for NE stabilization is the addition of salt, resulting in low treatment cost. It has been found that, in the case of using synergistic surfactants systems (i.e. ionic-surfactant plus non-ionic surfactant), salt content effectively reduces the thickness of the interfacial electrical double layer, allowing to be obtained a NE with less surfactant [332]. Maeda [333] and Ruiz et al. [334] stated that the stability between the ionic and non-ionic mixed micelles systems is controlled mainly by two factors. One is the interaction between the head groups, and the second one is the interaction between the hydrocarbon chains. The effect of adding monovalent electrolyte sodium chloride such as (NaCl) at different concentration (0 – 6 wt. % NaCl) have been studied in this section. Light scattering measurements show that at lower salinities (e.g. < 3 wt.%), more surfactant molecules were dispersed in the water phase. Therefore, the steric and electrostatic repulsion between oil droplets is too weak to overcome the hydrogen bonds of water molecules. As salinity increased, at 4 wt. %, the solubility of the surfactant in the water phase is increasingly reduced and most surfactants tend to distribute at the oil/water interface, which leads to the decrease of interfacial tension and decrease the droplet size. In addition, the electrostatic repulsion overcomes the van der Waals and hydrophobic attraction because it is still adequately strong. However, NaCl could destabilize NEs by weakening the electrostatic repulsion, whereby as the salt concentration increased (above 4 wt. %), the electrostatic repulsion among droplets became weaker and weaker due to the electrostatic screening of the charge, ultimately resulting in larger particle sizes [335].

The zeta potential of NE was also evaluated at different ionic composition (Figure 7-5 A). The results show that the zeta potential of the NE decreased slightly with increasing NaCl (e.g.< 4 wt.%), but this changed sharply (in the negative side) and shift toward zero upon the further addition of NaCl (e.g.> 4 wt.%). At optimum levels (4 wt.%), comparatively strong electrostatic repulsion persisted, thereby preventing droplets from approaching

each other. Similarly, the hydrodynamic size and refractive index in Figure 7- 5 B shows the same trend with zeta potential measurements. Therefore, 4 wt.% of NaCl was selected as the optimum salinity in the next experiments.

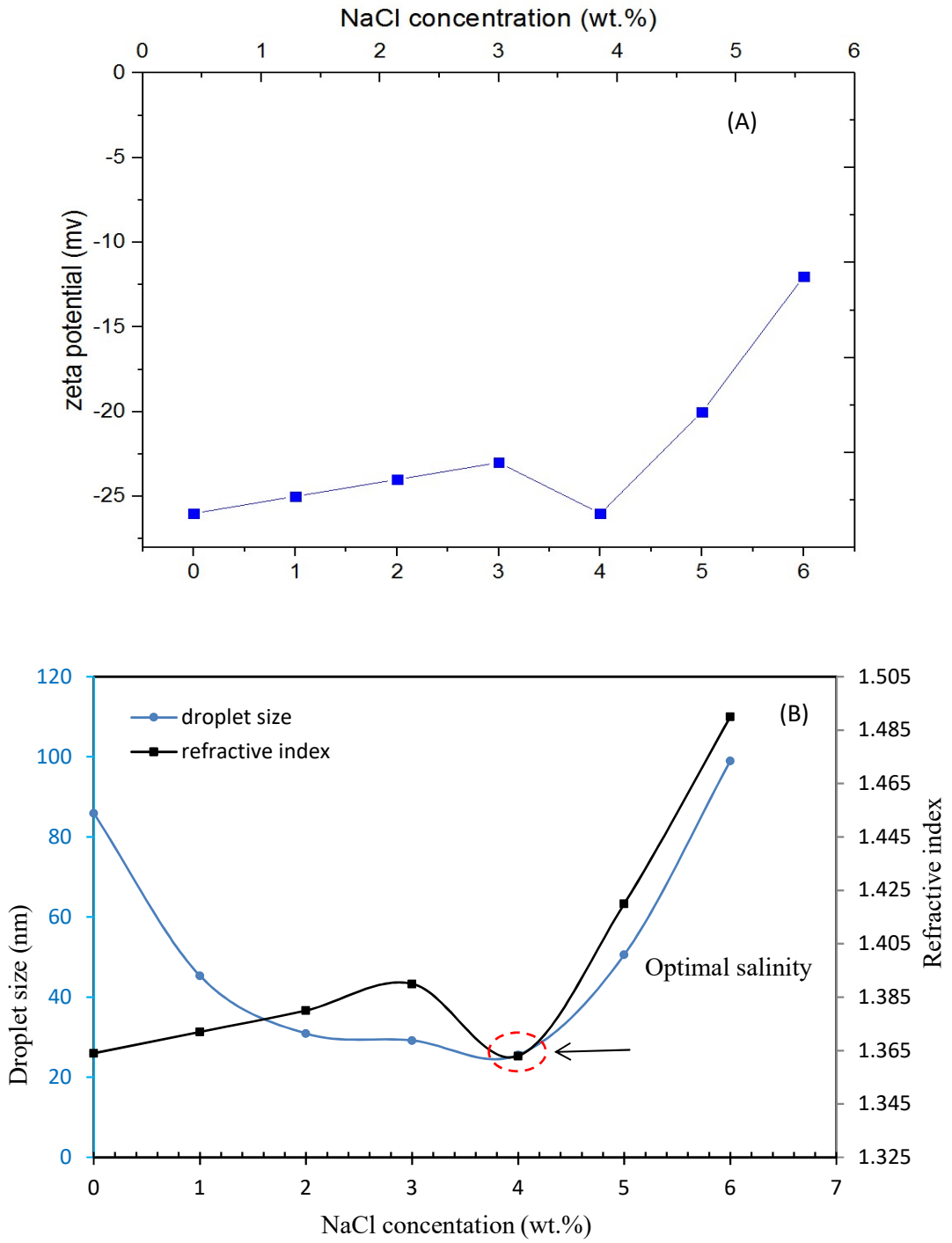

Figure 7-5. (A) Zeta potential for NEs, (B) Hydrodynamic size and the refractive index of NE samples with different NaCl concentrations

7.3.2. Dynamic adsorption experiments

The adsorption of asphaltene on porous media depends on the composition and petrophysical properties of porous media samples [336]. Therefore, different tests (as shown in Table 3) were conducted to evaluate the dependency of asphaltene adsorption on flow characteristics, concentration and composition of asphaltene, and the effect of clay content.

Figure 7-6 (A–C) shows the plot of the concentration profiles (i.e., breakthrough curves) vs. pore volumes injected for a 10000 mg/L asphaltene solution. The asphaltene injections were performed at 0.5 ml/min, 1 ml/min and 3 ml/min. The breakthrough curves for both the low and higher rates injection cycles are plotted. In the low flow rate (0.5 ml/min) case (i.e., test 1), a further shift to higher pore volumes injected at breakthrough is observed; indicating high adsorption in the accessible pore volume requiring about 1.6 PV to reach equilibrium concentrations in the effluent. It is probably due to entrapment in smaller openings between pore sand adsorption in the entire core that resulted in higher asphaltene loss in this case. Furthermore, mass separations between asphaltene molecules (i.e., smaller molecules have penetrated the pore sand were retained) and adsorption kinetics are perhaps, responsible for the spread out the aspect of the asphaltene in the low flow rate regime. At 1 ml/min (i.e., test 2) showed a similar early breakthrough at 0.5 PV but with a reduced concentration of asphaltene in the emerging fluid (C/C_0 = 79%), implying that up to 29 % of the injected asphaltene remained within the core. On the other hand, at a high flow rate (i.e., test 3), the breakthrough was achieved quickly with C_e/C_0 approaching unity at 0.4 PV just as the first drop of asphaltene emerged from the core. The different explanations have been reported for the effect of flow rate on asphaltene adsorption mechanism as the shear effects, residence time, and zone isolation in the pore space at higher flow rates [337].

Figure (7-6 B) shows the variation of concentration and adsorption amounts of asphaltene versus injected pore volumes of asphaltene solution at two different asphaltene concentrations of 5000 mg/L and 10000 mg/L (i.e., test 4 and 5). The early breakthrough in the concentration curves is the same for both concentrations; however, it takes longer for asphaltenes to reach the equilibrium asphaltene concentration at 10000 mg/L compared to 5000 mg/L. As expected, the adsorbed amount of asphaltene at 5000 mg/L asphaltene concentration is 0.58 mg/g rock smaller than that at 10,000 mg/L, as shown in Table 7-4.

More fluctuations for C_e/C_0 were also observed in Figure (7-5 C) compared to injection asphaltene inside rock without kaolinite clay (i.e., test 6), both implemented at flow rate 0.5 ml/min and asphaltene concentration of 10,000 mg/L, is due to the presence of kaolinite clay and the resulting heterogeneity that led to entrapment and re-entrainment of asphaltene particles.

When precipitant (heptane) was added to the asphaltene solution, a substantial amount of asphaltene was deposited on the rock surface due to the destabilization effect of heptane. This can be observed in Fig. (7-6 C) (i.e., test 7) with C_e/C_0 varying in the middle section of the graph and the breakthrough is shifted to higher pore volume injection. One can argue that the observed breakthrough level C_e/C_0 reduction is a result of the increase in asphaltene particle size and reduction in particle stability. As seen in this figure, the adsorption did not reach the saturation level and continued with the injection of asphaltene solution in the sand pack. Therefore, it can be said that adsorption in the presence precipitant and kaolinite is multi-layer adsorption with no saturation limit in contrary to tests conducted at higher flow rates and low concentrations that obeyed Langmuir type adsorption which reached the saturation level.

Each flooding experiment was followed by an injection of a further 3 PV of brine in order to check if the asphaltene particles were strongly adsorbed inside the rock. This brine post flooding process was conducted after the end of the asphaltene flooding at 3 PV for all experiments. The results (i.e., rightmost part of Figure 7-6 a, b and c) show that different amounts of asphaltene can be removed out from the sand following the brine flooding. However, after another about 3 PV of brine, no more asphaltenes can be driven out, suggesting that some asphaltenes remain trapped in the cores.

Further calculation shows that, for test 8 (highest concentration (10,000 mg/L) asphaltene flooding with the presence heptane and clay content at low flow rate), 193.5mg of asphaltene in total (48.1% of the total injected amount) were deposited in the rock during asphaltene flooding and remained trapped there, which corresponds to about 3.235 mg of asphaltene per gm of grain surface. The desorption of asphaltene via brine flooding shows that a significant amount of asphaltene (58.6 mg) is strongly adsorbed inside the packed bed column even after further 3 PV brine injection. We have focused more on test 8 in the rest of the chapter.

Table 7-4. Asphaltene adsorption/desorption in the core sample during asphaltene/ brine flooding.

	Asphaltene adsorption				Asphaltene desorption			
Test	Total Asph. Mass adsorbed (mg)	Ce/C_0 (%)	Γ(mg/g rock)	adsorbed asphaltene fraction %	Ce/C 0 (%)	Total Asph. adsorbed mass (mg)	Γ(mg/g rock)	desorbed asphaltene fraction, %
1	81.268	79	1.359	21.49	36	40.7238	0.681	50.11
2	58.00	85	0.97	15.34	26	41.561	0.695	71.65
3	30.916	92	0.517	8.17	22.5	22.0662	0.369	71.37
4	34.684	82	0.58	17.92	21.5	22.3652	0.374	64.48
5	116.071	70	1.941	30.70	35.5	52.5642	0.879	45.28
6	162.536	59	2.718	42.99	40	56.511	0.945	34.76
7	166.54	57	2.785	44.05	43	57.408	0.96	34.47
8	193.5	50	3.235	50.00	41	58.663	0.981	30.31

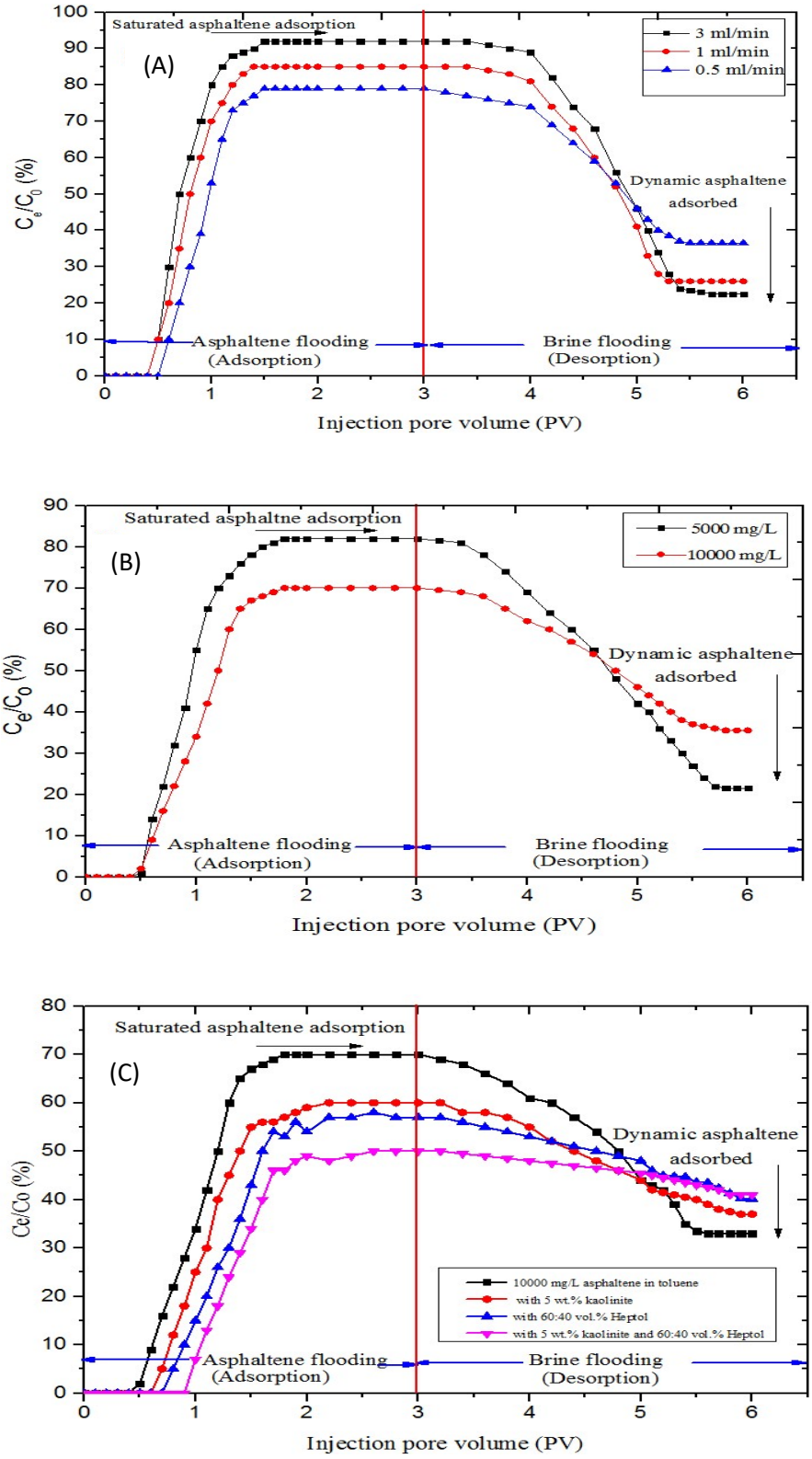

Figure 7-6. The effect of (A) injection flow rate, (B) asphaltene concentration, and (C) the addition of 60 vol. % heptane, and 5 wt.% kaolinite on the adsorption of asphaltene on sandstone.

As was described based on the behaviour of breakthrough curves versus the number of injected pore volumes of the asphaltene through the porous media, the mobility of asphaltene particles on porous media is affected by two asphaltene deposition mechanisms: adsorption and mechanical plugging (e.g., hydrodynamic bridging) [338,339]. The adsorption effect is related to the interactions between the asphaltenes functional groups and the porous media surface, involves surface polarity, affinity or other attractive forces. The adsorption of asphaltenes on porous media is the result of favourable interactions of the asphaltene species or its aggregates with chemical species on the porous media surface. Several interaction forces, individually or in combination with each other, can be responsible for it such as electrostatic (Coulombic) interactions, charge transfer interactions, Van der Waals interactions, repulsion or steric interactions and hydrogen bonding. The pore-throat blockage effect is highly dependent on the asphaltene concentration. This is supported by SEM analysis of the Berea sandstone (Figure 7-1), the latter of which shows that around 6% of pore throats are under 220 nm when subjected to quantitative image analysis [340], i.e., less than the hydrodynamic diameter of the asphaltene particles. These relative dimensions suggest strongly that the blockage could take place, especially when the fluid contains high concentrations of asphaltene. Additional mechanisms were hypothesized namely as ‘‘multilayer kinetic surface adsorption’’ based on manipulating the asphaltene composition (i.e., when heptane is added) and mineralogy (i.e., when kaolinite is added), and ‘‘pore throat plugging’’ based on high injection flow rate. These newly hypothesized mechanisms offer an understanding of the dynamic asphaltene adsorption kinetics in porous media. All these four mechanisms are schematically presented in Figure 7-7.

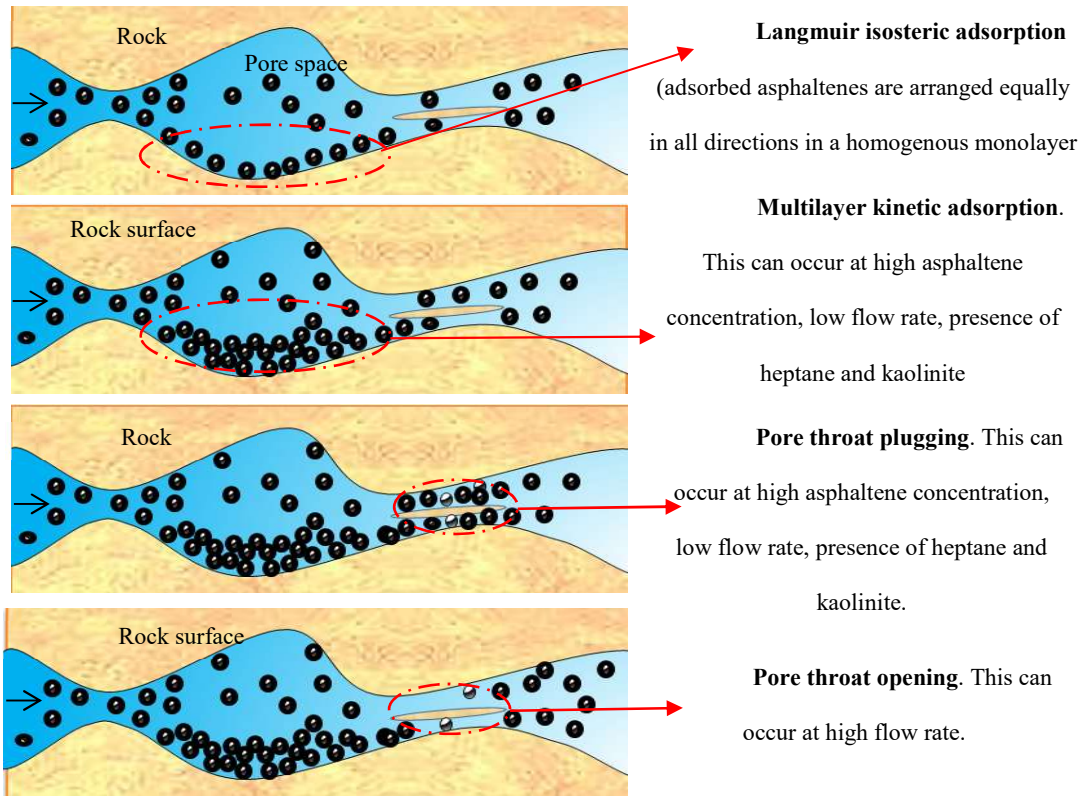

Figure 7-7. Schematic of different asphaltene deposition mechanisms in porous media originated from a continuous flow of asphaltene.

7.3.3. Removal of asphaltene from Berea sandstones using NEs.

It can be seen that the cumulative asphaltene recovery efficiencies of brine flooding for different three cases are quite close to each other (around 41%), which means that the tertiary flooding started from the similar residual saturation of asphaltene solution ($S_{as,r}$). From the data in Figure 7-8, it is apparent that the cumulative asphaltene recovery efficiency of 52.93 % OOIP by the end of tertiary DBSA with overflush brine flooding and blank NEs, meaning both DBSA molecules and blank NEs can mobilize about 11 % more adsorbed and trapped asphaltene after this step. However, injection 1.5 PV of DBSA NEs further improved the advanced asphaltene displacement efficiency of 13.21%.

After shutting-in for 24 h aging, the cumulative asphaltene recovery efficiency was increased from 52.93 % to 80.95 % after post brine injection, and E_{AAD} was correspondingly increased from 11 % to 28 % in the case of aging with DBSA. This suggests that the adsorbed and trapped asphaltene particles are sterically stabilized by the presence of DBSA molecules on the rock surface and hence the asphaltene displacement efficiency is increased. However, the aging with blank NEs shows an increase in the cumulative asphaltene recovery from 52 % to 76 % and advanced asphaltene displacement increases from 11 % to 23 %.

The most surprising aspect of the data is in the presence of DBSA NEs. Following the aging and post brine flooding, a significant increase in the cumulative asphaltene recovery and advanced asphaltene displacement efficiencies were recorded as 91.4 % and 36.3 % respectively, as shown in Table 7-5. These interesting results could be attributed to the slow release of DBSA and other NE's components (surfactants and oil phase) from NE during shutting-in for 24 h (i.e., aging time) and interact with asphaltene molecules, which are saturated the H-bonding sites of asphaltenes and the fact that it interacted with both the periphery and aromatic cores of asphaltenes. As a result, the adsorbed and trapped asphaltenes are eluted from sandstone rock surfaces and prevented interacting laterally between themselves and kept well-solubilized in the solution i.e., increasing the stability of asphaltene. These interactions are almost certainly due to acid-base interaction, hydrogen bond, polar-π interaction, cation-π interaction, and aromatic-aromatic interaction. These interactions also can promote further electrostatic interactions with other ion pairs. For example, the hydroxyl group in the chain length can form H- bonding with water or surfactants, whereas the nitrogen in the aromatic core can provide acid-base as well as H-bonding interactions with DBSA. In addition to higher asphaltene recovery ability, the proposed concept can significantly reduce the amount of AI and the total

chemicals by factors of 95% and 22% respectively, as shown clearly in the detailed materials balance in Table 7-6.

Furthermore, several past experimental works have shown that using pure inhibitors in the reservoir can induce the formation of viscous phases such as liquid crystals and viscous macroemulsions in o/w interface which is a challenge for oil recovery. Therefore, encapsulated DBSA inside NEs and then the slow release is effective to improve the distribution of DBSA molecules, minimize interfacial tension at the o/w interface, and prevent the formation of viscous phases.

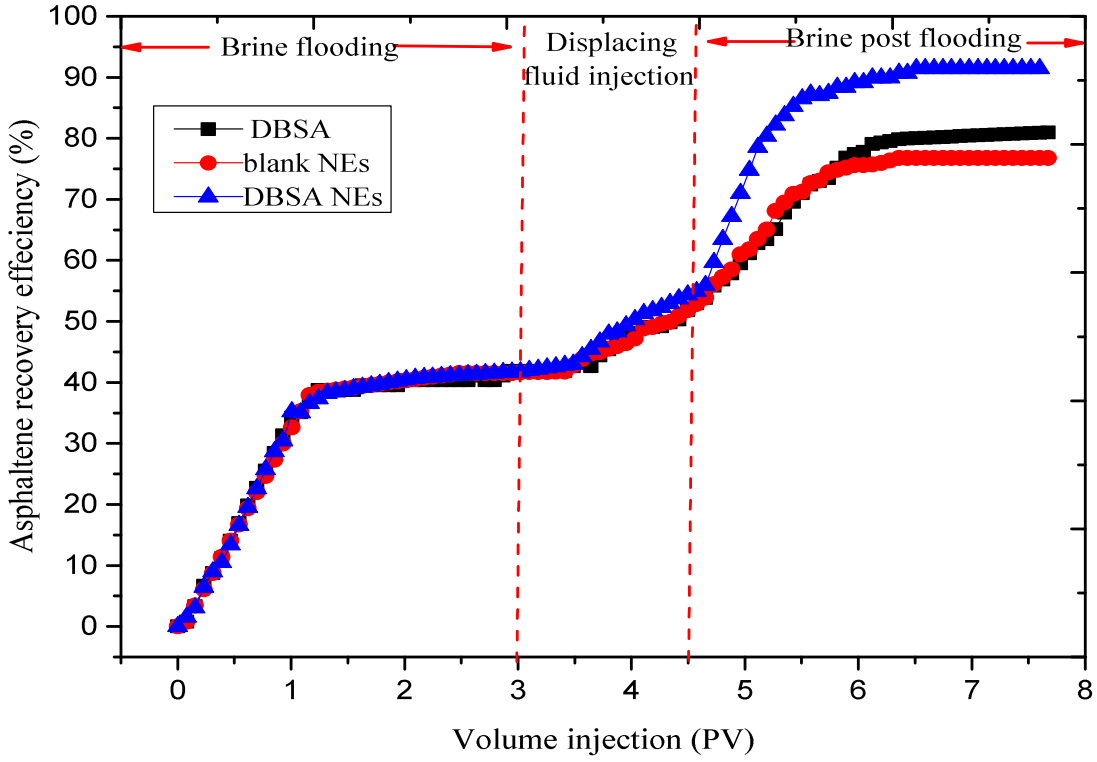

Figure 7-8. Enhanced asphaltene displacement efficiency by DBSA, blank NEs and DBSA NEs.

Table 7-5: The amount of asphaltene recovered at different stages, for flooding experiments with different displacing fluids.

Displacing fluids	E_{CAR} after brine flooding, %	E_{CAR} after displacing fluid injection, %	Ultimate asphaltene displacement efficiency %	E_{AAD} by displacing fluid, %	E_{AAD} by brine post flooding, %
DBSA	41.86	52.93	80.95	11.07	28.02
Blank NE	41.49	52.84	76.74	11.35	23.90
DBSA NE	41.70	54.91	91.47	13.21	36.57

Table 7-6. Displacing fluids compositions and material balance.

Displacing fluids	Total vol. injected (ml)	DBSA Vol.%	Vol. DBSA (ml)	Nacl %	Brine (ml)	xylene vol.%	Vol. xylene (ml)	Tween 80 vol.%	Vol. Tween 80 (ml)	SBDS vol.%	Vol. SBDS (ml)	Water vol.%	Vol. Water (ml)	% R_{AI}*	% R_{TC}**
DBSA	20	20%	4	4%	0.29	------	------	------	------	------	------	80	16	------	------
Blank NE	20	------	------	4%	0.36	7	1.4	6	1.2	1	0.2	82	16.4	------	------
BDSA NE	20	1.0 %	0.2	4%	0.36	7	1.4	6	1.2	1	0.2	81	16.2	95	30

7.3.4. Effect of asphaltene deposition on the morphology of the core sample.

The Berea sandstone sample was damaged in the adsorption process mentioned previously, deposited asphaltene layers and clusters were formed on the surface after asphaltene injection. The morphology and particle size of deposited carbon formed on sandstone samples by SEM are given in Figure 7-9 before and after injection of asphaltene, brine, DBSA NEs, and post brine injection. The SEM image gives a three-dimensional view of the core sample at a microscopic level. As mentioned earlier in the kinetic adsorption test, the variation in breakthrough level is caused due to two asphaltene deposition mechanisms: adsorption and mechanical plugging and these further supported

by SEM images. The amount of asphaltene deposition can represent that the surfaces seem rougher due to the deposited asphaltene in comparison to sandstone before asphaltene injection. SEM images show that the deposited asphaltene structures can aggregate together and form layers, which cover the surface of the rock sample. In addition, SEM analyses show the formation of large clusters on the layers of adsorbed asphaltene already adsorbed on the surface of sandstone rock with characteristic sizes that greatly exceed the monolayer characteristic size. Therefore, these experimental results suggest multilayer adsorption of asphaltene on sandstone core samples. The evidence of multilayer adsorption from SEM observation supports the mechanistic understanding of the asphaltene adsorption kinetics (Figure 7-7).

After brine injection, SEM image shows that large clusters of asphaltene are still absorbed. This can be attributed to the low efficiency of displacement of adsorbed and trapped asphaltene by brine flooding.

However, after DBSA injection and aging for 24 h (i.e., slowly release effect), solubilisation of adsorbed asphaltene on the sock surface was observed. It may be assumed that the DBSA was progressively released from NE and interact with asphaltene molecules, leading to asphaltene dissolution on the rock surface. After post brine flooding, no asphaltene clusters and layers were observed.

The EDX analyses (see Figure B-1 in Appendix B) show a significant increase in the amount of carbon (represents asphaltene) was counted after asphaltene injection, which again confirms the deposition of asphaltene in the pores of the core samples. However, the results for the sample extracted from the column after the post-flooding process, show that only a small amount of carbon was detected on the rock surface. Therefore, the results

of SEM and EDX also provide strong visualisation evidence for the efficacy of DBSA NEs in advanced asphaltene displacement.

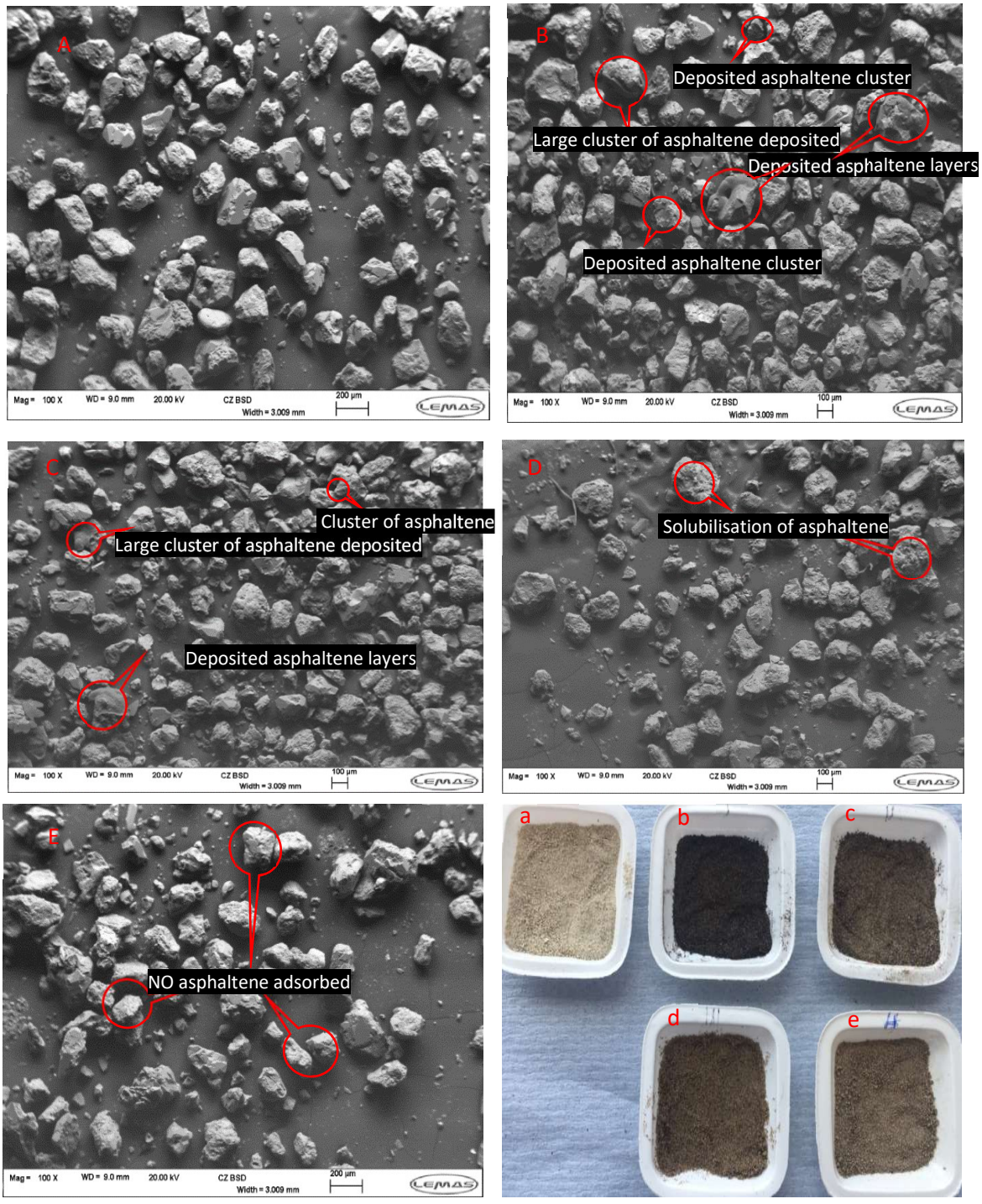

Figure 7-9. SEM images of studied Berea sandstone samples (A-E) and corresponding images (a-e): A) prior injection, B) after asphaltene injection, C) after DBSA NE injection, D) after release effect, and E) after post brine flooding.

7.3.5. Wettability alteration

Wettability is defined as the tendency of one fluid to spread on or adhere to a solid surface in the presence of other immiscible fluid. The fluid with the higher affinity toward the solid surface is called the wetting phase; the other fluid is the nonwetting phase. Wettability is very important in oil recovery processes and has a strong effect on distribution, location, and flow of oil and water in reservoir during production [341]. The wettability alteration of Berea sandstone over different aging times with asphaltene was evaluated through the measurement of the contact angle with brine alone, DBSA alone, blank NEs, and DBSA NEs. The substrates were immersed in asphaltene solution inside a sealed container for 21 days at 25 °C. During the aging process, asphaltene molecules adsorbed on the rock surfaces, altering their wettability [339]. Since adsorption is a kinetic process, wettability alteration is a function of aging time. After 7 days of aging, the contact angles became almost constant, indicating that a minimum of one week was needed to alter the wettability of the substrate, as shown in Figure 7-10. Aging the Berea sandstone for 21 days exhibited the highest wettability alteration with an increase in CA from 60° to 122° for asphaltene droplet with brine. This could be explained by the strong adsorption of asphaltene polars onto Berea sandstone [342]. Therefore, wettability was altered from water-wet to oil-wet after 21 days of aging. Generally, when the contact angle is between 0 to 75° and 115° – 180°, the system is defined as water wet and oil-wet state, respectively, and when the contact angle falls within the range of 75º-115°, the system is neutrally wet [343].

The effect of additives on the wettability alteration of Berea substrates was also investigated. Figure 7-10 shows that DBSA restored the wettability of aged Berea substrates from weakly oil-wet to water-wet, with a contact angle of 60°. It is possible

that DBSA molecules adsorbed with their hydrophobic tails on the mineral surface and created a hydrophilic layer with their polar heads [344]. Blank NEs also show a strong tendency to migrate and adsorb on the mineral surface due to the large surface area of the droplets and the presence of ionic/non-ionic surfactants, which restored the wettability with a contact angle of 57°.

The high performance of DBSA NE for wettability alteration explains its effectiveness in controlling asphaltene droplet. This suggests that DBSA NEs are slowly released AI and other NEs components and therefore the ability of these chemicals to penetrate and swell the adsorbed asphaltene layers, further altering rock wettability from 122° to 50° after 21 days of aging. Comparing with the effect of brine on CA, about 50 % and 53 % reduction in CA are achieved in the presence of DBSA and blank NE, respectively. While a significant reduction in CA (about 60 %) in CA is achieved with the addition of DBSA NEs.

The contact angle images are shown in Figure 7-11. The minor differences between the right and left angles in all the tests confirmed the smoothness and homogeneity of the Berea sandstone surface used. The results demonstrate that the addition of DBSA, blank NE, and DBSA NEs improve the rock wettability towards water wet. The brine produces an asphaltene CA of 64˚, which indicates the oil-wet system. Conversely, DBSA, blank NE, and DBSA NEs turn the system more water-wet.

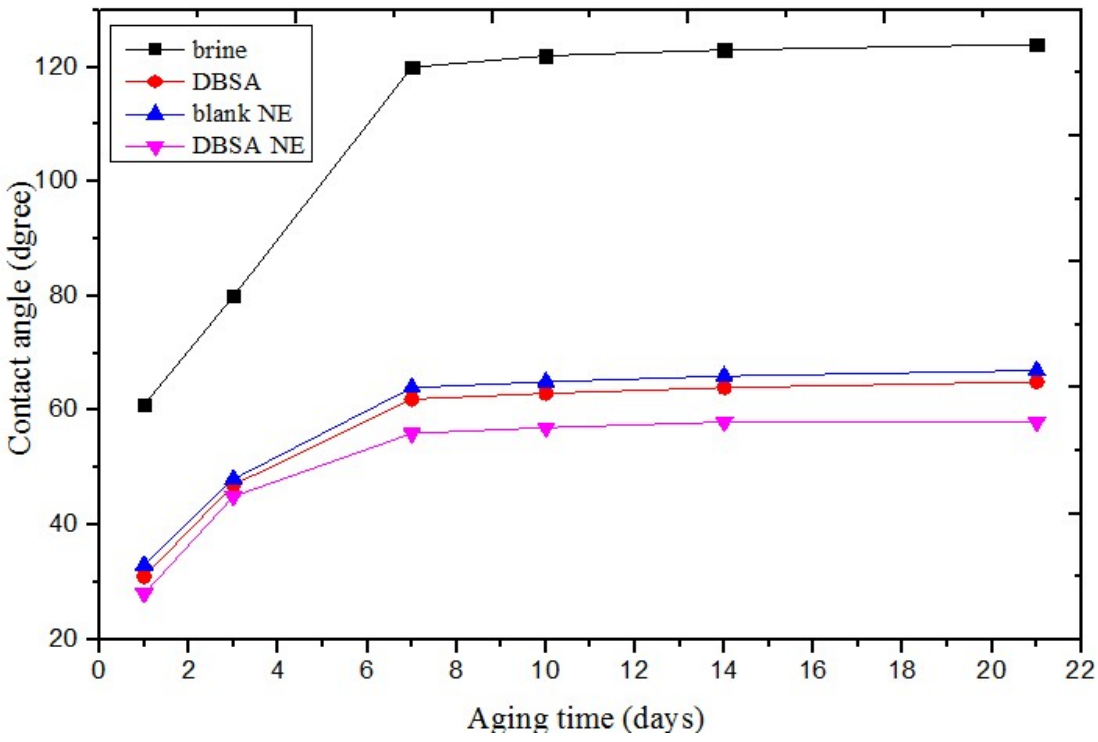

Figure 7-10. Average static contact angles of oil droplets released from aged Berea rock during imbibition in brine, DBSA, blank NE, and DBSA NE.

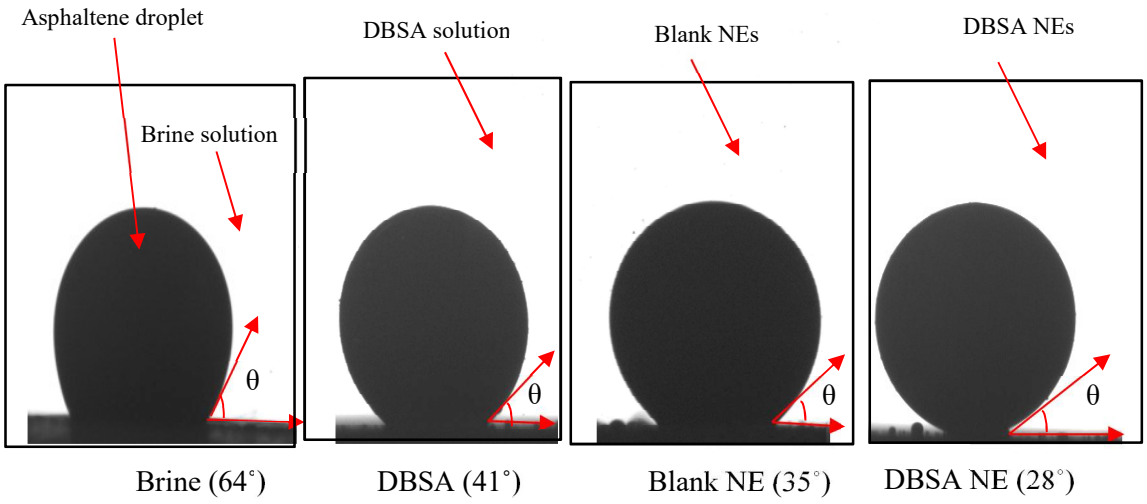

Figure 7-11. Contact angle images of asphaltene/rock in brine, DBSA, blank NE, and DBSA NE after 1-day of aging.

7.3.6. Interfacial tension (IFT)

Figure 7-12 shows the dynamic of the interfacial tension between asphaltene solution and brine, DBSA, blank NEs, and DBSA NEs. It is apparent that IFT decreases with the presence of salinity (i.e., 4 wt. % NaCl), which can be related to a reduction in electrostatic repulsion at the interfacial region. The IFT of brine starts at about 21.6 mN/m and approaches to the equilibrium value of 15.9, which is lower than that for asphaltene/deionized water (26.1 mN/m to reaches the equilibrium value of 22 mN/m). Apparently, monovalent cations (Na^+) have a more pronounced effect on IFT reduction than deionized water [345]. It has been reported that the Na^+ may interact with a polar organic component of asphaltenes, producing ionic complexes [333] and changing the surface charges on oil phase [347,348].

One may also observe in this figure, when DBSA molecules exist in the system, that IFT of asphaltene solution is decreased quickly, which means the DBSA molecules reach to the asphaltene drop surface in a short time. The diffusion of DBSA molecules starts from the onset of drop formation in the cuvette and before the onset of measurements. However, the IFT starts at about 14.1 mN/m and approaches the equilibrium value of 7.1 mN/m within about 30 min.

For the system containing blank NEs, the IFT start from values about 5.8 mN/m which is close to DBSA NEs /asphaltene IFT. Using 1 vol. % DBSA inside NE did not cause a significant change in the IFT. Thus, DBSA is likely located inside nanodroplets (i.e., in xylene) and stabilised by mixed surfactants, which acts as a very good carrier for controlled and delivery DBSA inside porous media and is an advantage for enhanced oil/asphaltene recovery process. In addition, in the presence of DBSA NEs system, the hydrophobicity of the systems becomes stronger because the electrostatic repulsion and

hydration are weakened. As a result, the molecules of this system absorb quickly and arrange close together at asphaltene/brine interface, acting to reduce the IFT. This can be attributed to the "release effect" of DBSA and other components from NEs towards asphaltene/water interface, which leads to reducing IFT.

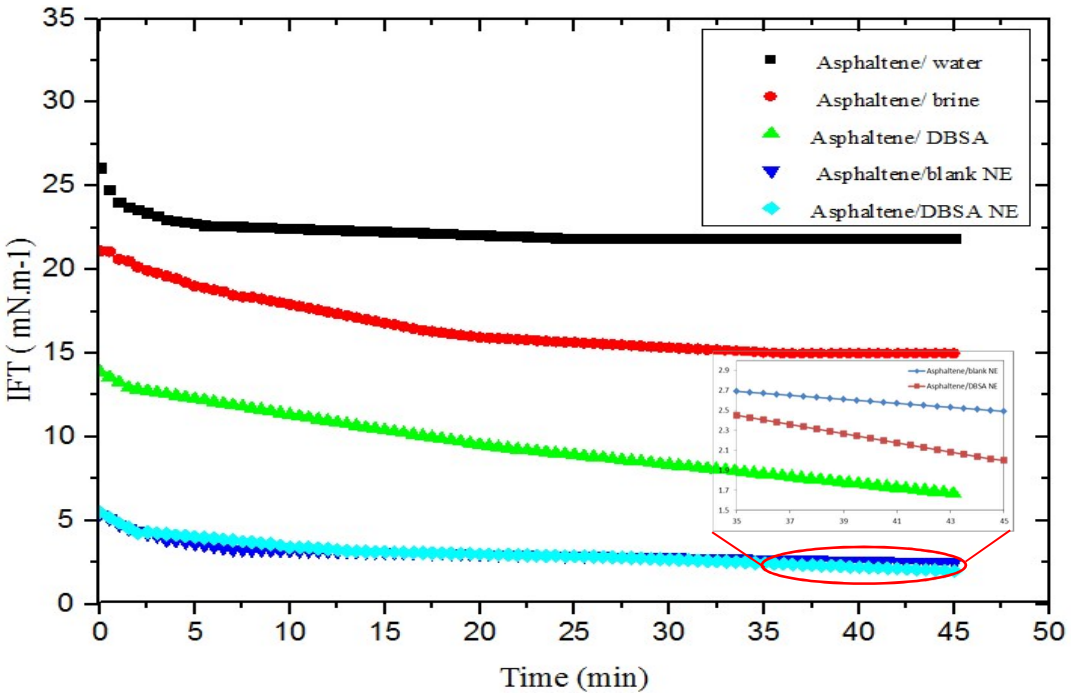

Figure 7-12. Dynamic IFT between asphaltene and different solutions deionized water, brine, DBSA, blank NEs, and DBSA NEs.

7.3.7. Potential asphaltene displacement mechanism in the presence of NE

7.3.7.1. Expansion of the electrical double layer (EDL)

The presence of brine may form an electrical double layer (EDL) (electrokinetics repulsive), which was likely to be the primary mechanism for displacement asphaltene during brine injection. The repulsive interaction hinders the adsorption of asphaltene on the rock surface, because the Na^+ may interact with a polar organic component of asphaltene producing ionic complexes [346], changing the surface charges of asphaltene droplets [347,348]. However, when extra clay mineral and precipitant are existence,

asphaltene exerts attractive forces towards mineral surfaces, destabilizing the thin film [349]. This could eventually lead to direct contact between asphaltene particles and sand surface facilitates the adsorption and as a result, the higher chance of wettability alternation toward less water-wet or more oil-wet changed the displacement performance toward lower cumulative production.

In the case of the addition of DBSA, DBSA molecules interact with asphaltene and adsorb at the interface, resulting reduction in IFT as well as increasing the negative charge at asphaltene/water interface. Blank NEs can also adsorb at the asphaltene/water interface due to its affinity towards the oil phase, and therefore more negative charges on rock sites would be expected.

The addition of DBSA NEs can induce significantly further expansion the EDL, augmenting hydration forces and creating a repulsive potential. The latter, in turn, overwhelms attractive hydrophobic forces and eventually results in more stable water films on mineral surfaces. This can be attributed to the adsorption of DBSA NEs at the asphaltene/brine interface, which is negative charge (-28 mv), and ultimately the DBSA and other components would slowly release to adsorb at asphaltene/brine and brine/rock interface, resulting in a further reduction in ITF and significant expansion EDL. Figure 7-13 illustrates the water film stability in the function of these competing phenomena.

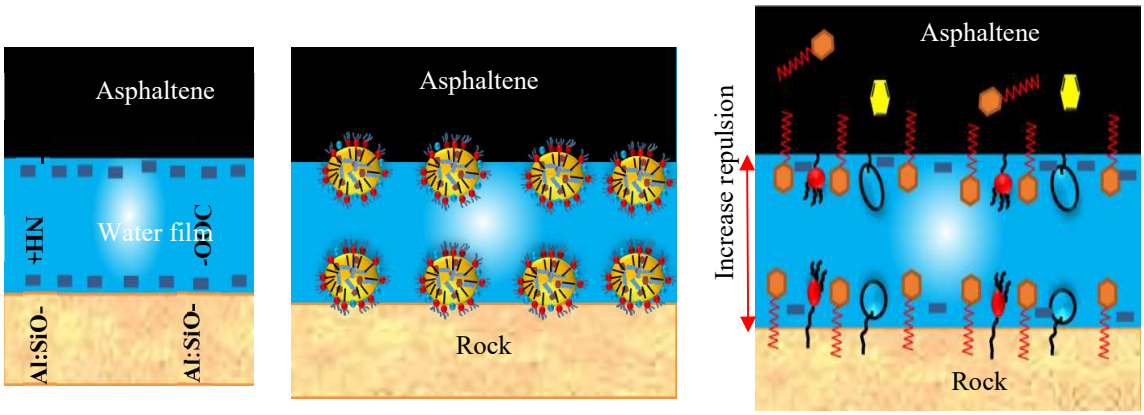

Figure 7-13. Illustrative representation of water film stability between asphaltene and rock surface in the absence and presence of DBSA NES.

7.3.7.2. Molecular mechanism of asphaltene removal by NE

It is postulated that the effectiveness of the NE relies on the reduction in the percentage of polar adsorptive molecules onto porous media. DBSA NEs shows a strong tendency to migrate and adsorb at the asphaltene/rock interface due to the large surface area of the droplets and the presence of ionic/non-ionic surfactants. This interfacial activity of DBSA NEs allows the displacement of asphaltenes from the interface because the very low asphaltene/brine interfacial tension (~3.7 mN/m) causes the asphaltene film to continually recede and eventually detach from the solid surface, as shown in Figure 7-14.

The slow release mechanism provides further intermolecular interaction between DBSA NE's components and asphaltene, resulting reduction the average size of asphaltene, IFT at the interface, and contact angle (i.e., wettability alteration). The released DBSA and other components act as linkers that swell the adsorbed asphaltene layers and minimize the adsorption at the asphaltene/rock interface, allowing the more-effective momentum across the interface. Consequently, less energy is needed at the same flow rate for the brine to mobilize the asphaltene as we observed in reducing the pressure drop. Therefore,

the asphaltene adsorbed on rock surface can be mobilized by the viscous forces caused by the flow of the injected brine in post-flooding case, reducing the available adsorptive molecules per unit mass.

In addition, the DBSA NEs can effectively reduce the Van der Waal's interactions between asphaltene molecules, allowing the asphaltene droplet to move more freely. Once mobilized, the asphaltene droplet would be surrounded by the DBSA and other components, which accumulates around the droplet periphery in micellar fashion (stabilisation mechanism). In this way, the droplet could be effectively dispersed into the oil phase once dislodged from the mineral surface. The total mechanism is summarized in Figure 7-15, as the slow release, IFT and CA reduction, electrokinetics repulsive expansion, and solubilisation may become the dominant mechanisms for the asphaltene displacement.

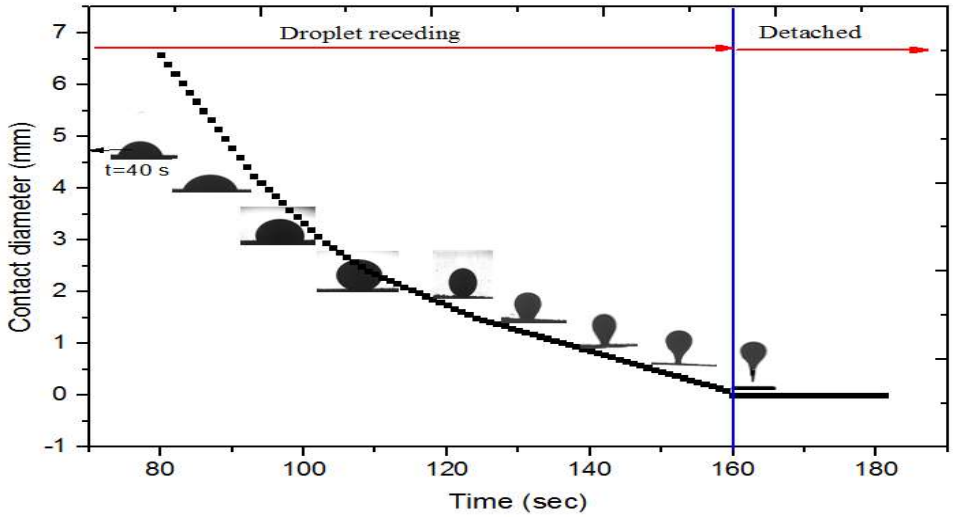

Figure 7-14. Asphaltene droplet dewetting with the DBSA NEs. The solid surface-oil droplet contact diameter reaches a minimum of 0.34 mm at the point of oil droplet detachment. Insets are images of asphaltene droplet on sandstone immersed in DBSA NEs.

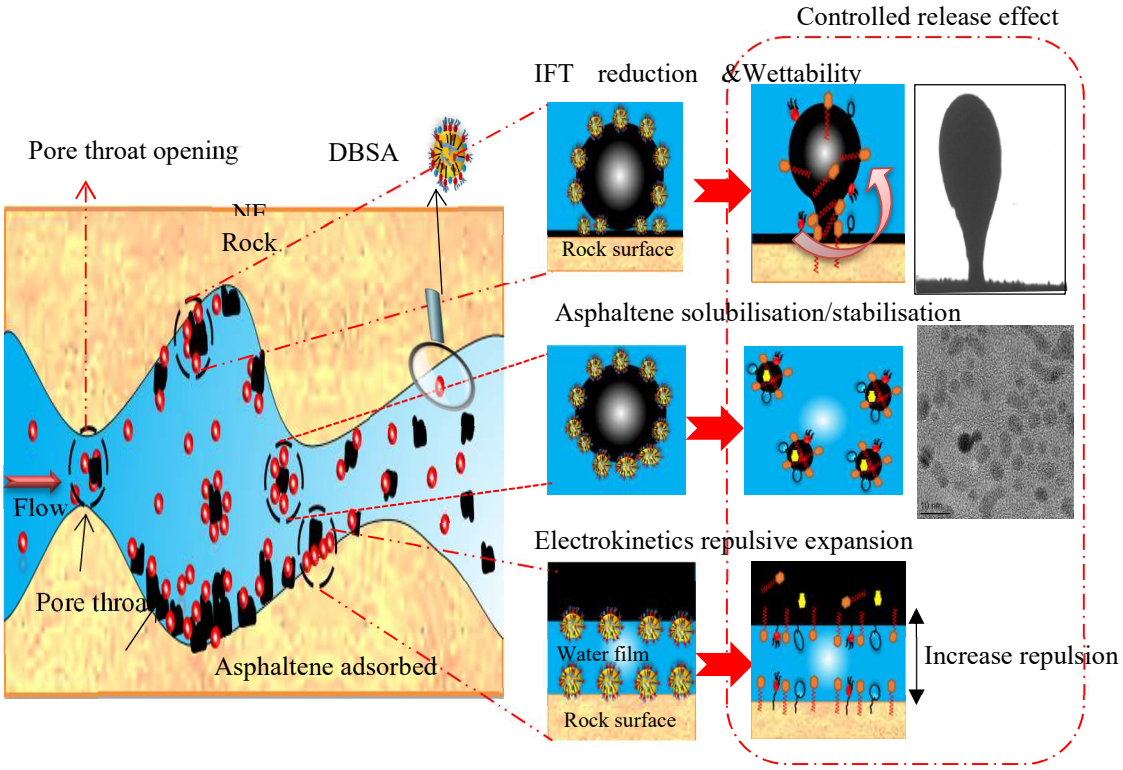

Figure 7-15. Proposed mechanism of NEs loaded AI interaction with asphaltene on the mineral surface.

7.4. Chapter summary

This Chapter studied the controlled delivery and release concept under flow conditions by using a core-flooding facility. The following conclusions can be drawn:

- Dynamic adsorption of asphaltene was dependent on injection flow rate, the concentration of asphaltene, the composition of asphaltene solution and mineralogy of porous media.
- Three possible mechanisms, i.e., multilayer kinetic, surface adsorption, and pore throat opening, should be considered for dynamic asphaltene adsorption kinetics in porous media.
- Comparing to DBSA flooding alone, DBSA NEs allowed significant asphaltene removal up to 15.81% and minimized the AI amount and the total chemicals usage by 95% and 22% respectively.
- A number of factors, including the slow release, IFT reduction and wettability alteration, electrokinetics repulsive expansion, solubilisation and molecular mobilization, could contribute to the efficiency of asphaltene displacement.
- DBSA NEs effectively displaced asphaltene particles by reducing the interfacial tension and fragment asphaltene particles into smaller droplets, allowing efficient recovery of fluids pumped and the onset of rapid production.

Chapter 8

Conclusions and future work

8.1. Conclusions

The aim of this thesis was to explore how emerging nanotechnology can be used to address the challenges that conventional asphaltene controlling are facing. Through a series of experiments, we developed a novel concept for controlled delivery and release of AI by using NEs to control asphaltene aggregation, precipitation and deposition under static and dynamic conditions. It showed that the new concept could provide tremendous value by i) improving the stability of the asphaltene; ii) reducing the usage of AI, and iii) extending the treatment time. In addition, NEs can be used as carriers for delivery and controlled release of AI inside porous media, leading to more stable asphaltene and higher oil recovery efficiency.

The main conclusions drawn via the experimental investigations are summarized as below:

1) **Nanoemulsion stability**

- The results showed that the type of mixed surfactants, type of oil phase and the content of AIs are important parameters to fabricate stable NEs.
- Both static and dynamic studies revealed that AI -reinforced NEs were more stable than blank NE.
- Stable viscosity values with shear thinning nature indicated better mobility control of nanoemulsions.

- DBSA NEs with unique properties of long-term kinetic stability, low IFT values, stable surface charge, and improved viscosity values implied its potential for improved oil recovery.

2) Controlled Releases of Asphaltene Inhibitors in bulk fluid

- NEs allowed a significant reduction of AI and chemical amounts in stabilizing the asphaltene. The inhibitor amount and total chemical usage could be reduced by 95 and 10 % respectively compared with the case of using pure DBSA.
- DBSA NEs allowed a significant delay of asphaltene precipitation, i.e. a delay from pure asphaltene solution of 450 sec to 1400 sec in the presence of NEs.
- The presence of DBSA NE also reduced the precipitation thickness of asphaltene up to 75 %.
- The release of DBSA from NE depended on the interactions of surfactants used for the fabrication of NEs, and the subsequent change of the overall polarity and hydrophobic characteristics.
- Both the surface effect and bulk effect were contributing to effectiveness the NE in releasing AIs, including the migration of NEs to the water/oil interface and slowly release of chemicals at the interface, and the formation of hydration layers around asphaltene particles in the bulk.

3) Kinetic Study of Controlled AI release

- DBSA and other NE's components were progressively released from NE and interact with asphaltene molecules, increasing the stability of asphaltene.

- DBSA NEs could significantly increase the efficiency of asphaltene inhibition by 84.12 % after 24 h, showing its effectiveness with increasing release time.
- DBSA NEs could reduce asphaltenes from precipitate to spherical nanometric particles (5 to 30 nm), delaying the onset of asphaltene precipitation.
- The released amount of DBSA (99 %) was much higher from NE than form the xylene (13 %). The release profile of DASA NEs follows that Korsmeyer-Peppas mode kinetic model.
- There was a significant advantage in using NEs loaded with DBSA to achieve prolonged asphaltene treatment with a reduced amount of inhibitor, rather than directly mixing DBSA in xylene.

4) Molecular structure of asphaltene

- The results from XRD and TEM confirmed the validity of asphaltene stability mechanism by the release of DBSA and other components from NE, which were able to increase both the stacking distance between aromatic rings and aliphatic chains and reduce the diameter of the aromatic sheet and the cluster size.
- These alterations in molecular structure led to a decrease in the aromaticity of asphaltene, which in turn increase the solubility of aromatic compounds in oil and improve the liberation of asphaltene aggregates. As a result, the disruption of the aromaticity implied a change of the π system over the aromatic zone that in turn disturbed eventual π–π interactions between asphaltene stacks, which was the main mechanism responsible for the formation of clusters at the nanoscale.

- The FTIR spectroscopic study verified that DBSA NE involved multiple interactions with asphaltene, building up a multicentric electron density in this region, which led to deeper isosurfaces of van der Waals forces in the interacting zone. In addition, the quantitative study indicated that asphaltenes with DBSA NEs have a lower number of carbon atoms per alkyl side chain, lower aromaticity, shorter side chain of aliphatic substituents, and more amount of aliphatic and aromatic groups compared with pure asphaltene.
- The TGA results further demonstrated the alteration of asphaltene structure. It was found that during the chemical reaction between asphaltene and DBSA NEs, the structure of asphaltene was improved considerably and the coke yield was decreased around 62% due to the decrease of the cluster sizes and the increase of the stacking distance between aromatic sheets.

5) Delivery and controlled release of inhibitor under flow condition

- Dynamic adsorption of asphaltene was dependent on injection flow rate, the concentration of asphaltene, the composition of asphaltene solution and mineralogy of porous media.
- Different to conventional thought that the mobility of asphaltene particles through porous media is controlled by two deposition mechanisms: adsorption and mechanical plugging, this work suggests that additional mechanisms, i.e., multilayer kinetic surface adsorption and pore throat opening, should be considered for dynamic asphaltene adsorption kinetics in porous media.

- Comparing to DBSA flooding alone, DBSA NEs allowed significant asphaltene removal up to 15.81% and minimize the inhibitor amount and the total chemicals used by 95% and 22% respectively.
- Several possible mechanisms, including slow release, IFT reduction and wettability alteration, electrokinetics repulsive expansion, solubilisation and molecular mobilization might become the dominant mechanisms for asphaltene displacement.

8.2 Future work

There is great potential to extend the current study and build upon the knowledge within this area. Such points are discussed below.

- This research has explored a novel method by using AIs inside NEs, which could not only significantly reduce the usage of AIs but also produce small oil droplets stabilized for a long time. An alternative method for future work will be suggested by using surfactant-free Pickering NEs stabilized with nanoparticles and encapsulating a model of hydrophobic AI, which will be able to reduce the total chemical amounts. Since nanoparticles can be used for remediation of asphaltenes, Pickering NEs will be able to deliver and controlled release both AI and nanoparticles to control asphaltene problems in the bulk and surfaces.
- The onset of asphaltene precipitation was investigated near onset kinetics in toluene- n-heptane mixture. At higher n-heptane dilution when toluene is present, allowing particle size distributions to be difficult measured. Therefore, for future work, it is recommended to investigate asphaltene

behaviour at high precipitant content and verify the onset with different techniques such as optical microscopy, UV-vis spectrophotometry, and interfacial tension.

- The kinetic processes of inhibitor release from NEs were found to be dependent upon a strong interaction among DBSA molecules and the NE's components, and inhibitor concentration in the NE. Further effort can be directed towards the study of surfactant types and concentrations, oil type, and NEs sizes effects. Studying these effects in both *in situ* and kinetic release approaches would optimize the process parameters for NEs preparation as a better inhibitor carrier with a prolonged release profile.
- Morphological features and structural characteristics of asphaltene with NEs loaded with AI were investigated in this thesis and led to propose novel insights into the stability and molecular modification structure of asphaltene. Therefore, it is proposed to carry out further studies to investigate the morphology and molecular structure for asphaltenes extracted from different crude oils based on the number of heteroatoms in the functional groups and acid number in asphaltenes.
- This thesis already gives a detailed understanding of asphaltene adsorption based on adsorption isotherm, flow rate, the concentration of asphaltene, and the presence of clay. As we mentioned previously in Chapter 2, the key of effectiveness for an inhibitor is getting it to have good adsorption on the formation surface and not be produced back too quickly, otherwise, treatment lifetimes become uneconomically short. Therefore, it will be interesting to understand the transport and retention mechanisms of NEs loaded with AI on porous media. The assumption is that the retention of

AI may be driven by physiochemical properties of NEs and mineralogy of porous media, although there did not exist in the literature a systematic study of the exact mechanisms of inhibitor adsorption/desorption onto rock minerals in the formation. Based on our understanding from this work, this can be achieved by; (a) measuring a breakthrough curve of the NEs as the change in the effluent NEs concentration as a function of the number of PV; (b) carefully characterizing the minerals to understand their detailed surface chemistry and their particle size distributions their influence of NEs retention.

- It may be interesting to use Quartz Crystal Microbalance with Dissipation (QCM-D) technique to study the effect of NEs loaded with AI on the adsorption/desorption of asphaltenes on different substrates. Comparison with the breakthrough and SEM data reported in Chapter 7, this approach will help to better understand the mechanism of asphaltene removal before and after injection of NEs.

APPENDIX A

Kinetic Study of Controlled Asphaltene Inhibitor Release from Nanoemulsions

Zero-order model

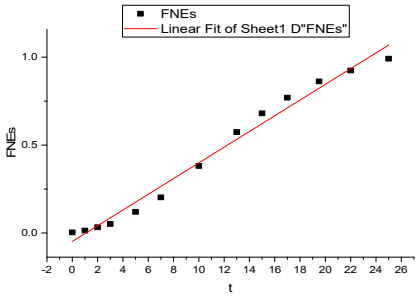

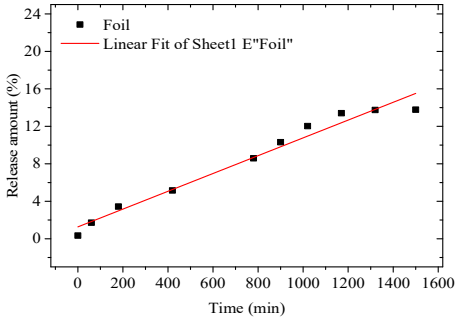

First order model

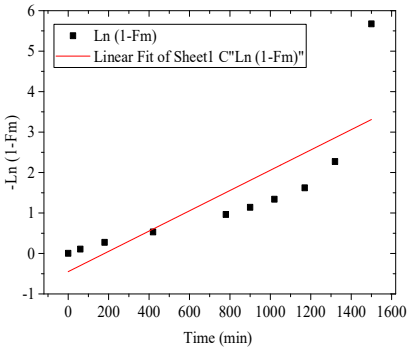

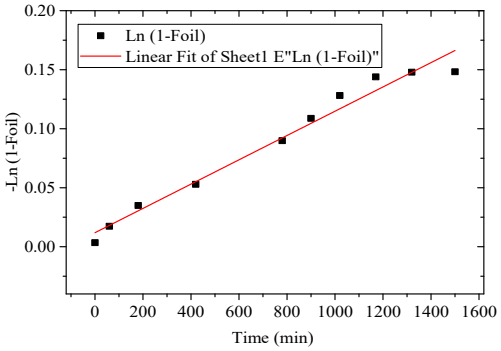

Huguchi model

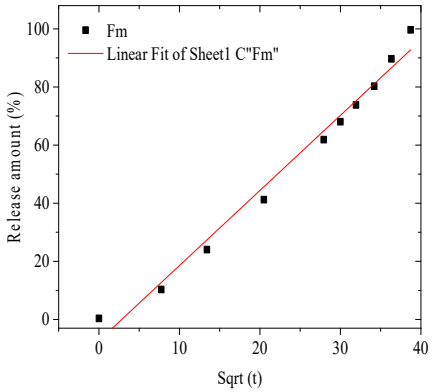

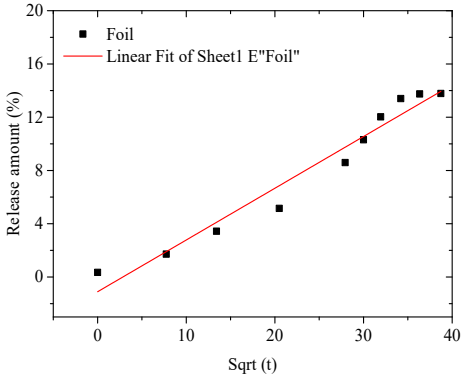

Korsmeyer-Peppas model

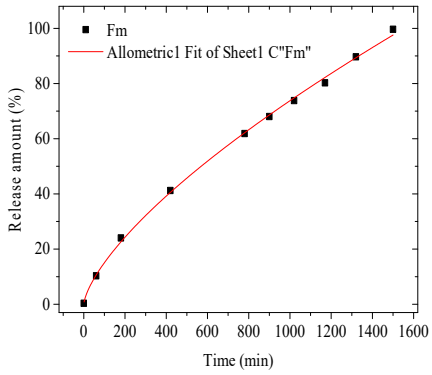

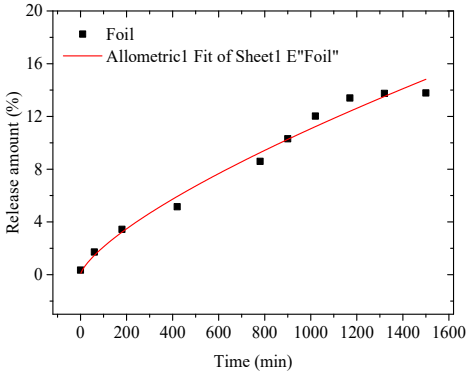

Baker-Lonsdale model

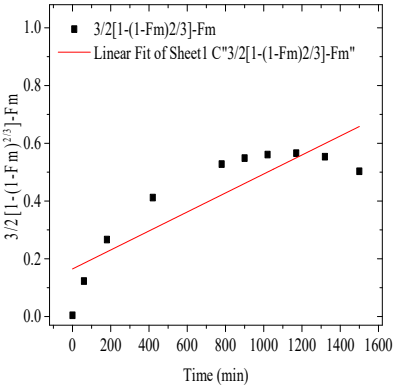

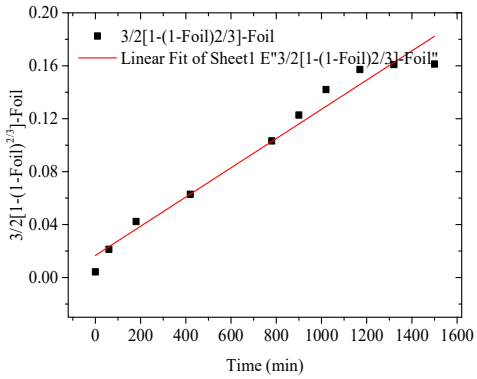

Hixon-Crowell model

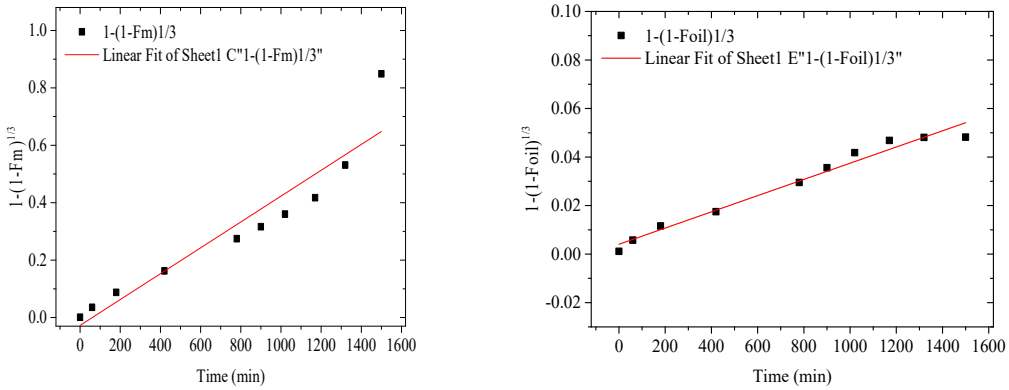

Square root of mass

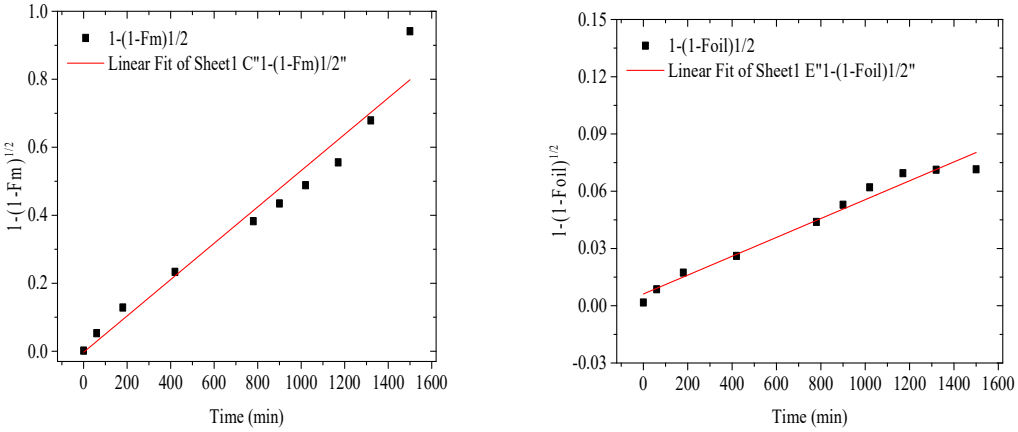

Three seconds root of mass

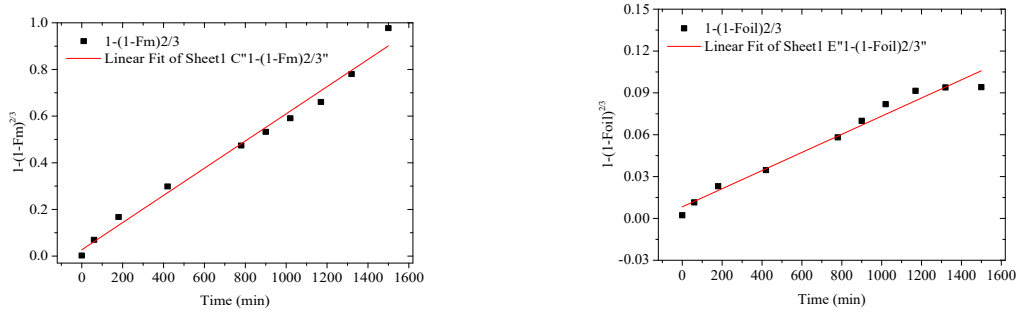

Figure A-1. The release profiles of DBSA (a) from NEs and fitted to the Korsmeyer-Peppas mode (n = 0.68), and (b) from oil phase and fitted to the first order mode.

APPENDIX B

Delivery and controlled release of inhibitor: A prospective method for enhanced oilfield asphaltene prevention

Pure sandstone

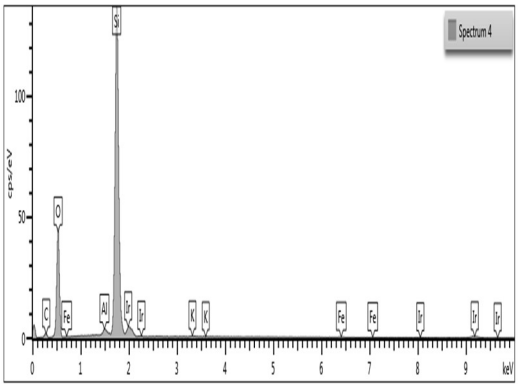

Element	Wt%	Wt% Sigma
C	13.64	1.15
O	57.29	1.15
Al	0.48	0.79
Si	28.32	0.41
K	0.11	0.02
Fe	0.17	0.05
Total:	100	

Sand stone after brine injection

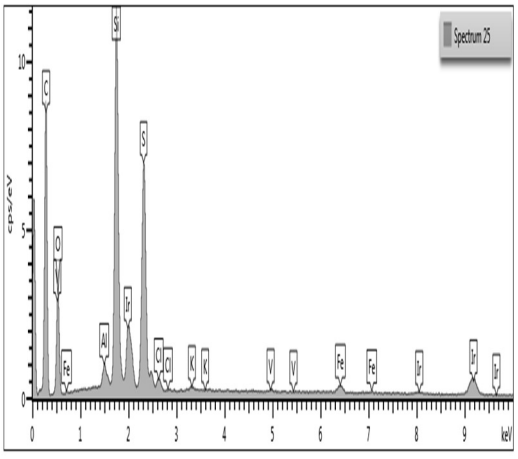

Element	Wt%	Wt% Sigma
C	71.87	0.37
O	19.1	0.33
Al	0.23	0.01
Si	4.26	0.05
S	3.72	0.05
Cl	0.22	0.02
K	0.06	0.01
V	0.08	0.02
Fe	0.47	0.03
Total:	100	

Sand stone after asphaltene injection

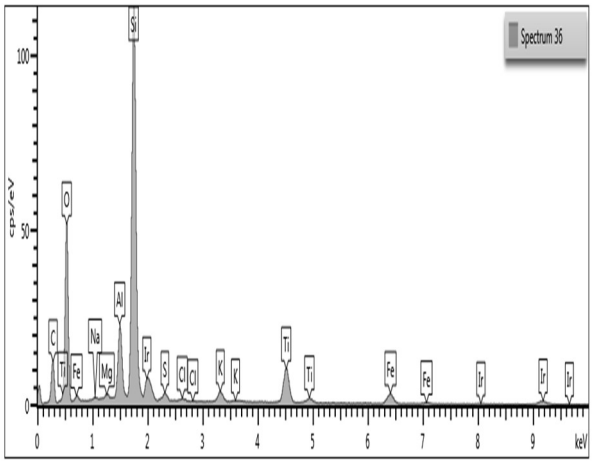

Element	Wt%	Wt% Sigma
C	34.52	0.7
O	46.34	0.54
Na	0.12	0.03
Mg	0.15	0.02
Al	2.3	0.04
Si	11.53	0.14
S	0.28	0.02
k	0.09	0.02
Cl	0.49	0.02
Total:	100	

Sand stone after DBSA NEs injection and aging for 24 h.

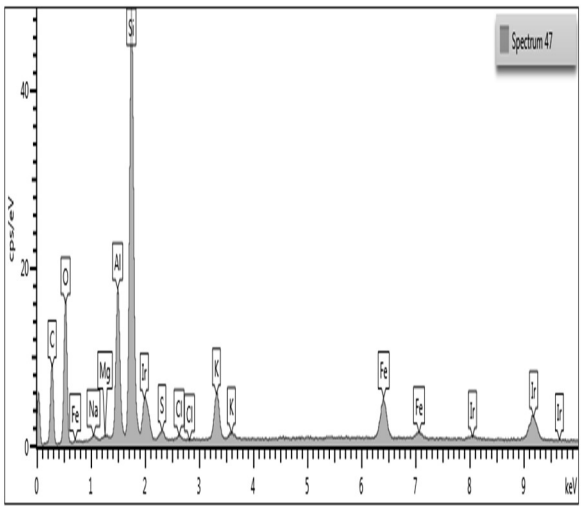

Element	Wt%	Wt% Sigma
C	46.28	0.73
O	33.53	0.53
Na	0.19	0.03
Mg	0.08	0.02
Al	3.55	0.07
Si	9.65	0.15
S	0.26	0.02
Cl	0.13	0.02
K	1.85	0.05
Fe	4.47	0.11
Total:	100	

Sand stone after post flooding

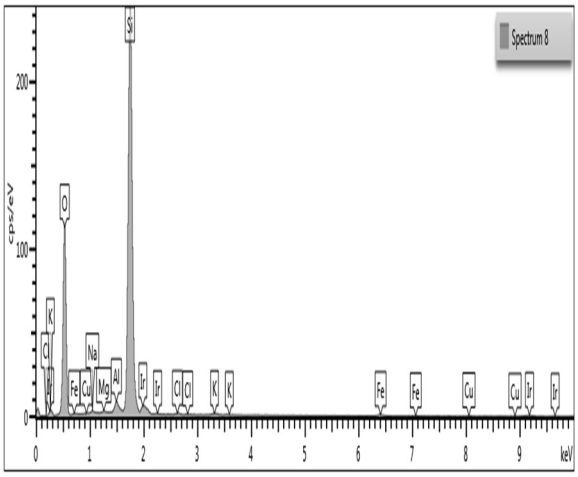

Element	Wt%	Wt% Sigma
C	16.18	1.1
O	56.28	0.19
Na	0.32	0.06
Mg	0.16	0.04
Al	0.8	0.04
Si	25.32	0.17
Cl	0.2	0.03
K	0.22	0.03
Fe	0.52	0.05
Total:	100	

Figure B-1. EDX elemental analysis for (A) Fresh Sandston, (B) particles after brine injection, (C) particles after asphaltene injection, (D) particles after DBSA NE injection, and (E) particles after DBSA NEs injection and release effect, and (F) particles after post brine flooding.

List of References

[1] Hammami, A. and Ratulowski, J., 2007. Precipitation and deposition of asphaltenes in production systems: a flow assurance overview. In *Asphaltenes, heavy oils, and petroleomics* (pp. 617-660). Springer, New York, NY.

[2] Novaki, L.P., Moraes, E.O., Goncalves, A.B., de Lira, R.A., Linhares, V.N., de Oliveira, M.C., Meireles, F.A., Gonzalez, G. and El Seoud, O.A., 2016. Solvatochromic and solubility parameters of solvents: equivalence of the scales and application to probe the solubilization of asphaltenes. *Energy & Fuels*, *30*(6), pp.4644-4652.

[3] Rogel, E., Miao, T., Vien, J. and Roye, M., 2015. Comparing asphaltenes: Deposit versus crude oil. *Fuel*, *147*, pp.155-160.

[4] Hosseini, A., Zare, E., Ayatollahi, S., Vargas, F.M., Chapman, W.G., Kostarelos, K. and Taghikhani, V., 2016. Electrokinetic behavior of asphaltene particles. *Fuel*, *178*, pp.234-242.

[5] Akbarzadeh, K., Hammami, A., Kharrat, A., Zhang, D., Allenson, S., Creek, J., Kabir, S., Jamaluddin, A., Marshall, A.G., Rodgers, R.P. and Mullins, O.C., 2007. Asphaltenes—problematic but rich in potential. *Oilfield Review*, *19*(2), pp.22-43.

[6] Ancheyta, J., Centeno, G., Trejo, F. and Speight, J.G., 2005. Asphaltene characterization as function of time on-stream during hydroprocessing of Maya crude. *Catalysis today*, *109*(1), pp.162-166.

[7] Alcázar-Vara, L.A., Zamudio-Rivera, L.S. and Buenrostro-González, E., 2016. Effect of Asphaltenes and Resins on Asphaltene Aggregation Inhibition, Rheological Behaviour and Waterflood Oil-Recovery. *Journal of Dispersion Science and Technology*, *37*(11), pp.1544-1554.

[8] Mullins, O.C., 2010. The modified Yen model. *Energy & Fuels*, *24*(4), pp.2179-2207.

[9] Wang, J., Li, C., Zhang, L., Que, G. and Li, Z., 2009. The properties of asphaltenes and their interaction with amphiphiles. *Energy & Fuels*, *23*(7), pp.3625-3631.

[10] Maqbool, T., Balgoa, A.T. and Fogler, H.S., 2009. Revisiting asphaltene precipitation from crude oils: A case of neglected kinetic effects. *Energy & Fuels*, *23*(7), pp.3681-3686.

[11] Mullins, O.C., 2011. The asphaltenes. *Annual review of analytical chemistry*, *4*, pp.393-418.

[12] Andreatta, G., Goncalves, C.C., Buffin, G., Bostrom, N., Quintella, C.M., Arteaga-Larios, F., Pérez, E. and Mullins, O.C., 2005. Nanoaggregates and structure− function relations in asphaltenes. *Energy & Fuels*, *19*(4), pp.1282-1289.

[13] Groenzin, H. and Mullins, O.C., 1999. Asphaltene molecular size and structure. *The Journal of Physical Chemistry A*, *103*(50), pp.11237-11245.

[14] Adams, J.J., 2014. Asphaltene adsorption, a literature review. *Energy & Fuels*, *28*(5), pp.2831-2856.

[15] Simon, S., Jestin, J., Palermo, T. and Barré, L., 2008. Relation between solution and interfacial properties of asphaltene aggregates. *Energy & Fuels*, *23*(1), pp.306-313.

[16] Haskett, C.E. and Tartera, M., 1965. A practical solution to the problem of asphaltene deposits-Hassi Messaoud Field, Algeria. *Journal of petroleum technology*, *17*(04), pp.387-391.

[17] Tuttle, R.N., 1983. High-pour-point and asphaltic crude oils and condensates. *Journal of Petroleum Technology*, *35*(06), pp.1-192.

[18] Thomas, F.B., Bennion, D.B., Bennion, D.W. and Hunter, B.E., 1992. Experimental and theoretical studies of solids precipitation from reservoir fluid. *Journal of Canadian Petroleum Technology*, *31*(01).

[19] Novosad, Z. and Costain, T.G., 1990, January. Experimental and modeling studies of asphaltene equilibria for a reservoir under CO2 injection. In *SPE Annual Technical Conference and Exhibition*. Society of Petroleum Engineers.

[20] Burke, N.E., Hobbs, R.E. and Kashou, S.F., 1990. Measurement and Modeling of Asphaltene Precipitation (includes associated paper 23831). *Journal of Petroleum Technology*, *42*(11), pp.1-440.

[21] Hirschberg, A., DeJong, L.N.J., Schipper, B.A. and Meijer, J.G., 1984. Influence of temperature and pressure on asphaltene flocculation. *Society of Petroleum Engineers Journal*, *24*(03), pp.283-293.

[22] Gruesbeck, C. and Collins, R.E., 1982. Entrainment and deposition of fine particles in porous media. *Society of Petroleum Engineers Journal*, *22*(06), pp.847-856.

[23] Garti, N. ed., 2008. *Delivery and controlled release of bioactives in foods and nutraceuticals*. Elsevier.

[24] Tsung, J. and Burgess, D.J., 2012. Fundamentals and applications of controlled release drug delivery. *Fundam Appl Control Release Drug Deliv*, pp.107-23.

[25] Pouton, C.W., *Formulation of self-emulsifying drug delivery systems.* Adv Drug Deliv Rev, 1997. 25(1): p. 47-58.

[26] Lawrence, M.J. and G.D. Rees, *Nanoemulsion-based media as novel drug delivery systems.* Adv Drug Deliv Rev, (0).

[27] Kalra, A., 2013. *Preparation and evaluation of oil-in-water self-nanoemulsifying systems with potential for pulmonary delivery* (Doctoral dissertation, University of Toledo).

[28] Torchilin, V., 2011. Fundamentals and Applications of Controlled Release Drug Delivery.

[29] Del Gaudio, L., Bortolo, R. and Lockhart, T.P., 2007, January. Nanoemulsions: a new vehicle for chemical additive delivery. In *International Symposium on Oilfield Chemistry*. Society of Petroleum Engineers.

[30] Acevedo, S., Ranaudo, M.A., García, C., Castillo, J., Fernández, A., Caetano, M. and Goncalvez, S., 2000. Importance of asphaltene aggregation in solution in determining the adsorption of this sample on mineral surfaces. *Colloids and Surfaces A: Physicochemical and Engineering Aspects*, *166*(1-3), pp.145-152.

[31] Mostowfi, F., Indo, K., Mullins, O.C. and McFarlane, R., 2008. Asphaltene nanoaggregates studied by centrifugation. *Energy & fuels*, *23*(3), pp.1194-1200.

[32] Mullins, O.C., Sabbah, H., Eyssautier, J., Pomerantz, A.E., Barré, L., Andrews, A.B., Ruiz-Morales, Y., Mostowfi, F., McFarlane, R., Goual, L. and Lepkowicz, R., 2012. Advances in asphaltene science and the Yen–Mullins model. *Energy & Fuels*, *26*(7), pp.3986-4003.

[33] Wang, S., Liu, J., Zhang, L., Masliyah, J. and Xu, Z., 2009. Interaction forces between asphaltene surfaces in organic solvents. *Langmuir*, *26*(1), pp.183-190.

[34] Simon, S., Jestin, J., Palermo, T. and Barré, L., 2008. Relation between solution and interfacial properties of asphaltene aggregates. *Energy & Fuels*, *23*(1), pp.306-313.

[35]Spiecker, P.M., Gawrys, K.L., Trail, C.B. and Kilpatrick, P.K., 2003. Effects of petroleum resins on asphaltene aggregation and water-in-oil emulsion formation. *Colloids and surfaces A: Physicochemical and engineering aspects*, *220*(1-3), pp.9-27.

[36] Yarranton, H.W., Alboudwarej, H. and Jakher, R., 2000. Investigation of asphaltene association with vapor pressure osmometry and interfacial tension measurements. *Industrial & engineering chemistry research*, *39*(8), pp.2916-2924.

[37] Tanaka, R., Sato, E., Hunt, J.E., Winans, R.E., Sato, S. and Takanohashi, T., 2004. Characterization of asphaltene aggregates using X-ray diffraction and small-angle X-ray scattering. *Energy & Fuels*, *18*(4), pp.1118-1125.

[38] Faus, F.M., Grange, P. and Delmon, B., 1984. Influence of asphaltene deposition on catalytic activity of cobalt molybdenum on alumina catalysts. *Applied catalysis*, *11*(2), pp.281-293.

[39] H. Alboudwarej, R. K. Jakher, W. Y. Svrcek and H. W. Yarranton, Spectrophotometric measurement of asphaltene concentration, Pet. Sci. Technol., 2004, 22(5–6), 647–664.

[40] P. C. Painter, M. Sobkowiak and J. Youtcheff, FT-IR study of hydrogen bonding in coal, Fuel, 1987, 66(7), 973–978.

[41] M. A. Anisimov, I. K. Yudin, V. Nikitin, G. Nikolaenko, A. Chernoutsan, H. Toulhoat, D. Frot and Y. Briolant, Asphaltene aggregation in hydrocarbon solutions studied by photon correlation spectroscopy, J. Phys. Chem., 1995, 99(23), 9576–9580.

[42] S. Acevedo, B. M´endez, A. Rojas, I. Layrisse and H. Rivas, Asphaltenes and resins from the Orinoco basin, Fuel, 1985, 64(12), 1741–1747.

[43] B. K. Wilt, W. T. Welch and J. G. Rankin, Determination of asphaltenes in petroleum crude oils by Fourier transform infrared spectroscopy, Energy Fuels, 1998, 12(5), 1008–1012.

[44] Zhao, R.; Zhang, R. Q. A new insight into π−π stacking involving remarkable orbital interactions. Phys. Chem. Chem. Phys. 2016, 18 (36), 25452−25457.

[45] Wang, H., Xu, H., Jia, W., Liu, J. and Ren, S., 2017. Revealing the Intermolecular Interactions of Asphaltene Dimers by Quantum Chemical Calculations. Energy & Fuels, 31(3), pp.2488-2495.

[46] Mullins, O.C., Seifert, D.J., Zuo, J.Y. and Zeybek, M., 2012. Clusters of asphaltene nanoaggregates observed in oilfield reservoirs. *Energy & Fuels*, *27*(4), pp.1752-1761.

[47] Mullins, O.C., 2010. The modified Yen model. *Energy & Fuels*, *24*(4), pp.2179-2207.

[48] Yen, T.F., 1974. Structure of petroleum asphaltene and its significance. *Energy Sources, Part Arecovery, Utilization, And Environmental Effects*, *1*(4), pp.447-463.

[49] Speight, J.G., 2004. Petroleum Asphaltenes-Part 1: Asphaltenes, resins and the structure of petroleum. *Oil & gas science and technology*, *59*(5), pp.467-477.

[50] Bahman, J., Nasiri, M., Sabeti, M. and Mohammadi, A.H., 2017. An Introduction to Asphaltenes Chemistry. *Heavy Oil: Characteristics, Production and Emerging Technologies. Nova Science Publishers, Inc., NY, USA*.

[51] Hotier, G. and Robin, M., 1983. Effects of different diluents on heavy oil products: measurement, interpretation, and a forecast of asphaltene flocculation. *Revue de l'IFP*, *38*, p.101.

[52] Srivastava, R.K. and Huang, S.S., 1997, January. Asphaltene deposition during CO2 flooding: a laboratory assessment. In *SPE Production Operations Symposium*. Society of Petroleum Engineers.

[53] Fakher, S. and Imqam, A., 2019. Asphaltene precipitation and deposition during CO2 injection in nano shale pore structure and its impact on oil recovery. *Fuel*, *237*, pp.1029-1039.
[54] Saraji, S., Goual, L. and Piri, M., 2010. Adsorption of asphaltenes in porous media under flow conditions. *Energy & Fuels*, *24*(11), pp.6009-6017.

[55] Murgich, J., 2002. Intermolecular forces in aggregates of asphaltenes and resins. *Petroleum science and technology*, *20*(9-10), pp.983-997.

[56] Dubey, S. T., and M. H. Waxman. "Asphaltene adsorption and desorption from mineral surfaces." *SPE Reservoir Engineering* 6, no. 03 (1991): 389-395.

[57] Gonzalez, G. and Travalloni-Louvisse, A.M., 1993. Adsorption of asphaltenes and its effect on oil production. *SPE Production & Facilities*, *8*(02), pp.91-96.
[58] Pernyeszi, T., Patzko, A., Berkesi, O. and Dékány, I., 1998. Asphaltene adsorption on clays and crude oil reservoir rocks. *Colloids and Surfaces A: Physicochemical and Engineering Aspects*, *137*(1-3), pp.373-384.

[59] Acevedo, S., Castillo, J., Fernández, A., Goncalves, S. and Ranaudo, M.A., 1998. A study of multilayer adsorption of asphaltenes on glass surfaces by photothermal surface deformation. Relation of this adsorption to aggregate formation in solution. *Energy & Fuels*, *12*(2), pp.386-390.

[60] Acevedo, S., Ranaudo, M.A., García, C., Castillo, J., Fernández, A., Caetano, M. and Goncalvez, S., 2000. Importance of asphaltene aggregation in solution in determining the adsorption of this sample on mineral surfaces. *Colloids and Surfaces A: Physicochemical and Engineering Aspects*, *166*(1-3), pp.145-152.

[61] Marczewski, A.W. and Szymula, M., 2002. Adsorption of asphaltenes from toluene on mineral surface. *Colloids and Surfaces A: Physicochemical and Engineering Aspects*, *208*(1-3), pp.259-266.

[62] Dudášová, D., Simon, S., Hemmingsen, P.V. and Sjöblom, J., 2008. Study of asphaltenes adsorption onto different minerals and clays: Part 1. Experimental adsorption with UV depletion detection. *Colloids and Surfaces A: Physicochemical and Engineering Aspects*, *317*(1-3), pp.1-9.

[63] Jouault, N., Corvis, Y., Cousin, F., Jestin, J. and Barré, L., 2009. Asphaltene adsorption mechanisms on the local scale probed by neutron reflectivity: transition from monolayer to multilayer growth above the flocculation threshold. *Langmuir*, *25*(7), pp.3991-3998.

[64] de la Cruz, J. M.; Castellanos-Ramı´rez, I.; Ortiz-Tapiac, A.; Buenrostro-Gonz_alez, E.; Dur_an-Valenciad, C.; L_opez-Ramı´rez, S. Colloid Surf., A 2009, 340, 149–154.

[65] Xing, C., Hilts, R.W. and Shaw, J.M., 2010. Sorption of Athabasca vacuum residue constituents on synthetic mineral and process equipment surfaces from mixtures with pentane. *Energy & Fuels*, *24*(4), pp.2500-2513.

[66] Piro, G., Canonico, L.B., Galbariggi, G., Bertero, L. and Carniani, C., 1996. Asphaltene adsorption onto formation rock: an approach to asphaltene formation damage prevention. *SPE Production & Facilities*, *11*(03), pp.156-160.

[67] Toth, J., 2003, January. Comparative Study of Asphaltene Adsorption on Formation Rocks under Static and Dynamic Conditions. In *International Symposium on Oilfield Chemistry*. Society of Petroleum Engineers.

[68] Haskett, C.E. and Tartera, M., 1965. A practical solution to the problem of asphaltene deposits-Hassi Messaoud Field, Algeria. *Journal of petroleum technology*, *17*(04), pp.387-391.

[69] Leontaritis, K.J., 2005. Asphaltene near-well-bore formation damage modeling. *Journal of energy resources technology*, *127*(3), pp.191-200.

[70] Darabi, H., 2014. *Development of a non-isothermal compositional reservoir simulator to model asphaltene precipitation, flocculation, and deposition and remediation* (Doctoral dissertation).

[71] Argillier, J., Henaut, I., Heraud, J.P. and Glenat, P., 2005, January. Heavy oil dilution. In *SPE International Thermal Operations and Heavy Oil Symposium*. Society of Petroleum Engineers.

[72] Taborda, E.A., Franco, C.A., Lopera, S.H., Alvarado, V. and Cortés, F.B., 2016. Effect of nanoparticles/nanofluids on the rheology of heavy crude oil and its mobility on porous media at reservoir conditions. *Fuel*, *184*, pp.222-232.

[73] Rogel, E., Miao, T., Vien, J. and Roye, M., 2015. Comparing asphaltenes: Deposit versus crude oil. *Fuel*, *147*, pp.155-160.

[74] Álvarez, E., Trejo, F., Marroquín, G. and Ancheyta, J., 2015. The effect of solvent washing on asphaltenes and their characterization. *Petroleum Science and Technology*, *33*(3), pp.265-271.

[75] Osaheni, J.A., Fyvie, T.J., O'neil, G.A. and Matis, H., General Electric Co, 2012. *Methods and system for removing impurities from heavy fuel*. U.S. Patent 8,088,277.

[76] Yeung, C.K., Value Creation Inc, 2009. *System for the decontamination of asphaltic heavy oil and bitumen*. U.S. Patent 7,625,466.

[77] Nwadinigwe, C.A., Anigbogu, I.V. and Ujam, O.T., 2015. Studies on precipitation performance of n-heptane and n-pentane/n-heptane on C7 and C5/C7 asphaltenes and maltenes from 350° C atmospheric residuum of three Nigerian light crudes. *Journal of Petroleum Exploration and Production Technology*, *5*(4), pp.403-407.

[78] Janssen, M.J., Ou, J.D., Heeter, G.A. and Van Oorschot, C.W., ExxonMobil Chemical Patents Inc, 2016. *Removal of asphaltene contaminants from hydrocarbon streams using carbon based adsorbents*. U.S. Patent 9,321,971.

[79] Pourabdollah, K., Moghaddam, A.Z., Kharrat, R. and Mokhtari, B., 2011. Improvement of heavy oil recovery in the VAPEX process using montmorillonite nanoclays. *Oil & Gas Science and Technology–Revue d'IFP Energies nouvelles*, *66*(6), pp.1005-1016.

[80] Nassar, N.N., Hassan, A. and Pereira-Almao, P., 2011. Metal oxide nanoparticles for asphaltene adsorption and oxidation. *Energy & Fuels*, *25*(3), pp.1017-1023.

[81] Bouts, M.N., Wiersma, R.J., Muijs, H.M. and Samuel, A.J., 1995. An evaluation of new aspaltene inhibitors; Laboratory study and field testing. *Journal of Petroleum Technology*, *47*(09), pp.782-787.

[82] Abdallah, D., 2012, January. Impact of Asphaltenes Deposition on Completion Design for CO2 Pilot in an Onshore Abu Dhabi Field. In *Abu Dhabi International Petroleum Conference and Exhibition*. Society of Petroleum Engineers.

[83] Subramanian, D. and Firoozabadi, A., 2015, November. Effect of Surfactants and Water on Inhibition of Asphaltene Precipitation and Deposition. In *Abu Dhabi International Petroleum Exhibition and Conference*. Society of Petroleum Engineers.

[84] Ortega, F.J., Navarro, F.J. and García-Morales, M., 2017. Dodecylbenzenesulfonic Acid as a Bitumen Modifier: A Novel Approach To Enhance Rheological Properties of Bitumen. *Energy & Fuels*, *31*(5), pp.5003-5010.

[85] Hashmi, S.M., Zhong, K.X. and Firoozabadi, A., 2012. Acid–base chemistry enables reversible colloid-to-solution transition of asphaltenes in non-polar systems. *Soft Matter*, *8*(33), pp.8778-8785.

[86] Goual, L. and Sedghi, M., 2015. Role of ion-pair interactions on asphaltene stabilization by alkylbenzenesulfonic acids. *Journal of colloid and interface science*, *440*, pp.23-31.

[87] Wang, J., Li, C., Zhang, L., Que, G. and Li, Z., 2009. The properties of asphaltenes and their interaction with amphiphiles. *Energy & Fuels*, *23*(7), pp.3625-3631.

[88] Chang, C.L. and Fogler, H.S., 1994. Stabilization of asphaltenes in aliphatic solvents using alkylbenzene-derived amphiphiles. 2. Study of the asphaltene-amphiphile interactions and structures using Fourier transform infrared spectroscopy and small-angle X-ray scattering techniques. *Langmuir*, *10*(6), pp.1758-1766.

[89] Goual, L. and Firoozabadi, A., 2004. Effect of resins and DBSA on asphaltene precipitation from petroleum fluids. *AIChE journal*, *50*(2), pp.470-479.

[90] Goual, L. and Sedghi, M., 2015. Role of ion-pair interactions on asphaltene stabilization by alkylbenzenesulfonic acids. *Journal of colloid and interface science*, *440*, pp.23-31.

[91] Wei, D., Orlandi, E., Simon, S., Sjöblom, J. and Suurkuusk, M., 2015. Interactions between asphaltenes and alkylbenzene-derived inhibitors investigated by isothermal titration calorimetry. *Journal of Thermal Analysis and Calorimetry*, *120*(3), pp.1835-1846.

[92] Ovalles, C., Rogel, E. and Moir, M., Chevron USA Inc, 2018. *Method for determining the effectiveness of asphaltene dispersant additives for inhibiting or preventing asphaltene precipitation in a hydrocarbon-containing material subjected to elevated temperature and presssure conditions*. U.S. Patent 9,921,205.

[93] Gochin, R.J. and Smith, A., Imperial College of Science Technology and Medicine, 2001. *Method of controlling asphaltene precipitation in a fluid*. U.S. Patent 6,270,653.

[94] Ascanius, B.E., Garcia, D.M. and Andersen, S.I., 2004. Analysis of asphaltenes subfractionated by N-methyl-2-pyrrolidone. *Energy & fuels*, *18*(6), pp.1827-1831.

[95] Newberry, M.E. and Barker, K.M., Baker Petrolite Corp, 1983. *Method for the removal of asphaltenic deposits*. U.S. Patent 4,414,035.

[96] Victorov, A.I. and Firoozabadi, A., 1996. Thermodynamic micellizatin model of asphaltene precipitation from petroleum fluids. *AIChE journal*, *42*(6), pp.1753-1764.

[97] Pan, H. and Firoozabadi, A., 1998. A thermodynamic micellization model for asphaltene precipitation: Part I: Micellar size and growth. *SPE Production & Facilities*, *13*(02), pp.118-127.

[98] Zendehboudi, S., Ahmadi, M.A., Mohammadzadeh, O., Bahadori, A. and Chatzis, I., 2013. Thermodynamic investigation of asphaltene precipitation during primary oil production: laboratory and smart technique. *Industrial & Engineering Chemistry Research*, *52*(17), pp.6009-6031.

[99] León, O., Rogel, E., Urbina, A., Andújar, A. and Lucas, A., 1999. Study of the adsorption of alkyl benzene-derived amphiphiles on asphaltene particles. *Langmuir*, *15*(22), pp.7653-7657.

[100] Silva, I., Borges, B., Blanco, R., Rondón, M., Salager, J.L. and Pereira, J.C., 2014. Breaking of water-in-crude oil emulsions. 5. Effect of acid-alkaline additives on the performance of chemical demulsifiers. *Energy & Fuels*, *28*(6), pp.3587-3593.

[101] Von Tapavicza, S., Zoellner, W., Herold, C.P., Groffe, J. and Rouet, J., Henkel AG and Co KGaA, 2002. *Use of selected inhibitors against the formation of solid organo-based incrustations from fluid hydrocarbon mixtures*. U.S. Patent 6,344,431.

[102] Miller, R.F., Atlantic Richfield Co, 1987. *Inhibiting polymerization of vinyl aromatic monomers*. U.S. Patent 4,654,450.

[103] Ovalles, C., Rogel, E., Morazan, H., Chen, K. and Moir, M.E., 2016. The use of nonylphenol formaldehyde resins for preventing asphaltene precipitation in vacuum residues and hydroprocessed petroleum samples. *Petroleum Science and Technology*, *34*(4), pp.379-385.

[104] Miller, D., Vollmer, A., Feustel, M. and Klug, P., Clariant Produkte (Deutschland) GmbH, 2001. *Synergistic mixtures of phosphoric esters with carboxylic acids or carboxylic acid derivatives as asphaltene dispersants*. U.S. Patent 6,204,420.

[105] Auflem, I., Havre, T. and Sjöblom, J., 2002. Near-IR study on the dispersive effects of amphiphiles and naphthenic acids on asphaltenes in model heptane-toluene mixtures. *Colloid and polymer science*, *280*(8), pp.695-700.

[106] Östlund, J.A., Nydén, M., Auflem, I.H. and Sjöblom, J., 2003. Interactions between asphaltenes and naphthenic acids. *Energy & Fuels*, *17*(1), pp.113-119.

[107] Miller, D., Vollmer, A., Feustel, M. and Klug, P., Clariant Produkte (Deutschland) GmbH, 1999. *Use of sarcosinates as asphaltene-dispersing agents*. U.S. Patent 5,948,237.

[108] Chávez-Miyauchi, T.E., Zamudio-Rivera, L.S. and Barba-López, V., 2013. Aromatic polyisobutylene succinimides as viscosity reducers with asphaltene dispersion capability for heavy and extra-heavy crude oils. *Energy & Fuels*, *27*(4), pp.1994-2001.

[109] Mena-Cervantes, V.Y., Hernández-Altamirano, R., Buenrostro-González, E., Beltrán, H.I. and Zamudio-Rivera, L.S., 2013. Development of oxazolidines derived from polyisobutylene succinimides as multifunctional stabilizers of asphaltenes in oil industry. *Fuel*, *110*, pp.293-301.

[110] Abrahamsen, E.L., 2012. *Organic flow assurance: Asphaltene dispersant/inhibitor formulation development through experimental design* (Master's thesis, University of Stavanger, Norway).

[111] Xu, Y., Wu, J., Dabros, T., Hamza, H. and Venter, J., 2005. Optimizing the polyethylene oxide and polypropylene oxide contents in diethylenetriamine-based surfactants for destabilization of a water-in-oil emulsion. *Energy & fuels*, *19*(3), pp.916-921.

[112] Larichev, Y.V., Nartova, A.V. and Martyanov, O.N., 2016. The influence of different organic solvents on the size and shape of asphaltene aggregates studied via small-angle X-ray scattering and scanning tunneling microscopy. *Adsorption Science & Technology*, *34*(2-3), pp.244-257.

[113] Bernasconi, C., Faure, A. and Thibonnet, B., Elf Antar France, 1986. *Homogeneous and stable composition of asphaltenic liquid hydrocarbons and additive useful as industrial fuel*. U.S. Patent 4,622,047.

[114] Wang, Y., Zhang, Y., Chen, F., Zheng, M., Zhao, L., Gao, J., Hao, T. and Xu, C., 2018. Direct Separation of Olefins from Aromatics or Sulfides: Influence of the Structure and Content of Olefins and Aromatics. *Energy & Fuels*, *32*(2), pp.2571-2581.

[115] Abrahamsen, E.L., 2012. *Organic flow assurance: Asphaltene dispersant/inhibitor formulation development through experimental design* (Master's thesis, University of Stavanger, Norway).

[116] León, O., Contreras, E. and Rogel, E., 2001. Amphiphile adsorption on asphaltene particles: adsorption isotherms and asphaltene stabilization. *Colloids and Surfaces A: Physicochemical and Engineering Aspects*, *189*(1-3), pp.123-130.

[117] Hu, Y.F. and Guo, T.M., 2005. Effect of the structures of ionic liquids and alkylbenzene-derived amphiphiles on the inhibition of asphaltene precipitation from CO2-injected reservoir oils. *Langmuir*, *21*(18), pp.8168-8174.

[118] Junior, L.C.R., Ferreira, M.S. and da Silva Ramos, A.C., 2006. Inhibition of asphaltene precipitation in Brazilian crude oils using new oil soluble amphiphiles. *Journal of Petroleum Science and Engineering*, *51*(1-2), pp.26-36.

[119] Breen, P.J., Baker Hughes Inc, 2001. *Inhibition of asphaltene deposition in crude oil production systems*. U.S. Patent 6,313,367.

[120] Leon, O., Contreras, E., Rogel, E., Dambakli, G., Espidel, J. and Acevedo, S., 2001. The influence of the adsorption of amphiphiles and resins in controlling asphaltene flocculation. *Energy & Fuels*, *15*(5), pp.1028-1032.

[121] Lima, A.F., Mansur, C.R., Lucas, E.F. and González, G., 2009. Polycardanol or sulfonated polystyrene as flocculants for asphaltene dispersions. *Energy & Fuels*, *24*(4), pp.2369-2375.

[122] Al-Sabagh, A.M., Nasser, N.M., El-Sukkary, M.M., Eissa, A.M.F., Kabel, K.I. and Abd El-Hamid, T.M., 2013. Surface Active and Thermodynamic Properties in Relation to the Demulsification Efficiency for Some Ethoxylated Derivatives of Alkyldiamines and Polyalkylenepolyamines. *Journal of Dispersion Science and Technology*, *34*(10), pp.1356-1367.

[123] Chang, C.L. and Scott Fogler, H., 1996. Peptization and coagulation of asphaltenes in apolar media using oil-soluble polymers. *Fuel Science and Technology International*, *14*(1-2), pp.75-100.

[124] Feustel, M., Krull, M. and Mörscher, M., Clariant International Ltd, 2017. *Additives For Low-Sulfur Marine Diesel*. U.S. Patent Application 15/501,381.

[125] Wang, T., Xu, J., Wang, M., Wei, X., Shen, M., Huang, J., Zhang, R., Li, L. and Guo, X., 2015. Synthesis of comb-type copolymers with various pendants and their effect on the complex rheological behaviors of waxy oils. *Journal of Applied Polymer Science*, *132*(11).

[126] Le, H.T., ConocoPhillips Holding Co, 1990. *Oil compositions containing terpolymers of alkyl acrylates or methacrylates, an olefinically unsaturated homo or heterocyclic-nitrogen compound and allyl acrylates or methacrylates*. U.S. Patent 4,954,135.

[127] Li, J., Ali, S.A., Bustos, O. and Miller, M.J., Schlumberger Technology Corp, 2014. *Asphaltene removal composition and methods*. U.S. Patent 8,695,707.

[128] Cornelisse, P.M.W., Shell Oil Co, 2006. *Method for solubilising asphaltenes in a hydrocarbon mixture*. U.S. Patent 7,122,113.

[129] Gundersen, S.A., Ese, M.H. and Sjöblom, J., 2001. Langmuir surface and interface films of lignosulfonates and Kraft lignins in the presence of electrolyte and asphaltenes: correlation to emulsion stability. *Colloids and Surfaces A: Physicochemical and Engineering Aspects*, *182*(1-3), pp.199-218.

[130] Mitra-Kirtley, S., Mullins, O.C., Van Elp, J., George, S.J., Chen, J. and Cramer, S.P., 1993. Determination of the nitrogen chemical structures in petroleum asphaltenes using XANES spectroscopy. *Journal of the American Chemical society*, *115*(1), pp.252-258.

[131] Argillier, J.F., Coustet, C. and Henaut, I., 2002, January. Heavy oil rheology as a function of asphaltene and resin content and temperature. In *SPE International thermal operations and heavy oil symposium and international horizontal well technology conference*. Society of Petroleum Engineers.

[132] Duenckel, R.J., Leasure, J.G. and Palisch, T., 2014, February. Improvements in Downhole Chemical Delivery: Development of Multifunctional Proppants. In *SPE Hydraulic Fracturing Technology Conference*. Society of Petroleum Engineers.

[133] Yang, J. and Jovancicevic, V., Baker Hughes Inc, 2009. *Microemulsion containing oil field chemicals useful for oil and gas field applications*. U.S. Patent 7,615,516.

[134] Ibrahim, J.M., Sorbie, K. and Boak, L.S., 2012, January. Coupled Adsorption/Precipitation Experiments: 1. Static Results. In *SPE International Conference on Oilfield Scale*. Society of Petroleum Engineers.

[135] Jordan, M.M., Sorbie, K.S., Chen, P., Armitage, P., Hammond, P. and Taylor, K., 1997, January. The design of polymer and phosphonate scale inhibitor precipitation treatments and the Importance of precipitate solubility in extending squeeze lifetime. In *International Symposium on Oilfield Chemistry*. Society of Petroleum Engineers.

[136] Collins, I.R., Stewart, N.J., Wade, S.R., Goodwin, S.G., Hewartson, J.A. and Deignan, S.D., 1997, January. Extending scale squeeze lifetimes using a chemical additive: from the laboratory to the field. In *solving oilfield scaling conference* (pp. 23-24).

[137] Fleming, N., Ramstad, K., Nelson, A.C. and Kidd, S., 2009. Innovative use of kaolinite in downhole scale management: squeeze-life enhancement and water shutoff. *SPE Production & Operations*, *24*(03), pp.439-449.

[138] Al-Zahrani, A.A., Saudi Arabian Oil Co, 2011. *Method of mixing a corrosion inhibitor in an acid-in-oil emulsion*. U.S. Patent 8,039,422.

[139] Zhang, P., Ruan, G., Kan, A.T. and Tomson, M.B., 2016. Functional scale inhibitor nanoparticle capsule delivery vehicles for oilfield mineral scale control. Rsc Advances, 6(49), pp.43016-43027.

[140] Gupta, D.S. and Kirk, J.W., BJ Services Co LLC, 2009. *Method of inhibiting or controlling formation of inorganic scales*. U.S. Patent 7,491,682.

[141] Brown, J.M., Gupta, D.V., Taylor, G.N., Shen, D. and Self, R., 2011, January. Laboratory and field studies of long-term release rates for a solid scale inhibitor. In *SPE International Symposium on Oilfield Chemistry*. Society of Petroleum Engineers.

[142] Lvov, Y.M., Shchukin, D.G., Mohwald, H. and Price, R.R., 2008. Halloysite clay nanotubes for controlled release of protective agents. *ACS nano*, *2*(5), pp.814-820

[143] Zhang, P., Shen, D., Kan, A.T. and Tomson, M.B., 2016. Synthesis and laboratory testing of a novel calcium-phosphonate reverse micelle nanofluid for oilfield mineral scale control. *RSC Advances*, *6*(46), pp.39883-39895.

[144] Haindade, Z.M.W., Bihani, A.D., Javeri, S.M. and Jere, C.B., 2012, January. Enhancing flow assurance using Co-Ni nanoparticles for dewaxing of production tubing. In *SPE International Oilfield Nanotechnology Conference and Exhibition*. Society of Petroleum Engineers.

[145] Charpentier, T.V., Neville, A., Baudin, S., Smith, M.J., Euvrard, M., Bell, A., Wang, C. and Barker, R., 2015. Liquid infused porous surfaces for mineral fouling mitigation. *Journal of colloid and interface science*, *444*, pp.81-86.

[146] Zheludkevich, M.L., Shchukin, D.G., Yasakau, K.A., Möhwald, H. and Ferreira, M.G., 2007. Anticorrosion coatings with self-healing effect based on nanocontainers impregnated with corrosion inhibitor. *Chemistry of Materials*, *19*(3), pp.402-411.

[147] Ghorbani, N., Wilson, M.C.T., Kapur, N., Fleming, N., Tjomsland, T. and Neville, A., 2017. Adsorption of polyphosphinocarboxylic acid (PPCA) scale inhibitor on carbon nanotubes (CNTs): A prospective method for enhanced oilfield scale prevention. *Journal of Petroleum Science and Engineering*, *150*, pp.305-311.

[148] Zhang, P., Shen, D., Ruan, G., Kan, A.T. and Tomson, M.B., 2016. Mechanistic understanding of calcium–phosphonate solid dissolution and scale inhibitor return behavior in oilfield reservoir: formation of middle phase. *Physical Chemistry Chemical Physics*, *18*(31), pp.21458-21468.

[149] Del Gaudio, L., Bortolo, R. and Lockhart, T.P., 2007, January. Nanoemulsions: a new vehicle for chemical additive delivery. In *International Symposium on Oilfield Chemistry*. Society of Petroleum Engineers.

[150] Maserati, G., Daturi, E., Del Gaudio, L., Belloni, A., Bolzoni, S., Lazzari, W., Leo, G., 2010. Nano-emulsions as cement spacer improve the cleaning of casing bore during cementing operations. In: Paper SPE-133033eMS, Presented at SPE Annual Technical Conference and Exhibition, Florence, Italy, 19-22 September

[151] Zea, C., Barranco-García, R., Alcántara, J., Chico, B., Morcillo, M. and de la Fuente, D., 2017. Hollow mesoporous silica nanoparticles loaded with phosphomolybdate as smart anticorrosive pigment. *Journal of Coatings Technology and Research*, *14*(4), pp.869-878

[152] G. Contri, G.M.O. Barra, S.D.A.S. Ramoa, C. Merlini, L.G. Ecco, F.S. Souza, A. Spinelli, Epoxy coating based on montmorillonite-polypyrrole: electrical properties and prospective application on corrosion protection of steel, Prog. Org. Coat. 114 (2018) 201–207

[153] Nourafkan, E., Hu, Z. and Wen, D., 2018. Controlled delivery and release of surfactant for enhanced oil recovery by nanodroplets. *Fuel*, *218*, pp.396-405.

[154] Nourafkan, E., Hu, Z. and Wen, D., 2018. Nanoparticle-enabled delivery of surfactants in porous media. Journal of colloid and interface science, 519, pp.44-57.

[155] Rosestolato JC, Pérez-Gramatges A, Lachter ER, Nascimento RS. Lipid nanostructures as surfactant carriers for enhanced oil recovery. Fuel. 2019 Mar 1; 239:403-12.

[156] YE, C., 2013. *Formulation design and development of transdermal delivery system-nanoemulsion of Schizandrol A* (Doctoral dissertation).

[157] Miles, A.F., Bourne, H.M., Smith, R.G. and Collins, I.R., 2003, January. Development of a novel water in oil microemulsion based scale inhibitor delivery system. In *International Symposium on Oilfield Scale*. Society of Petroleum Engineers.

[158] Amanullah, M. and Al-Tahini, A.M., 2009, January. Nano-technology-its significance in smart fluid development for oil and gas field application. In *SPE Saudi Arabia Section Technical Symposium*. Society of Petroleum Engineers.

[159] Kumar, R., Kaur, K., Uppal, S. and Mehta, S.K., 2017. Ultrasound processed nanoemulsion: A comparative approach between resveratrol and resveratrol cyclodextrin inclusion complex to study its binding interactions, antioxidant activity and UV light stability. *Ultrasonics sonochemistry*, *37*, pp.478-489.

[160] Mandal, A., Bera, A., Ojha, K. and Kumar, T., 2012, January. Characterization of surfactant stabilized nanoemulsion and its use in enhanced oil recovery. In *SPE International Oilfield Nanotechnology Conference and Exhibition*. Society of Petroleum Engineers.

[161] Wooster, T.J., Golding, M. and Sanguansri, P., 2008. Impact of oil type on nanoemulsion formation and Ostwald ripening stability. *Langmuir*, *24*(22), pp.12758-12765.

[162] McClements, D.J., 2015. *Food emulsions: principles, practices, and techniques*. CRC press.

[163] Shiloach, A. and Blankschtein, D., 1998. Predicting micellar solution properties of binary surfactant mixtures. *Langmuir*, *14*(7), pp.1618-1636.

[164] Garamus, V.M., 1998. A new method for the determination of the dehydration coefficient of ethylene oxide groups of non-ionic surfactants in mixed micelles. *Chemical physics letters*, *290*(1-3), pp.251-254.

[165] Aratono, M., Ohta, A., Minamizawa, H., Ikeda, N., Iyota, H. and Takiue, T., 1999. The excess thermodynamic quantities of adsorption of a binary nonionic surfactant mixture. *Journal of colloid and interface science*, *217*(1), pp.128-136.

[166] Kabalnov, A., 2001. Ostwald ripening and related phenomena. *Journal of Dispersion Science and Technology*, *22*(1), pp.1-12.

[167] Kabalnov, A.S. and Shchukin, E.D., 1992. Ostwald ripening theory: applications to fluorocarbon emulsion stability. *Advances in colloid and interface science*, *38*, pp.69-97.

[168] McClements, D.J., 2012. Nanoemulsions versus microemulsions: terminology, differences, and similarities. *Soft matter*, *8*(6), pp.1719-1729.

[169] Julian McClements, D., Henson, L., Popplewell, L.M., Decker, E.A. and Jun Choi, S., 2012. Inhibition of Ostwald ripening in model beverage emulsions by addition of poorly water-soluble triglyceride oils. *Journal of food science*, *77*(1), pp.C33-C38.

[170] Ziani, K., Chang, Y., McLandsborough, L. and McClements, D.J., 2011. Influence of surfactant charge on antimicrobial efficacy of surfactant-stabilized thyme oil nanoemulsions. *Journal of agricultural and food chemistry*, *59*(11), pp.6247-6255.

[171] Chen, H., Jin, X., Li, Y. and Tian, J., 2016. Investigation into the physical stability of a eugenol nanoemulsion in the presence of a high content of triglyceride. *RSC Advances*, *6*(93), pp.91060-91067.

[172] Taylor, P., 2003. Ostwald ripening in emulsions: estimation of solution thermodynamics of the disperse phase. *Advances in colloid and interface science*, *106*(1-3), pp.261-285.

[173] McClements, D.J. and Rao, J., 2011. Food-grade nanoemulsions: formulation, fabrication, properties, performance, biological fate, and potential toxicity. *Critical reviews in food science and nutrition*, *51*(4), pp.285-330.

[174] Galindo-Alvarez, J., Le, K.A., Sadtler, V., Marchal, P., Perrin, P., Tribet, C., Marie, E. and Durand, A., 2011. Enhanced stability of nanoemulsions using mixtures of non-ionic surfactant and amphiphilic polyelectrolyte. *Colloids and Surfaces A: Physicochemical and Engineering Aspects*, *389*(1-3), pp.237-245.

[175] Smith, R.J., Lotya, M. and Coleman, J.N., 2010. The importance of repulsive potential barriers for the dispersion of graphene using surfactants. *New Journal of Physics*, *12*(12), p.125008.

[176] McClements, D.J. and Rao, J., 2011. Food-grade nanoemulsions: formulation, fabrication, properties, performance, biological fate, and potential toxicity. *Critical reviews in food science and nutrition*, *51*(4), pp.285-330.

[177] K. Kumar, E.K. Dao, K.K. Mohanty, Atomic force microscopy study of wettability alteration by surfactants, *SPE J.* 13 (2) (2008) 137–145.

[178] Fanun, M., 2012. Microemulsions as delivery systems. Current Opinion in Colloid & Interface Science 17, 306-313.

[179] Danielsson, I., Lindman, B., 1981. The definition of microemulsion. *Colloids and surfaces*, 3, 391-392.

[180] Lawrence, M.J., Rees, G.D., 2000. Microemulsion-based media as novel drug delivery systems. *Advanced Drug Delivery Reviews*, 45, 89-121.

[181] Tadros, T., Izquierdo, P., Esquena, J. and Solans, C., 2004. Formation and stability of nano-emulsions. *Advances in colloid and interface science*, *108*, pp.303-318.

[182] Tamilvanan, S., 2008. Oil-in-Water Nanosized Emulsions: Medical Applications, in: Gad, S.C. (Ed.), Pharmaceutical Manufacturing Handbook: Production and Processes. John Wiley & Sons, Inc., pp. 1327-1366.

[183] Gao, X.-H., Zhang, L., Wei, H., Chen, H.-D., 2008. Efficacy and safety of innovative cosmeceuticals. *Clinics in Dermatology*, 26, 367-374.

[184] Bui, K., Akkutlu, I.Y., Zelenev, A., Saboowala, H., Gillis, J.R. and Silas, J.A., 2016. Insights into mobilization of shale oil by use of microemulsion. *SPE Journal*, *21*(02), pp.613-620.

[185] Müller-Goymann, C., 2004. Physicochemical characterization of colloidal drug delivery systems such as reverse micelles, vesicles, liquid crystals and nanoparticles for topical administration. *European Journal of Pharmaceutics and Biopharmaceutics*, 58, 343-356.

[186] Tadros, T.F., 2005. Surfactants in Nano-Emulsions. Applied Surfactants: Principles and Applications, 285-308.

[187] Vogt, A., Combadiere, B., Hadam, S., Stieler, K.M., Lademann, J., Schaefer, H., Autran, B., Sterry, W., Blume-Peytavi, U., 2006. 40 nm, but not 750 or 1,500 nm, Nanoparticles Enter Epidermal CD1a+ Cells after Transcutaneous Application on Human Skin. J. Invest. Dermatol. 126, 1316-1322.

[188] Capek, I., 2004. Degradation of kinetically-stable o/w emulsions. *Advances in Colloid and Interface Science,* 107, 125-155.

[189] Buckley, J.S., Liu, Y. and Monsterleet, S., 1998. Mechanisms of wetting alteration by crude oils. *SPE journal*, *3*(01), pp.54-61.

[190] Al Sultan, A., Zirrahi, M., Hassanzadeh, H. and Abedi, J., 2018. Effect of the Surfactant on Asphaltene Deposition on Stainless-Steel and Glass Surfaces. *Energy & Fuels*, *32*(4), pp.5635-5642.

[191] J.R. Baran, G.A. Pope, W.H. Wade, V. Weerasooriya, A. Yapa, Microemulsionformation with chlorinated hydrocarbons of differing polarity, *Environ. Sci.Technol*. 28 (7) (1994) 1361–1366.

[192] A.R. Duffield, R.S. Ramamurthy, J.R. Campanelli, Surfactant enhancedmobilization of mineral oil within porous media, *Water Air Soil Pollut*. 143(1-4) (2003) 111–122.

[193] C.C. West, J.H. Harwell, Surfactants and subsurface remediation, Environ. Sci.Technol 26 (12) (1992) 2324–2330.

[194] P.A. Winsor, Binary and multicomponent solutions of amphiphiliccompounds. solubilization and the formation, structure, and theoreticalsignificance of liquid crystalline solutions, *Chem. Rev*. 68 (1) (1968) 1–40.

[195] R.E. Jackson, Surfactant-enhanced remediation of DNAPL zones in granularaquifer systems, *Rem. J.* 4 (1) (1993) 77–91.

[196] Bettahar, M., SchÄfer, G. and Baviere, M., 1999. An optimized surfactant formulation for the remediation of diesel oil polluted sandy aquifers. *Environmental science & technology*, *33*(8), pp.1269-1273.

[197] Cowell, M.A., Kibbey, T.C.G., Zimmerman, J.B., Hayes, K.F., 2000. Partitioning of ethoxylated nonionic surfactants in water/NAPL systems: effects of surfactant and NAPL properties. *Environ. Sci. Technol*. 34 (8), 1583–1588.

[198] Javanbakht, G., Arshadi, M., Qin, T. and Goual, L., 2017. Micro-scale displacement of NAPL by surfactant and microemulsion in heterogeneous porous media. *Advances in water resources*, *105*, pp.173-187.

[199] D.J. McClements, Nanoemulsions versus microemulsions: terminology,differences, and similarities, *Soft Matter,* 8 (6) (2012) 1719–1729.

[200] A. Mandal, A. Bera, Surfactant stabilized nanoemulsion: characterization andapplication in enhanced oil recovery, *Int. J. Chem. Mol. Nucl. Mater. Metall.Eng*. 6 (7) (2012) 537–542.

[201] Qin, T., Javanbakht, G., Goual, L., Piri, M. and Towler, B., 2017. Microemulsion-enhanced displacement of oil in porous media containing carbonate cements. *Colloids and Surfaces A: Physicochemical and Engineering Aspects*, *530*, pp.60-71.

[202] Oliveira MCK, Lucas EF, Gonzalez G, Oliveira JF. Heavy oil fraction removal from sand using hydrotropes containing oil-in-water microemulsions. *Prog Colloid Polym Sci*, 2004;128:288–92.

[203] Lowry, E., Sedghi, M. and Goual, L., 2016. Molecular simulations of NAPL removal from mineral surfaces using microemulsions and surfactants. *Colloids and Surfaces A: Physicochemical and Engineering Aspects*, *506*, pp.485-494.

[204] Hernandez, H.W., Ehlert, W. and Trabelsi, S., 2019. Removal of crude oil residue from solid surfaces using microemulsions. *Fuel*, *237*, pp.398-404.

[205] L. Del Gaudio, R. Bortolo, T. P. Lockhart, Nanoemulsions: A new vehicle for chemical additive delivery, Proc. International Symposium on Oilfield Chemistry.

[206] Wiśniewska, M., 2010. Influences of polyacrylic acid adsorption and temperature on the alumina suspension stability. *Powder Technology*, *198*(2), pp.258-266.

[207] Kov scek A, Wong H and Radke C. A pore-level scenario for the development of mixed wettability in oil reservoirs. AIChE Journal. 1993. 39(6): 1072-1085

[208] Buc kley J S, Liu Y and Monsterleet S. Mechanisms of wetting alteration by crud e oils. SPE Journal. 1998. 3(1): 54-61 (paper SPE 37230)

[209] Wiśniewska, M., Urban, T., Nosal-Wiercińska, A., Zarko, V. and Gun'ko, V., 2014. Comparison of stability properties of poly (acrylic acid) adsorbed on the surface of silica, alumina and mixed silica-alumina nanoparticles—application of turbidimetry method. *Open Chemistry*, *12*(4), pp.476-479.

[210] Li, D., Li, L., Xiao, N., Li, M. and Xie, X., 2018. Physical properties of oil-in-water nanoemulsions stabilized by OSA-modified starch for the encapsulation of lycopene. *Colloids and Surfaces A: Physicochemical and Engineering Aspects*, *552*, pp.59-66.

[211] Anton, N., Gayet, P., Benoit, J.P. and Saulnier, P., 2007. Nano-emulsions and nanocapsules by the PIT method: an investigation on the role of the temperature cycling on the emulsion phase inversion. *International Journal of Pharmaceutics*, *344*(1-2), pp.44-52.

[212] McClements, D.J., 2015. *Food emulsions: principles, practices, and techniques*. CRC press.

[213] Troncoso, E., Aguilera, J.M. and McClements, D.J., 2012. Fabrication, characterization and lipase digestibility of food-grade nanoemulsions. *Food Hydrocolloids*, *27*(2), pp.355-363.

[214] Ozturk, B. and McClements, D.J., 2016. Progress in natural emulsifiers for utilization in food emulsions. *Current Opinion in Food Science*, *7*, pp.1-6.

[215] C.-Y. Lin, L.-W. Chen, Emulsification characteristics of three-and two-phase emulsions prepared by the ultrasonic emulsification method, *Fuel Processing Technology,* 87 (4) (2006) 309–317.

[216] Y. Chang, L. McLandsborough, D. J. McClements, Physical properties and antimicrobial efficacy of thyme oil nanoemulsions: influence of ripening inhibitors, *Journal of agricultural and food chemistry,* 60 (48) (2012) 12056–12063.

[217] R. Liang, S. Xu, C. F. Shoemaker, Y. Li, F. Zhong, Q. Huang, Physical and antimicrobial properties of peppermint oil nanoemulsions, *Journal of agricultural and food chemistry*, 60 (30) (2012) 7548–7555.

[218] T. Tadros, P. Izquierdo, J. Esquena, C. Solans, Formation and stability of nanoemulsions, *Advances in colloid and interface science,* 108 (2004) 303–318.

[219] Guerra-Rosas, M.I., Morales-Castro, J., Ochoa-Martínez, L.A., Salvia-Trujillo, L. and Martín-Belloso, O., 2016. Long-term stability of food-grade nanoemulsions from high methoxyl pectin containing essential oils. *Food Hydrocolloids*, *52*, pp.438-446.

[220] Lee, K.S., 2011. Performance of a polymer flood with shear-thinning fluid in heterogeneous layered systems with crossflow. *Energies*, *4*(8), pp.1112-1128.

[221] Sastry, N.V., Dave, P.N. and Valand, M.K., 1999. Dilute solution behaviour of polyacrylamides in aqueous media. *European polymer journal*, *35*(3), pp.517-525.

[222] Pérez-Masiá, R., Lagaron, J.M. and Lopez-Rubio, A., 2015. Morphology and stability of edible lycopene-containing micro-and nanocapsules produced through electrospraying and spray drying. *Food and bioprocess technology*, *8*(2), pp.459-470.

[223] Pal, R.A.J.I.N.D.E.R., 1996. Rheology of emulsions containing polymeric liquids. *Encyclopedia of emulsion technology*, *4*, p.93.

[224] Niraula, B., King, T.C., Chun, T.K. and Misran, M., 2004. Rheology properties of glucopyranoside stabilized oil–water emulsions: effect of alkyl chain length and bulk concentration of the surfactant. *Colloids and Surfaces A: Physicochemical and Engineering Aspects*, *251*(1-3), pp.117-132.

[225] Vlachos, N., Skopelitis, Y., Psaroudaki, M., Konstantinidou, V., Chatzilazarou, A. and Tegou, E., 2006. Applications of Fourier transform-infrared spectroscopy to edible oils. *Analytica chimica acta*, *573*, pp.459-465.

[226] Zheng, J. and Fayer, M.D., 2007. Hydrogen bond lifetimes and energetics for solute/solvent complexes studied with 2D-IR vibrational echo spectroscopy. *Journal of the American Chemical Society*, *129*(14), pp.4328-4335.

[227] American Society for Testing and Materials (ASTM), 2005. ASTM D6560, Standard Test Method for Determination of Asphaltenes (Heptane Insolubles) in Crude Petroleum and Petroleum Products.

[228] Speight, J.G. and Moschopedis, S.E., 1981. On the molecular nature of petroleum asphaltenes.

[229] Tan, X., Fenniri, H. and Gray, M.R., 2009. Water enhances the aggregation of model asphaltenes in solution via hydrogen bonding. *Energy & Fuels*, *23*(7), pp.3687-3693.

[230] He, Z., Jiang, S., Li, Q., Wang, J., Zhao, Y. and Kang, M., Facile and cost-effective synthesis of isocyanate microcapsules via polyvinyl alcohol-mediated interfacial polymerization and their application in self-healing materials, *Composites Science and Technology*, 2017, *138*, 15-23.

[231] Bonakdar, S., Emami, S.H., Shokrgozar, M.A., Farhadi, A., Ahmadi, S.A.H. and Amanzadeh, A., Preparation and characterization of polyvinyl alcohol hydrogels crosslinked by biodegradable polyurethane for tissue engineering of cartilage, *Materials science and engineering: c*, 2010, *30*(4), 636-643.

[232] Ketren, W., Zen, H., Ashida, R., Kii, T. and Ohgaki, H., Investigation on Conversion Pathways in Degradative Solvent Extraction of Rice Straw by Using Liquid Membrane-FTIR Spectroscopy, *Energies*, 2019, *12*(3), p.528.

[233] Hou, R., Bai, Z., Hao, P., Dai, X., Xu, J., Zheng, H., Guo, Z., Kong, L., Bai, J. and Li, W., Effects of temperature and solvents on structure variation of Yunnan lignite in preheating stage of direct liquefaction, *Fuel*, 2019, *239*, 917-925.

[234] Liu, X., Hirajima, T., Nonaka, M., Mursito, A.T. and Sasaki, K., Use of FTIR combined with forms of water to study the changes in hydrogen bonds during low-temperature heating of lignite, *Drying technology*, 2016, *34*(2), 185-193.

[235] Bledzki, A.K., Mamun, A.A. and Volk, J., Barley husk and coconut shell reinforced polypropylene composites: the effect of fibre physical, chemical and surface properties, *Composites Science and Technology*, 2010, *70*(5), 840-846.

[236] Wang, F.C., Feve, M., Lam, T.M. and Pascault, J.P., 1994. FTIR analysis of hydrogen bonding in amorphous linear aromatic polyurethanes. I. Influence of temperature. *Journal of Polymer Science Part B: Polymer Physics*, *32*(8), pp.1305-1313.

[237] Vikulov, K.A., Shelimov, B.N. and Kazansky, V.B., 1991. IR and UV-Vis spectroscopie studies of the surface Mo CH2 and Mo CH-CH3 carbene complexes produced by methylcyclopropane chemisorption over photoreduced silica-molybdena catalysts. *Journal of molecular catalysis*, *65*(3), pp.393-402.

[238] Keresztury, G., Holly, S., Besenyei, G., Varga, J., Wang, A. and Durig, J.R., 1993. Vibrational spectra of monothiocarbamates-II. IR and Raman spectra, vibrational assignment, conformational analysis and ab initio calculations of S-methyl-N, N-dimethylthiocarbamate. *Spectrochimica Acta Part A: Molecular Spectroscopy*, *49*(13-14), pp.2007-2026.

[239] Brzezinski, B., Radziejewski, P., Rabold, A. and Zundel, G., 1995. Hydrogen bonds and hydrogen-bonded systems in Mannich bases of 2, 2′-biphenol: an FTIR study of the proton polarizability and Fermi resonance effects as a function of temperature. Journal of molecular structure, 355(2), pp.185-191.

[240] Yang, Z., Chen, S., Peng, H., Li, M., Lin, M., Dong, Z., Zhang, J. and Ji, Y., 2016. Effect of precipitating environment on asphaltene precipitation: Precipitant, concentration, and temperature. *Colloids and Surfaces A: Physicochemical and Engineering Aspects*, *497*, pp.327-335.

[241] Gray, M.R., Tykwinski, R.R., Stryker, J.M. and Tan, X., 2011. Supramolecular assembly model for aggregation of petroleum asphaltenes. *Energy & Fuels*, *25*(7), pp.3125-3134.

[242] Buckley, J.S., 1999. Predicting the onset of asphaltene precipitation from refractive index measurements. *Energy & Fuels*, *13*(2), pp.328-332.

[243] Wattana, P., Wojciechowski, D.J., Bolaños, G. and Fogler, H.S., 2003. Study of asphaltene precipitation using refractive index measurement. *Petroleum science and technology*, *21*(3-4), pp.591-613.

[244] Wiehe, I.A., 2008. *Process chemistry of petroleum macromolecules*. CRC press.
Lerche, D. and Sobisch, T., 2007. Consolidation of concentrated dispersions of nano-and microparticles determined by analytical centrifugation. *Powder technology*, *174*(1), pp.46-49.

[245] Hildebrand, J. H.; Wood, S. E. The Derivation of Equations for Regular Solutions. J. Chem. Phys. 1933, 1 (12), 817−822.

[246] Wiehe, I. A.; Kennedy, R. J. The Oil Compatibility Model and Crude Oil Incompatibility. *Energy Fuel*s, 2000, 14 (1), 56−59.

[247] Wang, J. X.; Buckley, J. S. A Two-Component Solubility Model of the Onset of A sphaltene Flocculation in Crude Oils. *Energy Fuels*, 2001, 15 (5), 1004−1012.

[248] Chang, C.W. and Liao, Y.C., 2016. Accelerated Sedimentation Velocity Assessment for Nanowires Stabilized in a Non-Newtonian Fluid. *Langmuir*, *32*(51), pp.13620-13626.

[249] Primozic, M., Duchek, A., Nickerson, M. and Ghosh, S., 2017. Effect of lentil proteins isolate concentration on the formation, stability and rheological behavior of oil-in-water nanoemulsions. *Food Chemistry*, 237, pp.65-74.

[250] Schilling, C.H. and Aksay, I.A., 1992. Consolidation Behavior of Flocculated Alumina Suspensions. *J. Am. Ceram. Soc*, *75*(12), pp.3305-3314.

[251] Lange, F.F. and Miller, K.T., 1987. Pressure filtration: consolidation kinetics and mechanics. *American Ceramic Society Bulletin*, *66*(10), pp.1498-1504.

[252] Lamas, B., Abreu, B., Fonseca, A., Martins, N. and Oliveira, M., 2012. Assessing colloidal stability of long term MWCNT based nanofluids. *Journal of colloid and interface science*, 381(1), pp.17-23.

[253] Brochu, C., Pelletier, E., Caron, G. and Desnoyers, J.E., 1986. Dispersion of crude oil in seawater: The role of synthetic surfactants. *Oil and Chemical Pollution*, *3*(4), pp.257-279.

[254] Goual, L. and Firoozabadi, A., 2004. Effect of resins and DBSA on asphaltene precipitation from petroleum fluids. *AIChE journal*, *50*(2), pp.470-479.

[255] Chang, C.L. and Fogler, H.S., 1994. Stabilization of asphaltenes in aliphatic solvents using alkylbenzene-derived amphiphiles. 2. Study of the asphaltene-amphiphile interactions and structures using Fourier transform infrared spectroscopy and small-angle X-ray scattering techniques. *Langmuir*, *10*(6), pp.1758-1766.

[256] Goual, L. and Sedghi, M., 2015. Role of ion-pair interactions on asphaltene stabilization by alkylbenzenesulfonic acids. *Journal of Colloid and Interface Science*, *440*, pp.23-31.

[257] Hashmi, S.M. and Firoozabadi, A., 2013. Self-assembly of resins and asphaltenes facilitates asphaltene dissolution by an organic acid. *Journal of Colloid and Interface Science*, *394*, pp.115-123.

[258] Alhreez, M. and Wen, D., 2018. Controlled releases of asphaltene inhibitors by nanoemulsions. *Fuel*, *234*, pp.538-548.

[259] González, G. and Middea, A., 1991. Peptization of asphaltene by various oil soluble amphiphiles. *Colloids and Surfaces*, *52*, pp.207-217.

[260] Chang, C.L. and Fogler, H.S., 1994. Stabilization of asphaltenes in aliphatic solvents using alkylbenzene-derived amphiphiles. 1. Effect of the chemical structure of amphiphiles on asphaltene stabilization. *Langmuir*, *10*(6), pp.1749-1757.

[261] Sjöblom, J., Aske, N., Auflem, I.H., Brandal, Ø., Havre, T.E., Sæther, Ø., Westvik, A., Johnsen, E.E. and Kallevik, H., 2003. Our current understanding of water-in-crude oil emulsions: Recent characterization techniques and high pressure performance. *Advances in Colloid and Interface Science*, *100*, pp.399-473.

[262] Aslan, S. and Firoozabadi, A., 2014. Effect of water on deposition, aggregate size, and viscosity of asphaltenes. *Langmuir*, *30*(13), pp.3658-3664.

[263] Souza, V.B., Neto, J.S., Spinelli, L.S. and Mansur, C.R., 2013. Application of oil/water nanoemulsions as a new alternative to demulsify crude oil. *Separation Science and Technology*, *48*(8), pp.1159-1166.

[264] Dash, S.; Murthy, P. N.; Nath, L.; Chowdhury, P. Kinetic modeling on drug release from controlled drug delivery systems. *Acta Pol. Pharm.* 2010, 67(3), 217–223.

[265] Hoepfner, M. P.; Limsakoune, V.; Chuenmeechao, V.; Maqbool, T.; Fogler, H. S. A fundamental study of asphaltene deposition. *Energ Fuel* 2013, 27(2), 725–735.

[266] Juyal, P.; Ho, V.; Yen, A.; Allenson, S. J. Reversibility of asphaltene flocculation with chemicals. *Energ Fuel* 2012, 26(5), 2631–2640.

[267] de Almeida Borges, V.R., Simon, A., Sena, A.R.C., Cabral, L.M. and de Sousa, V.P., Nanoemulsion containing dapsone for topical administration: a study of in vitro release and epidermal permeation. *International journal of nanomedicine* 2013, *8*, p.535.

[268] Barradas, T.N., Senna, J.P., Cardoso, S.A., e Silva, K.G.D.H. and Mansur, C.R.E., Formulation characterization and in vitro drug release of hydrogel-thickened

nanoemulsions for topical delivery of 8-methoxypsoralen. *Materials Science and Engineering* 2018, *92*, pp.245-253.

[269] Nothnagel, L. and Wacker, M.G., How to measure release from nanosized carriers?.*European Journal of Pharmaceutical Sciences*. 2018

[270] Costa, P.; Lobo, J. M. S. Modeling and comparison of dissolution profiles. *European Journal of Pharmaceutical Sciences* 2001, 13(2), 123–133.

[271] Rodrigues, M. R.; Lanzarini, C. M.; Ricci-Junior, E. Preparation, in vitro characterization and in vivo release of naproxen loaded in poly-caprolactone nanoparticles. *Pharm. Dev. Technol.* 2011, 16, 12–21.

[272] Pereira, J. C.; Delgado-Linares, J.; Briones, A.; Guevara, M.; Scorzza, C.; Salager, J. L. The effect of solvent nature and dispersant performance on asphaltene precipitation from diluted solutions of instable crude oil. *Petroleum Science and Technology* 2011, 29(23), 2432–2440.

[273] Colomer, M. T.; Guzman, J.; Moreno, R. Determination of peptization time of particulate sols using optical techniques: Titania as a case study. *Chemistry of Materials* 2008, 20(12), 4161–4165.

[274] Alhreez, M.; Wen, D.; Ali, L. A novel inhibitor for controlling Iraqi asphaltene problems. International Conference on Environmental Impacts of the Oil and Gas Industries: Kurdistan Region of Iraq as a Case Study (EIOGI). Iraq; 2017, 37–41.

[275] Mansur, C. R.; de Melo, A. R.; Lucas, E. F. Determination of asphaltene particle size: influence of flocculant, additive, and temperature. *Energ Fuel* 2012, 26(8), 4988–4994.

[276] Hoepfner, M. P.; Vilas Bôas Fávero, C.; Haji-Akbari, N.; Fogler, H. S. The fractal aggregation of asphaltenes. *Langmuir* 2013, 29(28), 8799–8808.

[277] Aditya, N. P.; Shim, M.; Lee, I.; Lee, Y.; Im, M. H.; Ko, S. Curcumin and genistein coloaded nanostructured lipid carriers: in vitro digestion and antiprostate cancer activity. *Journal of Agricultural and Food Chemistry* 2013, 61(8), 1878–1883.

[278] Gao, A.; Liu, F.; Xiong, Z.; Yang, Q. Tunable adhesion of superoleophilic/ superhydrophobic Poly (lactic acid) membrane for controlled-release of oil soluble drugs. *Journal of Colloid and Interface Science* 2017, 505, 49–58.

[279] Jose, S.; Fangueiro, J. F.; Smitha, J.; Cinu, T. A.; Chacko, A. J.; Premaletha, K.; Souto, E. B. Predictive modeling of insulin release profile from cross-linked chitosan microspheres. *European journal of medicinal chemistry* 2013, 60, 249–253.

[280] Peppas, N.A. Commentary on an exponential model for the analysis of drug delivery: Original research article: a simple equation for description of solute release: I II. Fickian and non-Fickian release from non-swellable devices in the form of slabs, spheres, cylinders or discs, 1987. *Journal of Controlled Release* 2014, 190, 31–32.

[281] Elosaily, G. H. Formulation and in-vitro evaluation of nystatinnanoemulsion-based gel for topical delivery. *J. Am. Sci.* 2012, 8(12), 541–548.

[282] Rodríguez-Burneo, N.; Busquets, M. A.; Estelrich, J. Magnetic nanoemulsions: Comparison between nanoemulsions formed by ultrasonication and by spontaneous emulsification. *Nanomaterials* 2017, 7(7), 190.

[283] Alvarado, H. L.; Abrego, G.; Souto, E. B.; Garduño-Ramirez, M. L.; Clares, B.; García, M. L.; Calpena, A. C. Nanoemulsions for dermal controlled release of oleanolic and ursolic acids: in vitro, ex vivo and in vivo characterization. *Colloids and Surfaces B: Biointerfaces* 2015, 130, 40–47.

[284] Miastkowska, M.; Sikora, E.; Ogonowski, J.; Zielina, M.; Łudzik, A. The kinetic study of isotretinoin release from nanoemulsion. *Colloids and Surfaces A: Physicochemical and Engineering Aspects* 2016, 510, 63–68.

[285] Nanjwade, B. K.; Varia, P. J.; Kadam, V. T.; Srichana, T.; Kamble, M. S. Development and evaluation of nanoemulsion of repaglinide. *Nanotechnol. Nanomed.* 2013, 1(2), 1–8.

[286] Christopher, J.; Sarpal, A. S.; Kapur, G. S.; Krishna, A.; Tyagi, B. R.; Jain, M. C.; Jain, S. K.; Bhatnagar, A. K. Chemical structure of bitumen-derived asphaltenes by nuclear magnetic resonance spectroscopy and X-ray diffractometry. Fuel 1996, 75(8), 999–1008.

[287] S. Afra, H. A. Nasr-El-Din, D. Socci and Z. Cui, Green phenolic amphiphile as a viscosity modifer and asphaltenes dispersant for heavy and extra-heavy oil, Fuel, 2018, 220, 481–489.

[288] Yen, T. F.; Erdman, J. G.; Pollack, S. S. Investigation of the structure of petroleum asphaltenes by X-ray diffraction. Anal. Chem. 1961, 33(11), 1587–1594.

[289] AlHumaidan, F. S.; Hauser, A.; Rana, M. S.; Lababidi, H. M.; Behbehani, M. Changes in asphaltene structure during thermal cracking of residual oils: XRD study. Fuel 2015, 150, 558–564.

[290] Ebert LB, Scanion JC. Average structure determination for heavy ends in fossil fuels. Liquid Fuel Technol 1984;2(3):257–86.

[291] Shirokoff JW, Siddiqui MN, Ali MF. Characterization of the structure of Saudi crude asphaltenes by X-ray diffraction. Energy Fuels 1997;11:561–5.

[292] Rodrigues, M. R.; Lanzarini, C. M.; Ricci-Junior, E. Preparation, in vitro characterization and in vivo release of naproxen loaded in poly-caprolactone nanoparticles. Pharm. Dev. Technol. 2011, 16, 12–21.

[293] Alhreez, M. and Wen, D., 2019. Molecular structure characterization of asphaltene in the presence of inhibitors with nanoemulsions. *RSC Advances*, *9*(34), pp.19560-19570.

[294] J.M. Jacobson, M.R. Gray, Use of I.R. spectroscopy and nitrogen titration data in Structure Group Analysis of Bitumen, Fuel 66 (1987) 749– 752.

[295] H. Kallevik, O.M. Kvalheim, Sjoblom, Quantitative determination of asphaltenes and resins in solution by means of near-spectroscopy correlations to emulsions stability, Journal of Colloid and Interface Science 225 (2000) 494–504.

[296] J.F. McKay, T.E. Cogswell, J.H. Weber, D.R. Latham, Analysis of acids in high-boiling petroleum distillates, Fuel 54 (1975) 54–61.

[297] H.A. Akrami, M.F. Yardim, A. Akar, E. Ekinci, FT-IR characterisation of pitches derived from avgamasya asphaltite and raman-dinc¸ers heavy crude, Fuel 76 (1997) 1389– 1394.

[298] R.R. Coelho, I. Hovell, M.B. de Mello Monte, A. Middea, A. Lopes de Souza, Characterisation of aliphatic chains in vacuum residues (VRs) of asphaltenes and resins using molecular modelling and FTIR techniques, Fuel Process. Technol. 87 (2006) 325–333.

[299] Wu, H. and Kessler, M.R., 2015. Asphaltene: structural characterization, molecular functionalization, and application as a low-cost filler in epoxy composites. RSC Advances, 5(31), pp.24264-24273.

[300] M. Fossen, H. Kallevik, K. D. Knudsen and J. Sjoblom, Asphaltenes precipitated by a two-step precipitation procedure. 2. Physical and chemical characteristics, Energy Fuels, 2011, 25(8), 3552–3567.

[301] M. Mouazen, A. Poulesquen and B. Vergnes, Influence of thermomechanical history on chemical and rheological behavior of bitumen, Energy Fuels, 2011, 25(10), 4614–4621.

[302] T. Yan, K. Chen, L. Wang, Y. Liu, Y. Zhang, Z. Jiang, T. Fang, Experimental investigation of upgrading heavy oil with supercritical methanol, Energy Fuels 31 (2017) 5882–5890.

[303] D. Zhang, Z. Ren, D. Wang, K. Lu, Upgrading of crude oil in supercritical water: a five-lumped kinetic model, J. Anal. Appl. Pyrolysis 123 (2017) 56–64.

[304] J. Tong, X. Han, S. Wang, X. Jiang, Evaluation of structural characteristics of Huadian oil shale kerogen using direct techniques (solid-state 13C NMR, XPS, FTIR, and XRD), Energy Fuels 25 (2011) 4006–4013.

[305] Calemma, V., Iwanski, P., Nali, M. et al. 1995. Structural Characterization of Asphaltenes of Different Origins. Energy Fuels 9 (2): 225–230.

[306] M. Mouazen, A. Poulesquen and B. Vergnes, Influence of thermomechanical history on chemical and rheological behavior of bitumen, Energy Fuels, **2011**, 25(10), 4614–4621.

[307] Kabalnov, A. and Wennerström, H., 1996. Macroemulsion stability: the oriented wedge theory revisited. Langmuir, 12(2), pp.276-292.

[308] J.D. McLean, P.K. Kilpatrick, Comparison of precipitation and extrography in the fractionation of crude oil residua, Energy & Fuels 11 (1997) 570– 585.

[309] Poveda, J.C., Molina, D., Martínez, H., Florez, O. and Campillo, B., 2014. Molecular Changes in Asphaltenes within H2 Plasma. Energy & Fuels, 28(2), pp.735-744.

[310] Mullins, O.C., 2011. The asphaltenes. Annual Review of Analytical Chemistry, 4, pp.393-418.

[311] V. Savel'ev, A. Golovko, L. Gorbunova, V. Kamyanov, C. Galvalizi, Oil Gas Sci. Tech.- Rev. IFP 63 (2008) 57–67.

[312] Maity, S.K., Blanco, E., Ancheyta, J., Alonso, F. and Fukuyama, H., 2012. Early stage deactivation of heavy crude oil hydroprocessing catalysts. Fuel, 100, pp.17-23.

[313] Maity, S.K., Kumar, S., Srivastava, M., Kharola, A.S., Maurya, K.K., Konathala, S., Chatterjee, A.K. and Garg, M.O., 2015. Characterization of asphaltenic material obtained by treating of vacuum residue with different reactive molecules. Fuel, 149, pp.8-14.

[314] Sahoo, S.K., Ray, S.S. and Singh, I.D., 2004. Structural characterization of coke on spent hydroprocessing catalysts used for processing of vacuum gas oils. Applied Catalysis A: General, 278(1), pp.83-91.

[315] Velazquez-Jimenez, L.H. and Rangel-Mendez, J.R., 2014. Chemical and thermogravimetric analyses of raw and saturated agave bagasse main fractions with Cd (II), Pb (II), and Zn (II) Ions: adsorption mechanisms. Industrial & Engineering Chemistry Research, 53(20), pp.8332-8338.

[316] Mora, A.J., Avila, E.E., Delgado, G.E., Fitch, A.N. and Brunelli, M., 2005. Temperature effects on the hydrogen-bond patterns in 4-piperidinecarboxylic acid. Acta Crystallographica Section B: Structural Science, 61(1), pp.96-102.

[317] Zahabi, A., Gray, M.R. and Dabros, T., 2012. Kinetics and properties of asphaltene adsorption on surfaces. *Energy & Fuels*, *26*(2), pp.1009-1018.

[318] Gonzalez, G. and Travalloni-Louvisse, A.M., 1993. Adsorption of asphaltenes and its effect on oil production. SPE Production & Facilities, 8(02), pp.91-96.

[319] Pernyeszi, T., Patzko, A., Berkesi, O. and Dékány, I., 1998. Asphaltene adsorption on clays and crude oil reservoir rocks. Colloids and Surfaces A: Physicochemical and Engineering Aspects, 137(1-3), pp.373-384.

[320] Acevedo, S., Castillo, J., Fernández, A., Goncalves, S. and Ranaudo, M.A., 1998. A study of multilayer adsorption of asphaltenes on glass surfaces by photothermal surface deformation. Relation of this adsorption to aggregate formation in solution. Energy & Fuels, 12(2), pp.386-390.

[321] Acevedo, S., Ranaudo, M.A., García, C., Castillo, J., Fernández, A., Caetano, M. and Goncalvez, S., 2000. Importance of asphaltene aggregation in solution in determining the adsorption of this sample on mineral surfaces. Colloids and Surfaces A: Physicochemical and Engineering Aspects, 166(1-3), pp.145-152.

[322] de la Cruz, J.L.M., Castellanos-Ramírez, I.V., Ortiz-Tapia, A., Buenrostro-González, E., Durán-Valencia, C.D.L.A. and López-Ramírez, S., 2009. Study of monolayer to multilayer adsorption of asphaltenes on reservoir rock minerals. Colloids and Surfaces A: Physicochemical and Engineering Aspects, 340(1-3), pp.149-154.

[323] Dudášová, D., Simon, S., Hemmingsen, P.V. and Sjöblom, J., 2008. Study of asphaltenes adsorption onto different minerals and clays: Part 1. Experimental adsorption with UV depletion detection. Colloids and Surfaces A: Physicochemical and Engineering Aspects, 317(1-3), pp.1-9.

[324] Jouault, N., Corvis, Y., Cousin, F., Jestin, J. and Barré, L., 2009. Asphaltene adsorption mechanisms on the local scale probed by neutron reflectivity: transition from

monolayer to multilayer growth above the flocculation threshold. Langmuir, 25(7), pp.3991-3998.

[325] Xing, C., Hilts, R.W. and Shaw, J.M., 2010. Sorption of Athabasca vacuum residue constituents on synthetic mineral and process equipment surfaces from mixtures with pentane. Energy & Fuels, 24(4), pp.2500-2513.

[326] Franco, C.A., Nassar, N.N., Ruiz, M.A., Pereira-Almao, P. and Cortés, F.B., 2013. Nanoparticles for inhibition of asphaltenes damage: adsorption study and displacement test on porous media. Energy & Fuels, 27(6), pp.2899-2907.

[327] Xie, K. and Karan, K., 2005. Kinetics and thermodynamics of asphaltene adsorption on metal surfaces: A preliminary study. Energy & fuels, 19(4), pp.1252-1260.

[328] Saraji, S., Goual, L. and Piri, M., 2010. Adsorption of asphaltenes in porous media under flow conditions. Energy & Fuels, 24(11), pp.6009-6017.

[329] Nassar, N.N., Betancur, S., Acevedo, S., Franco, C.A. and Cortés, F.B., 2015. Development of a population balance model to describe the influence of shear and nanoparticles on the aggregation and fragmentation of asphaltene aggregates. Industrial & Engineering Chemistry Research, 54(33), pp.8201-8211.

[330] Betancur, S., Carmona, J.C., Nassar, N.N., Franco, C.A. and Cortés, F.B., 2016. Role of particle size and surface acidity of silica gel nanoparticles in inhibition of formation damage by asphaltene in oil reservoirs. Industrial & Engineering Chemistry Research, 55(21), pp.6122-6132.

[331] Kelland, M.A., 2014. Production chemicals for the oil and gas industry. CRC press.

[332] Lamas, B., Abreu, B., Fonseca, A., Martins, N. and Oliveira, M., 2012. Assessing colloidal stability of long term MWCNT based nanofluids. Journal of colloid and interface science, 381(1), pp.17-23.

[333] Maeda, H. and Kakehashi, R., 2000. Effects of protonation on the thermodynamic properties of alkyl dimethylamine oxides. Advances in colloid and interface science, 88(1-2), pp.275-293.

[334] Ruiz, C.C. and Aguiar, J., 2003. Mixed micellization of octaoxyethylene monododecyl ether and n-alkyltrimethylammonium bromides. Colloids and Surfaces A: Physicochemical and Engineering Aspects, 224(1-3), pp.221-230.

[334] McClements, D.J., 2005. Theoretical analysis of factors affecting the formation and stability of multilayered colloidal dispersions. Langmuir, 21(21), pp.9777-9785.

[336] Hu, C., Morris, J.E. and Hartman, R.L., 2014. Microfluidic investigation of the deposition of asphaltenes in porous media. Lab on a Chip, 14(12).

[337] Behbahani, T.J., Ghotbi, C., Taghikhani, V. and Shahrabadi, A., 2015. Experimental study and mathematical modeling of asphaltene deposition mechanism in core samples. Oil & Gas Science and Technology–Revue d'IFP Energies nouvelles, 70(6), pp.1051-1074.

[338] Hu, Z., Azmi, S.M., Raza, G., Glover, P.W. and Wen, D., 2016. Nanoparticle-assisted water-flooding in Berea sandstones. Energy & Fuels, 30(4), pp.2791-2804.

[339] Javanbakht, G. and Goual, L., 2016. Mobilization and micellar solubilization of NAPL contaminants in aquifer rocks. Journal of contaminant hydrology, 185, pp.61-73.

[340] Jada, A. and Salou, M., 2002. Effects of the asphaltene and resin contents of the bitumens on the water–bitumen interface properties. Journal of Petroleum Science and Engineering, 33(1-3), pp.185-193.

[341] Salehi, M., Johnson, S.J. and Liang, J.T., 2008. Mechanistic study of wettability alteration using surfactants with applications in naturally fractured reservoirs. *Langmuir*, *24*(24), pp.14099-14107.

[342] Thomas, M.M., Clouse, J.A. and Longo, J.M., 1993. Adsorption of organic compounds on carbonate minerals: 1. Model compounds and their influence on mineral wettability. Chemical geology, 109(1-4), pp.201-213.

[343] Anderson, A., William, G., 1986. Wettability literature survey-Part 1: rock/oil/brine interactions and the effects of core handling on wettability. Society of Petroleum Engineer 38 (11), 1125–1127.

[344] Nicolini, J.V., Ferraz, H.C. and Borges, C.P., 2017. Effect of seawater ionic composition modified by nanofiltration on enhanced oil recovery in Berea sandstone. Fuel, 203, pp.222-232.

[345] Anderson, W.G., 1986. Wettability literature survey-part 3: the effects of wettability on the electrical properties of porous media. Journal of petroleum technology, 38(12), pp.1-371.

[346] Bennett, B. and Larter, S.R., 1997. Partition behaviour of alkylphenols in crude oil/brine systems under subsurface conditions. Geochimica et Cosmochimica Acta, 61(20), pp.4393-4402.

[347] Arashiro, E.Y. and Demarquette, N.R., 1999. Use of the pendant drop method to measure interfacial tension between molten polymers. Materials Research, 2(1), pp.23-32.

[348] Besra, L., Sengupta, D.K. and Roy, S.K., 2000. Particle characteristics and their influence on dewatering of kaolin, calcite and quartz suspensions. International Journal of Mineral Processing, 59(2), pp.89-112.